Etude de matériaux polymères comme confinement solide dans l'application choc laser LSP

Corentin Le Bras

HESAM UNIVERSITÉ

Arts et Métiers Sciences et Technologies

ÉCOLE DOCTORALE SCIENCES ET MÉTIERS DE L'INGÉNIEUR
[Laboratoire de recherche - Campus de Paris]

THÈSE

présentée par : **Corentin LE BRAS**
soutenue le : **12 janvier 2022**

pour obtenir le grade de : **Docteur d'HESAM Université**

préparée à : **École Nationale Supérieure d'Arts et Métiers**

Spécialité : **Mécanique-matériaux**

Etude de matériaux polymères comme confineurs solides dans l'application choc laser LSP

THÈSE dirigée par :
M. Berthe Laurent

et co-encadrée par :
M. Fayolle Bruno, Gervais Matthieu, Valadon Stéphane et Ecault Romain

Jury

M. Laurent LAMAIGNERE	Dir de recherche, CESTA, CEA	Président
M. Laurent LAMAIGNERE	Dir de recherche, CESTA, CEA	Rapporteur
M. Yann MARCO	Professeur, IRDL, ENSTA Bretagne	Rapporteur
M. Laurent BERTHE	Dir de recherche, PIMM, ENSAM	Examinateur
M. Laurent DELBREILH	MdC HDR, Université de Rouen	Examinateur
M. Bruno FAYOLLE	Professeur, PIMM, ENSAM	Examinateur
M. Matthieu GERVAIS	MdC, PIMM, ENSAM	Examinateur
M. Laurent VIDEAU	Ing de recherche, DAM, DIF, CEA	Examinateur
M. Stéphane VALADON	Ing, Airbus Opérations, Toulouse	Invité

THÈSE

Remerciements

Je tiens tout d'abord à remercier mes encadrants tout au long de cette thèse qui m'ont toujours accompagnés impeccablement tout au long de ces trois années que ce soit scientifiquement ou humainement. Le mélange du milieu des lasers et des polymères n'aura pas toujours été simple mais grâce à votre patience et votre bienveillance ça a été un plaisir d'avoir à méler ces deux disciplines. Laurent Berthe, ta motivation et ton optimisme sans faille m'ont permis de persévérer les (rares) fois où le laser faisaient des siennes ou que d'autres difficultés se faisaient sentir. Tu m'as converti aux lasers, la preuve je continue dedans ! Bruno Fayolle, malgrès ton emploi de ministre, tu as pris le temps de m'expliquer et de me transmettre énormément dans le domaine des polymère, tes qualités humaine et ta bonne humeur permanente ont sans aucun doute beaucoup joué sur le bon déroulement de la thèse et même sur l'ambiance de l'équipe polymère de manière générale. Grâce à toi je suis maintenant un grand bichon prêt à partir vers de nouvelles aventures. Matthieu Gervais, même si l'aspect synthèse des polymères est malheureusement un peu passé à la trappe, tu as toujours été présent et réactif quand j'en ai eu besoin, d'autant plus pendant ma rédaction pour la corrections ! Au delà de ses aspects j'ai beaucoup apprécier toutes les discussions que l'on a pu avoir tout au long de ces trois années et j'espère que l'on se recroisera de temps en temps pour en avoir d'autres !

Je n'oublie pas non plus l'encadrement que j'ai reçu par les deux personnes qui m'ont suivi chez Airbus, à savoir Stéphane Valadon et Romain Ecault, même si l'on s'est moins croisé que ce qui été initialement prévu j'ai énormément apprécié travailler avec vous. Vous avez su m'orienter quand je commençais à m'éparpiller dans le sujet.

Je souhaite bien évidemment remercier tous les membres de mon jury Laurent Lamaignere, Yann Marco, Laurent Delbreilh et Laurent Videau, qui ont accepté et pris le temps de lire mon manuscrit et aussi de me donner des conseils afin de l'améliorer. Mon seul regret dans ce choix de jury sera de ne pas avoir réussi à créer un jury uniquement composé de Laurent.

Le travail présenté dans ce manuscrit à été réalisé dans le cadre de l'ANR FORGE et est donc le produit d'un travail collaboratif. Je tiens donc à remercier tous les gens qui ont pu prendre part à ce projets et plus spécifiquement Tomas Bergara ainsi que Domenico Furfari qui se sont fortement investis dans ce projet et qui ont beaucoup oeuvré dans le but de m'aider et m'aiguiller.

Cette thèse n'aurait pas été la même sans l'ambiance générale du PIMM qui donne envie de venir tous les matins. Je me dois donc de remercier tous les gens qui ont pu oeuvrer de près ou de loin à cette ambiance qui je l'espère ne changera pas de si tôt en essayant de ne pas en oublier en commençant par la halle polymère dans laquelle on a posé ma niche de bichon à mon arrivée. Je remercie donc: Tout le bureau $9\frac{3}{4}$: avec dans un premier temps Clément, Eeva puis Romain suivi plus tard de Fanon qui ont tous participé à faire de ce petit bureau en un endroit plutôt sympa dans lequel travailler. Je n'oublie pas l'équipe des bichons composée de Xavier, le meilleur imitateur de bruits mignons, Caroline, qui skie très bien, pour une parisienne, Simon, le déporté bordelais qui a de très bonnes idées en fin de soirée et Gwladys accompagnée de queen Shatouille qui fait les pires (meilleurs ?) cadeaux de secret Santa. On peut aussi citer Raphaël (Esh) sans oublier le petit Shot, Fréd pour son approvionnement en bière et son imitation de la poule, Alexis et sa belle moustiquaire, Anna (I am not a gros bébé anymore), Gianmarco for his teaching of formal, polite italian, Ana la grosse folle et pour finir Sara qui m'a appris à aimer l'Italie et sa cuisine même si j'arriverai à te convertir au beurre un jour.

Du côté de la halle laser j'appelle à la barre, Mohammad le chef raisonnable, Gwénaëlle et Lucas, les deux sudistes, Klauss et Maxime, les collègues d'escalade (ou peut-être de blessure), Julien toujours de bonne humeur en arrivant au bureau et Selen, la kedi queen la plus française d'entre-nous, je pense qu'on a plus grand chose à t'apprendre si ce n'est à uslu dur. j'ai eu aussi beaucoup l'occasion de passer vous voir (principalement pour prendre des cafés, on va pas se mentir) mais ça à toujours été très agréable de venir discuter avec vous dans ce grand bureau open-space même si je n'aurais jamais réussi à y travailler. Reste Marine, l'exilée dans son petit bureau à l'écart, toujours présente pour un petit thé ou pour se plaindre du laser, on aura dû se supporter du début à la fin et ça s'est pas trop mal passé au final je crois.

Pour cloturer ce tour du labo, je rajouterai les gens de la halle Manet qu'on aime même s'ils sont cachés au loin : Lucas lp, puisses-tu transmettre les enseignements de puppet yoda aux générations futures, sans oublier ses deux autres acolytes Antoine et Pouya.

Promesse oblige un petit message pour Tio: Oi tio, obrigado por tudo, não mude, afinal eu não

aprendi muito bem português, mas pelo menos posso dizer ótimo Cabo. Estou contando com você para não ser sábio entre os momentos em que nos encontrarmos novamente.

Pour finir je voudrais remercier l'équipe brestoise, Gwénaël, Jo, Méline, Erwan et Marc qui étaient déjà là bien avant, pendant et qui seront toujours là bien après cette thèse à moins que je finisse par trop vous saouler à vous demander de m'appeler docteur.

Je finirai ces remerciements déjà bien trop longs en remerciant mon papa et ma maman et plus généralement ma famille qui m'a toujours encouragé et donné la curiosité et le goût de la science, vous avez toujours été un exemple pour moi et j'espère que vous êtes quand même un peu fiers de moi !

Abstract

The laser shock peening process is commonly used in the aerospace industry. It consists in focusing a laser pulse at the surface of a metallic piece to reinforce its fatigue behaviour properties. When the laser pulse hits the surface of the material, a plasma is created and starts to expand in the air. This plasma release induces the creation of a shockwave with a typical pressure in the GPa range that plasticises the matter. As a result, compressive residual stresses are induced in the material. They are themselves the cause of the final improved fatigue behaviour. In order to produce sufficient pressures to treat the alloys of interest, a water layer is usually placed on top of the surface of the metallic target in the form of running water brought by a little hose. This configuration hinder the plasma expansion in the air and induces the production of higher maximum pressures during a longer duration. However, this configuration does not allow for the treatment of some specific parts of aircrafts that cannot support water in their environment. For this reason, an alternative to the water confined regime is necessary. In this work, the use of flexible, transparent polymers is studied and demonstrates good results allowing to consider polymer as a true candidate for all the laser peening applications where water cannot be used. After a state of the art and a presentation of the materials and methods used during the work, a first part describes the choice, parametric study and residual stresses measurements realised with polymer confinement on an aeronautic alloy while a second part presents the flexible polymer mechanical behaviour under laser conditions (high pressure and strain rate).

Keywords : Laser, Laser shock peening, Polymer, Pressure sensitive adhesive, Dynamic glass transition, Residual stresses, Fatigue.

Résumé

Le procédé de laser shock peening est couramment utilisé dans l'industrie aéronautique. Il consiste à focaliser une impulsion laser à la surface d'une pièce métallique dont il faut renforcer le comportement en fatigue. Quand l'impulsion laser atteint la surface de la cible métallique, un plasma se crée puis se détend dans l'air. Cette détente engendre la création d'une onde de choc avec une pression de l'ordre du GPa qui à pour effet de plastifier la matière qu'elle traverse. En conséquence, des contraintes résiduelles de compression sont induites dans le matériau et ce sont ces dernières qui sont la cause du meilleur comportement en fatigue obtenu. Afin de produire des pressions suffisantes au traitement d'alliages utilisés dans l'aéronautique, une couche d'eau est placée sur la surface de la pièce à traiter. Cette configuration à pour effet d'empêcher la détente du plasma dans l'air, provoquant des pressions plus fortes pendant un temps plus long. Cependant le régime confiné par eau ne permet pas le traitement de certaines zones spécifiques des avions dans lesquelles de l'eau ne peut pas être amenée. De ce fait, une alternative au confinement eau apparait comme nécessaire. Dans ce manuscrit de thèse l'utilisation d'un polymère transparent et flexible montre de bons résultats permettant de considérer les polymères comme de vrais candidats pour les applications de grenaillage laser dans lesquelles l'eau ne peut être utilisée en tant que confinement. Après un état de l'art et une présentation des outils utilisés au cours des différentes expériences, ce manuscrit décrit dans une première partie le choix d'un confinement suivi de son étude paramétrique et de résultats de mesures de contraintes résiduelles après traitement. Une seconde partie se concentre sur les propriétés mécaniques d'un polymère flexible sous un régime mécanique de type choc laser (haute pression et vitesse de déformation).

Mots-clés : Laser, Grenaillage laser, Polymère, Adhésif sensible à la pression, Transition vitreuse dynamique, contraintes résiduelles, Fatigue.

Contents

Remerciements **3**

Abstract **7**

Résumé **9**

Introduction **17**

1 Bibliography **27**
1.1 A brief laser shock peening history . . . 33
1.2 Laser shock peening process . . . 35
1.2.1 Direct regime . . . 36
1.2.2 Confined regime . . . 36
1.2.3 Breakdown . . . 38
1.2.3.1 Influence on transmitted pulse duration . . . 39
1.2.3.2 Triggering phenomena . . . 40
1.2.3.3 Pulse length influence . . . 42
1.2.4 Effects induced by the treatment . . . 43
1.2.4.1 General mechanical effects . . . 43
1.2.4.1.1 Depth of the plastified area . . . 45
1.2.4.1.2 Effect of laser shock on hardness . . . 46
1.2.4.2 General thermal effects . . . 47
1.2.4.3 Thermoprotective layer . . . 48
1.2.4.4 Residual stresses . . . 50
1.2.4.4.1 Treatment without thermal coating . . . 50
1.2.4.5 Roughness modification linked to LSP treatment . . . 52
1.2.5 Key process parameters . . . 54
1.2.5.1 Pulse profile and duration influence . . . 54
1.2.5.2 Wavelength influence . . . 55
1.3 Applications . . . 56
1.3.1 Fatigue life enhancement . . . 58
1.3.1.1 Fatigue life improvement induced by laser shock peening . . . 59
1.3.1.2 Crack propagation and initiation . . . 59
1.3.1.3 Fatigue crack growth . . . 60
1.3.1.4 Stress corrosion cracking resistance . . . 60

1.3.2 Other laser applications . . . 61
1.3.3 Laser peening compared to other peening strategies . . . 63
1.3.4 Industrialisation challenges with water confinement . . . 64
1.3.4.1 Parts to be treated . . . 65
1.3.5 Advantages of polymer confinement . . . 66
1.4 Polymers as confinement . . . 67
1.4.1 Laser interaction with polymer . . . 68
1.4.1.1 Heating inclusion model . . . 70
1.4.1.2 Bond breaking model . . . 71
1.4.1.3 Coloured center model . . . 71
1.4.2 Properties needed for a polymer confinement for LSP treatment . . . 71
1.4.2.1 Crystalline properties . . . 72
1.4.2.2 Bond strength . . . 72
1.4.2.3 Polymer choice . . . 72
1.4.3 Pressure Sensitive Adhesive description . . . 73
1.4.3.1 Mechanisms of PSAs . . . 75
1.4.3.2 Application requirements . . . 76
1.4.4 Overview of polymers material properties . . . 77
1.4.4.1 Viscoelasticity and viscoplasticity . . . 77
1.4.4.1.1 Stress relaxation . . . 79
1.4.4.1.2 Dynamic mechanical measurement . . . 79
1.4.5 Non-linear viscoelastoplasticity . . . 82
1.4.6 Elastomers under high stress rate . . . 82
1.4.6.1 Dynamic glass transition . . . 82
1.4.6.2 Pressure effect . . . 83
1.4.6.3 Strain rate effect . . . 84
1.4.7 Model to describe elasticity . . . 86
1.4.8 Model to describe glassy polymers . . . 87
1.5 Conclusion on the needed properties for the confinement . . . 88

2 Materials and methods **93**
2.1 Lasers . . . 94
2.1.1 Laser Description . . . 94
2.1.1.1 Héphaïstos . . . 94
2.1.1.2 Theïa . . . 95
2.1.2 Laser spot . . . 96
2.1.3 Pulse duration measurement . . . 96
2.1.4 Energy measurement . . . 98
2.2 VISAR . . . 98
2.2.1 Measurement principle . . . 100
2.2.2 PIMM's VISAR Setup . . . 101
2.2.3 Signals obtained by VISAR . . . 102
2.2.4 Advantages over other measurement techniques . . . 103
2.3 Numerical simulation . . . 104

2.3.1 Target geometry and boundary conditions . . . 104
2.3.2 Entry data . . . 105
2.3.2.1 Spatial profile . . . 105
2.3.2.2 Pressure profile . . . 106
2.3.3 Constitutive models . . . 107
2.3.3.1 Elasto-plastic . . . 107
2.3.3.2 Jonhson-Cook . . . 107
2.3.3.3 Mie-Grüneisen equation of state . . . 108
2.4 Material characterization . . . 110
2.4.1 Infra-Red spectroscopy . . . 110
2.4.2 Dielectric relaxation spectroscopy . . . 111
2.4.2.1 Principle . . . 111
2.4.2.2 Apparatus . . . 112
2.4.2.3 Data treatment . . . 114
2.4.2.3.1 Havriliak-Negami . . . 114
2.4.2.3.2 Vogel-Fulcher-Tammann . . . 114
2.5 Residual stresses measurement by XRD . . . 114

3 Confinement and parameters influencing laser shock 119
3.1 Synthesis and choice of the confinement . . . 125
3.1.1 Polymer synthesis . . . 125
3.1.2 Choice of the polymers of interest . . . 126
3.1.2.1 Energy transmission measurement . . . 126
3.1.2.2 Pressure measurements . . . 127
3.1.2.3 Transmission after mulitiple laser shots . . . 130
3.2 Wavelength influence on the produced pressure . . . 130
3.2.1 Pressure measurement . . . 131
3.3 Young's modulus influence on the pressure produced . . . 132
3.3.1 Expected effects . . . 132
3.3.2 Pressure measurement . . . 134
3.4 Confinement thickness influence on the LSP process . . . 137
3.4.1 Epoxy . . . 137
3.4.2 Acrylate . . . 138
3.4.2.1 Pressure and backface velocity measurements . . . 139
3.4.2.2 Full width half maximum shortening . . . 140
3.4.2.3 Plasma thickness versus confinement thickness . . . 142
3.4.2.3.1 Impedance calculation from literature . . . 143
3.4.2.3.2 Impedance calculation from experiments . . . 145
3.4.2.4 Tape damaging under laser irradiation . . . 146
3.4.2.4.1 Transmission after shot . . . 146
3.4.2.4.2 Tape imaging . . . 146
3.4.2.4.3 Infra-red characterization . . . 149
3.4.2.5 Conclusion on the confinement thickness effects . . . 149
3.5 Adhesion . . . 151

3.5.1 Silicone confinement . . . 152
3.5.2 Acrylate tape confinement . . . 153
3.6 Chemical composition . . . 155
3.7 Residual stresses measurements . . . 156
3.7.1 Laser shock set-up . . . 157
3.7.2 Surface state before and after treatment . . . 159
3.7.3 Residual stress measurement . . . 159
3.7.3.1 Surface measurement . . . 159
3.7.3.2 Residual stresses calculation experiment . . . 159
3.7.3.3 In-depth measurement . . . 162
3.8 Conclusion . . . 163

4 Polymer confinement under shock **167**
4.1 Dynamic glass transition . . . 170
4.1.1 Material choice . . . 171
4.1.1.1 Polymer synthesis . . . 171
4.1.1.2 Transmission measurement . . . 172
4.1.1.3 Dielectric relaxation spectroscopy setup . . . 172
4.1.2 Dielectric relaxation spectroscopy results on acrylate tape . . . 172
4.1.3 Polycarbonate and polydimethylsiloxane study . . . 175
4.1.4 Comparison with laser experiment . . . 178
4.1.4.1 Rear free surface velocity profiles . . . 179
4.1.4.2 Simulation parameters . . . 180
4.1.4.2.1 Constitutive model . . . 182
4.1.4.2.2 Spatial and pressure profiles . . . 183
4.1.4.3 Simulation results - Strain rates extracted . . . 184
4.2 Acrylate tape mechanical characterization . . . 187
4.2.1 Shock experiment setup . . . 187
4.2.2 Spallation threshold . . . 187
4.2.3 Changes induced in the material . . . 193
4.2.3.1 Behaviour before damaging threshold . . . 193
4.2.3.2 Properties at higher pressures . . . 197
4.2.3.3 Mie-Grüneisen parameters extraction . . . 201
4.2.3.3.1 S parameter determination . . . 202
4.2.3.3.2 Grüneisen parameter determination . . . 204
4.2.3.3.3 Speed of the sound determination . . . 204
4.3 Conclusion on the acrylate behaviour under laser shock conditions . . . 205

Conclusion **207**

Appendixes **217**

A Ballard's model **219**

B Impedance mismatch and shockwave theory **221**

B.1 State equations . . . 221
B.1.1 $P_x < P_H$ Elastic regime . . . 222
B.1.2 $P_x > P_H$ Plastic regime . . . 223
B.2 Shockwave propagation . . . 223
B.2.1 Front shock stiffening . . . 223
B.2.2 Release spreading . . . 224
B.3 Hugoniot curve . . . 225
B.4 Shock polar . . . 226
B.4.1 Shock polar properties . . . 227
B.4.1.1 Isentropic approximation . . . 227
B.4.1.2 Unique polar approximation . . . 228
B.4.1.3 Unique adiabatic approximation . . . 228
B.5 Shock transfer between two media A and B . . . 229
B.5.1 General case: A and B are solids . . . 229
B.5.2 B is a gas or void . . . 230
B.5.3 Example of a shockwave propagating between two media . . . 231

C Fatigue testing principle **235**
C.1 Fatigue testing methods . . . 236

D Paris' law **239**

E Mullins and Payne effects **241**
E.1 Mullins effect . . . 241
E.2 Payne effect . . . 242

References **256**

Introduction

Context

The context of this PhD thesis is intertwined with a global problematic concerning the service life of aircrafts, be them new or already in service. The problematic of cyclic fatigue affecting metallic parts, especially the openwork ones, is a major challenge in the long-term goal of increasing the service life of aircrafts. Replacing such pieces instead of trying to make them last longer is not a viable alternative, considering the price and sustainability of the operation. In some case, that approach would mean replacing the entire aircraft which is obviously too expensive. An alternative to this option is to reinforce the mechanical behaviour of the material subject to high cyclic loading, stress concentration or crack initiation. In this context laser shock peening or laser peening (LSP) is a solution of choice. Although the process is really close to classical peening (or shot-blasting) using metallic or ceramic balls to hit the matter to be treated, LSP offers many advantages. First of all, the process is non contact, allowing treatment in claustrated area that are normally difficult to access. Moreover the compressive residual stresses imparted in the work-piece by the process are higher and applied more in depth in the material than what can be achieved with classical peening. Broadly speaking, the fatigue properties can increase by up to 400% after the LSP treatment.

The laser shock peening process consists in focusing a laser pulse of high intensity (in the GW/cm^2 range) at the surface of the piece to be treated. When the pulse hit the target, a plasma is created and then expands in the air. This phenomenon leads to the creation of a shockwave that propagates in the target and plastifies it, thus inducing the creation of compressive residual stresses, themselves responsible of the increased fatigue behaviour properties.

To optimise the process a transparent later to the laser pulse is placed on top of the target's surface. This layer prevents the plasma expansion in the air by confining it. This method allows at

equivalent laser energies to produce pressures up to six time higher than in direct regime (i.e. no confinement) while also maintaining this pressure for two times longer, in the order of two time the pulse duration. This configuration presents one major limitation; at laser intensities higher than a threshold dependent on the confining material. a breakdown plasma is created at the surface or inside of the confining material and starts to absorb the incident laser energy, thus limiting the maximum pressure produced as well as it time of application with this configuration. Today, two main laser peening configuration are used in the industry

- The "classical" LSP that uses high laser energies (> to some joules) with pulse duration in the order of 10 ns, laser spot diameters of multiple mm, a relatively low overlap between laser shots (as low as 30%) and a low pulse frequency. With this configuration a thermal coating is also used in order to avoid thermal effects at the surface of the treated piece which induce tensile residual stresses as well as oxidation of the surface. This type of configuration is mainly used in the aeronautic industry for the reinforcement of the fatigue and crack propagation behaviour.
- The second configuration is a method developped by Yuji Sano in 1997 for the treatment of immersed nuclear tanks for Toshiba. This method uses low laser energies (100's of mJ), pulse durations in the 5 ns range, laser spot diameters typically inferior to 1 mm and a high overlap ratio between shots. This allows for the use of laser with a high pulse frequency up to 100's of Hz. A major advantage of this configuration lies in the absence of the necessity to use a thermal coating to protect the surface treated. Even though the thermal effects are detrimental to the treatment, the compressive residual stresses imparted in the materials treated are high enough to guaranty an increase of the final fatigue behaviour and crack propagation resistance.

In the aeronautic industry, the first configuration is currently exclusively used, coupled with the use of water as a confinement. However the use of such a confinement limits the use of the process. As of now, it is impossible to treat some specific claustrated surfaces such as interior of wings due to the presence of kerosene in this place, small bore holes because of the impossibility to obtain a good water flow in such a small space or some specific parts of cockpits were the treatment would be used in maintenance and the presence of on-board electronic would prevent the use of water.

In these conditions the development of an alternative confinement for the laser shock peening application to be able to treat these specific application is necessary. Following preliminary results

from Damien Courapied PhD's work, the use of an adhesive elastomer already showed promising results by producing important pressure when used as a confinement for the application. In these conditions, polymers appears a good candidates to be used as confining medium for the laser shock peening application. Moreover this type of material can be tuned by playing on their chemistry and thus be adapted to a particular use.

It is in this context that the FORGE project, in which this PhD work takes place, was created. It gathers the PIMM laboratory, CNRS, CEA as well as industrial actors (Thales, Rescoll, Imagine Optics and Airbus) in order to develop the laser shock peening method to be able to use it with a solid confinement for aircraft still in construction and the ones already in-service.

Objectives

The objectives of this PhD work are multiple. First a finer comprehension of the laser/matter interaction during the laser shock process while using polymer confinement is necessary. An understanding of the other processes taking place at the different interfaces (air/confinement and target/confinement) during the laser shots is also necessary. A study of the water confinement is also realised along the study of polymer confinements in order to have a reference point of comparison that are also compared with the already existing literature on the subject.

One of the research axis is to compare the results obtained while using different types of confinements to observe the underlying effects taking place during the process. Another part of the work studies the damaging mechanisms, thermal and mechanical, at work in the polymers used as confinement during the interaction as the literature on these phenomena is not comprehensive with the laser energies and materials of interest aimed.

The laser parameters aimed for the final application by Airbus are laser energies of some GW/cm^2 with a pulse duration of some ns and a laser spot diameter of less than 1 mm. The wavelengths used were first 532 nm for the characterization at the laboratory to then transition to a 1064 nm laser developed by Thales and with an overall parametric closer to the end use. The change of final wavelength is important for the industrial use if the laser has to be transported by optic fiber in order to have access to the concerned areas. Indeed, the use of a 1064 nm laser avoids non-linear effects in the optic fiber that would prevent its use. The rest of the parameters, closer to the Toshiba method

than the classical aeronautic configuration allows to reduce the thermal effects and be dispensed of the use a thermal coating. If the comprehension of the laser/matter interaction in such a configuration is understood, the design and properties of the polymer can be tuned to fit the end use better and can even be adapted depending on the material to be treated by LSP and/or the laser used for said treatment.

This manuscript presents the work realised during three years to find, characterize and study a potential alternative to the water confined regime by using polymers instead for the laser shock peening application in an industrial setting. The first chapter will describe the laser shock peening process as well as the phenomena involved in it while also presenting in a second part the polymer mechanical and chemical characteristics needed for the final application.

The second chapter presents the materials and methods used for the different studies realised during this PhD work. From the choice of materials used as targets to the tools chosen for the confinements choice, characterization and evaluation when used for the LSP process.

The third chapter focuses in a first part on the choice of a confinement for the application while a second part study the effect of different parameters on the process capability. A last section describes the residual stresses approach used and the results obtained with it.

The fourth chapter describes all the results obtained from experiments aiming at better understanding the mechanical behaviour of the chosen materials for confinement under laser shock conditions (i.e. high strain rate and pressure).

A conclusion on the realised work closes the manuscript and is accompanied with perspectives giving an insight on future possible works that could be done to further the control and efficiency of the LSP process with polymer confinements.

Contexte FR

Le contexte de cette thèse s'inscrit dans une problématique plus globale qui concerne la durée de vie des aéronefs, qu'ils soient neufs ou en service. La fatigue cyclique qui touche des pièces métalliques, souvent ajourées dans le but de les alléger est un problème important, le remplacement de ces pièces étant très onéreux voire impossible dans certains cas. Une des alternatives apparaissant logiquement est le renforcement du comportement de résistance en fatigue. Dans ce contexte, le choc laser ou LSP pour Laser Shock Peening, aussi appelé grenaillage laser apparaît comme une solution de choix. En effet, le LSP bien que proche du grenaillage mécanique, présente de nombreux avantages : Il s'agit d'un procédé sans contact, ce qui facilite sa mise en place dans des environnements exigus ou difficiles d'accès. Les contraintes résiduelles de compression créées par le traitement sont plus fortes et sont appliquées plus profondément par rapport au grenaillage classique. De manière générale, les propriétés de résistance à la fatigue peuvent augmenter jusqu'à 400% à l'issue du traitement.

Le procédé LSP consiste à focaliser un rayonnement laser de haute intensité (de l'ordre de quelques GW/cm^2) à la surface d'une pièce à traiter. Au contact de la pièce, un plasma se forme puis se détend. Cette détente du plasma engendre la formation d'une onde de choc qui se propage dans la cible et la plastifie, entraînant la création de contraintes résiduelles de compression, étant elles-mêmes responsables des propriétés en fatigue accrues.

Afin d'optimiser le procédé, une couche transparente au rayonnement laser est apposée à la surface de la cible afin de former un contact intime avec cette dernière. Cette couche permet d'empêcher l'expansion du plasma dans l'air en le confinant. Cette méthode permet, à énergie égale, de produire des pressions jusqu'à six fois plus élevées qu'en régime direct (i.e. sans couche de confinement) tout en maintenant la pression appliquée pendant une durée deux fois plus élevée, de l'ordre de deux fois la durée d'impulsion laser. Cette configuration présente cependant une limitation importante. Au delà d'une intensité seuil, un plasma de claquage se crée à la surface ou à l'intérieur du matériau de confinement. Ce plasma a pour effet d'absorber une partie de l'énergie laser incidente et par conséquent de réduire l'énergie effective apportée en surface de la pièce à traiter, diminuant de fait les pressions produites ainsi que leurs durées d'application. Aujourd'hui deux configurations de LSP confiné industrielles existent : Le LSP "classique" pour lequel les énergies laser sont élevées (de l'ordre de quelques J), avec des durées d'impulsion de l'ordre de 10 ns, des diamètres de tâche laser de plusieurs

mm, des taux de recouvrement tir à tir assez faibles et une fréquence d'impulsion faible. Avec ces paramètres, un revêtement thermoprotecteur est aussi utilisé afin d'éliminer les effets thermiques induits en surface par le rayonnement laser et qui engendrent des contraintes résiduelles de traction s'opposant aux effets recherchés. Cette configuration est principalement utilisée dans le domaine de l'aéronautique pour le renforcement du comportement en fatigue et la résistance à la propagation des fissures des pièces traitées. La deuxième configuration est une méthode de traitement mise au point par Sano en 1997 pour le traitement de cuves immergées dans le domaine du nucléaire par la société Toshiba. Cette confiuration appelée méthode Toshiba utilise des énergies faibles (quelques centaines de mJ), des durées d'impulsions de l'ordre de 5 ns, des diamètres de tâche laser inférieurs au mm et un taux de recouvrement tir à tir élevé, le tout avec une fréquence d'impulsion de plusieurs dizaines voire centaines de Hz. Aucun revêtement thermoprotecteur n'est utilisé ce qui pose la question des potentiels effets thermiques en surface de la pièce traitée. Malgré ces effets potentiellement délétères les contraintes résiduelles de compressions induites dans le matériaux sont suffisantes pour assurer une amélioration du comportement en fatigue ainsi que de la résistance à la propagation des fissures des pièces traités. Dans le domaine aéronautique, c'est la première configuration qui est actuellement exclusivement utilisée en régime confiné par eau. Cependant l'utilisation d'un tel confinement amène des contraintes. Ainsi, il est impossible de traiter les surfaces claustrées telles que l'intérieur d'ailes d'avion ou encore des alésages de petites dimensions dans lesquels l'écoulement de l'eau ne peut être correctement contrôlé, rendant impossible la mise en place du procédé. L'autre limitation du traitement par le confinement eau réside dans l'impossibilité de son utilisation sur des surfaces proches d'équipements électroniques comme on peut en trouver dans les cockpits par exemple. Dans ces conditions le développement d'une alternative au confinement par eau pour répondre à ces applications spécifiques est indispensable. A la suite d'études menées par D. Courapied en 2016, l'utilisation d'un élastomère adhésif acrylate comme confinement a permis de générer des niveaux de pression prometteurs. Les adhésifs polymères apparaissent donc comme étant des candidats potentiels pour ce type d'application du fait de leurs nombreux avantages. En effet, leur flexibilité leur permet de s'adapter à différentes formes complexes. De plus, les nombreuses possibilités de formulation laissent entrevoir des possibilités d'adaptation du polymère en fonction de l'application visée ou encore du matériau à traiter pour s'orienter vers un matériau "sur mesure" en fonction de la situation. C'est dans ce cadre que le projet FORGE, dont ce travail de thèse fait partie, à été mis en place. Il regroupe

le PIMM, le CNRS, le CEA ainsi que des acteurs industriels tels que Thalès, Rescoll, Imagine Optic et Airbus afin de développer une méthode de traitement par Laser Shock Peening en utilisant un confinement solide pour traiter des pièces pour l'instant inaccessibles avec la configuration actuelle, que ce soit en pré-traitement ou en entretien sur les appareils déjà en service.

Objectifs FR

Les objectifs de ce travail de thèse sont multiples. Tout d'abord obtenir une compréhension plus fine de l'intéraction laser-matière durant le procédé de laser shock peening lors de l'utilisation d'un confinement polymère. Un travail sur les autres procédés prenant place aux différentes interfaces (air/polymère et polymère/cible) pendant le choc laser est aussi nécessaire. Une étude du confinement eau soit aussi être menée en parallèle afin d'avoir un point de comparaison de référence et des données comparables avec la littérature déjà existante sur le sujet.

Un des axes de recherche consiste à comparer les résultats obtenus en utilisant différents types de confinements polymères afin d'observer les effets sous-jacents prenant place au cours du procédé laser. Une autre partie du travail se concentre sur l'étude des mécanismes d'endommagement, à la fois thermiques et mécaniques qui prennent place dans le polymère de confinement au cours de l'intéraction. En effet, la littérature disponible sur ce sujet est inexistante dans la gamme des énergies atteinte par laser et sur les matériaux d'intérêt de cette étude.

Les paramètres laser visés pour l'application finale par Airbus sont des énergies laser de l'ordre de quelques GW/cm^2 avec une durée d'impulsion de quelques ns et un diamètre de tâche laser de moins de 1 mm. La longueur d'onde utilisée était dans un premier temps de 532 nm pour la caracterisation en laboratoire pour ensuite passer à un laser 1064 nm développé par Thales avec un set de paramètres correspondants à l'utilisation finale. Le changement de longueur d'onde est crucial dans le cadre d'une utilisation industrielle avec transport par fibre optique, l'utilisation d'un laser 1064 nm permettant d'éviter des effets non-linéaires dans la fibre qui servira à atteindre les zones difficiles d'accès. Le reste des paramètres est proche de ceux utilisés par la méthode Toshiba qui permet la réduction des effets thermiques et donc évite l'utilisation d'un revêtement thermo-protecteur.

Si la compréhension de l'intéraction laser-matière dans une telle configuration est bien comprise, le design des polymères de confinement pourra être adapté en faisant varier leur propriétés en fonction

de l'utilisation choisie.

Ce manuscrit présente le travail réalisé au cours des trois années de ce doctorat qui consiste à trouver , caractériser et étudier un polymère pouvant être un candidat potentiel pour être utilisé comme alternative au régime confiné eau de l'application laser shock peening en environnement industriel. Le premier chapitre présente le procédé de laser shock peening ainsi que les principaux phénomènes y prenant place alors qu'une deuxième partie présente les propriétés mécaniques et thermiques des polymères attendues pour une utilisation en tant que confinement.

Le deuxième chapitre présente les matériaux et méthodes utilisés pour les différentes expériences réalisées durant ce travail de thèse. Cette description part du choix des matériaux utilisés comme cible et confinement tout en décrivant aussi les techniques utilisées pour les caractériser au cours du procédé LSP.

Le troisième chapitre se concentre dans une première partie sur le choix d'un confinement remplissant les critères nécessaires à son utilisation en tant que confinement pendant qu'une seconde partie étudie les effets des différents paramètres de ce confinement sur la pression produite par choc laser. Une dernière partie présente des résultats de mesures de contraintes résiduelles réalisées en utilisant le confinement polymère sélectionné au préalable.

Le quatrième chapitre décrit tous les résultats obtenus d'expériences visant à obtenir une meilleure compréhension du comportement mécanique des matériaux polymères choisis sous des conditions de chargement trouvées lors d'un choc laser (haute pression et vitesse de déformation).

Une conclusion sur le travail réalisé vient clore le manuscrit et est accompagnée de perspectives sur les expériences futures possibles à réaliser afin de pouvoir mieux comprendre les phénomènes mis en jeu lors du procédé de LSP avec en régime de confinement polymère.

Bibliography

1 | Bibliography

Content

1.1 A brief laser shock peening history . . . 33
1.2 Laser shock peening process . . . 35
1.2.1 Direct regime . . . 36
1.2.2 Confined regime . . . 36
1.2.3 Breakdown . . . 38
1.2.3.1 Influence on transmitted pulse duration . . . 39
1.2.3.2 Triggering phenomena . . . 40
1.2.3.3 Pulse length influence . . . 42
1.2.4 Effects induced by the treatment . . . 43
1.2.4.1 General mechanical effects . . . 43
1.2.4.1.1 Depth of the plastified area . . . 45
1.2.4.1.2 Effect of laser shock on hardness . . . 46
1.2.4.2 General thermal effects . . . 47
1.2.4.3 Thermoprotective layer . . . 48
1.2.4.4 Residual stresses . . . 50
1.2.4.4.1 Treatment without thermal coating . . . 50
1.2.4.5 Roughness modification linked to LSP treatment . . . 52
1.2.5 Key process parameters . . . 54
1.2.5.1 Pulse profile and duration influence . . . 54
1.2.5.2 Wavelength influence . . . 55
1.3 Applications . . . 56
1.3.1 Fatigue life enhancement . . . 58
1.3.1.1 Fatigue life improvement induced by laser shock peening . . . 59
1.3.1.2 Crack propagation and initiation . . . 59
1.3.1.3 Fatigue crack growth . . . 60
1.3.1.4 Stress corrosion cracking resistance . . . 60
1.3.2 Other laser applications . . . 61
1.3.3 Laser peening compared to other peening strategies . . . 63
1.3.4 Industrialisation challenges with water confinement . . . 64
1.3.4.1 Parts to be treated . . . 65

1.3.5 Advantages of polymer confinement 66
1.4 Polymers as confinement 67
1.4.1 Laser interaction with polymer 68
1.4.1.1 Heating inclusion model 70
1.4.1.2 Bond breaking model 71
1.4.1.3 Coloured center model 71
1.4.2 Properties needed for a polymer confinement for LSP treatment 71
1.4.2.1 Crystalline properties 72
1.4.2.2 Bond strength 72
1.4.2.3 Polymer choice 72
1.4.3 Pressure Sensitive Adhesive description 73
1.4.3.1 Mechanisms of PSAs 75
1.4.3.2 Application requirements 76
1.4.4 Overview of polymers material properties 77
1.4.4.1 Viscoelasticity and viscoplasticity 77
1.4.4.1.1 Stress relaxation 79
1.4.4.1.2 Dynamic mechanical measurement 79
1.4.5 Non-linear viscoelastoplasticity 82
1.4.6 Elastomers under high stress rate 82
1.4.6.1 Dynamic glass transition 82
1.4.6.2 Pressure effect 83
1.4.6.3 Strain rate effect 84
1.4.7 Model to describe elasticity 86
1.4.8 Model to describe glassy polymers 87
1.5 Conclusion on the needed properties for the confinement 88

Introduction

This chapter presents the different elements that take place this project work. It is separated in two distinct parts, one pertaining to the laser aspect of the work while the other is focused on the polymer aspect of project.

The first part begins with a comprehensive laser shock peening history is presented in order to give the reader a sense of the process as a whole from where is started to the way it is used nowadays with its advantages and drawbacks. Thereafter, a detailed presentation and explanation of the laser shock peening process is given and opens to the effects induced by the process, be they beneficial or detrimental to the piece treated. Thus the different breakdown triggering phenomena as well as their effects on the laser shock peening process are detailed. The potential thermal effect are described followed by the residual stress induced by the treatment. After the description of the process as a whole, the key parameters of laser shock peening are also covered and linked to the specific needs of the project and the final aim targeted. The laser part is concluded with the challenges of the application described and the means that will be used to tackle them.

The second part, is focused on the polymer aspect of the project work. First, a presentation of the literature available on the interaction between polymers and laser is presented as well as the damaging mechanisms involved in such a type of interaction. Then, properties that a polymer needs to have in order to be a good candidate for the laser shock peening application are described. Thereafter, a potential class of polymers, the pressure sensitive adhesives are presented as good candidate to be used as confinement for the laser shock peening process. Their properties are then described as well as the general phenomena that take place in this type of materials. The chapter is continued with a description of the mechanical behaviour of such material under high strain rate and/or pressure, followed by a brief overview of the models available to represent these effects. The chapter is then closed with a conclusion on the needed properties for the confinement that will be chosen for the treatment of the work pieces involved in this project.

Historique du laser shock peening

Les premières découvertes ayant mené au développement du laser shock peening (LSP) moderne ont commencé dans les années 60 avec l'expansion des technologies de lasers pulsés [1]. L'étude de

l'interaction laser-matière avec différents matériaux a conduit à des mesures de pression sur les surfaces ablatées par impulsion laser avec des sondes piézoélectriques [2]. Une avancée majeure a été réalisée en 1970 quand Anderholm découvrit que la pression produite par un choc laser pouvait être grandement augmentée en confinant le plasma produit en plaçant un matériau diélectrique (dans ce cas un quartz), transparent au rayonnement laser, sur la cible [3]. Au début des années 70, des études ont commencé sur les effets du grenaillage laser appliqué sur des cibles métalliques à l'institut Battelle à Columbus en Ohio. Ces travaux ont montré une amélioration des propriétés mécaniques de la zone traitée par LSP [4]. Les études menées durant cette période étaient limitées par le faible nombre d'échantillons étudiés ainsi que par le manque de méthodes de caractérisation précises. Par la suite, le développement du procédé de grenaillage laser a ralenti aux USA par manque de source laser utilisable dans un cadre industriel. Dans le même temps, cette période correspond au début d'un certain nombre d'étude en France sur différents aspects du procédé de LSP : l'interaction confinée [5, 6, 7, 8], la caractérisation des ondes de choc [9], les effets mécaniques induits [10, 11, 12], les propriétés en fatigue [13, 14], l'écaillage [15, 16] ou encore la densification de poudre [17]. Pendant les années 90, de nouvelles sources laser ont été développé, accompagnées par des diagnostiques d'analyse des ondes de chocs plus précis [16, 18, 19]. Ces nouveaux outils ont lancé un renouveau dans la recherche associée au domaine du choc laser et ont permis le début de l'industrialisation du procédé au travers le traitement de pales [20]. Au même moment, le procédé était aussi développé pour son utilisation dans l'industrie nucléaire [21]. Cet intérêt de la part de l'industrie fut motivé par les avantages du grenaillage laser par rapport au grenaillage « classique » ; un matériau traité par LSP a une profondeur de zone affectée par le traitement plus grande qu'un matériau traité par grenaillage. Les contraintes résiduelles dans le matériau sont aussi plus fortes, conduisant à de meilleures propriétés de comportement en fatigue ou en résistance à la corrosion. En parallèle au développement industriel, de nouvelles études furent lancées, notamment en France pour étudier plus en détail les propriétés en fatigue [22], en résistance à la corrosion [23] et en propagation de fissures [24]. Cette période vit aussi le début de la recherche dans le domaine par la Chine par des chercheurs comme Zhang [25]. Dans les années suivantes, le nombre de brevets associés au procédé de grenaillage laser a augmenté de manière importante avec l'industrialisation rapide de la technique (fig. 1.1a). A partir de cette période, l'utilisation du LSP en industrie a commencé à décoller avec la création d'entreprises comme LSP Technologies en 1995 qui a commencé à offrir des solutions de LSP à l'échelle industrielle ou encore la Metal Improvement

Company, créée en 1945 mais qui commence à proposer des traitements par grenaillage laser en 2003. Grâce à ces acteurs le procédé se démocratise dans le monde industriel mais aussi dans celui de la recherche afin de mieux comprendre les phénomènes mis en jeu lors de l'interaction laser-matière. Depuis le début des années 2000, la simulation du procédé couplée à des expériences est aussi devenue un enjeu majeur dans le but de produire des outils précis permettant l'optimisation des différents paramètres du procédé et d'accélérer le développement du LSP tout en réduisant son coût.

Aujourd'hui, le LSP est de plus en plus utilisé à l'échelle industrielle bien qu'il soit réservé à des applications spécifiques sur des pièces critiques dans le but de renforcer leur durée de vie. D'autres domaines évoluent rapidement vers des applications industrielles comme le traitement de pièces produites par fabrication additive laser. Le traitement par LSP de ces pièces permet de corriger leur forme grâce au grand contrôle apporté par la maîtrise des différents paramètres laser comparé au grenaillage classique [27, 28]. Le grenaillage laser, malgré son coût de mise en œuvre plus élevé à désormais montré son efficacité pour le renforcement des propriétés mécaniques de pièces critiques.

Lors de la mise en œuvre du procédé, le matériau de confinement classiquement utilisé est l'eau pour sa transparence, et sa facilité à créer un contact efficace avec la cible à traiter. Un des obstacles à l'extension de l'utilisation du LSP est l'impossibilité d'utiliser dans l'eau dans le cas du traitement de certaines pièces dans des lieux avec des atmosphères réactives, des zone dans lesquelles on peut trouver de l'électronique embarqué ou encore toutes les zones ou les projections d'eau ne peuvent être nettoyées avec certitude dans le cas du traitement de structure déjà assemblées. Une solution serait de remplacer l'eau de confinement par un matériau solide, comme déjà montré dans les travaux de Anderholm avec l'utilisation de quartz comme matériau confineur [3]. Cependant, l'utilisation de verres rigides pour le traitement de pièces de géométrie complexe n'est pas possible, il faut donc trouver un matériau flexible s'adaptant à ces formes particulières. Un polymère flexible apparait comme un candidat prometteur pour de telles applications. Des polymères, sous forme rigides ont déjà été étudié dans la littérature par Hong et al. [29]. Dans ce travail les auteurs ont évalué l'influence du matériau de confinement sur l'impédance réduite du système et sur la pression finale produite par les chocs laser sans étudier le potentiel de ces matériaux pour éventuellement remplacer l'eau en tant que confinement pour des applications à l'échelle industrielle. Une autre approche développée pour le traitement par grenaillage laser consiste à utiliser une paramétrie différente développée par Y. Sano et al. [30, 21] en utilisant des tâches laser plus petites couplées à un taux de répétition élevé qui permet de s'affranchir

de l'utilisation d'un revêtement thermo-protecteur tout en évitant les effets thermiques de surface induits par le plasma lors du traitement.

Si toutes les étapes du procédé, du dimensionnement jusqu'au traitement laser, sont correctement maitrisées, le LSP en régime confiné par eau ou par polymère pourra devenir de plus en plus usité, entre autres sur des pièces critiques légères nécessitant une durée de vie élevée.

1.1 A brief laser shock peening history

The first discoveries leading to the development of modern-day laser shock peening (LSP) started in the 1960s with the spread of pulsed laser technology [1]. The study of laser interaction with different materials led to pressure measurements on a surface ablated by a pulsed laser with piezoelectric momentum transducer [2]. A major breakthrough occurred in 1970 when Anderholm discovered that the pressure delivered through a laser shock could be greatly improved by confining the plasma produced by placing a dielectric (in this case a quartz overlay), transparent to the laser beam, on the target [3]. At the beginning of the 1970s, studies on the effect of LSP applied on metallic targets began at the Battelle institute in Columbus, Ohio and demonstrated an improvement of mechanical properties in the treated area [4]. The studies from that period were still limited due to the low numbers of sample studied and the lack of fitting and accurate characterization methods.

After that, the development of the subject was slowed down in the United State since no laser sources allowed for an industrial application yet. On the other hand this period corresponded to the beginning of a number of studies in France on different aspects of the process: confined interaction [5, 6, 7, 8], shockwave characterization [9], mechanical effects induced [10, 11, 12], fatigue properties enhancement [13, 14], flaking [15, 16] or powder densification [17].

During the 90's new laser sources were developed as well as more accurate characterization diagnostics for shockwaves [16, 18, 19]. These new tools gave a second breath to the research in the domain and started the industrialisation of the process in the aerospace industry with fan blade treatment [20] while the process was also developed for applications in the nuclear industry [21]. This industrial interest steams from the advantage of laser peening compared to conventional peening. A material treated by LSP has a much larger affected depth than a material treated by conventional peening as well as higher compressive residual stresses induced, leading to better fatigue and corrosion resistance properties.

In parallel of the industrial development, new studies began in France among others on fatigue properties [22], corrosion [23] and crack propagation [24]. This period also saw the start of research in China on the subject by Zhang [25].

In the incoming years, and with the understanding that the process could be industrialised quickly, the number of patent started to drastically increase (fig. 1.1a).

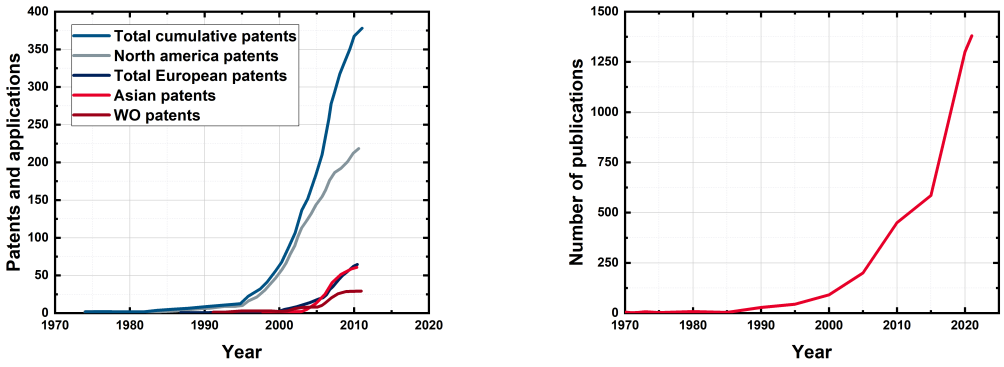

(a) (b)

Figure 1.1: (a) Growth of the number of patents associated with laser shock peening through the years (from [26]), (b) Growth of the number of publication associated with laser shock peening through the years.

From this period, laser peening use started steadily rising with companies like LSP Technologies created in 1995 which began offering industrial laser peening solutions or the Metal Improvement Company, created in 1945 and that started proposing laser peening solutions in 2003. Thanks to that, the process became more popular in the industry while also being researched to understand the underlying phenomena occurring during the laser treatment. Since the beginning of the 2000's modelling is also coupled with the experiments in order to produce tools to ease the optimization of the different parameters of the process, further accelerating industrial implementation.

Today, LSP at an industrial scale, although chosen for specific applications, is more and more applied in the aerospace and automotive industry for the treatment of sensitive areas on certain parts to increase their lifetime. Other fields are rapidly evolving towards industrial applications such as the treatment of parts produced by additive manufacturing. LSP treatment of these types of materials allows more shaping and forming possibilities as well as shape correction treatment due to the highly controlled nature of the process compared to conventional shot peening [27, 28]. Coupled with the deeper levels of residual stress produced, it has shown to be highly cost effective despite its higher operating cost compared to conventional shot peening.

Water is the usual confining material because it is cheap, transparent to the laser, and ensures contact with surfaces. One of the obstacles to extending LSP's applications is the impossibility of using water in a reactive atmosphere or near electronic devices as well as areas where water can be retained if

not collected properly in the case of treatment of already assembled structures. A solution to this issue should be a solid material, as demonstrated by the pioneering work on laser shock [3]. However, the use of rigid glasses for the treatment of pieces presenting complex geometries such as the ones encountered in the aerospace industry is impossible. In contrast, a soft polymer confinement, with its adaptability, shaping possibilities, and wide range of formulations and properties, is an ideal candidate for this type of need. Laser shock peening with polymer confinement has been studied only by Hong et al. [29]. The authors evaluated only the influence of the confining medium used on mechanical impedance, without carrying out a complete investigation of the performances exhibited by these materials. Consequently, a large field is open to carry out studies on potential new confinement, from their capacity to treat a material to there implementation to maybe replace water in some applications.

Another approach to optimize the laser shock peening process lies in the use of a different parametric. As shown in the Work of Y. Sano et al. [30, 21] the use of smaller laser spot coupled with a high shot repetition rate allow to avoid the use of a thermal coating usually placed on top of the surface to treat to remove the thermal effects induced by the laser treatment and can lead to new development in the way LSP will be applied in the future.

If every step of the process is correctly mastered, LSP could, with water and/or polymer confinement, become more and more used, especially on light critical structures with high service life by coupling optimized dimensioning with accurate modelling of the parts from their machining to the LSP treatment they will be treated with.

1.2 Laser shock peening process

Laser Shock Peening consists of focusing a pulsed laser (usually a ns pulse, GW/cm^2 energy) at the surface of a material. The incident energy is absorbed by a thin layer of the material up to its vaporisation and ionisation to form a plasma. The release of the plasma induces, by kickback effect, a pressure which is applied on the surface of the treated material. The stress created propagates through the material as a shockwave which modifies the matter properties while another shockwave is propagated in the opposite direction through the air. This configuration is generally used in laboratory setting for the study. A recap of the different effects taking place during the process depending on the use or not of a thermal coating is given in figure 1.2.

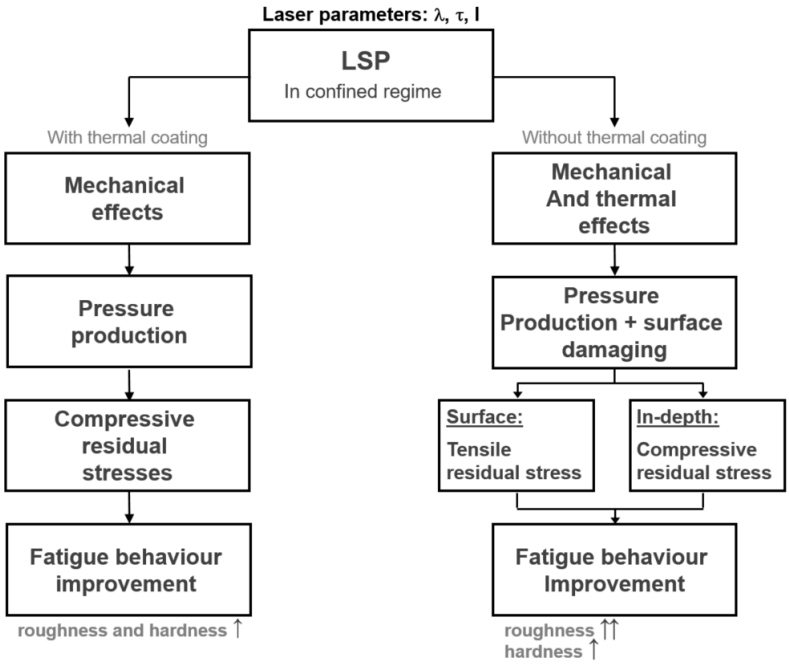

Figure 1.2: Different effect induced by the laser shock peening process when used with or without a thermal coating and the different physical parameters involved.

1.2.1 Direct regime

If the interaction occurs directly at the surface of the material, the plasma created is released in vacuum or void and the pressure induced will be low and applied for a time equivalent to the length of the laser pulse (< 1 GPa) (fig. 1.3a). This configuration is mainly used in lab setting for the study of the laser-matter interaction or pressure produced in large facilities [31, 32].

1.2.2 Confined regime

The confined regime consists of applying a transparent overlay, a dielectric material (water, quartz, polymer), on top of the surface to be treated. Under this configuration, the plasma generates at the interface dielectric/target and its expansion is hindered by the confinement. Since the plasma is contained in a smaller volume, its heating through the incident laser energy from the pulse is favoured compared to the direct regime. As a result, the pressure produced will be higher (6 to 10 times) and its time of application will be approximately two times longer than the laser pulse duration (fig. 1.3b).

The higher pressures produced induce higher residual stresses but also allow to treat materials

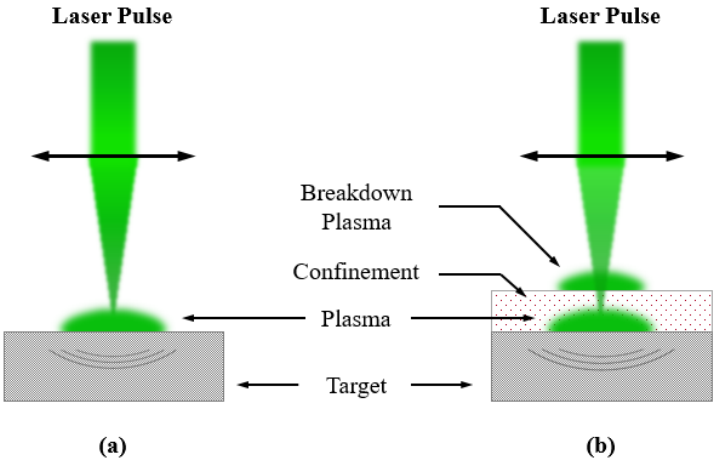

Figure 1.3: Laser Shock Peening principle, (a) direct regime and (b) confined regime

with higher elastic limits and thus gives a broader range of possibility to the application of the LSP treatment.

The phenomena at work during confined regime laser shock were studied by some such as Anderholm [3], Fournier [5], Devaux [7] and Berthe [33] or modelled by others like Fabbro [6] or Sollier [34] in order to calculate the pressures induced by a laser shock depending on the laser intensity used. An important parameter to characterize the laser-matter interaction is the laser energy absorption. It is influenced by other parameters such as the laser wavelength, the pulse duration and the laser intensity. The studies cited above brought up three main steps to describe the pressure production during the laser shock process:

- During the laser pulse, the incident energy is completely deposited at the interface dielectric/target. If the absorbed energy is sufficient, the target starts to vaporize to create a plasma. The pressure generated induces a shockwave which propagates both in the confinement and in the shocked material. These two shockwaves D_1 and D_2 put into motion the matter behind them at the material speeds u_1 and u_2 (see figure 1.4. Consequently, the interface between the two media simultaneously starts to separate with a growing width L(t):

$$L(t)(\mu m) = 2.10^{-4}\frac{P(t)(GPa)\tau(s)}{Z(g.cm^{-2}.s^{-1})} \tag{1.1}$$

  With $P(t)$ the pressure depending on the time, τ the pulse duration and Z the reduced impedance of the system ($Z = (1/Z_1) + (1/Z_2)$).

- After the laser pulse the plasma starts to adiabatically cool down. At this point the thermal exchange with the surrounding materials are neglected. As a result, the pressure slowly decreases while following the cool down trend.

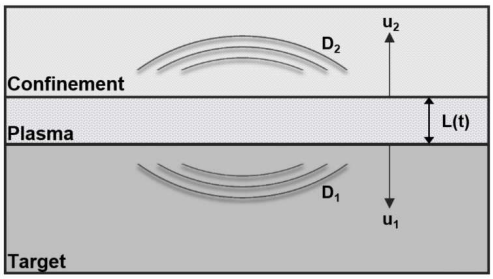

Figure 1.4: Geometry for the confined laser shock scenario.

In every step the gas is considered perfect and the heat exchange with cold materials are neglected. The first step is more detailed in Fabbro's work [6]. It shows that the laser absorption is higher in confined regime than in the direct one. Figure 1.5 demonstrates that the incident laser absorption is not linear depending on the laser intensity. At low intensities (<1 GW/cm²) the reflectivity is close to the normal reflectivity of the cold target. As the intensity increases, the reflectivity decreases as it becomes governed by an inverse bremsstrahlung phenomenon. This inflexion is a witness of the initiation of the confined plasma. When the power density reach a threshold (I>10 GW/cm²) the $R\%$ becomes constant which show the apparition of a breakdown plasma.

1.2.3 Breakdown

Although the confined regime is the one currently used for laser peening treatment, this configuration have some drawbacks. Mainly the potential creation of a breakdown plasma at the surface of the confinement at high energies on top of the "normal" plasma. This breakdown plasma can absorb a part of the incident laser pulse, thus reducing the pressure produced by the treatment and also shortening the length of the pressure application. Details on this phenomenon can be found in Berthe work [35] (see figure 1.6):

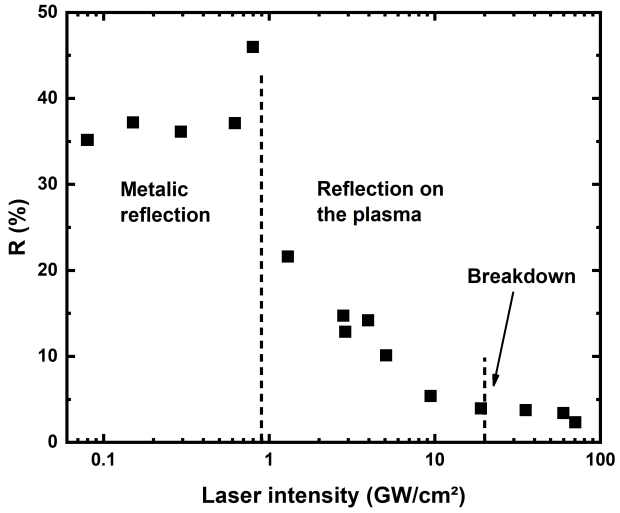

Figure 1.5: Reflectivity depending on the laser intensity for an aluminium target, water confinement, shocked with a 3 ns Gaussian pulse with a 1064 nm lase (from [7])

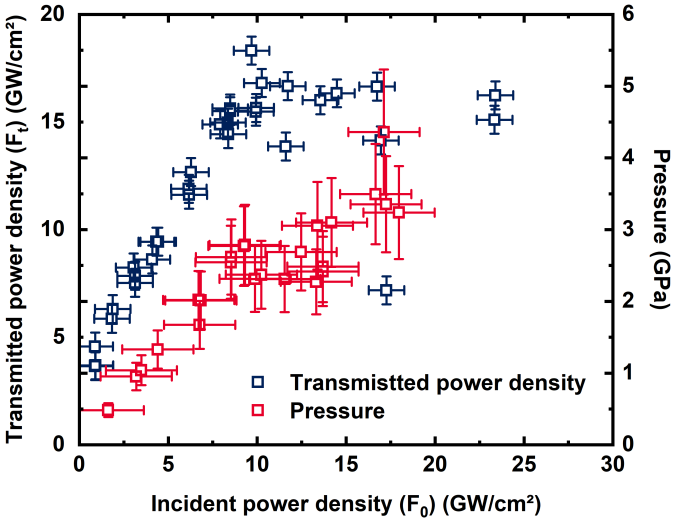

Figure 1.6: Peak pressure measurements from reference [36], and transmitted power density F_t as a function of incident power density F_0 (from [35]) for a 1064 nm laser, 25-30 ns laser pulse duration at full width at half maximum, spot diameter = 3 mm.

1.2.3.1 Influence on transmitted pulse duration

A way to characterise the apparition of a breakdown plasma is by measuring the Full Width Half Maximum (FWHM) of the transmitted laser pulse (Figure 1.7). The breakdown plasma initiation

induces a shortening of the FWHM. Depending on the laser intensity the breakdown plasma can appear before or after the peak pressure. That means that at laser intensities a little bit higher than the breakdown threshold, the maximum of the laser pulse pressure is reached but the pulse duration is shortened (figure 1.7.2). At higher power densities the breakdown plasma is formed before the maximum pressure of the shot is attained causing both the pressure and pulse duration to decline (figure 1.7.3) [37].

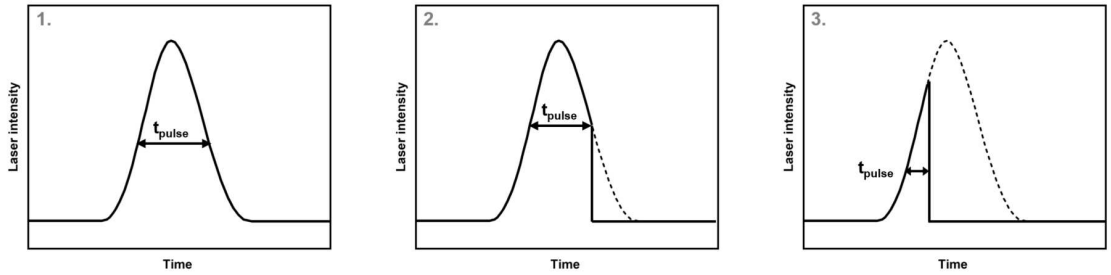

Figure 1.7: Breakdown plasma initiation depending on the laser intensity - influence on the transmitted pulse. (1.) Normal pulse, (2.) Transmitted pulse at a laser intensity a little higher than the breakdown threshold and (3.) Transmitted pulse at a laser intensity even higher than (2.).

1.2.3.2 Triggering phenomena

Two main phenomena govern the breakdown plasma initiation: namely the multiphotoionisation and electronic avalanche processes.

- **Multiphotoionisation:** One of the breakdown inducing phenomenon is the multiphotoionisation (MPI) that appears during laser irradiations of the confinement. It is dependent on parameters such as the wavelength, the pulse duration or the intensity. A breakdown plasma is triggered when the electronic density goes higher than the energy threshold of the atoms illuminated. In the case of laser shock, it takes the form of a plasma created at the surface of the confinement used an absorbs the incident laser energy, thus reducing the overall efficacy of the process. The electronic density threshold which induces the breakdown plasma is called the critical density n_c. The phenomenon of photoionisation consists in bringing energy is the form of photons to a surface. If the photon energy is higher than the ionization threshold, the atom will be ionized.

$$k(h\nu) \rightarrow e^- + A^+ \tag{1.2}$$

In the case of multiphotoionisation, multiple photons with an energy lower than the ionization threshold combine their energy in order to reach the sufficient energy to ionizes the atom. The triggering of the phenomenon is dependent on the energy threshold compared to the photons energy (i.e. number of combined photons energy in order to reach the threshold). Experiments showed that MPI is favoured by lower wavelengths whereas the pulse duration has no significant effect on the threshold even though is slightly decreases with long pulses. Overall the process only needs 3 to 4 photons to be triggered making it hard to avoid during a typical laser shot.

- **Electronic avalanche:** The second phenomenon taking place in the breakdown plasma formation is the electronic avalanche. If the atoms ionized by the laser pulse have sufficient energy, they can ionize surrounding atoms by collision through the inverse bremmstrahlung process. At each collision a new electron is produced, which leads to an exponential growth of the electron number until the critical density n_c is reached. The phenomenon is described with the following equation:

$$e^- + h\nu + A \rightarrow 2\, e^- + A^+ \tag{1.3}$$

For this process to take place, seed electrons are needed in the area seeing the laser shock. The energy needed to reach the ionization threshold is increased by the use of short pulses and shorter wavelengths. Generally, during a laser interaction the multiphotoionisation at low laser energies first takes place, and produces the seed electrons required for the electronic avalanche to take place and trigger the formation of a breakdown plasma. The seed electrons can also be present naturally in the material.

The laser parameter influence can be considered as follow: high laser intensity favours the start of both the phenomena while a short pulse duration reduce the probability of the two phenomena. The wavelength influence is dependent on the mechanism concerned. At shorter wavelengths the MPI process is favoured while the electronic avalanche is attenuated. During experiments at 532 nm, electronic avalanche will be the breakdown triggering factor while at 1064 nm it will be the MPI. [38, 39]. In the case of a polymer confinement, the laser shot repetition in the material is expected to induce the creation of thermal damaging that will act as seed electrons for the electronic avalanche phenomenon to be triggered. The MPI triggering will be more influenced by the transparency of the confinement (i.e its capacity to absorb the incident laser energy).

1.2.3.3 Pulse length influence

Measurements have been realised with different pulse duration to assess its effect on the pressure produced by laser shock. The results of different works with 1064 nm lasers on water confined aluminium targets is given in figure 1.8. The maximum pressure produced were measured for 600 ps, 10 and 25 ns Gaussian pulses and 3 ns square pulse [40, 39, 36]. For each configuration the results is divided in two parts:

- Under the breakdown threshold the pressure grows with the laser intensity following a $P \propto \sqrt{I}$ trend
- Once the breakdown threshold is reached, the pressure starts to saturate.

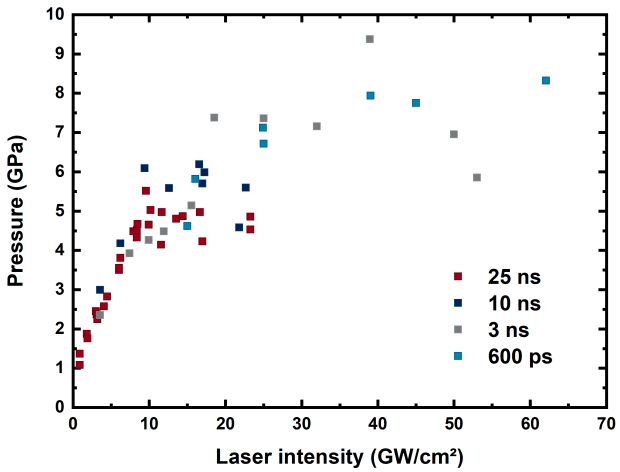

Figure 1.8: Maximum pressure depending on the laser intensity with a 1064 nm laser with pulse duration of 600 ps, 3 ns, 10 ns and 25 ns (Respectively from [40, 39, 36]).

The breakdown threshold is modified depending on the pulse duration used, it is decreasing with a shorter pulse duration. For the 10 ns and 25 ns pulse duration the pressure plateau starts around 10 GW/cm². For a 3 ns square pulse it appears only at 30 GW/cm² and at 60 GW/cm² with a 600 ps Gaussian pulse. The decrease in pulse duration is accompanied by a lower maximum pressure: the maximum pressure for 10 and 25 ns pulse is 5 to 6 GPa while for the 3 ns and 600 ps shots the maximum pressure reaches up to 7 - 8 GPa. One could think that decreasing further the pulse duration could be an easy way to reach higher pressures but studies by Schoen showed that with a

1053 nm, 10 ps pulse on copper targets with a glass confinement the pressure vary linearly with the laser intensity as opposed to what was observed with longer pulses before [41]. The plasma expansion in this type of configuration takes place in a distance so short the it is inferior to the rugosity of the glass confinement, causing the plasma to expand in air like in a direct regime.

The shape of the pulse can also plays a role. Devaux [7] demonstrated that using pulses with a sharp rising edge was beneficial by comparing laser shot with the same pulse duration but different pulse shapes. His experiments showed that compared to a regular Gaussian pulse showing a pressure saturation at 5 - 6 GW/cm², the use of a pulse with a sharp rising edge allowed to reach 10 GW/cm² before saturation.

These studies direct the choice of laser pulse parameters toward short pulse with sharp rising edge. However, for laser shock peening treatment the pulse duration also influence heavily the depth of plastification, so to say the depth of the compressive residual stresses. Thus a compromise is found with pulse durations between 3 to 10 ns.

1.2.4 Effects induced by the treatment

Laser Shock Peening treatment induces different effects in the treated material. First, an increase of the default density due to the plastic deformation of the matter. The plastification also creates a residual stress field cause by the heterogeneity of plastic deformation between the surface and the core of the material. Another factor is the sinking of the surface matter and the change in rugosity as well as the hardness. In the case of a treatment without using a thermoprotective layer, thermomechanical (stress relaxation, melting) and thermochemical (corrosion) effects can be observed.

1.2.4.1 General mechanical effects

The laser shock peening treatment is a process where the material treated undergoes a mechanical loading. The pressure loading induces an uniaxial compression of the targeted area while the planes parallel to the surface in the surrounding matter are put under tensile loading. The plasticised matter pushes the neighbouring material (fig. 1.9 (a)) while the still elastic matter responds by compressing the plasticised area, thus inducing compressive residual stresses (fig. 1.9b).

In order to further develop laser shock peening treatment and to optimize it, Ballard studied modelling of the mechanical effects of a fast impacts (high strain rate $\dot{\varepsilon}$) with an elasto-plastic model

which responds to Von-Mises yield criterion [42] in the case of a system of longitudinal plane waves with a purely uniaxial deformation [10]. The model shows the importance of the Hugoniot Elastic Limit (HEL) noted P_H of the material. The HEL draws the line between two shockwave propagation regimes:

- If the impact pressure is $< P_H$ the shockwave propagates has an elastic wave having no effect on the matter is goes through.
- If the impact pressure is $> P_H$ the shockwave propagates as a mix of elastic and plastic waves inducing plastic deformation and resulting residual stresses.

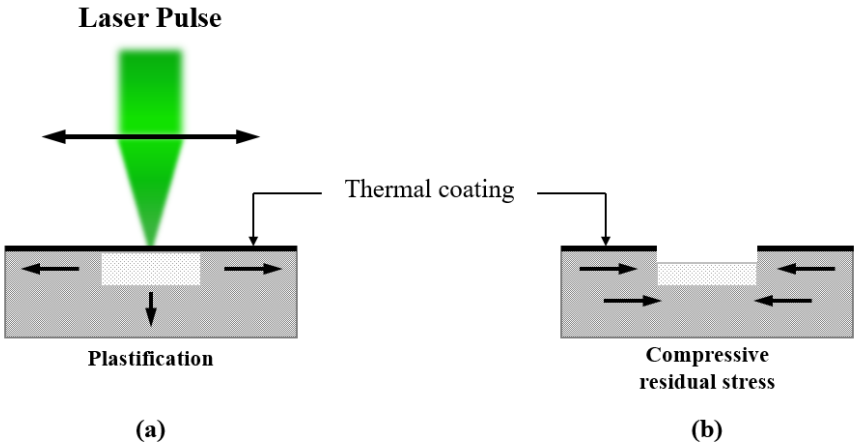

Figure 1.9: Mechanical effects induced by LSP treatment. (a) Plastification and (b) Compressive residual stress production

Ballard's work shows that the plastic deformation induced by the treatment begins at $P > P_H$ and saturates at pressure $> 2P_H$ (figure 1.11). The optimal treatment pressure is shown to be around 2 to $2.5P_H$ and exhibit the highest deformation at the surface of the material. This result shows that the optimal pressure treatment is only dependant on the mechanical properties of the target shocked. The model also allows for the calculation of the maximum induced residual stress and compares it with experimental results from Ballard [10] and Peyre [43]. The maximal amplitude for residual stresses is close to 0.6 to 0.7 σ_Y (or R_{ec}), the elastic limit for compressive load of the base material (fig. 1.10) ($R_{ec} \approx R_e$, the elastic limit under traction).

The results given are residual stresses located at the surface of the target where the pressure and deformation are maximal. It also does not cover cases of multiple shots and overlapping (shots

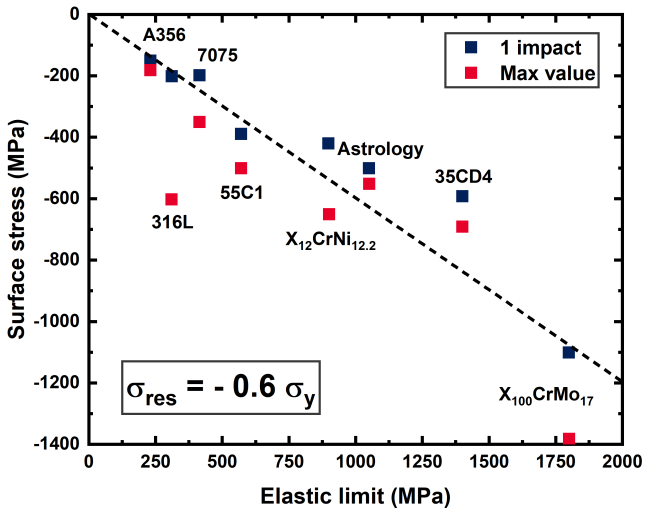

Figure 1.10: Maximum superficial residual stresses for mono-impact laser shots depending on the mechanical properties of the metal treated from [34]

location share an area depending on the spacing between shots) in which strain-hardening can play an important role depending on the metal. Some other results of Ballard's work are given in appendix A.

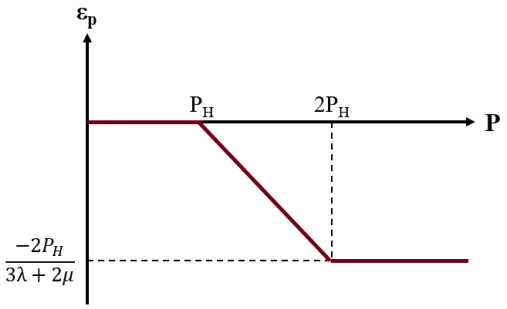

Figure 1.11: Evolution of the plastic deformation induced by laser peening in function of the impact pressure

1.2.4.1.1 Depth of the plastified area

It is possible to obtain the plastified depth by a laser shock thanks to Ballard's calculations for any shock conditions P and τ and for any material (P_H) for a nearly Gaussian pressure profile (between rectangular and triangular):

$$\mathrm{L_p} = \frac{\mathrm{c_p c_e}\tau}{\mathrm{c_e} - \mathrm{c_p}} \frac{P}{2P_H} \tag{1.4}$$

With L_p the plastified depth, c_p the plastic celerity of the wave, c_e the elastic celerity of the wave and P the pressure. The calculation is based on an elasto-plastic model with a Von-Mises criterion, put into motion by an uniaxial deformation composed of a system of longitudinal plane waves.

1.2.4.1.2 Effect of laser shock on hardness

The hardness of a material is a measurement of its resistance to localized plastic deformation induced either by mechanical indentation or abrasion. An increase of the hardness can be linked to an improvement of the elastic limit (σ_y) of the material. This change of elastic limit is important in the case of laser shock peening treatment with high overlap and/or multiple pass. Shots applied on an already plastified surface with a different tensile strength induce different effect. Because of that an appropriate law to represent the strain hardening of the material must be chosen if one wants to accurately model the laser shock peening process. The LSP process induces an increase of the treated material surface hardness caused by the increase in dislocation density (linear defect or irregularity in the crystal lattice [44]). The plastification induced by laser shock is also caused by the dislocations being generated at the shock front. There are three types of hardness measurements:

- Scratch hardness
- Rebound hardness
- Indentation hardness

In the case of laser shock peening, indentation measurements are used to evaluate the effect of the treatment generally with a Vickers hardness tester. For pure aluminium an improvement of 37.5% (from 40 to 55 HV) was obtained after a single pass of LSP without coating (1064 nm , 7 mm diameter spot, 20 J, 23 ns pulse, water confined) [45]. Comparison of the effect of a thermal coating were studied for 6061-T6 aluminium (1064 nm, 1.5 mm diameter spot, 2.5 J, 8 ns, water confined, black paint thermal coating) and are given in figure 1.12.

On surface, the hardness reaches higher values after laser treatment than the untreated alloy (respectively 120 and 121 for the LSPed ones and 110 for the untreated one). On the surface the

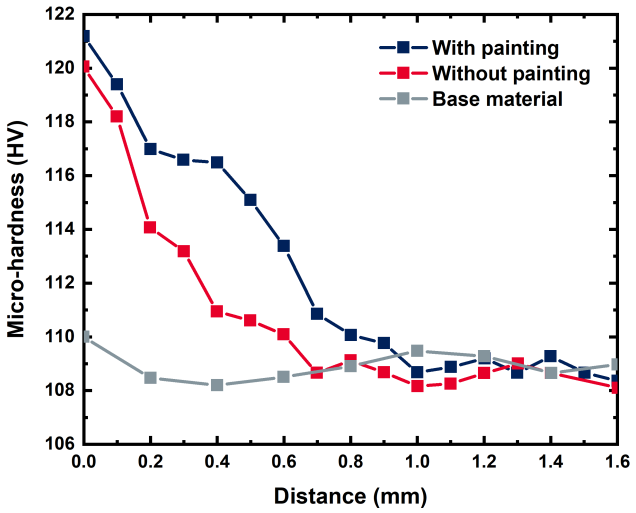

Figure 1.12: Micro-hardness profile on a 6061-T6 aluminium sample cross section treated with 1064 nm, 1.5 mm diameter spot, 2.5 J, 8 ns, water confined shots (From [46]).

thermal coating appears not to play a significant role but 200 μm under it induces a slightly higher hardness compared to the sample treated without thermal coating. After 1 mm depth the hardness of all the sample reach a plateau around 108 HV. The same trend of improvement is reported for other materials, for example aluminium alloys [47, 48], steels [49, 50] or titanium alloys [51].

1.2.4.2 General thermal effects

In the case of laser peening without thermoprotective coating, besides the mechanical aspect, the surface of the material is also affected by thermal effects. Multiple thermal effects are observed at the surface of the material:

- Ablation of the superficial layers ($\sim$ 1 to 5 μm)
- Fusion of the underlying matter ($\sim$ 5 to 10 μm)
- Creation of superficial residual oxide at the surface ($\sim$ 1 μm)
- Creation of residual tensile stresses at the thermally affected surface ($\sim$ 10 to 80 μm)

The creation of tensile residual stress is the exact opposite of the effect wanted with laser peening. The phenomenon is explained on fig. 1.13. During the pulse the targeted area is thermally dilated and

push the surrounding matter not affected by the laser shot. The matter not heated push the shocked area to create compressive stresses (fig. 1.13 (a)). However, at the end of the laser pulse the matter starts to cool down and contracts to have a smaller volume than at the beginning. To compensate the loss of volume the surrounding matter has to pull the treated area to force it to retrieve its initial volume (fig. 1.13 (b)). This effect induces tensile residual stresses. Under the thermally affected area compressive residual stresses are imparted in the material the same way as a treatment with thermal coating.

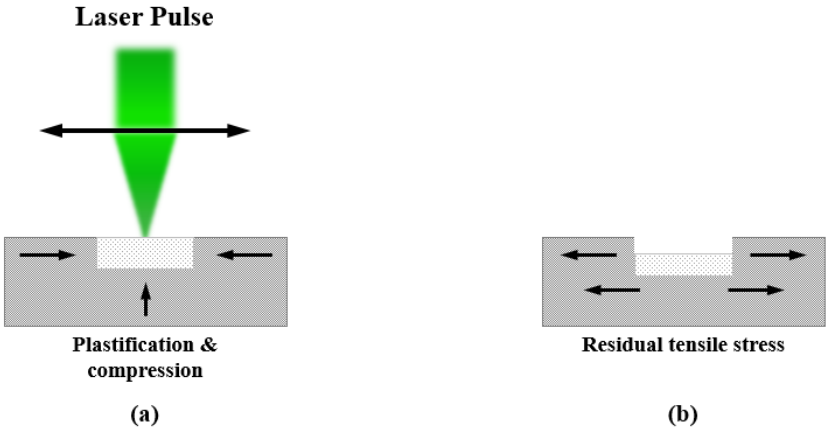

Figure 1.13: Mechanisms involved in the creation of tensile stress at the surface of a shocked material. (a) during the shock and (b) after the laser pulse.

1.2.4.3 Thermoprotective layer

In the classical laser peening configuration, a thermal coating is placed on the surface of the material to be treated to avoid detrimental thermal effects induced by the plasma heating. Typically, during a laser shock treatment without any thermal coating, the heating of the surface will cause:

- Ablation of a layer of matter at the surface (around 1 to 5 μm)
- Creation of residual oxides at the surface of the treated area
- Fusion of matter under the oxidized layer (around 5 to 10 μm)

An example of the difference of surface after laser treatment with or without thermal coating is given in figure 1.14 for inconel 718 with a Nd:Yag laser (1054 nm) using a 20 ns pulse duration.

The use of a thermal coating causes the plasma to be formed at the surface of the coating. The thermal damages induced by the plasma heating are applied at the surface of the coating while only transmitting a mechanical loading at the surface of the material of interest. Generally black paint is used for its easy application of the surface of the material but aluminium tape is also used is some cases [52]. For some in-lab experiments, the confinement chosen was more original with some research using quartz crystals, Polymethylmethacrylate (PMMA) blocks or glass mainly for the demonstration of the impedance mismatch theory such as in Hong et al. work [29] (more information in Appendix B) but the thermal coating stays the same as opposed to another treatment method created by Y. Sano [30, 21] which does not use any thermal coating to protect the surface on the materials treated. This configuration induces differences on the surface finish such as:

- Topology/Roughness of the shocked piece
- Surface hardness
- Surface residual stresses

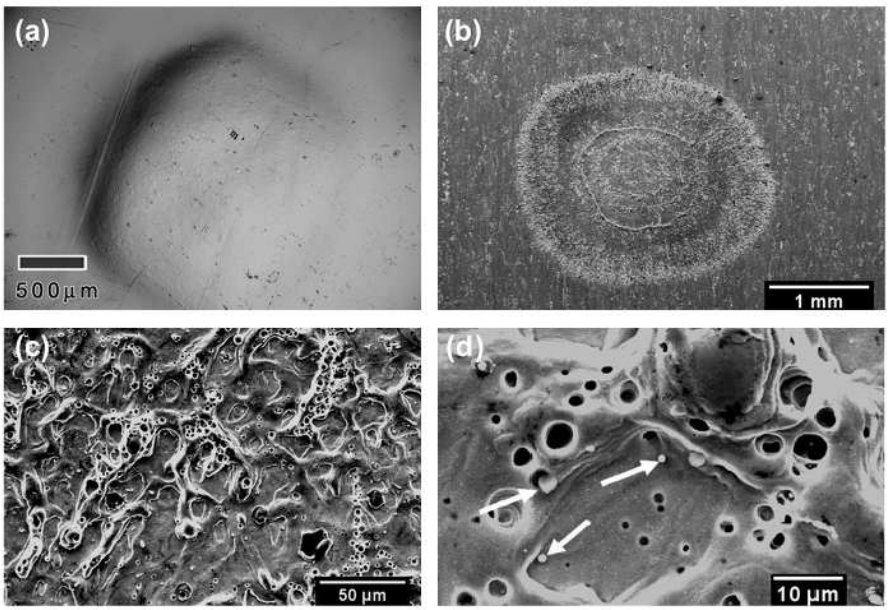

Figure 1.14: Representative images of (a) a single dimple after shot with a protective overlay and (b), (c) and (d) without any thermal coating (taken from [53])

1.2.4.4 Residual stresses

As said earlier, the laser shock peening process improves the mechanical properties (fatigue and corrosion resistance) of the treated material thanks to the compressive residual stresses imparted in the treated material through its plastification. In the case of a treatment with a protective coating, inducing only a mechanical effect, the residual stresses are compressive on the surface through up to a certain depth depending on the laser parameters and the type of material treated (see Equation 1.4). The plastified depth can reach up to 2 mm for aluminium [54], 1.5 mm for steel [55], 1.2 mm for titanium alloys [56, 57]. These experimental results show the importance of the elastic limit of the material in the plastified depth. The reduced depth affect by compressive residual stresses for titanium alloys is explained by the higher yield stress (σ_y) of the titanium alloys compared to aluminium alloys and steels. Figure 1.15a shows an example of the change of the residual stresses measured on a 2024-T3 aluminium alloys depending on the pressure applied, stressing the importance of the control over the laser parameters and pressure optimisation while taking into account the limit of the application of the process.

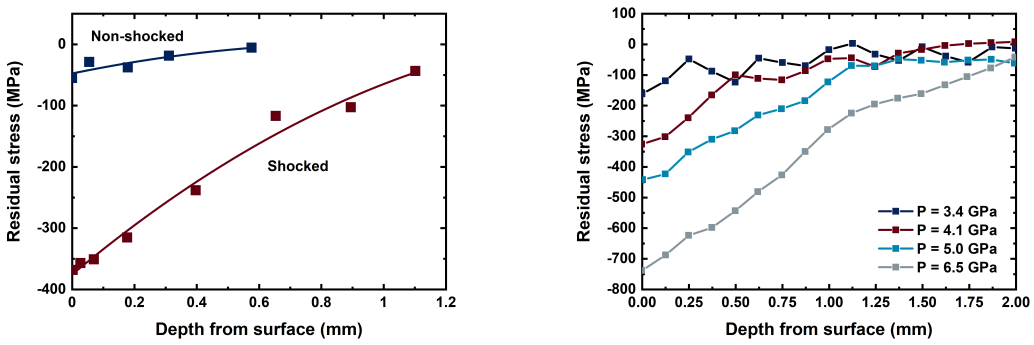

(a) (b)

Figure 1.15: (a) Residual stress measurement in a 6 mm thick 2024-T3 aluminium alloy (from [58]). (b) Distribution of residual stresses with different impact pressures (finite element modelling results) (from [55]).

1.2.4.4.1 Treatment without thermal coating

During treatment without protective coating the surface is affected by mechanical and thermal effects. As a consequence, during a shock, the already plastified surface is heated while the subsurface

is plastified to induce compressive residual stresses. When the heated surface cools down it participates to the relaxation of the compressive residual stresses present underneath and is thus put under tensile residual stresses. Consequently, the resulting residual stresses at the thermally affected surface of the treated part are tensile stresses.

A way to counter these drawbacks while not using a thermal coating is to use another configuration which was first presented by Mukai in 1995 [30] and was then developed mainly by Y. Sano for Toshiba for the treatment of immersed nuclear tank [59, 60, 61, 62]. It uses high overlap between shots and small laser spot diameter (< 1 mm). The use of a small laser spot induces the production of smaller plasmas that, in turn, induce less thermal effects on the surface due to the shortening of the plasma release [63]. This process also uses a low energy laser (around some hundreds of mJ) with a wavelength of 532 nm. As a result, the material treated shows improvement in its resistance against fracture and stress corrosion cracking thank to the high compressive residual stresses imparted in the work piece. The depth affected by the residual stresses is a bit lower than with the classical treatment. The advantages of such a configuration are as follow:

- No need for thermoprotective coating
- For small laser energy, the laser can be transported through a flexible optic fiber if the wavelength chosen is 1064 nm (at 532 nm non-linear effects are observed in the fiber)
- Water-immersed object can be treated thank to the 532 nm wavelength of the lasers used
- No surface preparation before laser peening

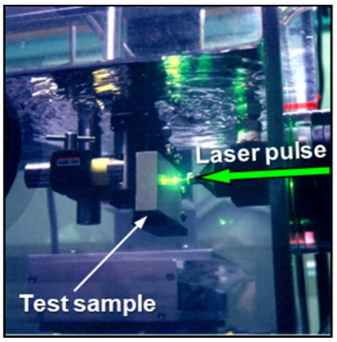

Figure 1.16: Experimental setup for Laser Peening without Coating (LPwC) (from [62]).

The treatment uses a low 532 nm laser with an energy of around 300 mJ and a pulse duration of some ns. To compensate for the low energy the number of pulses applied (i.e the pulse density) is increased. The increase of the number of shots does not really have an impact in the treatment time since the low energy needed for the shots allows the use of high frequency laser (tens to hundreds of Hz of repetition rate). One of the drawback of this process lies in the depth affected by the compressive residual stresses which is lower than what can be achieved with a more classical set of parameters.

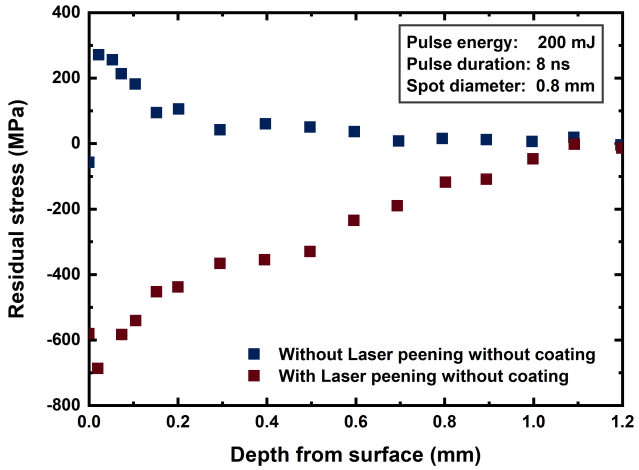

Figure 1.17: Residual stresses in depth of a 20% cold-worked type-304 austenitic stainless steel (from [64]).

1.2.4.5 Roughness modification linked to LSP treatment

The ablation and fusion of the surface layers of matter is an important matter during treatment without protective coating. In the case of alloys for aerospace applications, the surface roughness must meet strict criteria, especially for exterior critical parts that can disrupt the air flow on the fuselage. Gill et al. studied the difference in roughness caused by applying the same laser shock treatment to inconel 718 with and without thermal coating. As shown in figure 1.18. For a laser shot with a 1.8 mm laser spot with thermal coating, the dimple observed has a diameter of 2 mm and a depth of 5.5 μm with an homogeneous crater whereas if no coating is used the diameter of the dimple becomes 2.4 mm and the depth 8.5 μm while having and heterogeneous crater. Figure 1.19 shows the profile from a laser patch with different energy conditions. Once again, the use of a thermal coating showed an increase in the overall surface quality after treatment (from a Ra of 0.120 μm before shock to 1.87 μm

with coating and 19 μm without any).

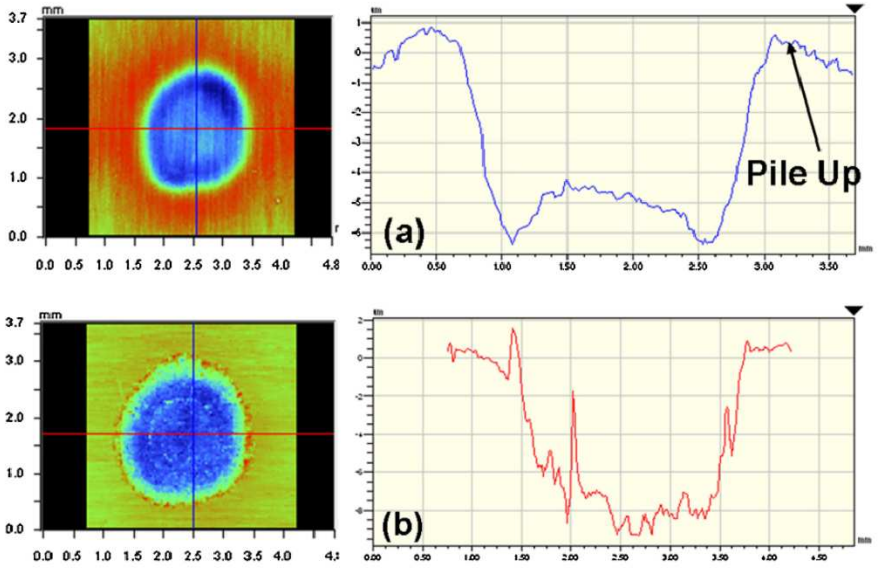

Figure 1.18: Profiles of a single water confined 3.9 J shot with a 1054 nm, 20 ns pulse, 1.8 mm laser spot equal to 7.7 GW/cm^2. (a) with thermal coating consisting of a vinyl tape and (b) without thermal coating (Taken from [53]).

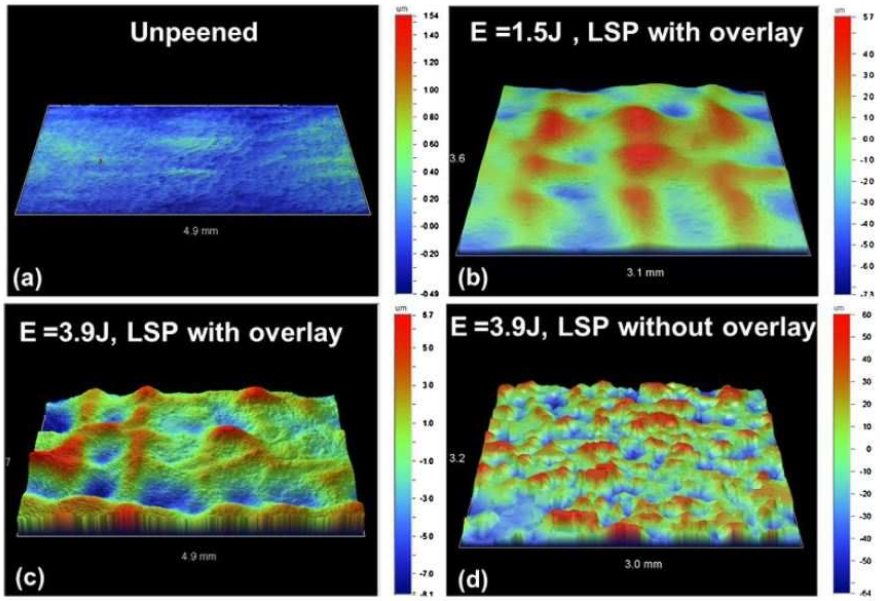

Figure 1.19: Surface profile from (a) unpeened, (b) peened with thermal coating (black vinyl tape) with 1.5 J, (c) with thermal coating with 3.9 J and (d) without thermal coating with 3.9 J (Taken from [53]).

Moreover their work demonstrated that the absence of protective coating led to potential changes

in the surface microstructure as well as the apparition of small cracks near the surface. In a study on an Si - 3% Fe alloy Clauer et al. showed that the thermally affected depth of the material could be roughly calculated with:

$$x = 2\sqrt{kt} \tag{1.5}$$

With k being the thermal diffusivity and t the pulse duration. In their study, only about 10 μm under the surface was affected by the thermal effects [65].

1.2.5 Key process parameters

To achieve a mastering in the laser shock peening process, the most important parameter is the pressure produced by a laser shot with defined parameters. By being able to accurately represent the pressure profile of a laser shot, the other steps of the process can be modelled accurately. For example, the modelling the compressive residual stresses imparted in the material by the process can be accurately represented if the exact pressure of each shot used for the treatment is known. Many studies were conducted in order to evaluate the influence of different laser parameters on the laser shock peening process. To achieve such an understanding of the process, it is crucial to know the effect of the different key parameters (mainly the laser wavelength and its spot profile and duration) of the process.

1.2.5.1 Pulse profile and duration influence

As shown in 1.2.3.3 measurements have been realised with different pulse duration an demonstrated the influence of this parameter on the apparition of a breakdown plasma. Indeed, using longer laser pulse will apply the pressure produced by the shot for a longer duration and in turn, induces the resulting compressive residual stresses deeper. However, such a configuration, as shown before, induces the apparition of a breakdown plasma at lower laser intensities due to the accumulation of photons at the surface of the treated material for a longer duration. For the treatment of alloys typically used in the aerospace industry, a pressure of at least 4 to 6 GPa must be reached. A 10 ns laser pulse appears as a good compromise between maximum pressure produced and its time of application.

1.2.5.2 Wavelength influence

The wavelength of the laser chosen is an important parameter for the laser-matter interaction but also for the application of the laser shock peening treatment. The laser wavelength chosen has an effect on the following aspects:

- The optical transmission in the polymer confinement.
- The laser-matter interaction yield.
- The breakdown plasma initiation.
- The laser protection.

First, the laser energy absorption by the metallic target and the plasma is influenced. From a practical aspect, the laser has to go through the confinement before inducing the plasma formation, depending on the absorption of the confinement at the wavelength of the laser, a consequent fraction of the incident energy can be lost before reaching the target or even induce a breakdown plasma. At first, most of the measurements were made at 1064 or 1053 nm. Later others studies showed the influence of smaller wavelengths. The pressures obtained depending on laser intensity for shots with a 1064, 532 and 355 nm laser, corresponding respectively to the first, second and third harmonics of an Nd:YAG laser are given in figure 1.20.

The confinement chosen is also a factor that have to be taken into account when choosing the laser wavelength to be used. The transmission of the chosen confining medium will influence the final energy deposited at the surface of the target. A low transparency confinement will allow for less energy to be deposited at the surface of the target. At the same time, if the layer absorbs more energy, its breakdown threshold will also be lower and by extension, lower the maximum pressures achievable with said confinement. In the classical water confined regime for example, the transmission is nearly 100% for a water layer from 1 mm to 10 cm thick with a 355 and 532 nm wavelength. However, at 1064 nm the energy absorbed becomes highly dependent on the layer thickness chosen. A 1 mm layer will allow for 94% of the energy to go through while only 0.2% will pass for a 10 cm thickness. Table 1.1 give the transmittance values obtained for different thickness of water confinement depending on the laser wavelength.

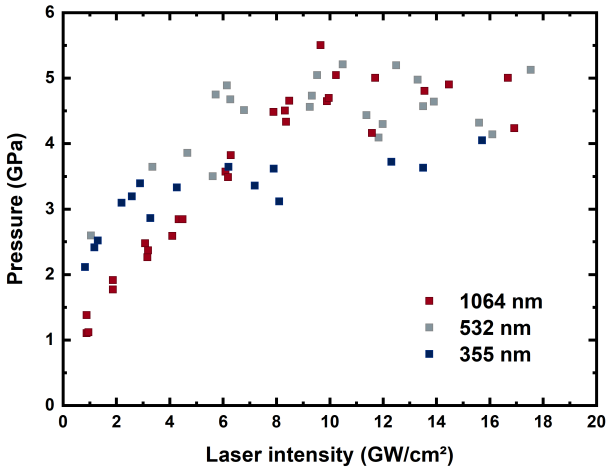

Figure 1.20: Maximum pressure depending on the laser intensity for different laser wavelengths (taken from [39, 66]).

Table 1.1: Water transmission at different wavelengths depending on the water confinement thickness layer (Values from [67]).

Water thickness	**355 nm**	**532 nm**	**1064 nm**
1 mm	99.97%	99.99%	94.12%
1 cm	99.79%	99.96%	54.55%
10 cm	97.93%	99.64%	0.23%

As one can see when working at 1064 nm, knowing the thickness of the layer of water used is of crucial importance. A more detailed transmission curve is given in figure 1.21 for thickness varying from 1 μm to 20 cm. In practical application, treatment are done with a laminar water flow by bringing a hose close to the treatment location. The layer thickness with this type of setup is typicality around 1 mm which allow most of the laser energy not to be lost.

1.3 Applications

Since the end of the 90's, LSP is more and more industrially used, mainly in two domains:

- The treatment of fan blades of military planes. Thanks to the deeper residual stress the results obtained are much more interesting than with a classic peening approach. The fatigue life of the parts is significantly lengthened and reduces the problems caused by FOD (Flying Object

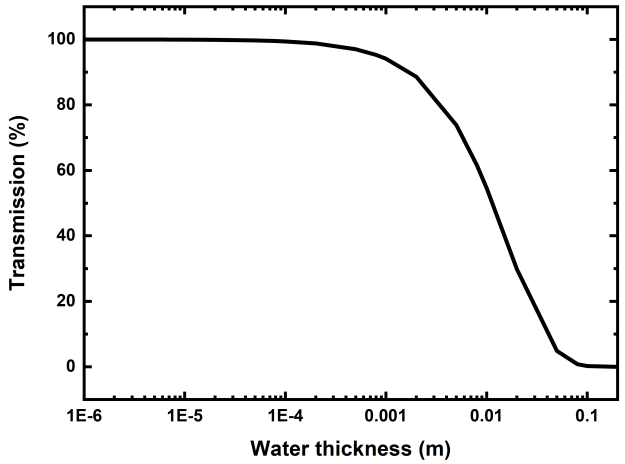

Figure 1.21: Laser energy transmission depending on the water confinement thickness at 1064 nm (Values taken from [67]).

Damage) on these types of aircrafts. A fan blade treated by LSP retrieves mechanical properties equivalent or superior to an undamaged part [26]. To avoid material deformation a beam splitter is used to divide the laser pulse into two and shock the part on both sides to generate symmetrical deformations [26] (fig. 1.22).

- In the nuclear industry, Toshiba Corporation developed a system to reinforce by laser shock welded joints of nuclear 304 steel tanks of water pressurised reactor subject to stress corrosion (fig: 1.23. The first results of the project were presented in 1995 by Mukai [30]. To be able to make an in-situ treatment, a compact portable system was developed with a YAG green laser (532 nm, 0.2 J, 10 ns, 10 Hz) and a rotating optic cane allowing transportation of the laser to the bottom of the tank (30 to 40 meters depth). This method showed good results despite not using any thermal coating to avoid thermal effects. The tensile stress at the surface is compensated by a high overlapping of the shots (2000%, so 20 impacts on the same point) and a small laser spot (0.7 mm). The use of the 532 nm laser instead of a near-infrared one is essential in this configuration to avoid the loss of transmission through water thickness.

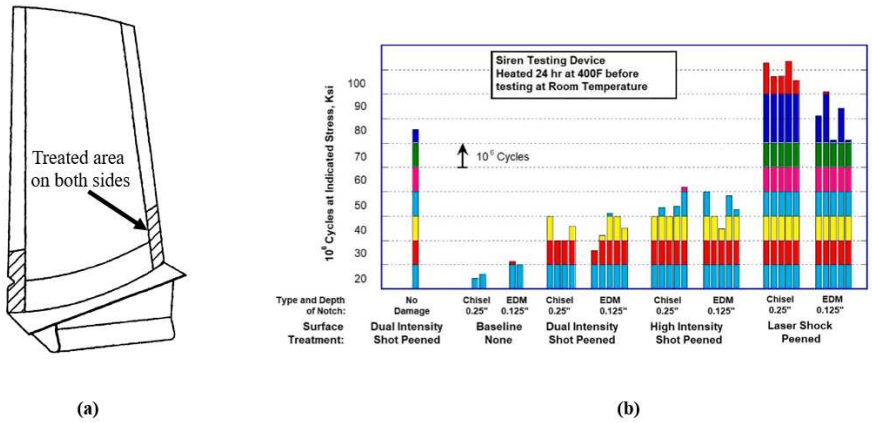

Figure 1.22: Fan blade reinforcement, (a) area treated (from [68]) and (b) gains expected from laser peening treatment on fan blades (from [26])

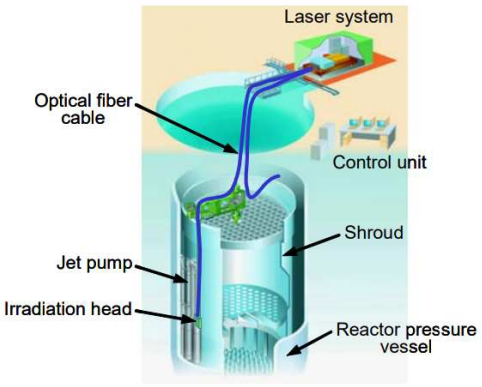

Figure 1.23: Laser peening setup used for nuclear tank treatment by Toshiba (from [60])

1.3.1 Fatigue life enhancement

As shown in figure 1.22 laser shock peening treatment produces substantial fatigue life gains on the treated parts. This improvement is due to the compressive residual stresses and strain hardening imparted in the area treated. Generally the fatigue life behaviour improvement can be expected to go as high as 350 to 400% [69] but can vary depending on the material or alloy treated. Different values are found in the literature with varying set of parameters and for different classically used alloys in the aerospace field. It is also important to note the difference between the fatigue measurement technique used. More information on the fatigue testing methods is given in appendix C. In the case of laser shock peening the 4-points-bending technique is usually used.

1.3.1.1 Fatigue life improvement induced by laser shock peening

In general, the improvement in fatigue life behaviour expected after a laser peening treatment can vary from 150 to more than 400% on aluminium alloys. Improvement of up to 412% were reported by Hu et al. on AA2024-T351 [69]. For AA6061-T6, a 185% enhancement was obtained by Huang et al. after laser treatment [70]. In the case of 316L steel, the fatigue life increase described by Correa et al. after treatment reaches 471% [71]. The differences of results between materials are influenced by the properties of the alloys treated but also by the laser parameters chosen in each of theses studies. For example, laser peening of AA2024-T351 can lead to improvement ranging from 412% to 243% [69, 72] depending on the set of parameters chosen. Thus multiple parameters can be tuned and modify the efficiency of the laser peening process on the final fatigue life behaviour. The pulse duration, the energy, the overlap, the pulse diameter as well as the peening pattern [73] all have a role to play in the final properties of the material treated [74, 75].

1.3.1.2 Crack propagation and initiation

The compressive residual stresses induced in the metallic piece treated by laser peening prevent crack propagation or initiation. As explained before in 1.2.4.1 (fig. 1.9) the compressive residual stress is caused by the surrounding matter pushing the laser shocked spot. Thus, potential crack initiation and propagation is harder to induce. In the case of a pre-existing crack it also slows down it propagation.

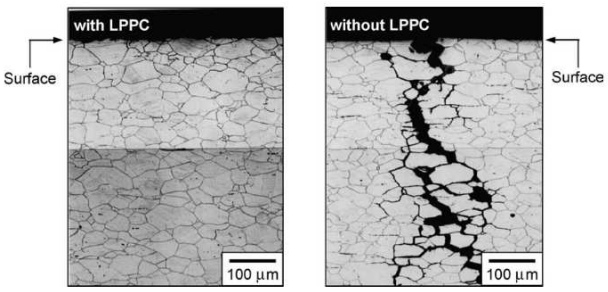

Figure 1.24: Stress corrosion cracking test results on SUS304 alloy (from [60])

1.3.1.3 Fatigue crack growth

The formation of a crack is heavily influenced by the surface state of the material. The presence of oxides, asperities, plasticity are important factors that can stimulate a crack formation. Phase change and viscous fluid can also play a role in crack induction although they play a smaller part.

The repeated loading and unloading of a material leads to the triggering of crack formation at the microscopic level due to the accumulation of localized irreversible slips at the stress concentration sites (i.e. grain boundaries). The orientation of the crack growth is then dictated by the defects present in the structure. The propagation of the crack is separated in two stages:

- **Stage I - Small cracks**: They are shear driven, interact with the micro-structure and are mostly analyzed by continuum mechanic approaches. The crack size is that of a material grain. The cracks grows along the slip system with the maximum shear stress. However this varies from grain to grain thus the cracks are tortuous. The stage I crack growth undergoes fluctuations but gradually slows down due to its encounter with multiple boundaries. As the crack grows larger the importance of the micro-structure decreases because of the accumulation of irreversible slips. This induces a plastic area ahead of the crack. The presence of a high amount of tip slips creates a high pile up stress. At this point the boundaries offer little resistance and the crack grow larger.

- **Stage II - Large cracks**: They are tension driven, relatively insensitive to micro-structure and mostly analyzed by fracture mechanics models. Theses types of cracks propagate in the normal direction to the applied stress with a propagation rate of microns per cycle. At some point the crack will reach a critical size and failure will occur.

A classic way to represent the fatigue crack growth of a materials the Paris' law. More information of the model can be found in appendix D.

1.3.1.4 Stress corrosion cracking resistance

Stress-corrosion cracking (SCC) needs a crack to propagates from. It can be an already existing crack in the material, like a defects such as a porosity [76], a weld [77] or even the result of machining [78]. In other case the crack is initiated through shock, in the aerospace industry a common crack

cause is FOD (Foreign Object Damage), which are generally birds hitting the plane during service and causing cracks on the cockpit nose or on the wings and motors [79]. The SCC cannot be dissociated from the fatigue cracks as it can originate from one. For example, in a plane, fatigue crack can develop at altitude during the fly while the stress corrosion crack will happen after the flights caused by the condensation of water.

The initiation of SCC generally occur in corrosion pits which are the caused by metallurgical inhomogeneities like inclusions or grain boundaries where oxide films does not offer a protection as efficient as in the surrounding area. The transmission from a pit to an SCC is dependent on the pit shape and depth but also on the local stress, strain and stress intensity factor. Figure 1.25 gives an example of a crack emanating from a corrosion pit.

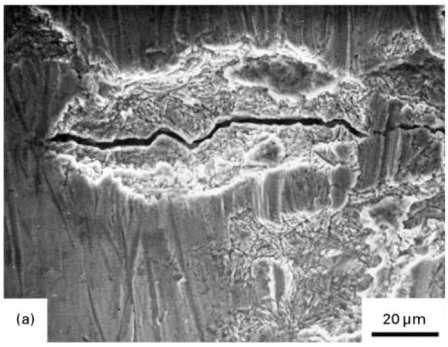

Figure 1.25: Scanning Electron Microscope (SEM) image showing crack initiation from a corrosion pit in a high-strength martensitic-steel aircraft component (taken from [80]).

LSP is a method of choice to improve the resistance to stress crack corrosion of metals. In the case of steel Sano [81] and Peyre [82] showed that laser peening leads to a better pitting resistance regardless of the use of a thermal coating or not. In a coated configuration, the mechanical effects (work-hardening and residual stresses) reduce the number of active sites to initiate pitting at lower potential while when thermal effects are also at play they are negligible for SCC susceptibility. Many material SCC resistance have been studied, from aluminium alloys [83, 84, 85] to titanium alloys [86, 87] and steels [88, 89] and found improvement of the SCC behaviour whatever the treated metal.

1.3.2 Other laser applications

Appart from laser shock peening, many other applications of laser shock are possible such as:

- **Laser Adhesion Test:** or LasAT. It consists in generating a high tensile stress at a material interface with a coating, it is mainly used for material properties control. The aerospace and biomedical field both use coating on some materials and the adherence of these coatings with the main piece need be assessed accurately. Classical tests used for these properties like bond pull tests [90], bulge test or scratch tests [91] are not adapted to this type of configuration and assembly and need more samples to produce relevant results compared to LasAT. The first demonstration of LasAT capability was realised by Vossen et al in 1978 [92]. Laser Adhesion Test use the laser shock process, a laser pulse is focused at the surface of a material to produce a shockwave inside of the material tested. During the wave propagation, reflections at the interfaces are going to create tensile stress waves. In the case of symmetrical shock, two compressive waves can cross one another and create a tensile stress at the meeting point. These tensile stresses are used to debond the coatings. By knowing the pressure applied by each shots at the point of interest, it is possible to evaluate the strength of the bond of the pieces. The diagnostic is realised through rear free surface velocity measurement with a Velocity Interferometer System for Any Reflector (VISAR)

- **Paint stripping:** It consists in using a laser pulse to destroy surface coatings from airplane fuselage and other materials. It has been developed since the early 1980s and allows for the recycling of some materials like aluminium. The paint on an airplane must be replaced on average every four years [93]. For this reason, the most common use of the paint stripping process is to remove the old paint layers before reapplying new ones. It offers controlled and accurate performances and has the advantage of being non-contact which makes it a solutions of choice. Some new applications are currently studied and aims at changing the way of using paint stripping. Instead of targetting the laser pulse at the surface of the materials to be treated, the laser is focused on the back face of the target to induce a shockwave that is mechanically removing the coatings thus avoiding potential surface oxidation and thermal damaging usually induced by the process [94].

- **Laser propulsion:** The process was first proposed in 1972 by Kantrowitz [95] to replace chemical propulsion to send spacecraft to near earth orbit. In the pulse laser propulsion a laser pulse is focused on a target to generate a plasma. The momentum transition occurring during the process is impinged by the plasma expansion counterforce exerted at the surface of the target. The main

advantage of the laser propulsion process compared to propulsion by classic chemical fuels is that a spacecraft using laser propulsion does not need to carry additional fuels or propellant sources as the propellant is acquired from the target itself thus reducing the launch costs [96].

1.3.3 Laser peening compared to other peening strategies

Multiple peening process exist, their choice depends on the situation, cost, industrial feasibility and needs. The most used one is still shot peening but new techniques arised through the years such as ultrasonic peening which is mostly used for the cold treatment of welded structures and based on an ultrasonic magnetostrictive oscillating system attached to a peening tool [97]. Another one would be cavitation peening which uses the collapsing of ultrasonic cavitation bubbles near a material surface immersed in liquid thus producing high pressure on the area of interest [98]. Water jet peening is also an alternative, close to cavitation peening as the two of them use projected water although cavitation peening use the bubble collapsing created while water jet peening uses the water column impact. Although theses techniques are gaining some traction, they are still marginally used compared to the classical shot peening since the fatigue results obtained with those treatment are less good than with classic peening, be it in terms of fatigue strength but also in depth affected by the treatment. Fatigue strength results are given for different types of peening techniques on figure 1.26 for the treatment of stainless steel.

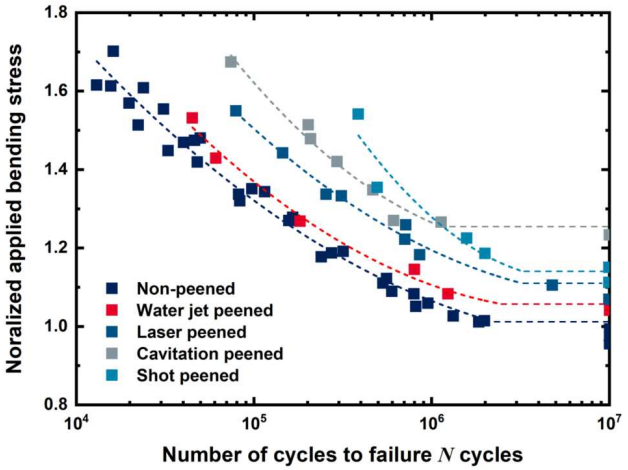

Figure 1.26: Improvement in fatigue strength of stainless steel by water-jet-peening, laser peening, cavitation peening and shot peening compared with a non-peened specimen (from [98]).

One of the major advantage of laser shock peening compared to classical peening is the depth affected by the treatment. For laser shock peening, the residual stresses are located at a depth up to ≈1.5 mm compared to ≈300 μm for shot peening [54] of Al alloy materials. In addition, the LSP-induced work hardening is generally limited (about +10% to +30%) compared to conventional shot peening [28]. This can be explained by the fact that the loading duration is very short (generally some ns), which consequently does not allow the activation of all the sliding systems of the material and thus generates fewer cross dislocations. Only cyclic hardening materials such as 304L and 316L have their hardness and their level of residual stresses increase with impact repetition.

Overall laser shock peening appears to be a better mechanical treatment option compared to shock peening for a material lifetime thanks to the controlled deformation. Indeed, the worse surface roughness produced through shot peening is detrimental to the residual stresses imparted in the material. For laser shock peening this effect is mitigated thanks to the low work-hardening induced by the treatment. Not only the surface is less deformed but it is also uniform because of the controlled path of the laser while for shot peening the impacts are random on the treatment area, leading to more differences overall. This deformation uniformity is another factor leading to higher fatigue behaviour.

1.3.4 Industrialisation challenges with water confinement

Although laser shock peening in water confined regime is widely used in the aerospace and automotive industry, it still has some drawbacks and limitations that prevent its use in some cases. First, the water flow needs to be thin enough not to absorb the incident laser energy with near infra-red lasers which are the majority of the lasers used for LSP in industrial setting. The flow of water brought must also be laminar to stay consistent. This has some implications, for example in the case of the treatment of small bore holes, this laminar flow cannot be achieved and thus make it impossible to implement laser shock peening in this type of configuration. In the same way, for the maintenance treatment of already flying aircrafts, some parts cannot be LSPed with a water confining regime due to the impossibility to bring water in those places. An example is the reinforcement of some interior parts of the wings that see a lot of stress concentration and cyclic loading. Due to the presence of kerosene tanks in the wings it is impossible to bring water in order to avoid water to contamination of the fuel tanks. For cockpit treatment also, the same type of problem arises. The presence of electronic devices inside of the cockpit prevent the use of water which would be too dangerous with the water

splashing caused by treatment. More generally, the presence of water can trigger corrosion phenomena if a metal has a small scratch or defect. For all of these reasons, finding an alternative to the water confined regime is a crucial point. It would allow the reinforcement of areas that cannot be correctly treated by laser shock peening but also potentially simplify already existing processes that use water as of now.

1.3.4.1 Parts to be treated

The parts to be treated with flexible confinement in place of the water confined regime are mainly cockpit areas as well as wings and small bore holes. Figure 1.27 gives an illustration of the concerned parts. The cockpits and wings presented are highly susceptible to cracks initiation and propagation due to Flying Object Damages (FOD) caused most of the time by birds hitting the plane in altitude or the inclusion of glasses in the cockpit that induce stress concentrations. Another cause of crack initiation and propagation resides in the natural cyclic loading happening in some area of the structure of these parts which induce fatigue damaging over long period of time.

Figure 1.27: Areas of interest for the laser shock peening treatment with polymer confinement: wing area and cockpit.

Although the confinement used for this work is not the classically used water, the end result after treatment aimed are the same. Improved fatigue life behaviour through the introduction of compressive residual stresses at the surface but also in depth of the treated material are desired. From this, the crucial parameters for the treatment are the same. The breakdown phenomenon must be avoided in order to be able to develop a sufficient pressure and induce high compressive residual stresses. This effect is affected by both the laser parameters and the confinement parameters. The laser parameters that can be tuned are the pulse duration, its wavelength and the spot size (respectively τ, λ and $\emptyset$):

- The pulse duration τ, influences the breakdown threshold. The longer the pulse duration is, the lower the breakdown threshold will be.
- The wavelength λ, also influences the breakdown threshold. The use of a 1064 nm wavelength compared to a 532 nm one will induce a lower breakdown threshold since the interaction yield is lower with this wavelength.
- The spot size Ø, influences the edge effects. The use of a smaller laser spot will induce the apparition of more edge effects which can cause tensile residual stresses in the treated piece.

The other part of the problem lies in the polymer used as a confining medium effect on the laser shock peening process. Since the choice of the material is not determined yet, one can only find the different polymer parameters that can potentially have an influence on the process and direct the choice of the polymer confining medium according to the supposed optimal properties or at least the best compromise that can be found through a literatures study.

The choice of polymers as potential confinement for the laser shock peening application stems from their flexible properties which appear compatible with the process. The advantages and the criteria chosen for the determination of the different confinements studied is given in the part hereinafter.

1.3.5 Advantages of polymer confinement

In order to be able to apply laser shock peening to every scenario a flexible adhesive polymer confinement seems to be a good alternative. It can potentially present many advantages:

- Depending on its flexibility it can be adapted to any complex geometry even though the applying process might require some engineering. Even in such case it would still be similar to the problems caused by the water flow management needed in a water confined regime to keep a laminar flow.
- Its chemical and mechanical properties can be tailored up to a certain point to make it more resistant to the potential damaging caused by the laser. In the same way its chemical structure can be modified to grant it a better transmission depending on the laser wavelength used.
- Similarly, by tuning its mechanical properties, typically by improving its Young's modulus and/or density, the pressure produced could be improved thanks to the impedance mismatch phenomenon applied at the transmission of a shock between two media (see appendix B)

- Depending on the way the polymer is made, it could contain multiple layers to incorporate a thermal coating which also protect the surface of the material treated from thermal damaging as well as further enhance the pressure gains from impedance mismatch.

With the desired properties of a polymer confining medium under laser shock already established, the choice of polymers for the LSP application can be oriented depending on polymer properties:

- **Flexible:** A way to obtain a flexible polymer is to choose one with a glass transition temperature lower than the ambient temperature in the area of treatment. By doing so the material is in a rubbery state allowing its shape to be modified and thus making adaptable to different work-piece geometries.
- **Transparency to the laser wavelength:** The transparency of a polymer in the wavelengths of interest (532 and 1064 nm) can be easily obtained by doing measurements with a calorimeter (see figure 3.2). In order to be sure that this transparency stays high throughout a laser shot, a solution is to chose amorphous material to avoid cristallization that affect the optical properties of the materials. Ideally, the choice should be oriented toward polymers that stays amorphous under high pressure and strain rates.
- **Good bonding and debonding properties:** To have a polymer able to stick to a surface and be easily removed without leaving any trace, pressure sensitive adhesives (PSA) are a good solution. More information on this type of material is given in 1.4.3.

1.4 Polymers as confinement

The choice of a polymer to use as a confinement instead of water must be based on a certain number of criteria:

- The polymer chosen should be flexible in order to be adaptable to a curved and potentially more complex surfaces.
- It has to have a good transparency to both the laser wavelengths used, respectively 532 nm for the laser used in the laboratory for the characterization and 1064 nm for the lasers used for the treatment and in an industrial setting.

- The confinement should be able to allow the production of pressures high enough for the laser shock peening treatment to yield sufficient compressive residual stresses and impart good fatigue life behaviour improvement into the shocked alloy.
- The material should be easily bonded and debonded not to leave any residues in the areas treated and pollute them.
- A high temperature resistance is preferable to limit potential thermal damaging of the confinement during the laser shock.
- In the same way, a high chemical stability is prefered to avoid modifications of the polymer properties in between laser shots but also for storage reason over time.

1.4.1 Laser interaction with polymer

The response of a polymer to a laser irradiation is highly dependent on its transparency. This property is referred as the optical strength in the literature and describes the capability of a material to resist optical damage. The process of polymer damaging through repeated shots is referred as the incubation process and describes the dependence of the damage threshold fluence (given by equation 1.6) on the number of laser pulses [99]. It is related to an incomplete dissipation of the incident energy brought to the material in between repeated shots. It can take the form of plastic stress/strain or can be considered stored in the shot region in the form of crystallographic change as well as chemical modification. Figure 1.28 gives an example of the decreasing damage threshold, represented as F, the laser energy (or fluence) necessary to induce damage depending on the number of shots on the same area in two different polymers.

$$F = \frac{E}{S} \tag{1.6}$$

With F the laser fluence, E the energy in Joules and S the surface in cm^2.

In the case of a polymer that is not fully transparent, the laser energy results in surface modifications. Both the chemical composition and the crystal structure of the first few layers of polymer are modified and some damages can be created in the thickness of the material shot. The different parameters affecting the damaging of a polymer under a laser pulse have been studied extensively by Manenkov's team. First, they evaluated the optical strength of polymethylmetacrylate (PMMA), an "organic glass" and showed that its optical strength was influenced by its propensity to carbonize

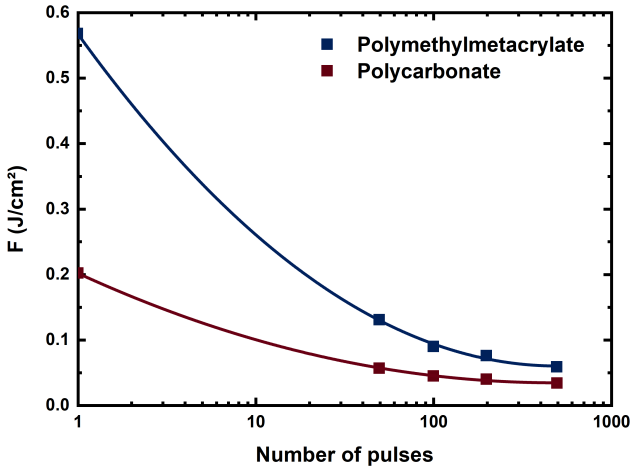

Figure 1.28: Measured N^{th} pulse ablation threshold, F_{th}^{N}, for polycarbonate and polymethylmetacrylate as a function of the number of pulses. Solid lines represent fitting using the incubation function given in [100] (taken from [101]).

during photolysis (i.e chemical decomposition under light) [102, 103] as well as by the presence and size of absorbing inclusion or defects in the material that can act as the seed for further damaging. The damages induced by these phenomena are dependent on different parameters:

- The material type (metal [104], semiconductor [105], dielectric [106], etc)
- The laser parameters: The wavelength [107], pulse duration [108] and repetition rate [109] all have an influence over the damage threshold

But the underlying processes are the same. In dielectric material potentially used as a confinement, the energy deposition proceeds through multiphotoionisation (see 1.2.3.2) and induces damaging. To define the damaging of a material, the common parameter used is the damage or ablation threshold which corresponds to the lowest fluence (energy per surface unit) that can induce damaging of the shot material, that is to say the removing of matter with the lower limit being one atom. The processes that can induce initiation and propagation of the damages and reduce the fluence threshold are described by three models:

- The heating inclusion model for thermal damage creation and expansion. Taking into account the rate of chemical degradation of material depending on the temperature and the geometrical

dimension of the impurities.

- The bond breaking model for structural default (i.e bond breaking) accumulation
- The coloured center model for lattice default accumulation.

1.4.1.1 Heating inclusion model

The reference study on this subject was realised by Hopper and Ulmann [110] and highlights the role of impurities in the laser damages. An ultimate strain of the shocked material containing heated inclusion is defined as a limit for damage formation. The model shows the absence of influence of the fusion of inclusions on the thermoelastic strain around the inclusions. During heating, if the strain does not exceeds the ultimate strain, no irreversible modification will be induced in the target material.

Manenkov and al. demonstrated that the accumulation of degradation products is accelerated by a gradual increase of the mechanochemical reaction rate constant according to relation from [111, 112]:

$$K \simeq exp\left(-(U_0 - \gamma\sigma)/kT\right) \tag{1.7}$$

With U_0 the activation energy, γ a structure dependent factor, σ the residual stress and k the Boltzmann constant.

Another point developed in Hopper's and Ulmann's concerns the influence of the temperature on the rate of chemical reaction triggered by the laser pulse. This case is particularly prevalent in the field of polymer treatment as they usually contain heating absorbing particles used as catalyst and stabilizer. The last point stressed concerns the thermodiffusion of the heating inclusion in the material matrix. In certain conditions this effect can induce a self enhancing growing of the light absorption. The heating of an inclusion is dependent on its size d and on λ the laser wavelength:

- If $d \ll \lambda$, the heating is negligible because the light absorption is too low by the inclusion and the heat loss too great into the surrounding environment.
- If $d > \lambda$, the large mass of the particle prevents a focalised heating but at the same time it can still cause damage due to the high surface affected.

- If d is slightly $< \lambda$, the damage is favoured due to the focused high heat absorption of the impurity.

1.4.1.2 Bond breaking model

The laser pulse succession induces multiple bond breaking in the shot material that can lead to macroscopic damages. With that in mind, knowing the bond strength of the different bond of a polymer can help predicting damaging by knowing the first bonds to break under irradiation. With damage accumulation, the shocked polymer evolves towards a state where only one shot is enough to induce damaging due to the lowering of the damage threshold. The minimum time needed to initiate the nucleation of an elementary defect varies from 10^{-11} to 10^{-13} s and corresponds to the time of thermal density fluctuations (the time during which the atoms can move due to thermal effects). The bond breaking model is valid only in a certain range of fluence that is dependent on the material shot. Thus equation 1.7 is only valid for $F > 0.7\,F_{th}$ for glasses and crystals while $F > 0.2\,F_{th}$ for polymers.

1.4.1.3 Coloured center model

The coloured center model or lattice defects model assumes that the laser induced damage in a material are caused by the action of mechanical stress resulting from Frenkel's defaults formed by multi photon production. Frenkel's default are a type of point defect (default that occurs only at a single lattice point) in crystalline solids consisting of an atom or ion leaving its place in the lattice and creating a vacancy while filling an interstice in a nearby location thus inducing strain in the lattice. During repeated laser shot, the local stress grows since the associated local expansion is blocked by the non affected surrounding matrix. Material damage occurs if the local stress exceeds the failure stress. Contrary to the bond breaking model, the coloured center model does not need any initial defect or seed inclusion to be triggered. This has been demonstrated by Glebov and al. [113] and then by Kitriotis and Merkle [114] that the accumulation of the stable coloured centers cannot be considered a process leading to breakdown by itself.

1.4.2 Properties needed for a polymer confinement for LSP treatment

In order to fulfil the maximum of criteria the choice of polymer can be oriented to maximize certain properties and ensure the efficacy of the chosen confinement. The first objective is to have

a transparent flexible polymer while limiting its damaging by laser. Considering the mechanisms presented above it appears that an ideal polymers confinement should be highly transparent with minimum inclusion and high bond strength while being amorphous to avoid any Frenkel's default due to crystallinity. The search must be oriented to find an equilibrium between each of these properties while still being able to easily bond and debond from the surface to treat by laser shock peening and producing sufficient pressures.

1.4.2.1 Crystalline properties

In order to obtain a fully transparent material, the confinement chosen for the laser shock peening process should be amorphous as a way to avoid the presence of crystals in the polymer matrix and limit potential reflection of the laser pulse inside the material that could create damaging or breakdown plasmas.

1.4.2.2 Bond strength

The bond energy of chemical bonds can give us information on a polymer, for example a polymer with a carbon based back-bone chain composed of C-C bonds (with an average bond energy of 346 kJ/mol [115]) will be more prone to decomposition under a laser pulse than a silicone polymer with a Si-O back-bone (average bond energy of 452 kJ/mol [115]). The choice of the polymer of confinement can be oriented to maximize bond energy in order to obtain more resistance against degradation. The simplest way would be to use silicones which are notorious for their stability and temperature resistance. The bond energy can also be taken into account for the choice of the groups added in the polymer chain to grant it properties.

1.4.2.3 Polymer choice

Considering the different properties explored, it appears that the choice of the polymer should be set on an elastomer with a glass transition temperature lower than the ambient temperature to have a flexible material. The elastomer should be amorphous to limit crystallization even if some could happen while under high stress/strain. Finally two types of backbone chains should be tested (i.e. C-C chain and Si-O chain) to see if the bond strength has a significant influence on the bond breaking process under laser irradiation.

A literature study shows that a category of material that fulfil these criteria are Pressure Sensitive Adhesives (PSAs). The choice of the potential confinement for the laser shock peening application is consequently oriented to this category of polymers.

1.4.3 Pressure Sensitive Adhesive description

PSA or Pressure Sensitive Adhesives are thin films that stick on nearly every surfaces by simple contact and can be removed without any residue. This type of adhesive is the most used by consumers and as such represents a big market. PSAs present multiple advantages like: instant formation of a contact with a substrate on touch, permanent tack, easy debonding and uniform thickness [116]. However up until recently the comprehension of the mechanisms at work in these types of polymers were not very well understood except by the companies involved in the manufactures themselves. Even if PSAs's purpose is to joint two surfaces together, the approach used is very different that in other types of adhesives. First they are not used in structural applications like epoxy resins, on the contrary, they are principally used in non-structural applications. The second difference is that PSAs do not need a chemical reaction to stick to their substrate, they bond with the surface upon contact. It is important to note that, as opposed to the term pressure sensitive, the bonding strength is not really dependent on the pressure applied on the adhesive. Thanks to this set of properties, these materials are easy and safe to use since the user does not have to worry about solvent evaporation or curing parameters. Even though the application is varying compared to other adhesives the principle is the same. The polymer needs to bond to the surface it is applied on, independently of its roughness and then needs to be able to sustain a certain amount of stress without debonding. A difference with more classical adhesives is that the bonding of non-PSA occurs at a liquid state and is then tested at a solid state after curing by UV radiation, temperature change or chemical reaction. PSAs are mixing liquid and solid properties since they are soft viscoelastic solids. Their properties are obtained from the hysteresis of the thermodynamic work of adhesion. However, there is still a difference with a proper hysteresis since here, there is a variation between the energy used to form the bonds and the energy dissipated to break them. For short periods of time, only the Van Der Waals forces are active in the PSA adhesion process [117, 118]. The drawback associated with these kinds of materials based on supramolecular interaction [119] is that their properties need to be much more finely tuned than for other types of adhesives, therefore a precise understanding of the mechanisms involved during the

process is necessary.

All commercial PSAs are based on polymers, mainly from three families: acrylics, styrenic block copolymers and natural rubbers. Silicones PSAs also exist but are reserved for niche uses like extreme temperatures were price is not an important factor. Historically, the first PSAs used were rubber based and are still the cheapest to make and the easiest to formulate. They are typically made of natural rubber and low-molecular-weight tackifying resin, miscible with the rubber in nearly equal proportions.

- **Acrylic PSAs:** They are the ones that allow the most liberty in term of formulation and optimization. They are generally composed of a copolymer of a long side-chain acrylic with a low glass transition combined with a short side-chain acrylic to adjust the T_g and completed with acrylic acid to improve adhesion and further maximize elongation properties. Tackifiers can be added in order to adjust the T_g and to hone the dissipative properties. In case of natural rubber PSAs, a cross-linking step is generally added after coating to prevent creep [120].

- **Copolymers PSAs:** Styrenic block copolymers adhesives have been the last available on the market. The usual material is a blend of styrene-isoprene-styrene (SIS) triblocks and styrene-isoprene diblocks compounded with a low-molecular-weight but high T_g resin based on C5 rings. The resin is miscible with the isoprene phase but immiscible with the styrene phase. To obtain usable properties in these PSAs, the proportion of styrene must be on the order of 4-12%, the molecular weight of the styrene block must be above 10-11 kg/mol in order to stay immiscible with the isoprene phase. The weight fraction of polymer in the blend must vary between 25 to 45%. The use of immiscible phase allows the formation of nanophase-separated edifices constituted of styrene domains dispersed in an isoprene matrix. The presence of these styrenes enables a physical cross-link, conferring better creep properties to the PSA [121].

- **Silicone PSAs:** They are widely used in medical [122], industrial [123] and tapes for insulation [124]. Multiple advantages justify their use despite their higher cost; good thermal stability, higher UV transparency and excellent flexibility, overall higher capabilities when it comes to chemical resistance, electrical properties and weathering resistance compared to organic PSAs. Finally thanks to their structure they are able to adhere to materials such as Kapton or Teflon contrary to other types of PSAs. Similar to the acrylic PSAs, their properties can be improved

through the use of tackifiers.

1.4.3.1 Mechanisms of PSAs

The mechanisms at work in PSAs were not really understood for a long time. It is thanks to a BASF scientist, Albrecht Zosel, that a mechanistic approach has been realized to understand the PSA adhesion system as opposed to the empirical approach used up until that point [125, 126]. Before, peel test was used to try to understand the mechanisms involved because as any other adhesive PSAs need a certain amount of energy dissipation to separate the two surfaces bonded. Peel test, however, is a little flawed because the peel force measured depend on the peel velocity, angle and adhesive thickness used. A strong coupling between geometry and mechanical properties was observed and limiting the interpretation and correlation between different results. Zosel developed a new test consisting of a cylindrical flat-ended probe. The probe is indented into a thin layer of adhesive and then removed orthogonally. During the operation, the force and position are constantly monitored.

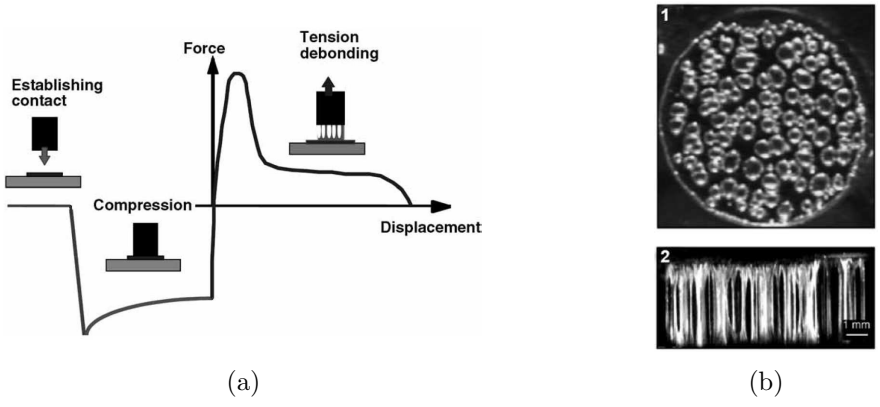

(a) (b)

Figure 1.29: (a) Schematic illustration of a tack test performed with a cylindrical flat-ended probe. (b)1. cavities observed during the tack test (view from above) and (b)2. fibrillation processes occurring during debonding of pressure-sensitive adhesives (view from the side) (taken from [127]).

Thanks to this apparatus and further studies, it has been shown that the debonding process is composed of three main steps described by figure 1.29a.

- The first peak corresponds to the formation of cavities growing from the interface. (see figure 1.29b1.).
- The growth of the cavities provokes a loss in force just before the plateau

- The expansion of the cavities without coalescing causes the formation of the fibrils. (see figure 1.29b2.).

It is important to note that the fibril formation is only observed on PSAs exhibiting high peeling forces. The final elongation of the fibrils is directly linked to the elongational properties of the adhesive.

Applied to the laser shock peening process, only the debonding phase needs to be taken into account. The fibril formation does not really have an impact as the plasma expansion will debond everything from the surface of the target.

1.4.3.2 Application requirements

From an application point of view, a PSA needs to possess three major properties: a good degree of stickiness, a controlled peel force depending on the peel velocity to induce adhesive fracture with the surface it is linked to and finally a good creep resistance to sustain stresses over a long period of time. Generally, with commercial formulation a compromise needs to be found to balance properties and price.

To adjust and have a good stickiness on an adhesive, it must be based on polymers used well above their T_g (25-45°C above). The T_g should also be as broad as possible to maximize the viscoelastic dissipation properties at low-modulus end of the glass transition. Once these specifications are met, other parameters can now be tuned like: molecular weight, molecular architecture or supramolecular structure. Another way used to adjust the stickiness is to add other molecules like tackifiers to the base polymer. They dilute the entanglement network and thus lower the modulus of the PSA in the plateau region of the curve shown on figure 1.29a. The lowering of the modulus is linked to the augmentation of the molecular weight of a polymer and allows the adhesive to form a good bond with a surface just by a light pressure. This means the adhesive must have a relatively high viscous component G'' of the shear modulus at the test frequency used (10 - 30% of the elastic component for removable PSAs, ≈100% for the ones exhibiting fibrils). This condition supposes that the material will dissipate energy through deformation, meaning a broadening of the G'' peak associated with the T_g [121]. To control the peel force an adhesive should strain-harden at high levels of strain. This property allows the material to induce completely adhesive failures, leaving no residue on the surface it was sticking to. Thus, the level of elongation exhibited and how progressive the strain-hardening

is are key parameters in PSA design [128]. For homopolymers and random copolymers, the degree of strain hardening is controlled by the choice of a suitable molecular weight distribution and degree of cross-linking. Typically, PSAs contain between 50 to 70% of insoluble fraction. Finally the creep properties are also controlled by chemical or physical cross-links. However the parameters necessary to obtain good creep properties and a good peel force are different. During creep, a shear force is constantly applied and no fibrils are formed, the optimum degree of cross-linking is higher than what would be used to obtain a good peel force.

For the applications targeted, an adhesive failure is preferred not to leave any residue on the surface treated an simplify the cleaning process. A good way of modulating the properties of interest for the laser shock peening process will be to play on the cross-linking of the adhesives chosen. To accompany the polymer choice, a good understanding of its mechanical properties is necessary. The following section presents a study of the global properties of polymers and more specifically elastomers with viscoelasto-plastic properties under static conditions and high strain rates such as the one that can be found during laser shock experiments.

1.4.4 Overview of polymers material properties

1.4.4.1 Viscoelasticity and viscoplasticity

Viscoelasticity

Viscoelasticity describes the behaviour of a material exhibiting both viscous and elastic properties during deformation. Viscoelastic deformation introduces a number of parameters that are not involved in a simple elastic deformation like stress relaxation, creep, dynamic mechanical behaviour or volume retardation. This type of behaviour can be found in polymers near their glass transition temperature when they reach a leathery state due to the improvement of molecular mobility with the temperature (figure 1.30). With the increasing temperature the molecular motion also increases and causes a change in the length and angle of chemical bond thus inducing a rising of the system energy. If the chain mobility is high enough, large-scale rearrangements are possible on a time-scale of the 10^{-12} sec order. A further increase of temperature will cause a fully rubbery behaviour.

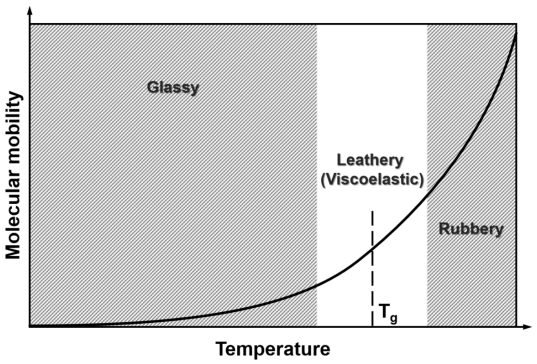

Figure 1.30: Temperature dependence of the rate of molecular movement in a polymer

Viscoplasticity

Viscoplasticity describes the mechanical response of solids under time-dependent plastic strains. Two main mechanisms are involved in the material rate-dependency:

- Vacancy formation and grain boundary sliding, processes that are usually studied for creep and stress relaxation experiments.
- Slip-induced plastic deformation due to the displacement and multiplication of dislocations

In the case of polymers, viscoplasticity takes place both in crystalline and amorphous phases. In the crystalline phase, slips are formed while in amorphous phases chain segment rotations are observed. Compared to a classical platicity a viscoplastic phenomenon is similar in terms of strain hardening and elasticity but a viscosity function must be added. The Norton's power law [129] is usually used and link the plastic strain rate $\dot{\epsilon}_p$ to the applied stress σ through two temperature-dependent parameters; $\lambda_{(T)}$, the kinematic viscosity of the material and $N_{(T)}$, a fitting parameter.

$$\dot{\epsilon_p} = \left(\frac{\sigma}{\lambda_{(T)}}\right)^{N_{(T)}} \tag{1.8}$$

The effect of strain-hardening on the stress/strain plot of a viscoplastic material is given in figure 1.31, the stress σ needed to attain a defined strain ϵ is higher when the strain rate $\dot{\epsilon}$ used is increased since the material damaging and relaxation is not able to fully take place during the time of the experiment.

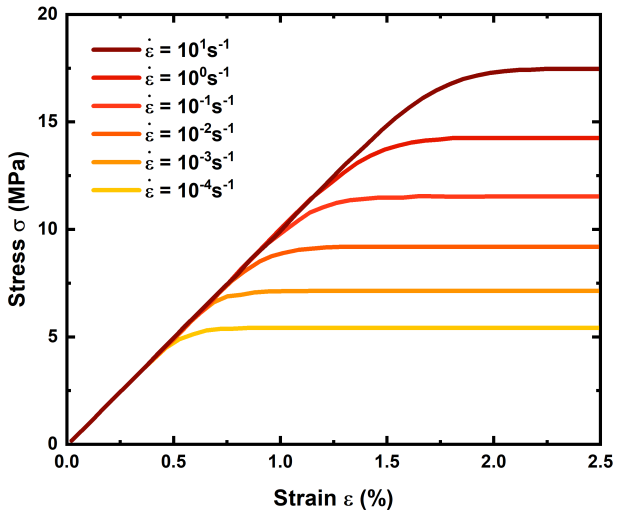

Figure 1.31: Stress-strain response at different strain rates from an elastomer containing fillers (taken from [130]).

1.4.4.1.1 Stress relaxation

In stress relaxation, a sample stressed by a tensile deformation ϵ_0 or a shear deformation γ_0 is studied. The decreasing stress is measured as a function of the time $\sigma(t)$ or $\sigma_{sh}(t)$ respectively. The link between the stress and deformation are given by the Young's modulus $E(t)$ and the shear modulus $G(t)$

$$E(t) = \frac{\sigma(t)}{\epsilon_0} \quad \text{and} \quad G(t) = \frac{\sigma_{sh}(t)}{\gamma_0} \tag{1.9}$$

The link between the two modulus is also given by:

$$E(t) = 2(1 + \nu(t))G(t) \tag{1.10}$$

With $\nu(t)$ the Poisson's ratio depending on the time.

1.4.4.1.2 Dynamic mechanical measurement

The classic creeps and stress relaxation tests are convenient for the study of a material response at long times (from minutes to days) but are not as accurate for effects happening at shorter times (of

the second order or less). The dynamic tests consist in applying a sinusoidal stress or strain to obtain the short-time range of the studied polymer response. When a viscolelastic material is put under a sinusoidally varying stress, the resulting strain reaches a steady state at some point. The strain also vary sinusoidally with the same angular frequency but retarded in phase by a δ angle called the loss angle. If the deformation is sinusoidal the stress and strain are given by:

$$\epsilon = \epsilon_0 sin(\omega t) \quad \text{(tensile strain)} \tag{1.11}$$

$$\sigma = \sigma_0 sin(\omega t + \delta) \quad \text{(tensile stress)} \tag{1.12}$$

With:

ϵ_0 : The amplitude of the sinusoidal tensile deformation.

σ_0 : The amplitude of the sinusoidal tensile stress (N/m).

ω : The angular frequency (rad/s). It is equal to $2\pi\nu$ where ν is the frequency in Hz.

δ : The phase angle (rad).

Experimentally, the strain is obtained by measuring the difference between the length of the sample before and after the experiment:

$$\epsilon = \frac{l - l_0}{l_0} \tag{1.13}$$

With:

l_0 : the initial length of the sample

l : the length of the sample after the experiment

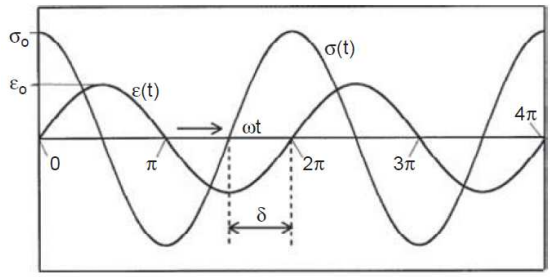

Figure 1.32: Sinusoidal strain and stress with phase angle δ (taken from [131]).

Dynamic modulus

The dynamic modulus is measured via multiple techniques like dynamic mechanical analysis (DMA) or dielectric relaxation spectroscopy (DRS) by applying a small oscillatory stress and measuring the resulting strain.

- For a purely elastic material the stress and strain are in phase, meaning the response of stress to strain or the other way around is immediate ($\delta = 0$)
- For a purely viscous material the strain lag stress by a $\delta = \pi/2$ phase
- A viscoelastic material exhibit behaviour somewhere in the middle of these two types of material ($0 < \delta < \pi/2$).

The behaviour of a linear viscoelastic material is a mix between that of an elastic solid symbolized by a spring with a modulus E (or G) and that of a Newtonian viscous liquid represented by a dash pot with a viscosity η. The material elasticity confers it a capacity to conserve and restitute energy after deformation. The viscosity of the material on the other hand, regards the capacity to dissipate energy. The complex dynamic modulus $G*$ is used to represent the relation between the oscillating stress and strain:

$$G^* = G' + iG'' \tag{1.14}$$

With: G' the storage modulus and G'' the loss modulus

$$G' = \frac{\sigma_0}{\epsilon_0} cos\ \delta \tag{1.15}$$

$$G'' = \frac{\sigma_0}{\epsilon_0} sin\ \delta \tag{1.16}$$

From this it is possible to obtain the loss factor $tan\,\delta$ which represents the dissipated energy during a loading cycle. The higher the $tan\ \delta$, the more energy is dissipated by the material.

$$tan\ \delta = \frac{G''}{G'} \tag{1.17}$$

Since the glass transition is accompanied by a large energy dissipation a peak in the $tan\ \delta$ depending on the temperature is indicative of the glass transition phenomenon.

1.4.5 Non-linear viscoelastoplasticity

Due to the different effects taking place in viscoelastoplastic materials, most of the properties exhibited by this class of material are non-linear. The non-linear nature of these effects imposes the use of models that take the different mechanical response of these materials into account. Two commonly encountered non-linear effects are the Mullins and Payne ones, used to describe the variation of the mechanical properties of filled elastomers under low and high strains. Both of these effects are described more in depth in appendix E

1.4.6 Elastomers under high stress rate

Elastomers are widely used in the industry thanks to their viscoelastic properties. Due to their flexibility and broad range of formulation, it is possible to tailor the elastomers, to some extent, to the use required. Today, elastomers can be found in areas as diverse as: Insulating materials [140], seals [141] or shock absorbers through their magnetorheological properties [142, 143]. The key factor of each of these application lies in the mechanical hysteresis of the elastomer used and the associated energy dissipation. The cause of the energy loss is the transition of an elastomer of interest from a rubbery state to a glassy state under defined condition of strain rate, pressure and temperature. If said condition are met the elastomer goes beyond the rubbery plateau and starts to exhibit a leathery behaviour to which is associated a large energy dissipation [144]. This type of effect can be induced by high strain rate and/or pressure. In the case of laser shock peening both of these solicitation are present and can induce property changes in the polymer during the laser shock such as the dynamic glass transition phenomenon.

1.4.6.1 Dynamic glass transition

The glass transition temperature is the usual quantity used to delimit the rubbery regime from the glassy one and is described as a temperature where a loss of molecular mobility is observed. It is caused by a loss of thermal energy and an increased molecular packing. When an elastomer is put under high strain rate or pressure the transition to a glassy state cannot be only explained by the

temperature anymore. Under such conditions a shift of the glass transition temperature depending on the strain rate and pressure applied is observed. To take into account the rate dependent aspect of the phenomenon, the glass transition temperature can be defined as the temperature at which the polymer chains mobility under the stress or strain applied becomes significantly slower than the time scale of the experiment. If this condition is respected the polymer chains becomes unable to move during the time of interest, thus leading to a glassy state since the chain are "frozen" [145]. When an elastomer passes to the glassy state, the mechanical energy absorption increases drastically. The mechanical properties also evolve. In the case of a rubber, the Young's modulus goes from tens of MPas to the GPa order. Multiple experiments exist to study material under a broad range of strain rates, from 10^{-8} s^{-1} with creep experiment to 10^{8} s^{-1} in the case of some shocks [146]. The classical experiment used to obtain the behaviour of materials under high strain rate is the Hopkinson bar test ($< 10^{5}$ s^{-1}) [147, 148]. Laser shock produces strain rates even higher ($> 10^{6}$ s^{-1}) while also applying pressure of the GPa order on the shocked material [43].

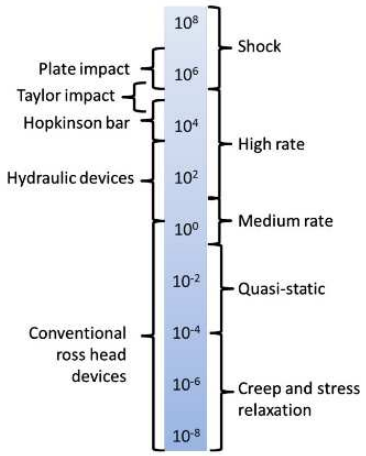

Figure 1.33: Experiments used to investigate different strain rates (taken from [146]).

1.4.6.2 Pressure effect

The effect of pressure on the dynamic glass transition have been studied by Zoller [149, 150] who found a linear correlation between the glass transition temperature and the pressure applied:

$$T_g(P) = T_g(0) + s_g P \tag{1.18}$$

s_g represents the shift in glass transition temperature per MPa of pressure applied. For example the average $s_g = 0.23$ K.MPa^{-1} for polystyrene means that and increase of ≈ 4 MPa will shifts the T_g by around 1 °C. More values for different polymers were given by Aharoni [151] and are reported in table 1.2:

Table 1.2: Changes in T_g of some amorphous and semi-crystalline polymers as function of applied pressure (taken from [152]).

Polymer	**T$_g$ (°C)** (at 1 atm)	**P** (MPa)	**T$_g$ (°C)** (at P MPa)	**s$_g$** (K.MPa^{-1})
Polystyrene	108	100	131	0.23
Polystyrene	100	200	182	0.41
Poly(methyl methacrylates)	103	100	121	0.18
Poly(vinyl chloride)	75	100	89	0.14
Poly(vinyl acetate)	32	80	49	0.21
Amorphous poly(etylene terephtalate)	70	100	93	0.23
Semi-cryst poly(etylene terephtalate)	70	100	93	0.23
Poly(butylene terephtalate)	0.69	200	89	0.10
Polyamide-6	52	200	99	0.24
Polyamide-6,6	60	200	109	0.25
Polyamide-6,9	60	200	102	0.21
Flexible aliphatic polymers (in general)	/	/	/	≈ 0.20
Amorphous polymers (in general)	/	/	/	≈ 0.28
Semi-cryst polymers (in general)	/	/	/	≈ 0.20

1.4.6.3 Strain rate effect

The strain rate of the experiment or treatment applied on an elastomer can have an effect on its glass transition temperature and induce a dynamic glass transition. Dynamic Mechanical Analysis (DMA) or Dielectric relaxation spectroscopy (DRS) are tools of choice to study the effect of high strain rate on materials thanks to the frequencies attained by the two techniques (≈ 100 s^{-1} for DMA and higher than 10^9 s^{-1} for DRS. The difference with laser shock experiment which produces deformation of the 10^6 s^{-1} range is that during laser shock, the strain is considerably higher than what is achieved during DMA or DRS experiment. Another point is that laser shot induces the production of a large pressure that influences the behaviour of the shocked materials while the pressure during DMA or DRS is low. Figure 1.34 shows the effect high strain rate (in the form of a high frequency applied through DRS experiment) on molecular mobility and by extension, the glass transition temperature of amorphous Poly(ethylen-vinyl acetate) (PVAc) [153]. The results show a shift of the T_g to higher

temperature along the increase of the strain rate. (from ≈ -10 °C at $\dot{\epsilon} = 10^{-1}$ s^{-1} to ≈ 60 °C at $\dot{\epsilon} = 10^{6}$ s^{-1}).

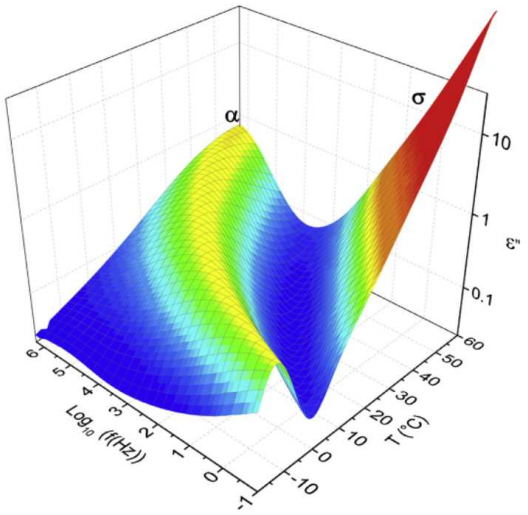

Figure 1.34: 3-D plot from a DRS analysis for EVA70: dielectric loss (ϵ") versus frequency (f) and temperature (T) (taken from [153]).

Time-Temperature Superposition

The Time-Temperature Superposition (TTS) is used to describe the viscoelastic behaviour of linear polymers over a broad range of times. Mechanical experiments such as DMA or DRS are realised at a set frequency and different temperatures. Each curve is then translated by a factor a_T to produce a mastercurve that covers a wide range of frequencies. The shift factor is expressed by using an Arrhenius equation and the Williams-Landel-Ferry (WLF) equation [154].

$$log(a_T) = \frac{-C_1(T - T_r)}{C_2 + (T - T_r)} \tag{1.19}$$

With:

T : the temperature

T_r : the reference temperature chosen for the master curve C_1 and C_2 : empirical constants

The Time-Temperature Superposition can be interesting to study the behaviour of material under high strain rates like the one that are observed during laser shock peening (≈ 10^6 s^{-1}). It can

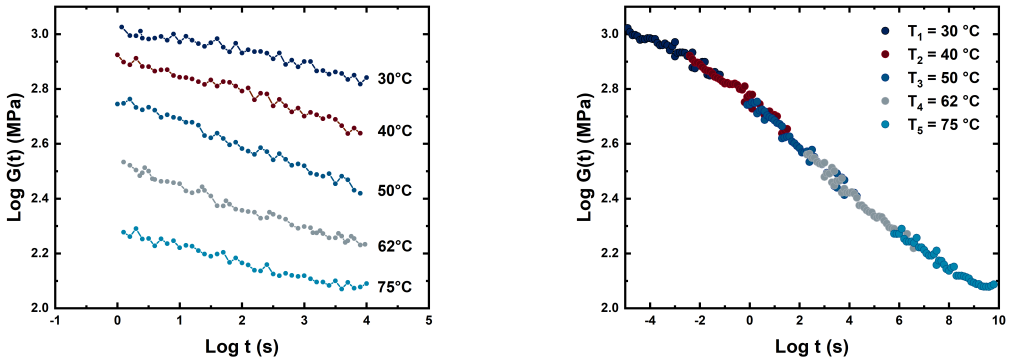

(a) (b)

Figure 1.35: (a) Segments of shear relaxation modulus at different temperatures, (b) master surve of shear relaxation modulus at reference temperature for Polyamide-6 (taken from [155]).

also be used the other way around to predict the behaviour of a viscoelastic polymer at really low temperature by doing experiments at high frequency. Although the use of DRS compared to DMA appears to be largely preferable considering its extensive frequency range, the set-up is more complex and the apparatus more difficult to find. The last problem lies in the treatment of the data which is also more complex with DRS through the use of the Havriliak-Negami model to treat the data and extrapolate the results to an even higher range of frequency and temperature [156, 157]. For these reasons DMA experiments are a lot more common to find in the literature.

1.4.7 Model to describe elasticity

To model the mechanical behaviour of elastomers, hyperelastic models are often used. These model are able to describe the behaviour of a material at large strains. A plethora of models exist to describe this type of material behaviour but all the models are phenomenological. A list of some of the existing models is given in table 1.3:

Table 1.3: List of hyperelastic models sorted by their year of publication and number of material parameters (partially taken from [158]).

Model	**Year**	**Number of material parameters**	**Reference**
Mooney	1940	2	[159]
Neo-Hookean	1943	1	[160, 161]
3-chains	1943	2	[162]
Ishihara	1951	3	[163]
Biderman	1958	4	[164]
Gent and Tomas	1958	2	[165]
Hart-Smith	1966	3	[166]
Valanis and Landel	1967	1	[167]
Ogden	1972	6	[168]
Haines-Wilson	1975	6	[169]
Slip-link	1981	3	[170]
Constrained junctions	1982	3	[171, 172]
van der Waals	1986	4	[173]
Arruda-Boyce	1993	2	[174]
Gent	1996	2	[175]
Yeoh and Fleming	1997	4	[176]
Tube	1997	3	[177]
Extended-tube	1999	4	[178]
Shariff	2000	5	[179]
Micro-sphere	2004	5	[180]
Khajehsaied	2013	3	[181]
Külcü	2020	2	[182]

Usually the most used ones are the Neo-Hookean, Mooney-Rivlin, Ogden and Arruda-Boyce models as their are implanted in most Finite Element Modelling (FEM) softwares. Figure 1.36 gives an example of the fit between experimental data and simulated ones with the Arruda-Boyce model:

1.4.8 Model to describe glassy polymers

A glass is by definition rigid and should resist plastic deformation. Cohen and Turnbull showed that an ideal glass have zero entropy [183]. This affirmation means that there is only one configuration accessible to the glass or that the energy needed to pass to another configuration would have an activation barrier of nearly infinite energy. In practice the configurational entropy of a glass is never zero as it has been shown by calorimetric measurements [184]. The classic definition of polymer under glassy state is that its chains are frozen so the position of each atoms stays constant over any time

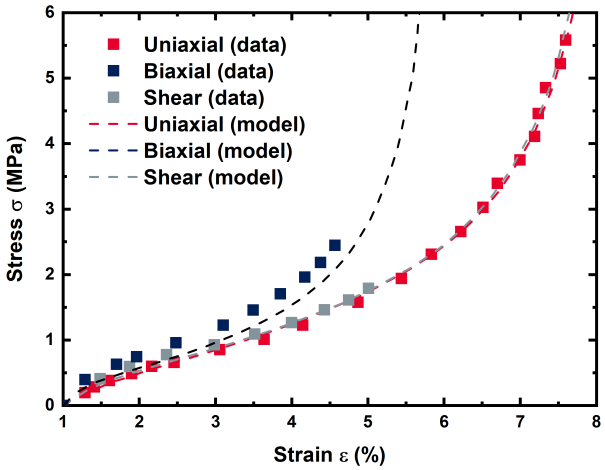

Figure 1.36: Results of simulations using the eight chain model versus data in uniaxial extension, biaxial extension and shear (taken from [174]).

interval even if in practice a glass is considered to be a material in a metastable state but with a needed time to rearrange itself far too big to be taken into account. The rigidity of a glassy structure steams from van der Waals and dipolar forces between neighbouring chains coupled with intramolecular forces. These forces block the rotation of backbone bonds thus increasing the segments over which intermolecular forces can act by blocking rearrangements. Some models exist to describe these effect like the one developed by Boyce in 1988 [185].

In the materials of interest for this study, a complete model would need to include an elastic part at the beginning of the loading and then a plastic part when the pressure and strain rate go up. The relaxation time of the polymer chains would also be needed to accurately represent the deformation of an hyperelastic material under these specific conditions. No model has been found in the literature to represent this type of interaction as of now.

1.5 Conclusion on the needed properties for the confinement

This chapter showed the different phenomena involved during the laser shock peening process and their effect on the target and polymer confinement chosen. It also presents the specifications needed for the polymer confinement to be efficient as well as the laser parameters aimed for the LSP treatment. These specifications are summarized below:

Confinement polymer properties:

- Good pressure produced ($\approx$ 4 GPa)
- Good optical transmission
- Easy bonding/debonding
- Flexible
- Thermally resistant

Laser parameters:

- Laser spot $\leqslant$ 1 mm
- No thermal coating
- Fiber transportation
- 1064 nm
- High repetition rate

If all these specifications are met, the treatment of claustrated areas, impossible to treat with water confined LSP will be implementable. However, to reach a mature process, the first step is to reach sufficient pressure with a laser shot using polymer confinement to be able to induce high compressive residual stresses in the alloy treated. Secondly, a mastering of the process with polymer confinement necessitate an understanding of its behaviour under shock to optimize the process. The different tools and apparatus used for these characterizations and experiments are described in the next chapter.

Materials and methods

2 | Materials and methods

Content

2.1 Lasers . . . 94
2.1.1 Laser Description . . . 94
2.1.1.1 Héphaïstos . . . 94
2.1.1.2 Theïa . . . 95
2.1.2 Laser spot . . . 96
2.1.3 Pulse duration measurement . . . 96
2.1.4 Energy measurement . . . 98
2.2 VISAR . . . 98
2.2.1 Measurement principle . . . 100
2.2.2 PIMM's VISAR Setup . . . 101
2.2.3 Signals obtained by VISAR . . . 102
2.2.4 Advantages over other measurement techniques . . . 103
2.3 Numerical simulation . . . 104
2.3.1 Target geometry and boundary conditions . . . 104
2.3.2 Entry data . . . 105
2.3.2.1 Spatial profile . . . 105
2.3.2.2 Pressure profile . . . 106
2.3.3 Constitutive models . . . 107
2.3.3.1 Elasto-plastic . . . 107
2.3.3.2 Jonhson-Cook . . . 107
2.3.3.3 Mie-Grüneisen equation of state . . . 108
2.4 Material characterization . . . 110
2.4.1 Infra-Red spectroscopy . . . 110
2.4.2 Dielectric relaxation spectroscopy . . . 111
2.4.2.1 Principle . . . 111
2.4.2.2 Apparatus . . . 112
2.4.2.3 Data treatment . . . 114
2.4.2.3.1 Havriliak-Negami . . . 114
2.4.2.3.2 Vogel-Fulcher-Tammann . . . 114
2.5 Residual stresses measurement by XRD . . . 114

Introduction

This chapter describes the different materials, diagnostics and tools used for the different experiments realised during this PhD work. First, the two different lasers used for the laser shots are presented and described followed by a presentation of the measurement of their typical laser spot, pulse duration and energy measurements. In a second part, the velocity interferometer system for any reflector (VISAR), the main tool used for the laser shock characterization during this project work, is extensively described, from the measurement procedure and the physical principles involved to a description of typical signals collected. The description of the VISAR is closed by a description of the advantages of the technique compared to the other measurement techniques. The next part presents the numerical tools used for the simulation of the backface velocity profiles collected with the VISAR measurements. The description covers the target geometry and boundary conditions, the entry data and the consitutive model chosen for the simulations. A description of the material characterization tools is then presented. An extensive description of the dielectric relaxation spectroscopy is given completed with the Hariliak-Negami and Vogel-Fulcher-Tammann equations used for the data treatment. To finish, the chapter final part describes the residual stress measurements procedures chosen for the study of the materials treated by laser shock peening.

2.1 Lasers

2.1.1 Laser Description

2.1.1.1 Héphaïstos

Héphaïstos facility at PIMM laboratory (Laboratory for Processes and Engineering in Materials and Mechanics, Paris, France). The laser is a Gaïa HP laser from THALES (Elancourt, France) and is composed of two Nd:YAG synchronised lasers. Both lasers have a wavelength of 532 nm and deliver each up to 7 J of energy with a Gaussian temporal profile showing a Full Width Half Maximum (FWHM) of 7 ns.

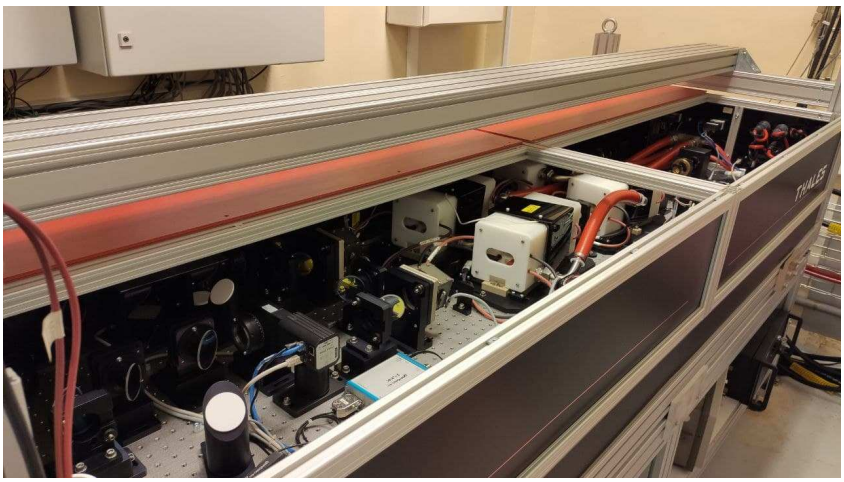

Figure 2.1: Gaïa HP laser used in the Héphaïstos facility.

2.1.1.2 Theïa

The Theïa laser is a Nd:YAG diode-pumped solid-state laser from Thales (Elancourt, France) working at a wavelength of 1064 nm. The energy delivered can go up 1 J with a Gaussian pulse duration varying from 6.9 to 21 ns at Full Width Half Maximum (FWHM) with a frequency of 200 Hz.

Figure 2.2: Theïa laser used in the Héphaïstos facility.

2.1.2 Laser spot

An accurate measurement of the laser spot size is crucial for the laser shock experiments and also for treatment. Since the entry information known from the laser is the energy, knowing the surface of the laser spot used is needed in order to correctly assess the laser intensity produced in GW/cm^2. This information is all the more important when small spots (typically < 1 mm) are chosen since the flux density vary way more with their size variation. Another important aspect when defining a laser spot characteristic is its homogeneity. In the case of the presence of surintensity, a breakdown plasma can be triggered at laser intensities lower than the breakdown threshold, the treatment can also be affected with large spots since the applied pressure resulting from the shock won't be evenly distributed throughout the spot surface. This effect is mitigated when small spots are used with the potential surintensities being mixed together due to the small spot size. Thanks to this, using laser spot sizes inferior to 1 mm does not necessitate the use of a Diffractive Optical Element (DOE) to obtain a fairly homogeneous energy repartition.

To homogenize laser spot with a size superior to 1 mm, a DOE is placed under the focusing lens. This type of lens is manufactured to have beam shaping properties while allowing the incident laser to retain its different properties such as beam size, polarization or wavelength. Figure 2.4 gives an example of the difference obtained with and without using a DOE on the Héphaïstos platform for fairly large spot.

To obtain the image of the laser spot a camera (Basler acA2040-25gm/ gc, Monochrome, CMOS 1" with a Pixel Size of 5,5 μm $\times$5,5 μm) is used, the camera is placed on the lasers trajectory at a defined focal length. To protect the camera, densities are used at the top of the focusing lens and before the camera entry. The last density also serves as a filter for the ambient light that could bring noise on the images. The measurement on the Théïa laser were done only with the use of a DOE. Figure 2.3c gives the laser spot profile used for the shot with a laser spot size of 1.2 mm.

2.1.3 Pulse duration measurement

The duration of the laser pulse used has an influence on the mechanical properties imparted in the material shocked. A longer pulse will induce a deeper plastification but will also have a lower breakdown threshold which will limit the maximum pressure produced by the laser shock process

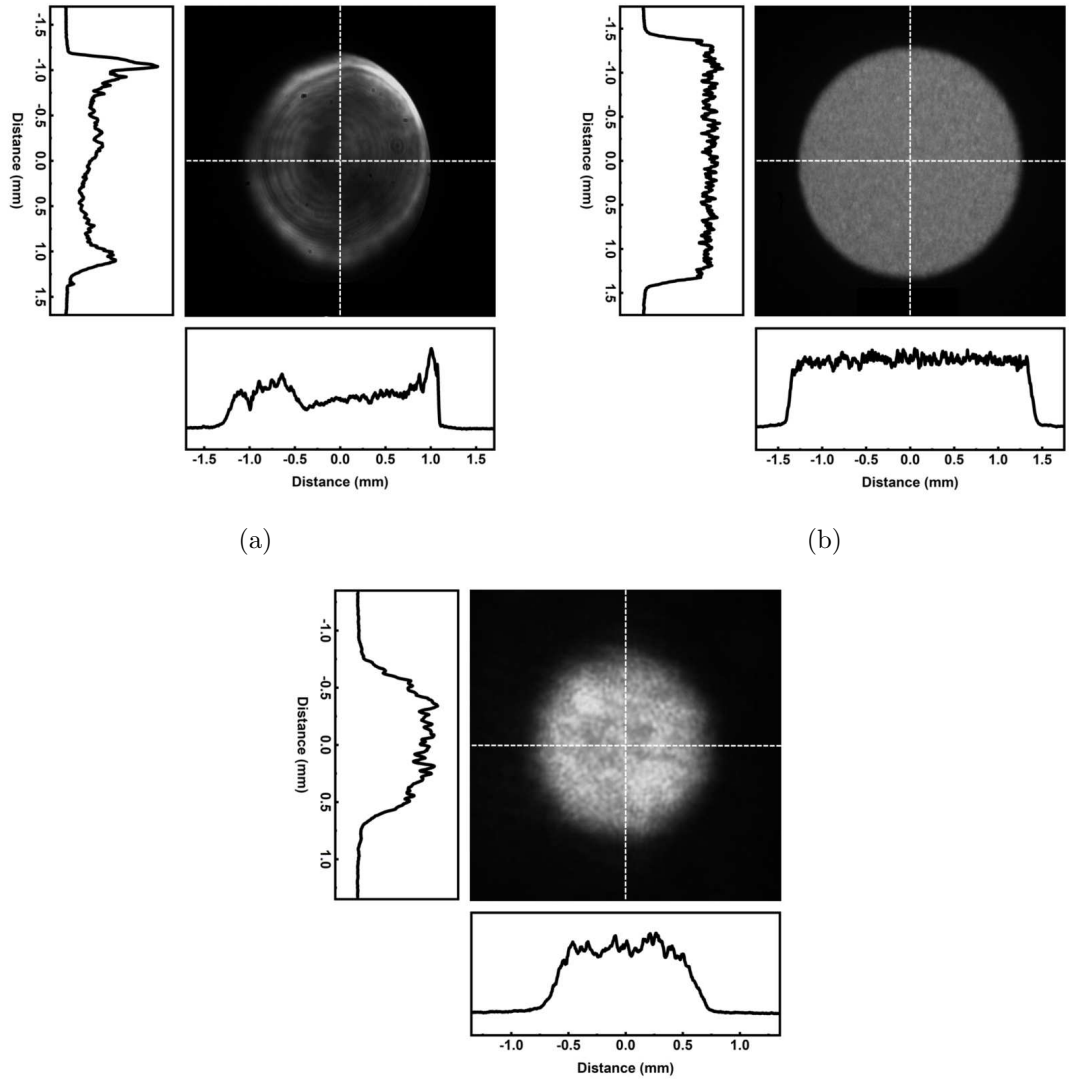

Figure 2.3: Laser spot profile obtained by direct camera measurement, 2D profiles are extracted with ImageJ software [186]. (a) Laser spot on the Héphaïstos laser without the use of a DOE. (b) Laser spot on the Héphaïstos laser with a DOE. (c) Laser spot with a DOE on the Théïa laser.

(see 1.2.2 and 1.2.3.1). The measurement of the pulse duration is done with a photodiode (Thorlabs DET10A1) located on the path of the laser before focalisation. The experiment was done on the Héphaïstos laser with one of the two beams and both of them to compare. The pulse duration was calculated at the Full Width at Half Maximum (FWHM).

The measured pulse duration was 7 ns, the measurements were made at each shot to take into

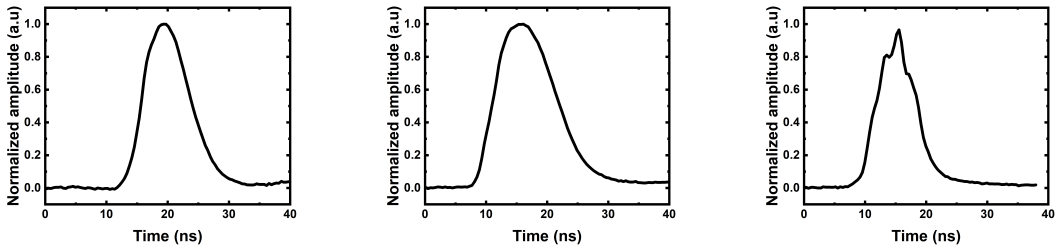

(a) (b) (c)

Figure 2.4: Laser pulse measured by photodiode on Héphaïstos laser, the intensity is normalized. (a) beam A, (b) beam B, (c) beam A+B.

account potential driftings of the result depending on the laser maintenance. The laser intensity did not have an influence on the pulse duration measured as normalized profiles at different laser intensities gave the same duration. In the case of the Théïa laser, two different pulse durations were used, respectively 9 and 21 ns to study the influence of this parameter on the pressure produced and on the breakdown phenomenon triggering.

2.1.4 Energy measurement

During a laser shot the energy delivered by the laser is given in the associated software piloting the laser. The measurement is done by an internal calorimeter inside of the laser so the values given do not take into account the optic path loss associated with the reflections of the laser pulse on the different mirrors to bring the pulse to the target. For example the loss through the last lens and DOE assembly is around 10% of the total energy. To calibrate the internal calorimeter, energy measurements are realised directly on the target after all optics. The energy is measured on the whole range of energy of the laser. Figure 2.5 give an example of a calibration on the laser with a slope of 0.914. A $\approx$ 10% correction is observed.

2.2 VISAR

Laser interferometry is a technique of choice to obtain the velocity versus time of a shocked object. The configuration usually used uses a laser beam reflected on the mirrorized surface of the shocked target. The laser shock induces a small shift in the laser wavelength. The reflected beam is separated in two, one part is delayed by a Michelson interferometer before being recombined with the other. It

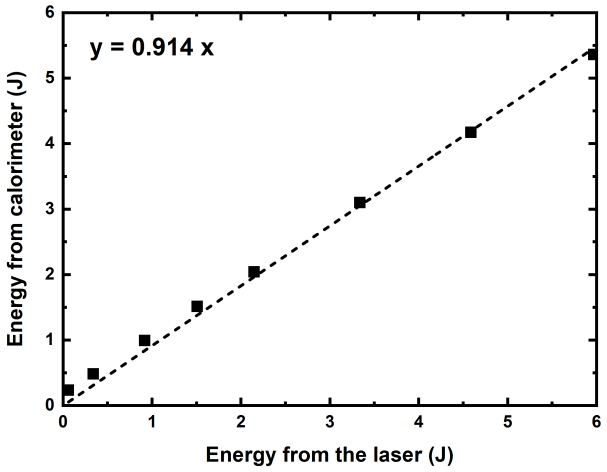

Figure 2.5: Result of the energy calibration showing the difference between the energy given by the laser software and the energy calculated at the surface of the material shocked for beam A of the Héphaïstos facility.

results in the light being combined with itself at a time $t - \tau$, with τ being the delay time. It it then possible to link the fringe count $f(t)$ to the target's surface velocity $u(t - \frac{1}{2}\tau)$ following the equation given by Barker [187].

$$u(t - \frac{1}{2}\tau) = \frac{\lambda F(t)}{2\tau(1 + \Delta\nu/\nu_0)(1 + \delta)} \tag{2.1}$$

With:

t: the time.

λ: the wavelength of the laser.

$(1 + \Delta\nu/\nu_0)$: a correction for the index-of-refraction variation with the shock stress if a transparent "window" material is used. If none is used $\Delta\nu/\nu_0 = 0$.

$(1 + \delta)$: a correction factor which is a function of the refraction index of the etalon material and of the laser wavelength.

The problem of most laser interferometry technique lies in that it needs very little surface tilt from the target. Another problem is the need of a mirrorized surface on the backface on the sample due to the different length of the two branches of the interferometer which can cause spatial incoherence

in the laser beam. Due to these limitations, high velocity impacts where difficult to study up to the apparition of the VISAR (Velocity Interferometer System for Any Reflector) [188].

This system allowed for the use of a diffuse specimen surface thank to the fact that the two legs of the interferometer were now appearing to be the same length. With this new setup the use of diffuse specimen surface also make the system nearly insensitive to tilting. This setup is based on the use of the WAMI (Wide Angle Michelson Interferometer) configuration [189] which allows for an easier observation of the fringe patterns with low light levels (i.e. diffuse light). A particularity of this VISAR is the monitoring of two fringes signals which are 90° out of phase thanks to a polarizer. A quarter-wave plate is then used to retard the P component of the light by a phase angle of 90° compared to the S component. This leads to a circular polarization on the oscilloscope as shown of fig. 2.6.

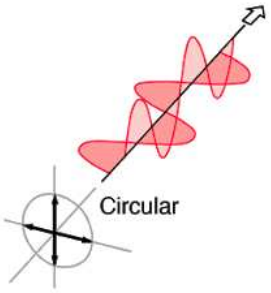

Figure 2.6: Circular light polarization used on the VISAR setup

This configuration leads to the formation of two 90° out-of-phase fringe pattern when the P and S components are reunited. The recording of two signals 90° out-of-phase is very important because if the interferometer's output light intensity I versus the fringe count F is plotted, it will take the form of a sine wave. Because of that at the maximum and minimum of the wave ($dI/dF = 0$) a slight change in the fringe count will not be noticeable. By having a 90° out-of-phase fringe pattern if a point is situated on a minimum or a maximum of the sine wave it will be in a region of good resolution on the other fringe pattern. This method also permits to discriminate between acceleration and deceleration.

2.2.1 Measurement principle

As said before, the VISAR allows for the measurement of the Doppler shift of a laser wavelength on the backface of a target moved by a shockwave. This shockwave is travelling through the thin target

from the front face of the material where the laser shock created a plasma release which produced a shockwave. The speed of the backface is linked to the wavelength shift following:

$$\lambda(t) = \lambda_0(1 - 2\frac{u(t)}{c}) \tag{2.2}$$

With:

- λ_0: The initial wavelength of the probe laser (in this case 532 nm)
- $u(t)$: The material speed in function of the time
- c: The speed of light

The fringe scrolling $F(t)$ produced by the interferometer is linked to the speed following:

$$u(t) = K.F(t) \tag{2.3}$$

- K: The fringe factor in $m/s/fringe$, determined by the length of the etalon standard on the second arm of the setup since the signal is interfering with itself, refelcted at a time $t - \tau$. Each fringe corresponds to a predetermined increment of speed K.
- $F(t)$: The fringe count

The fringe factor can also be linked directly to the initial laser wavelength λ_0 and the delay τ which is directly linked to the length of the etalon standard used:

$$K = \frac{\lambda_0}{2\tau} \tag{2.4}$$

2.2.2 PIMM's VISAR Setup

PIMM'S VISAR is based on the one from Barker [188, 187] with some added modifications from Tollier [190, 191]. The VISAR's setup is given in figure. 2.7. The system is composed of a VERDI probe laser (5W, 532 nm). This laser is reflected at the surface of the target and is then directed through the optic fiber through a mirror with a hole. At the beginning of the VISAR the beam is

polarized and then goes through a beam splitter to be separated and sent in the two arms of the VISAR. The first arm is between the phase plate and the M1 mirror is the reference branch. The wave goes through it at a time t. The polarizer and the $\lambda/8$ plate are used to create two interference system 90° out-of-phase. The second arm is between the phase and the mirror M2 and is the delay branch. The standard used in it is a BK7 glass standard with an optical index superior to the one of air. It is use to delay the wave by a time τ (so it allows changing K) which depends on the length of the used standard. The mirror M3 is used to direct the recombined waves in another beam splitter to send each 90° out-of-phase interference system in a distinct photomultiplicator PM1 and PM2.

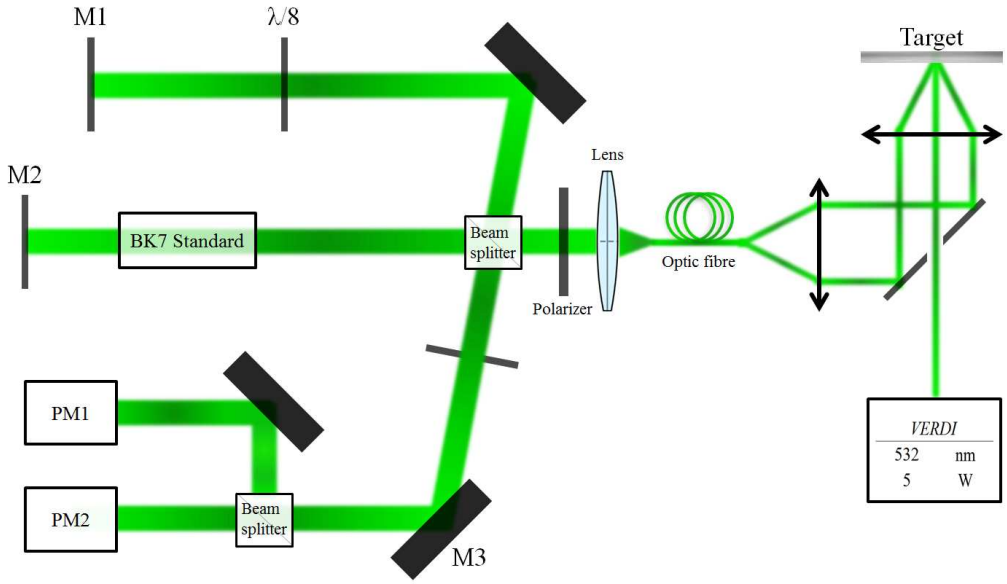

Figure 2.7: Schema of the PIMM's VISAR principle

2.2.3 Signals obtained by VISAR

The signals obtained from the two photomultiplicators are not directly useable and need to be treated through à Python code called PVisar. An example of signals obtained is given in figure. 2.8a.

The result obtained once the data are treated through PVisar is given in figure. 2.8b. The two main peaks show the wave going back and forth in the material shocked while the first one near 0 ns is the photodiode seeing the laser pulse.

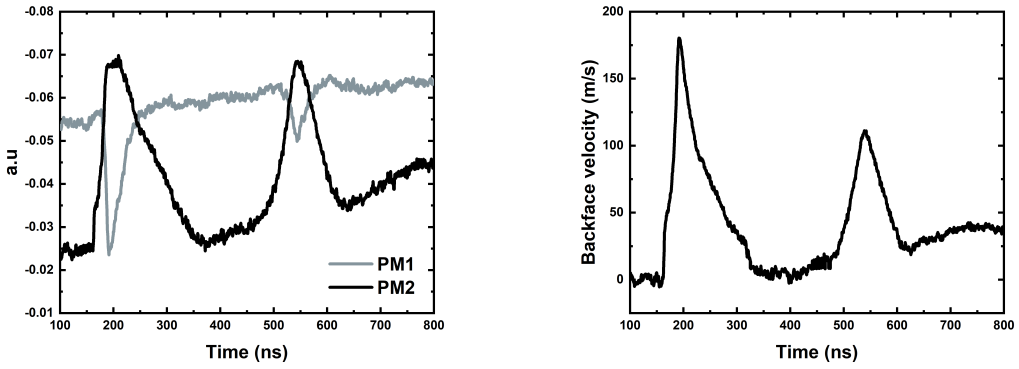

(a) (b)

Figure 2.8: (a) Signal obtained by VISAR on an aluminium target, 1 mm thick, solid acrylate confinement, shot with a Gaussian 7.5 ns pulse, a 3.74 mm laser spot and an intensity of 2.08 GW/cm^2. (b) Free surface speed profile corresponding to the signals shown in (a).

2.2.4 Advantages over other measurement techniques

Apart from VISAR other methods can be used to measure the backface speed of a target after a shock. Two main methods were used before the VISAR, namely the PVDF captor and the EMV gauge.

- The PVDF captor is a piezoelectric captor. It has a stronger response than a classical quartz piezoelectric. The drawback of this type of captor lies in that it has to be in contact with the shocked target. The pressure measured by this type of captor is also limited to around 13 GPa.
- The EMV gauge is another option but the electromagnetic field is difficult to measure during the shock, leading to bigger uncertainties than with VISAR.

VISAR measurement has some pro and cons but is overall the best technique when it comes to backface speed acquisition during laser shock.

- Cons: The target needs to diffuse the light. The signals obtained need to be post processed in order to be of use. The probe laser can in some cases (when working with epoxy for example) damage the target or specifically with polymers, post-cure them. Last, VISAR measurement is not adapted for short pulses (<1 ns) and/or sharp front shock rise ($\approx$ hundreds of ps) due to the response time of the photomultiplicators used)

- Pros: VISAR measurement is a non-contact method which only depends on the target properties and with no pressure measurement limit as long as the length of the etalon standards useable is large enough.

2.3 Numerical simulation

For the simulation of the different experiments the finite element analysis software Abaqus was used [192]. The modelling of the different shock experiment allows confronting the results obtained with the finite element modelling associated but also to extract supplementary information. For example with the accurate simulation of a backface velocity profile from a VISAR measurement it is possible to extract the pressure produced by the shock on the front face of the shocked material. For all the simulation, an axisymmetric model was used in order to reduce the computation time. Laser shock is well indicated for this time of simplification since the laser spot is round although it once again highlights the need of a good beam quality to have the same loading during the shock at each point of the area illuminated.

2.3.1 Target geometry and boundary conditions

The materials modelled used CAX4R (4-node bilinear axisymmetric quadrilateral, reduced integration, hourglass control) elements except for the residual stresses simulation where infinite elements were also used outside of the interest area to avoid the shockwave going back and forth. In this case the elements chosen were CINAX4 (4-node linear axisymmetric one-way infinite quadrilateral). The mesh used was finer in the area of interest with a size of 1 μm x 1 μm. outside of the area of interest a BIAS function in the X direction was used to reduce the time of calculation. For the boundary condition, the bottom right corner of the modelled materials, opposed to the shocked area was fixed to represent the sample holder used during the experiment. Figure 2.9 shows the typical geometry of a target used for the simulation of the laser shock peening process. Figure 2.10 gives a typical mesh used for the finite element modelling of a single pulse laser shock process.

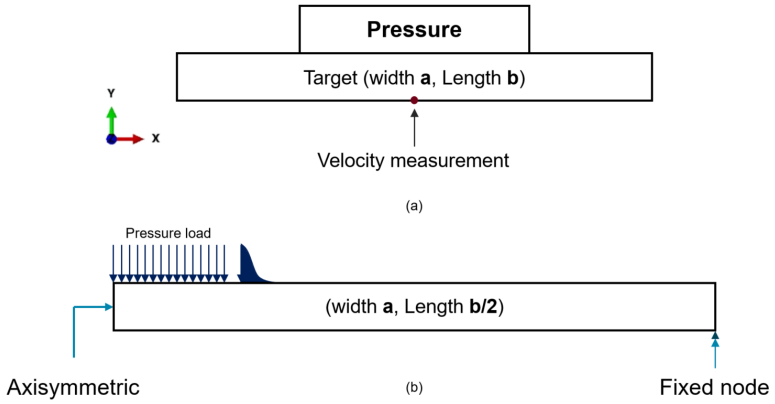

Figure 2.9: (a) typical target geometry used for LSP simulation, (b) 2D axisymmetric Finite Element model.

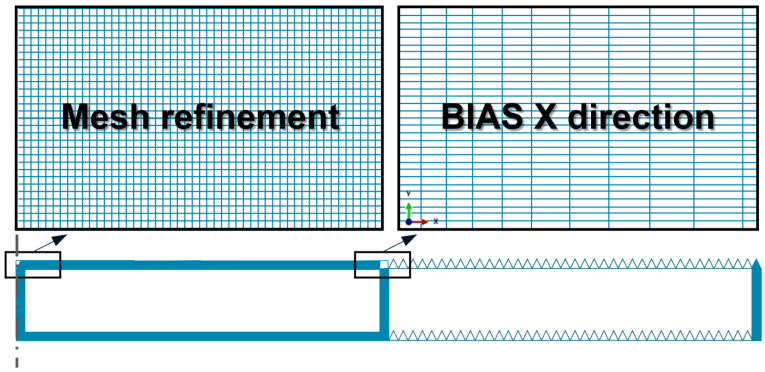

Figure 2.10: Typical mesh refinement used for the LSP simulation.

2.3.2 Entry data

2.3.2.1 Spatial profile

The spatial profiles were produced by filtering real laser spot profiles measured with a camera (Basler acA2040-25gm/ gc, Monochrome, CMOS 1" with a Pixel Size of 5,5 μm $\times$5,5 μm). The filter used was the Butterworth filter from python [193, 194]. The filtering is used to avoid errors during the calculations as with the local oscillations observed at the top of a classic laser spot profile that can induce multiple pressure in one cell causing the calculation to crash. The "flattening" of the top of the laser spot profile is also justified by the fact that at the beginning of the plasma creation, the incident laser energy is absorbed uniformly by the plasma thus justifying the approximation. Figure 2.12 shows the difference between a laser spatial profile before and after filtering for a 1 mm spot.

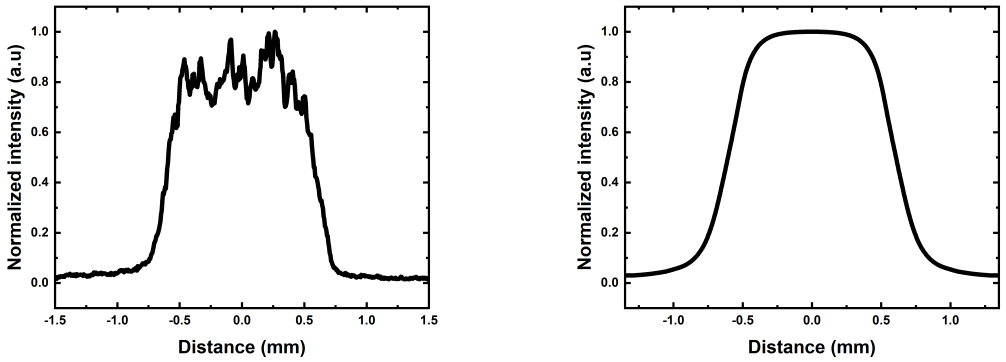

(a) (b)

Figure 2.11: (a) non filtered laser spatial profile obtained from a 1 mm laser spot with camera imaging and treatment via imageJ software. (b) Filtered laser spatial profile obtained with the Butterworth filter through a Python code and used for the simulation.

2.3.2.2 Pressure profile

The pressure profiles used for the simulations were either generated from a VDLOAD subroutine at the beginning of the PhD work or through a Python code using the one developed M. Scius-Bertrand et al. in [195] for laser irradiationat 532 and 1053 nm. The pressure profiles generated from the VDLOAD subroutine are normalized in intensity, the loading is then adjusted on Abaqus to accurately represent the backface velocity profile simulated. The same method is applied with the profiles generated from [195] work even if in most case the pressure obtained before normalization is close to the one obtained after varying the loading by inverse method. For each shot a pressure profile is generated and the loading adapted to be able to accurately reproduce the back face velocity profile. Figure 2.12 shows a typical pressure profile generated through the Python code for a 7 ns Full Width half Maximum (FWHM)shot and a profile obtained with the code, adapted in the paper for a 1053 nm, 7 ns FWHM interaction with a laser intensity of 4.05 GW/cm².

The difference between the two profiles is explained by the pulse shape of the lasers used. Figure 2.12a uses the Héphaïstos laser which produces Gaussian pulses while the GCLT laser used in the study for the code uses Top-Hat pulses.

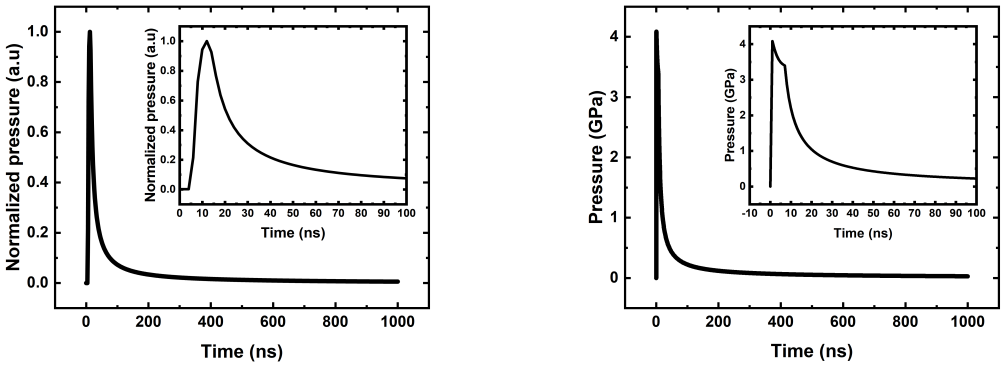

(a) (b)

Figure 2.12: (a) Normalized pressure profile obtained with the Python code for a 7 ns FWHM, 532 nm Gaussian pulse laser shot (b) Pressure profile obtained with the Python code for a 7 ns, 1053 nm, 4.05 GW/cm^2 top-hat pulse laser shot.

2.3.3 Constitutive models

Multiple constitutive models exist to describe the behaviour of metals and viscoelastic materials. In this manuscript the metals and alloys used where mainly pure aluminium (99.0%) and aluminium 7175-T7351. The polymers modelled were epoxies. The values for the simulations were either obtained from previous studies realised by other researchers and post-doc or directly taken from Abaqus or material characterization. For the epoxies, general values were taken the same way but are subject to more possible errors as the diversity or epoxies is broad with varying Young's modulus and densities.

2.3.3.1 Elasto-plastic

An elasto-plastic model is an easy-way to represent the behaviour of metallic material under laser shock since the loading is considered uniaxial. The model is constituted of few parameters, in this case only four: the Young's modulus E, the density ρ, the Poisson's coefficient ν and the yield stress σ_Y to represent the behaviour of the material modelled under loading. This type of model by itself induces some error compared to the others presented after and moreso when they are coupled together.

2.3.3.2 Jonhson-Cook

The Jonhson-Cook constitutive law is classically used to describe laser shock experiments. Compared to other models it takes into account the strain rate, strain-hardening and temperature effects.

It is also easily accessible since it is directly implemented in Finite Element Modelling (FEM) softwares such as Abaqus and LS-Dyna and finally it can be coupled with Equation of State to refine the results. Another main advantage is the fact that the parameters needed are generally easily available and if not, can be obtained through multiple experiments: torsion tests at different strain rates, static tensile tests or Hopkinson bar tests at ambient and high temperature.

The model defines a Von mises yield criterion (equivalent to the yield strength σ_y) with the equation:

$$\sigma = (\sigma_y + B\epsilon_p^n)\Big(1 + Cln\Big(\frac{\dot{\epsilon}}{\dot{\epsilon}_0}\Big)\Big)\Big(1 - \Big(\frac{T - T_0}{T_{melt} - T_0}\Big)^m\Big) \tag{2.5}$$

With:

σ_y: Yield stress

B: Strain hardening modulus

ϵ_p: Equivalent plastic deformation

n: Hardening coefficient

C: Strain rate sensitivity

$\dot{\epsilon}$: Strain rate during the experiment

ϵ_0: Reference strain rate

T_0: Room temperature

T_{melt}: Fusion temperature

m: Thermal softening coefficient

The first part of the equation describes the strain hardening effect, the second characterizes the strain rate effect and the last part is used to take into account the stress evolution with temperature during the plastic deformation. The thermal is not used in the modelling of this manuscript. Preliminary simulation were made in [196] and showed that the local temperature increase caused by the plastic deformation and the shockwave propagation did not have a noticeable influence on the backface velocity profile results obtained from the modelling.

2.3.3.3 Mie-Grüneisen equation of state

The Mie-Gruneisen equation of state is an equation of state that link pressure and volume in a solid at a defined temperature. It is generally used in a solid to determine the pressure during a shock. The equation stem from the Grüneisen model used to describe the effect of a crystal lattice volume variation on its vibrationnal properties. The basic Mie-Gruneisen equation is as follow:

$$\Gamma = V\left(\frac{dp}{de}\right)_V \tag{2.6}$$

With:

Γ: The Grüneisen parameter, representing the thermal pressure from a set of vibrating atoms.

V: Volume

P: Pressure

e: Internal energy

With the assumption that Γ is independent from p and e the Grüneisen model can be integrated to obtain:

$$p - p_0 = \frac{\Gamma}{V}(e - e_0) \tag{2.7}$$

With:

p_0: Pressure at a reference state (T = 0 K)

e_0: Energy at a reference state (T = 0 K)

With this assumption, the value of p_0 and e_0 is decorrelated from the temperature and their value can be estimated trough the Hugoniot equations.

Hugoniot equations

The Hugoniot equation governs energy, momentum and mass with the three equations:

$$E_H - E_0 = \frac{1}{2}(P_H + P_0)(V_0 - V) \tag{2.8}$$

$$P_H - P_0 = \rho_0 u_s u_p \tag{2.9}$$

$$\rho(u_s u_p) = \rho_0 u_s \tag{2.10}$$

With:

E: the specifc internal energy

P: the pressure

V: the volume

u_s: the shockwave velocity

u_p: the particle velocity

ρ: the density

The relation between the shockwave velocity u_s and the particle velocity u_p can be expressed linearly by:

$$u_s = C_0 + Su_p \tag{2.11}$$

With C_0 the sound velocity, meaning the speed of an elastic wave in the material and S the Hugoniot constant specific to the material. The particle velocity u_p is obtained through the maximum speed of a backface profile measured with a VISAR while the shockwave velocity u_s is extracted from the same backface velocity profile by calculating the time between two peaks corresponding to the shockwave going back and forth in the material shocked. Databases of material parameters exist for the Mie-Gruneïsen equation of state and can be found at [197, 198]

2.4 Material characterization

2.4.1 Infra-Red spectroscopy

Infra-red (IR) spectroscopy consists in identifying the energy level change when radiation passes through the material. It allows for the identification of chemical groups through the characteristic vibration of their covalent bond under irradiation. This technique is a good way of monitoring the polymer damaging via the reduction or apparition of certain bands, characteristic of broken bonds and the new groups attaching to them. Each molecule absorbs frequencies characteristic of their structure. When the IR radiation frequency is equal to the frequency of a chemical bond, the molecule absorbs the radiation, causing a band on the IR spectra. The information obtained is the transmitted light which allows the calculation of the transmitted energy at a specific wavenumber.

2.4.2 Dielectric relaxation spectroscopy

The Dielectric Relaxation Spectroscopy (DRS) experiments were realised with an Alpha Analyzer from Novocontrol Technologies GmbH while the temperature was controlled with a stability of ± 0.5° C with a Quatro Cryosystem (Novocontrol Technologies GmbH). The experiements were realised at GPM (Groupe de Physique des Matériaux) at university of Rouen by Clément Fosse who also did the fitting of the plots. The experiment under pressure was performed by Abdoulaye Soumaila Sounakoye. The experiment were used as a mean to obtain information on the strain rate and pressure effect on the physical state of the different polymers that were studied.

2.4.2.1 Principle

Dielectric relaxation spectroscopy is used to measure the dielectric properties of a material depending on the frequency applied. The external field created by the experiment interacts with the material's dipoles moment. Generally, the dielectric properties are represented by the permittivity ϵ through Maxwell's equation:

$$\epsilon^*(\omega) = \epsilon' - i\epsilon'' \tag{2.12}$$

ω represents the angular pulsation ($\omega = 2\pi f$ with f the frequency). A peak in the imaginary part of the permittivity ϵ'' is characteristic of the dynamic glass transition that induces segmental relaxation of the chains. Another way to represent the dynamic glass transition is through the calculation of the loss factor using:

$$tan\ \delta = \frac{\epsilon''}{\epsilon'} \tag{2.13}$$

In practice the DRS apparatus is going to measure the complex impedance Z^* of the system studied. The measured value will be the intensity I_0 at same frequency (ω) than U_0 but with a phase angle δ.

$$Z^* = \frac{U^*}{I^*} \tag{2.14}$$

With $U^* = U_0$ and $I^* = I' + iI''$. The two components of the complex intensity are then determined with the intensity I_0 obtained from the measurement at a phase angle δ:

$$I_0 = \sqrt{I'^{\,2} + I''^{\,2}} \tag{2.15}$$

$$tan\ \delta = \frac{I''}{I'} \tag{2.16}$$

To link these values with the permittivity to accurately describe the dielectric properties of the material studied, the following equation is used:

$$\epsilon^*(\omega) = \epsilon' - i\epsilon'' = \frac{-i}{\omega Z^*(\omega) C_0} \tag{2.17}$$

With C_0 the initial capacity of the system without any sample in the apparatus. The real and imaginary parts of the permittivity are determined with:

$$\epsilon' = \epsilon_\infty + \frac{\epsilon_s - \epsilon_\infty}{1 + \omega^2\tau^2} \tag{2.18}$$

$$\epsilon' = \frac{(\epsilon_s - \epsilon_\infty)\omega\tau}{1 + \omega^2\tau^2} \tag{2.19}$$

The complex permittivity is also obtained directly from the Debye relaxation:

$$\epsilon^*(\omega) = \epsilon_\infty + \frac{\Delta\epsilon}{1 + i\omega\tau} \tag{2.20}$$

With:

$\Delta\epsilon = \epsilon_s - \epsilon_\infty$

ϵ_∞: The permittivity at the high frequency limit

ϵ_s: The quasi-static permittivity (at low frequency)

τ: The characteristic relaxation time of the material

In practice, the permittivity is measured at different temperatures and frequency to produce a 3D relaxation map showing the different transitions potentially happening in the measured material in function of the parameters applied. Figure 2.13 shows an example of the data that can be obtained with DRS measurement. The α transition shown on the plot indicates the shift of dynamic glass transition depending on the frequency applied, giving information on the molecular mobility under high strain rates up to 2.10^6 s^{-1}. The peak called σ is the witness of a ionic conductivity phenomenon.

2.4.2.2 Apparatus

The DRS apparatus used was a Alpha Analyzer from Novocontrol technologies GmbH with a frequency range going from 10^{-1} to 2.10^6 Hz. The samples were 20 mm wide round and 500 μm thick

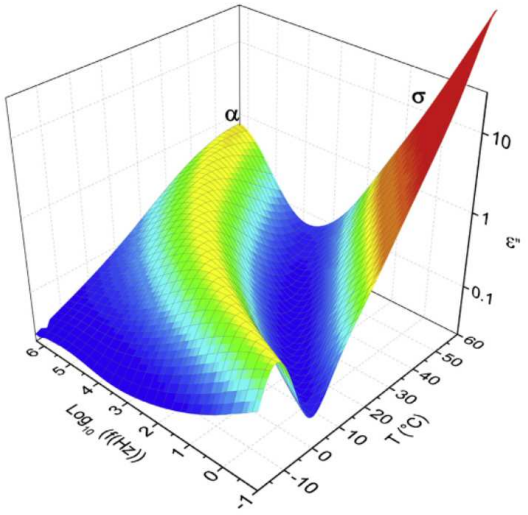

Figure 2.13: 3-D plot from DRS analysis for EVA70: dielectric loss (ϵ'') versus frequency (f) and temperature (T) (Taken from [153]).

pellets. The samples were placed between parallel fold electrodes. The temperature was controlled with a Quatro Cryosystem from Novocontrol technologies GmbH with an accuracy of ± 0.5 °C. The equipment can go up to 10^{11} Hz but would necessitate a setup change so the measurement have been stopped at 2.10^6 Hz to avoid setup changes. Figure 2.14 shows a classic DRS apparatus schema:

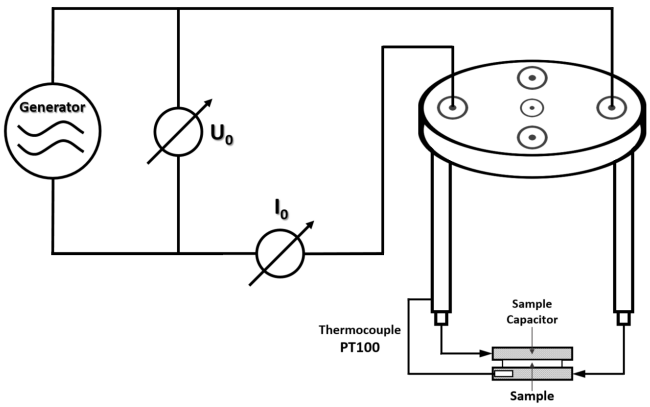

Figure 2.14: Schema of the DRS setup with the Alpha Analizer from novocontrol technologies GmbH (from [200]).

2.4.2.3 Data treatment

2.4.2.3.1 Havriliak-Negami

To extrapolate the data obtained to higher temperatures or frequencies, the Havriliak-Negami model is used [156]. It is an extension of the Debye relaxation equation (see equation 2.20) used for the description of the relaxation of polymers that takes into account the asymmetry of the permittivity peaks.

$$\epsilon^*(\omega) = \epsilon_\infty + \frac{\Delta\epsilon}{\left(1 + (i\omega\tau)^\alpha\right)^\beta} \tag{2.21}$$

Through the fitting the relaxation strength $\Delta\epsilon$, the relaxation time τ and the symmetric and asymmetric broadenning factors α and β can be determined [156, 157].

2.4.2.3.2 Vogel-Fulcher-Tammann

The Vogel-Fulcher-Tammann equation is used to obtain the relaxation time of the chains.

$$\tau_{max} = \tau_0 \, exp\left(\frac{D\,T_0}{T - T_0}\right) \tag{2.22}$$

The fragility index (m) is the quantification of the speed of transition of solid to liquid of a material dependent on the temperature. This index is used in the temperatures close to the glass transition and is defined at $\tau = 100$ s. The higher the fragility index is, the more the polymer will be fragile. This index is obtained with the Angell's equation [199]:

$$m = \frac{d\ log(\tau_{max})}{d(T_g/T)}_{T=T_g} \tag{2.23}$$

An example of the results and fit obtained with the Havriliak-Negami and VTF equation is given in figure 2.15 for the same copolymer but with varying ratios.

2.5 Residual stresses measurement by XRD

The calculation of the residual stresses is done using Bragg's law (see figure 2.16:

$$n\lambda = 2d\ sin\Theta \tag{2.24}$$

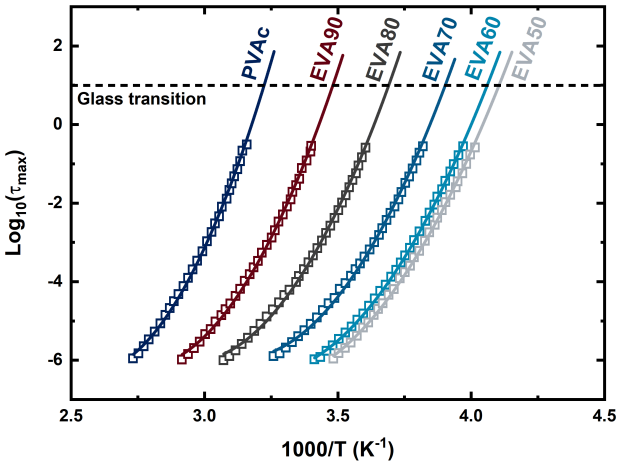

Figure 2.15: Temperature dependence of the glass transition temperature time for PVAc and EVA copolymers (from [153]).

With:

n : the diffraction order

λ : the wavelength of the cathode (here Cr cathode so $\lambda = 2.291$ Å)

d : interplanar spacing

Θ : the scattering angle

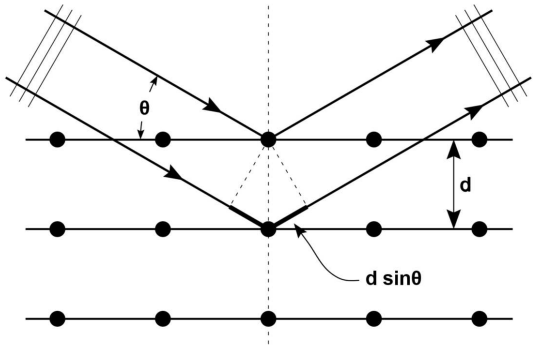

Figure 2.16: Bragg diffraction. Two incident beams with a known wavelength λ are reflected with a Θ angle on two different atoms separated by a plane distance d.

In the configuration used, all the parameters are known, the varying parameter is the angle Ψ. The definition of the two angles Θ and Ψ is given in figure 2.17

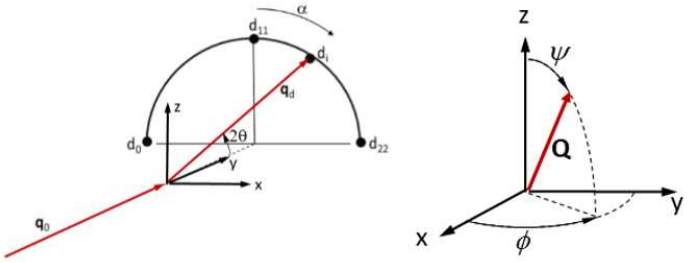

Figure 2.17: Representation of the two angles Θ and Ψ.

Due to the laser shock treatment, the plastification of the surface induces a shift in the interplanar spacing value d. This shift is then used to extract a strain ε:

$$\varepsilon_{hkl} = \frac{d_{hkl} - d^0_{hkl}}{d^0_{hkl}} \tag{2.25}$$

The above equation allow the extraction of the strain following the X and Z planes. Considering the sample geometry and the nature of the laser shock treatment (an uniaxial stress hypothesis is used) it is possible to assume that $\varepsilon^x = \varepsilon^y$. The stress calculation is then realised using:

$$\sigma^i = \frac{E}{1+\nu}\left[\varepsilon^i + \frac{\nu}{1-2\nu}(\varepsilon^x + \varepsilon^y + \varepsilon^z)\right] \tag{2.26}$$

With i the direction in which the stress is calculated. The $\sin^2(\Psi)$ method is then used. It consists in sweeping a Ψ angle and record the broadening of the diffraction peak caused by the plastification of the matter provoked by the laser peening treatment. This broadening is observed through a modification of the d value of the interplanar length depending on the Ψ angle:

$$\varepsilon^\Psi = \frac{1}{2}S_2(\sigma^x - \sigma^z)sin^2(\Psi) + \frac{1}{2}S_2\sigma^z + S_1(\sigma^x + \sigma^y + \sigma^z) \tag{2.27}$$

Finally, the slope and intercept of ε depending on $\sin^2(\Psi)$ gives the stress by linear combination.

Confinement and parameters influencing laser shock

3 | Confinement and parameters influencing laser shock

Content

3.1 Synthesis and choice of the confinement . . . 125
3.1.1 Polymer synthesis . . . 125
3.1.2 Choice of the polymers of interest . . . 126
3.1.2.1 Energy transmission measurement . . . 126
3.1.2.2 Pressure measurements . . . 127
3.1.2.3 Transmission after mulitiple laser shots . . . 130
3.2 Wavelength influence on the produced pressure . . . 130
3.2.1 Pressure measurement . . . 131
3.3 Young's modulus influence on the pressure produced . . . 132
3.3.1 Expected effects . . . 132
3.3.2 Pressure measurement . . . 134
3.4 Confinement thickness influence on the LSP process . . . 137
3.4.1 Epoxy . . . 137
3.4.2 Acrylate . . . 138
3.4.2.1 Pressure and backface velocity measurements . . . 139
3.4.2.2 Full width half maximum shortening . . . 140
3.4.2.3 Plasma thickness versus confinement thickness . . . 142
3.4.2.3.1 Impedance calculation from literature . . . 143
3.4.2.3.2 Impedance calculation from experiments . . . 145
3.4.2.4 Tape damaging under laser irradiation . . . 146
3.4.2.4.1 Transmission after shot . . . 146
3.4.2.4.2 Tape imaging . . . 146
3.4.2.4.3 Infra-red characterization . . . 149
3.4.2.5 Conclusion on the confinement thickness effects . . . 149
3.5 Adhesion . . . 151
3.5.1 Silicone confinement . . . 152
3.5.2 Acrylate tape confinement . . . 153
3.6 Chemical composition . . . 155

3.7 Residual stresses measurements 156
3.7.1 Laser shock set-up 157
3.7.2 Surface state before and after treatment 159
3.7.3 Residual stress measurement 159
3.7.3.1 Surface measurement 159
3.7.3.2 Residual stresses calculation experiment 159
3.7.3.3 In-depth measurement 162
3.8 Conclusion 163

Introduction

This chapter presents the different parameters in this specific study that can influence the laser shock process. A first part describes the synthesis and choice of the confinement with transmission and pressure measurements realised for different polymer confining materials. Other pressure measurements are then presented with different varying parameters such as the laser wavelength, the Young's modulus of the confining layer, the adhesive properties , chemical composition of the confinement. An extensive study of the confinement material thickness is also realised and details the effects induced as well as the damaging depending of the confinement depending on its thickness. Lastly, the chapter closes on residual stresses measurements compared to the results obtained in the literature in order to assess the efficiency of our choice of confinement when compared to the classic water confined configuration used in other works.

Synthèse et choix du confinement

De multiples confinements ont été évalués dans le but de déterminer leur transmission optique, leurs propriétés adhésives et leur capacité à produire une pression suffisante quand utilisés comme confinement pour le procédé LSP. Des silicones, epoxys et des polymères acryliques ont été étudiés en parallèle de l'eau classiquement utilisée comme confineur et utilisée comme référence pour la pression maximale produite par un choc laser. Six confinements différents sont ici présentés dans cette partie préliminaire afin d'en montrer les pressions maximales atteignables. Les trois confinement de la famille des silicones sont: un polydiméthylsiloxane fourni par Nicolas Gay, le vDT-431 choisi pour ses bonnes propriétés adhésives et le Sylgard184 pour ses propriétés mécaniques et optiques stables. Dans l'idéal, le confinement choisi à l'issue de cette étape de sélection doit posséder toutes les propriétés présentées dans le cahier des charges donné à la fin du chapitre I (1.5).

Synthèse des polymères

Les différents polymères utilisés pour les applications de choc laser ont été soit directement achetés à un fournisseur commercial, soit synthétisés au laboratoire PIMM. Le polymère acrylique a été acheté à la société Coroplast alors que les autres polymères décrits plus haut ont été synthétisés au laboratoire par une réaction entre une base et un durcisseur.

Dans le cas des époxys , le matériau présenté (figure 3.1) est un test réalisé pour des mesures de transmission optique. En effet, contrairement aux autres confinements, l'époxy ne possède pas de propriétées adhésives une fois la réticulation terminée. De ce fait, les cibles confinés avec un époxy ont dues être réticulées directement sur les cibles aluminium utilisées pour les expériences de choc laser. Cette méthode induit l'apparition de contraintes résiduelles à l'interface epoxy/cible aluminium. Ce phénomène n'induit pas d'effets notables sur les résultats des expériences de tir à l'exception d'une certaines sensibilité des échantillons à une séparation de l'assemblage si l'échantillon n'est pas manié soigneusement. Un cas spécifique concerne le polycarbonate (PC) utilisé dans le chapitre 4, qui a été directement réticulé sur la cible aluminium par le biais d'une presse chauffante, provoquant une grande sensibilté de l'échantillon au décollage du fait de sa faible épaisseur et des contraintes résiduelles provoquées par la réticulation sur cible.

Mesures de transmission d'énergie

Les mesures de transmission optiquese sur les polymères de confinement ont été réalisé en plaçant un calorimètre (QE50LP-H-MB-QED, Gentec) sous le porte-échantillon utilisé dans les éxpériences VISAR. La transmission d'énergie à été calculée en utilisant la plus faible énergie laser possible tout en plaçant le calorimètre le plus loin possible du point focal du laser dans le but de répartir l'énergie laser sur le calorimètre et réduire son possible endommagement. La mesure à été réalisée avec et sans polymère de confinement sur le chemin optique. La figure 3.2 montre le montage utilisé pour les mesures.

Les mesures de transmission optique ont été réalisé sur l'eau et les différents confinements polymère. Chaque mesure à été répétée plusieurs afin de garantir la stabilité et la répétabilité de l'expérience. Les données obtenues montrent un comportement différent entre l'eau et le confinement acrylique à 1064 nm. Au lieu d'une diminution de la transmission optique en passant à une longeur d'onde laser de 1064 nm au lieu de 532 nm, une légère augentation de la transmission est obtenue alors qu'une diminution est observée dans le cas de l'eau. De ce fait, les pressions maximales produites par le confinement acrylique devraient augmenter légèrement lors d'un passage d'une longeur d'onde laser de 532 à 1064 nm contrairement à l'eau qui voit sa transmission optique décroitre légèrement lors d'une telle modification de longueur d'onde. Le tableau 3.1 donne un récapitulatif des données obtenues par les mesures de transmission sur les différents matériaux de confinement.

En partant de ces résultats, les pressions maximales produites à 532 nm avec le confinement acrylique devraient être légèrement plus basse que celle produites avec le régime confiné eau (respectivement $\approx$ 90% de transmission contre 100% avec l'eau). A l'inverse les résultats attendus à 1064 nm devraient être équivalents du fait des transmissions égales de l'eau et confinement acrylique à 1064 nm. Cette hypothèse n'est cependant valide que dans le cas ou seule cette transmission optique intervient dans le processus et ou les modes d'interaction laser-matière sont les mêmes entre les deux confinements.

Mesures de pression

Pour déterminer un confinement qui sera utilisé pour le procédé de laser shock peening dans un cadre industriel et pour la caractérisation de l'interaction laser-matière en régime confiné par polymère, les différents polymères présentés précedemment ont été évalués par des mesures VISAR afin d'obtenir les pressions maximales produites en les utilisant comme confinement pour des expériences de choc laser. Les pressions ont été extraites des profils de vitesse en face arrière par la méthode de simulation numérique présentée dans la partie 2.3. Tous les tirs ont été réalisés sur des cibles d'aluminium 99.0% d'1 mm d'épaisseur avec une tache laser de 3 mm à 532 nm et une durée d'impulsion de 7 ns sur le laser Gaïa HP de la plateforme Héphaïstos. Les résultats des mesures de pression sont donnés dans la figure 3.3.

Les résultats montrent que les différents confinements ne permettent pas tous de produire des pressions égales lors d'un choc laser. De plus, toutes les courbes peuvent être séparées en deux parties. Dans un premier temps, la pression maximale augmente avec l'intensité laser de manière quasiment linéaire puis atteint un seuil auquel la pression sature. Cette deuxième partie de courbe correspond au déclenchement d'un plasma de claquage à la surface ou dans le matériau de confinement. Les pressions maximales et les seuils de claquages des différents matériaux de confinement étudiés sont données dans le tableau 3.1. Avec ces informations, il est alors possible de résumer les perfomances des différents confinements polymères en fonction de leur famille:

- L'eau produit les plus hautes pressions à toutes les intensités laser étudiées. Le phénomène de claquage apparait à 7.0 GW/cm^2 et la pression maximale atteinte est de 7.0 GPa.

- Le confinement acrylique donne des résultats équivalents au régime confiné par eau. Le plasma

de claquage se déclenche aussi à 7.0 GW/cm^2 et est couplé à une pression maximale produite de 7.6 GPa. Bien que la pression produite à cette intensité spécifique soit plus haute que celle produite par l'eau, les pressions globalement extraites sont équivalentes ou très légèrement inférieures au régime confiné par eau. Les pressions obtenues à partir du seuil de claquage ne sont pas prises en compte puisqu'instables à cause l'énergie incidente amenée à la cible qui n'est plus précisement connue.

- L'époxy utilisé comme confinement permet l'obtention de bons résultats en terme de pressions maximales produites mais aussi en terme de seuil de claquage bien que l'eau et l'acrylate reste meilleurs. La pressions maximale produite atteint 5.3 GPa pour une intensité laser de 5.6 GW/cm^2, intensité à laquelle le seuil de claquage est également atteint.

- Les silicones donnent tous les trois des résultats similaires, inférieurs à ceux obtenus avec les autres types de confinements. En fonction du type de silicone, le seuil de claquage varie entre 3.7 et 5.5 GW.cm^2 avec des pressions maximales comprises entre 4.1 et 4.7 GPa. Ces résultats sont en partie dûs à la transmission optique plus basse de ces polymères comparés à l'acrylate et à l'époxy. Le Sylgard184, qui possède la plus haute transmission optique (90% contre 82% pour le PDMS) produit les plus hautes pressions des trois silicones étudiés.

Bien que l'eau et le confinement acrylate sortent du lot en terme de performances, les autres polymères étudiés produisent eux aussi des pressions suffisamment hautes pour envisager le traitement de matériaux aéroanautique par choc laser en les utilisant comme confinement. Le tableau 3.1 donne un récapitulatif des seuils de claquage et des pressions maximales produites par chaque confinement. En considérant les résultats obtenus avec les matériaux polymères testés, le confinement acrylique apparaît comme le plus adapté à une utilisation comme confineur pour une application en laser shock peening de manière industrielle. Pour cette raisonn, ce matériau est aussi choisis pour des expériences de caractérisations complémentaires. De la même manière, l'époxy ainsi que le Sylgard184 sont aussi choisi pour des expériences complémentaires du fait de la possibilité de les synthétiser au laboratoire et d'en faire varier certaines propriétés. En utilisant ces deux autres polymères, une étude sur l'influence du module d'Young ainsi que sur les effets d'épaisseur et de propriétés adhésives sur le procédé de LSP devient possible.

3.1 Synthesis and choice of the confinement

Multiple confinements were tested in order to assess their performances as well as their optical transmission and bonding properties. Silicones, acrylate based polymers and epoxies were studied in parallel of water used as a reference for the maximum pressure produced by the laser shock experiment. Six different confinements are presented in this preliminary part to show the range of capabilities in terms of pressure produced by different types of confinement. The three different silicones chosen are described as follow: A polydimethylsiloxane supplied by Nicolas Gay, VDT-431 chosen for its good adhesive properties and Sylgard184 for its overall good and stable properties from mechanical to optical ones. Ideally the final chosen confinement will have all the needed properties presented at the end of chapter I (1.5).

3.1.1 Polymer synthesis

The different polymers used as confinement for the laser shock application were either directly bought to a commercial manufacturer or synthesized at the laboratory. The acrylate based polymer for example was bought to a manufacturer while all the other confinement were obtained by a classical two parts reaction with a base and a hardener.

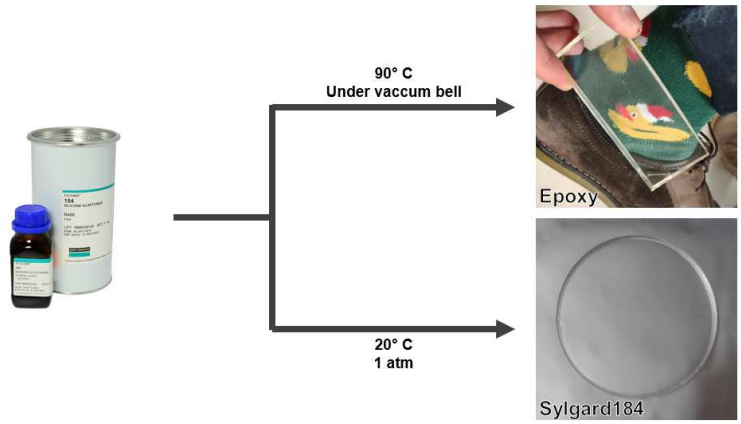

Figure 3.1: Typical reaction used for the synthesis of Sylgard184 and epoxy and final result of the syntheses.

In the case of the epoxy, the material presented is only a test realised for optical transmission and feasibility purposes. Contrary to the other polymer material, the epoxy does not have any adhesive

properties once it is fully cross-linked. Consequently, the epoxy confined samples had to be produced by directly cross-linking the polymer on the metallic target used for the laser shock. A resulting effect of this method is that the epoxy polymer undergoes shrinkage during its cross-linking which lead to residual stresses at the interface target/epoxy. This phenomenon does not induce any real noticeable effect on the 1 mm aluminium targets chosen for this confinement except a higher propensity to debonding of the epoxy layer is the target is bent or cut. In the specific case of the polycarbonate (PC) used in chapter 4, the material was directly cured on the surface of the aluminium target by heating and pressing it on the material to be confined.

3.1.2 Choice of the polymers of interest

In order to assess the efficiency of each polymer confinement chosen, the first step is to be able to accurately measure the laser energy brought to the surface of the metallic target. To do that, the optical transmission of the different polymers used as confinement need to be measured.

3.1.2.1 Energy transmission measurement

The optical transmission measurement on the polymer confinement is realised by placing a calorimeter (QE50LP-H-MB-QED, Gentec) under the sample holder used for the experiments. The transmission is calculated using the lowest possible laser energy while placing the calorimeter the farthest away from the focal point to diffuse the energy of the maximum surface of the calorimeter to avoid any damaging of the device. The energy received is recorded with and without the confinement on the laser path. Figure 3.2 shows the transmission setup used for the characterization of the confinements.

Transmission measurements were performed on the water and polymer confinements. Each measurement was done multiple time to ensure the stability and repeatability of the results. The data obtained show a behaviour different than the one observed with water. In the case of the polymer confinement and especially for the acrylate based one, instead of a diminution of the optical transmission with the wavelength change, a slight increase was observed when subjected to an infra-red irradiation. This should lead to a pressure production equivalent between water and the acrylate tape confinement under the two wavelengths. Even slightly higher pressures should be observed from the polymer confinement when shot with a 1 μm range laser. Table 3.1 gives a recap of the results obtained with the experiments.

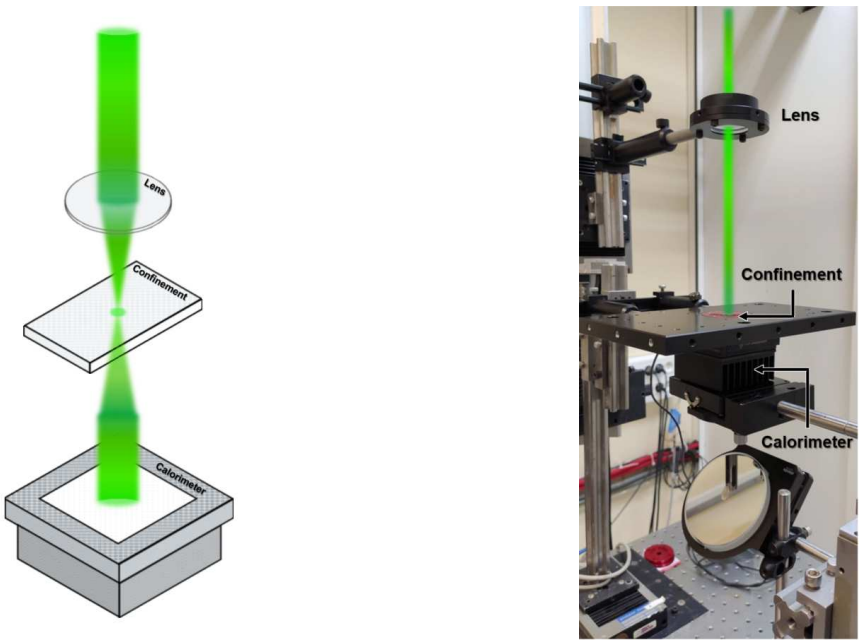

(a) (b)

Figure 3.2: (a) Schema of the transmission setup used on the Héphaïstos laser for the optical transmission characterization of the polymer confinements. (b) photo of the setup on the Héphaïstos platform.

From these results the pressure produced at 532 nm should be slightly lower with the polymer than with water as confinement since around 10% of the incident laser energy is lost when the laser goes through the polymers compared to water. The results expected from an infra-red laser should be equivalent at least for the acrylate tape polymer considering that they have the same transmission at this wavelength and if the laser-matter interaction does not differ between the two confinements.

3.1.2.2 Pressure measurements

To determinate the confinements of choice that will be used for the laser shock peening process and for the characterization of the polymer/target interaction, different polymer confinements were assessed by VISAR measurement to obtain the pressures produced while using them instead of the classical water confinement under laser shock configuration. The pressure was obtained following the method of numerical simulation method described in 2.3. All of the shots were realised on 1 mm thick 99.0% aluminium with a 3 mm laser spot size on the 532 nm, 7 ns pulse duration, Gaïa HP laser from the Héphaïstos platform. The pressures obtained depending on the laser intensity is given in figure 3.3 while figure 3.4 gives a zoomed in view of the pressure and laser intensity area of interest for an

industrial treatment (P ≈ 4 GPa).

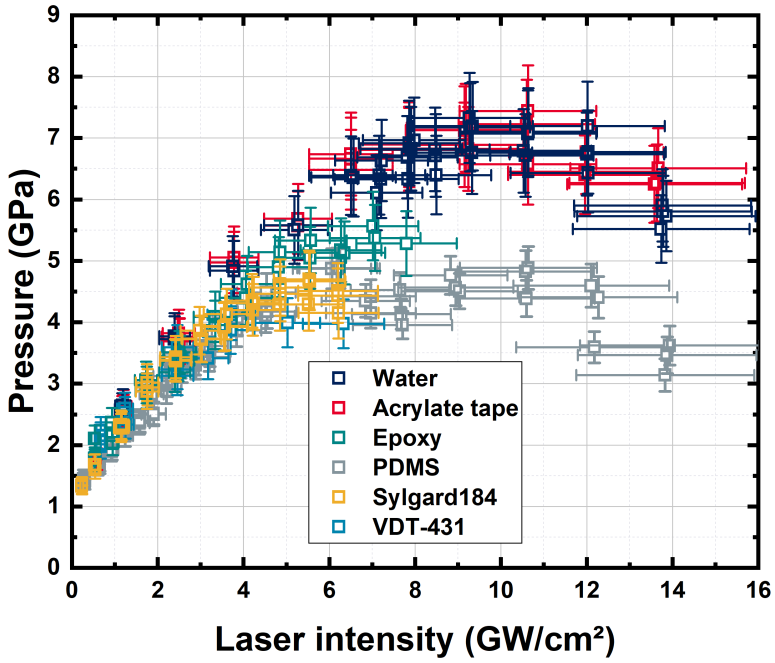

Figure 3.3: Pressure depending on the laser intensity for different polymer confinements and water for laser shots on a 1 mm 99.0% aluminium targets, 532 nm, 7 ns pulse duration, 3 mm spot size.

The results shows that the different confinements do not permit the same pressure production when used for a laser shock. All the curves can be separated in two parts. First, the maximum pressure increases along with the laser intensity until it reaches a threshold where the pressure saturate. This phenomenon corresponds to the breakdown occurrence in the material confinement. The maximum pressures and breakdown thresholds are given in table 3.1. The different material performance can be divided following their polymer family:

- Water produces the highest pressures for nearly all the laser intensities chosen. The breakdown appears at 7.0 GW/cm^2 while producing a pressure of 7.0 GPa.
- The acrylate tape gives equivalent results to the obtained with a water confined laser shock. The breakdown plasma initiation happens also at 7.0 GW/cm^2 and is coupled with a produced pressure of 7.6 GPa. Although the pressure produced at this specific laser intensity is higher than the one obtained with water, the overall pressures extracted are equivalent or just a little bellow

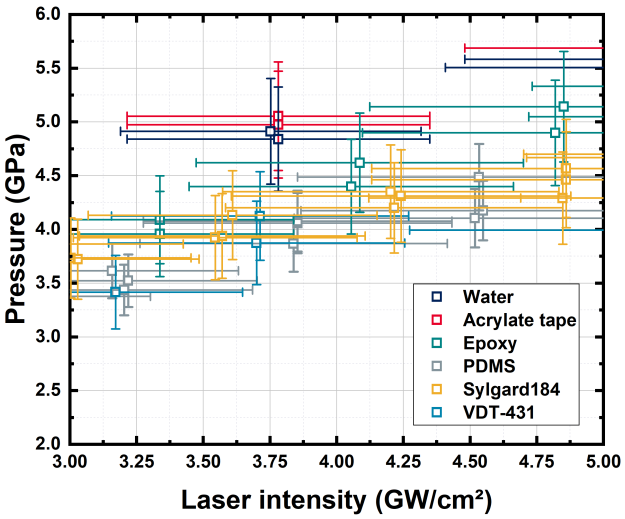

Figure 3.4: Pressure depending on the laser intensity for different polymer confinements and water for laser shots on a 1 mm 99.0% aluminium targets, 532 nm, 7 ns pulse duration, 3 mm spot size. Zoomed in on the 3 to 5 GW/cm^2 range, corresponding to the produced pressures needed for an industrial treatment.

the water confined regime. The pressure obtained after the breakdown threshold are not taken into account as the incident laser energy effectively brought to the surface of the aluminium surface cannot be accurately calculated anymore.

- Epoxy used as a confinement produces good results in terms of maximum pressure and breakdown threshold although it is not as good as water and acrylate tape. The Maximum pressure produced of 5.3 GPa is attained at 5.6 GW/cm^2, when the breakdown threshold is also reached.

- The three silicones give similar results, inferior to what can be achieved with the other types of confinement tested, be they water or polymers. Depending on the type of silicone the breakdown threshold vary between 3.7 and 5.5 GW/cm^2 while the pressure oscillates from 4.1 to 4.7 GPa. These results are likely due to a slightly lower optical transmission from these polymers compared to the acrylate tape and epoxy. The Sylgard184 which exhibit the highest optical transmission (90% while the PDMS has an 82% transmission), incidentally produces the highest pressures in the silicones studied.

Even though the water and acrylate tape confinements stand out, the other polymers studied still

produce high enough maximum pressure to be used for the treatment of most metal alloys with elastic limits in the range of 0.2 to 2 GPa. For the industrial treatment of aluminium alloys, a pressure around 4 GPa is necessary. Table 3.1 gives a recap of the breakdown threshold and maximum pressures produced by each confinement. Considering the results obtained with the different materials studied to be used as a replacement for the water in the laser shock application, the acrylate tape polymer is chosen as the reference material for the final industrial application and for the different experiments to better understand the specificities of the use of such a type of confinement for laser shock peening applications. The Sylgard184 silicone and the epoxy are also chosen for experiments because of the possibility to synthesize them in the laboratory, hence allowing a control of their respective properties depending of the protocol chosen. By using these two other polymers, it is possible to vary their Young's modulus, thickness or adhesive properties to study the effect of these properties on the process.

Table 3.1: Breakdown threshold and maximum pressure obtained from the VISAR experiments with the different confinements.

Confinement	**Breakdown threshold**	**Maximum pressure**	**Transmission**	
	GW/cm^2	GPa	532 nm	1064 nm
Acrylate based	7.6	7.0	92%	95%
Water	7.0	7.0	100%	95%
Epoxy	5.6	5.3	90%	
Sylgard184	5.5	4.7	90%	
PDMS	4.7	4.6	82%	
VDT-431	3.7	4.1	90%	
PC			87%	

3.1.2.3 Transmission after mulitiple laser shots

3.2 Wavelength influence on the produced pressure

Defining the range of use of the confinement is crucial to accurately assess its possible use. Héphaïstos' laser has a working wavelength of 532 nm, similar to the parametric used in Sano's work [21]. As detailed in 1.2.5.2 the wavelength mainly used for industrial treatments is infra-red, generally with 1064 nm lasers. The use of a 1064 nm wavelength avoids non-linear effects during fiber transportation of the beam. On the other hand, the laser energy transmission through water with a 1 μm wavelength

is highly dependent on the water confinement layer thickness whereas at 532 nm the transmission stays > 99% up to a thickness of 28 cm [67] of water. In this part, a study of the transmission of the confinement with green and infra-red laser is presented to assess the capability of potential polymer confinements under different irradiations.

3.2.1 Pressure measurement

Multiple pressure measurements through modelling of the back face velocity profiles obtained by VISAR measurements were performed in order to assess the effect of the wavelength on the pressure produced by laser shock. This type of experiment also gives an idea of the breakdown thresholds reached with this type of confinement depending on the laser wavelength chosen, an area where a few paper can be found. The confinement tested for these experiments was the acrylate tape polymer. Choosing an industrial material has the advantage of ensuring that the material used as confinement for the laser shots is always the same in chemical composition and thickness. Figure 3.5 gives the pressure depending on the laser intensity measured for 3 different wavelengths, respectively 532, 1053 and 1064 nm from Héphaïstos, GCLT (from CEA) and Théïa. The results show that similar to water the acrylate polymer tape shows a slightly less efficiency than when used in the infra-red range (1064 nm).

The maximum pressure obtained with an infra-red laser (1064 nm) is 5.8 GPa produced for a laser intensity of 7.48 GW/cm^2. The pressure produced at 532 nm is 19% higher (6.89 GPa at 7.86 GW/cm^2) even thought the laser intensity chosen is a little bit higher. The lower results obtain with the 21 ns pulse duration at 1064 nm from the Théïa laser are explained by the longer pulse that induce the initiation of a breakdown plasma at lower energy. Overall the use of a green laser allows for production of pressure around 15% higher whatever the incident energy used compared to infra-red wavelengths.

Figure 3.6a shows no difference between the pressures produced with the water or acrylate tape confinement under a green laser irradiation of 532 nm. Figure 3.6b, on the contrary demonstrates a slight decrease for shots at 1053 nm with water and acrylate tape confinement even though their optical transmission under a laser irradiation of such wavelength is the same.

Overall the wavelength influence between 532 nm and the 1 μm range seems to be rather modest with a loss of pressure produced of $\approx$ 15% in the infra-red range.

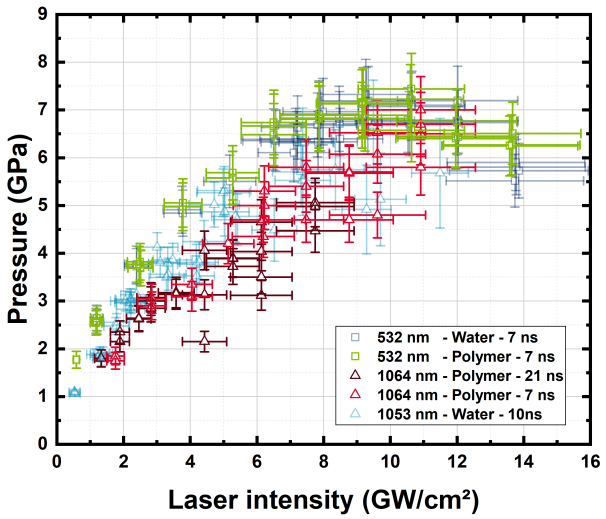

Figure 3.5: Influence of the laser wavelength on the pressure produced by laser shot, for green and infra-red lasers, the shots are realised on 1 mm 99.0% aluminium target with 1 mm acrylate tape confinement. The data at 532, 1053 and 1064 nm respectively come from Héphaïstos, GCLT and Théïa respectively.

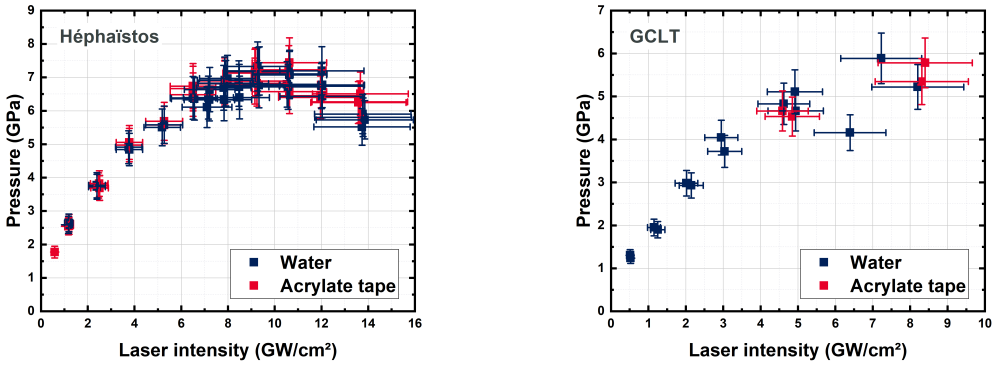

(a) (b)

Figure 3.6: Pressure depending on the laser intensity for water and acrylate tape confinement for two different wavelengths, (a) 532 nm on the Héphaïstos laser and (b) 1053 nm of the GCLT laser.

3.3 Young's modulus influence on the pressure produced

3.3.1 Expected effects

The Young's modulus of the confinement have an effect on the final pressure produced by the laser shock interaction through its influence on the reduced impedance Z of the system target/confinement,

respectively with an impedance Z_1 and Z_2. From Fabbro's model [201] the reduced impedance intervene in the pressure calculation:

$$P\,(GPa) = 0.01\,\sqrt{\frac{\alpha}{2\alpha+3}}\,\sqrt{Z\,(g.cm^{-2}.s^{-1})\,I_0\,(GW/cm^2)} \tag{3.1}$$

With:

Z: the reduced impedance of the system ($Z = \frac{1}{Z_1} + \frac{1}{Z_2}$) Z_1 being the impedance of the target shocked and Z_2 the impedance of the confinement.

α: a factor which corresponds to the thermal energy used for the plasma heating.

The impedance Z_2 of the confinement is calculated following:

$$Z = \rho\,D \tag{3.2}$$

With:

D: The shockwave velocity in the polymer.

ρ: The density of the polymer.

From this equation the shockwave velocity "D" can be decomposed using:

$$D = C_0 + S\,u \tag{3.3}$$

With:

C_0: the speed of the sound in the material.

S: the Hugoniot constant specific to the material.

Finally C_0 is obtained following:

$$C_0 = \sqrt{\left(\frac{E}{\rho}\right)\left(\frac{(1-\nu)}{(1-2\nu)(1+\nu)}\right)} \tag{3.4}$$

With:

E the Young's modulus of the material.

ν: the Poisson's coefficient of the material.

From these equation it is possible to theoretically predict the pressure produced by a confinement while treating an aluminium target. The aluminium impedance is 1.48x10^6 g.cm^{-2}.s^{-1} [34]. Figure 3.7

shows the pressure produced by laser shock depending on the Young's modulus of the confinement used while shocking a pure aluminium target with an intensity of 3 GW/cm^2. The confinement considered is an elastomer and has the same density as the acrylate tape polymer which was caculated with a density scale ($\rho = 0.935$). The Poisson's coefficient of the material is considered to be 0.499 since it is a rubber like material.

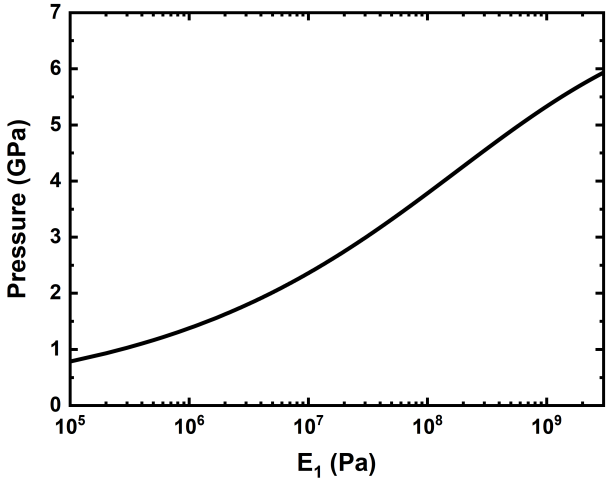

Figure 3.7: Pressure produced by a laser shock at an intensity of 3 GW/cm^2 on a pure aluminium target depending on the Young's modulus of the confinement.

The final pressure produced is heavily influenced by an E_1 modulus variation from 0 to 10^6 Pa and starts an inflexion between 10^6 to 10^9 Pas. Once the GPa range is attained, a plateau is reached and the pressure does not drastically change with pressure increase within this decade. Considering these results, the pressure produced by the flexible acrylate tape with a modulus of $\approx$ 70 MPa should produce 1 GPa with the chosen parameters while using a confinement with a Young's modulus in the GPa range would produce at least 5 GPa.

3.3.2 Pressure measurement

To assess the influence of the Young's modulus of the confinement material for laser shock on the pressure produced, VISAR measurement were realised while using a 250 μm epoxy as confining medium. The epoxies were synthesized by Rescoll with different mechanical properties and a thickness of around 250 μm. One batch had a modulus comprised between 1 to 2 GPa while the other one had a

modulus of 10 MPa. The laser spot used was 2.85 mm with laser intensities of 1.86 and 3.55 GW/cm^2 with a pulse duration of 7 ns.

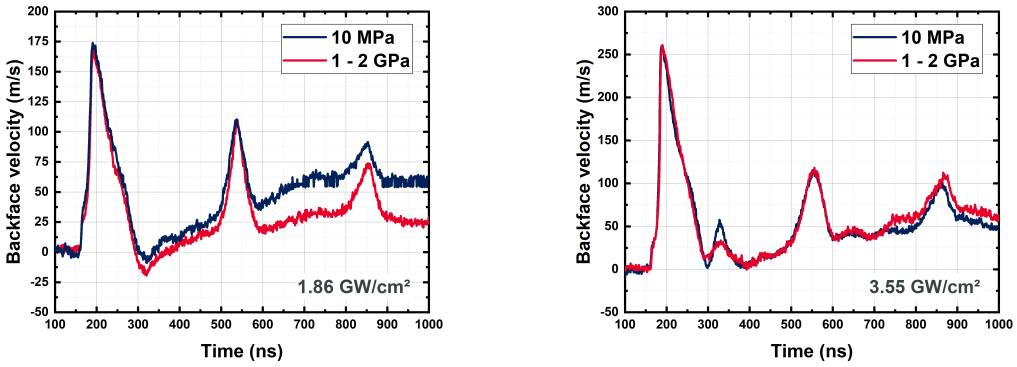

(a) (b)

Figure 3.8: Backface velocity profiles obtained by VISAR for laser shots on pure aluminium 1 mm thick (laser spot size 2.85 mm, pulse length 7 ns) with an epoxy confinement of either 1 - 2 GPa or 10 MPa. (a) shots at I = 1.86 GW/cm^2 and (b) at I = 3.55 GW/cm^2.

Figure 3.8 presents the backface velocity profiles obtained from shot at two different laser intensities on 1 mm pure aluminium on epoxy confinements with different Young's modulus. On figure 3.8a the same backface velocity is reached on the first and second peak even though the Young's modulus of the two confinement present a difference of two decades (10 MPa versus 1 - 2 GPa). The FWHM is also the same on the first and second peaks. After 550 ns, the 10 MPa profile starts to separate from the 1 - 2 GPa one due to the target starting to fly during the shock, moving it farther away from the probe laser of the VISAR, thus affecting the back face velocity profile. The third peaks still display the same FWHM even with the flying of the target and confirms the consistency of the results. On figure 3.8b the same trend is observed although in this case no flying of target is noticed and the two profiles stay overlapped during the whole time frame displayed. A small peak is observed between the first and second main one at 300 ns and is the witness of spallation of the aluminium target due to the high pressure produced by the shock with a pressure reached of 4.3 GPa. This suggests that the Young's modulus of the confinement used plays little to no influence on the final pressure produced by laser shock. A possible explanation is the increasing of the Young's modulus of the 10 MPa epoxy under high strain rate and pressure up to the GPa range through a transition to a glassy state. This would make the elastic modulus of both the epoxies similar during the laser irradiation, resulting

in the same pressure produced with two materials with vastly different mechanical properties under normal conditions.

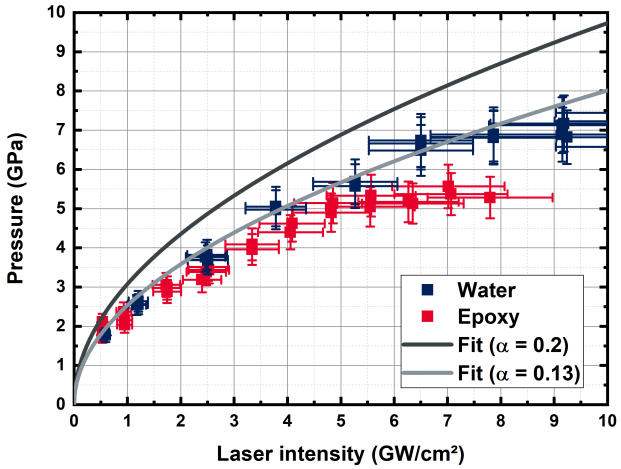

Figure 3.9: Comparison between the pressures experimentally obtained for water and epoxy confinement and the one calculated from equation 3.1 with an $\alpha = 0.2$ and with a corrected $\alpha = 0.13$ to fit the water used as reference.

From the comparison of the theoretical pressure reached with a laser intensity I of 3 GW/cm^2 and the pressures observed during the experiments a gap is observed with the theoretical pressure produced during laser shock on pure aluminium being around 5 GPa while the pressure developed during real shock with an higher intensity is 4.3 GPa. This suggests that either other factors may be involved in the pressure production during laser shock and that they are probably linked to experimental considerations more than mechanical one. This can also suggest that the α (=0.2, from [34] for a 1064 nm, 3 ns square pulse) coefficient used in equation 3.1 is not accurate and gives a overestimation of the pressure produced with the used set of laser parameters. Figure 3.9 gives the difference between the experimental pressure obtained with epoxy and water confinements and the calculation with Fabbro's model, using $\alpha = 0.2$ and with a corrected $\alpha = 0.12$. The α is calculated to fit the water confined interaction since the lower pressures found starting 4.5 GW/cm^2 for the epoxy confinement can be explained by the optical transmission difference which induces the production of a breakdown plasma at lower laser intensities and limits the maximum pressure that can be reached. The difference between the fit and the water experiments after 7 GW/cm^2 is also caused by the apparition of the breakdown plasma at the surface of the confining water droplet. The breakdown plasma created absorbs the

incident energy and causes the pressure to stop rising with an increasing laser intensity while the Fabbro model does not take this phenomenon into account

3.4 Confinement thickness influence on the LSP process

Confinements with different thicknesses were used for laser shock experiments to study their potential effect on the process. The confining medium chosen were epoxies and acrylate tapes with different controlled thicknesses. The difference of mechanical properties that can be induced by the variation of thickness has been shown to have no influence on the final pressure produced during the laser shock earlier. Solid epoxies and soft acrylate tapes were tested in order to confirm or infirm their thickness effect on the laser shock peening process.

3.4.1 Epoxy

The same epoxies from Rescoll, used for the mechanical properties study, with a Young's modulus in the GPa range were used. Two different thicknesses were studied, 250 and 500 μm to assess the effect of this parameter on the potential pressure produced with these materials.

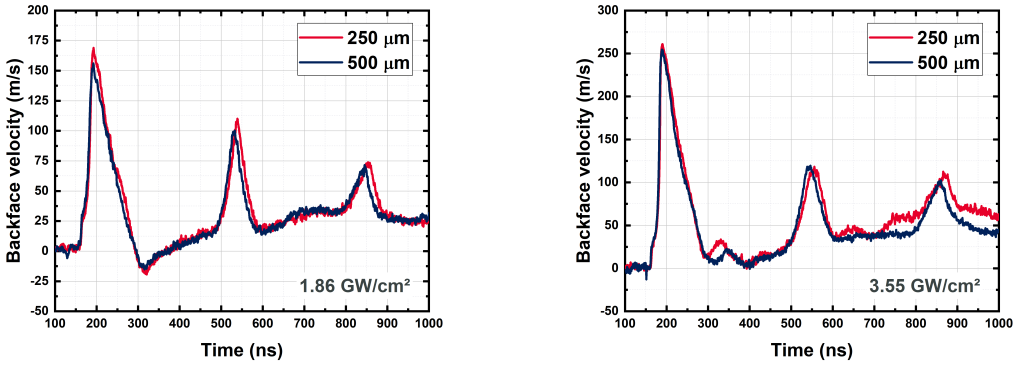

(a) (b)

Figure 3.10: Backface velocity profiles obtained by VISAR for laser shots on pure (99.0%) 1 mm thick aluminium (laser spot size 2.85 mm, pulse length 7 ns) with an epoxy confinements of 1 - 2 GPa with two different thicknesses. (a) shots at I = 1.86 GW/cm^2 with a confinement thickness of 250 and 500 μm and (b) at I = 3.55 GW/cm^2 with a confinement thickness of 250 and 500 μm.

Figure 3.10 shows that no difference are observed between the backface velocity profiles obtained from shots on 1 mm pure aluminium with epoxy confinement of 250 and 500 μm and a change of

laser intensity does not induce a change either. This implies that the transmission of the epoxies used are fully transparent in their thickness and that the optical losses happen at the interface due to reflections. In figure 3.10a the profile of the 250 μm epoxy arrives slightly earlier than the other, presumably due to the thickness of the aluminium target that must be a little bit higher than 1 mm since the tolerance of the seller are $\pm$ 10%.

3.4.2 Acrylate

The acrylate tape used is bought from an industrial manufacturer, the one usually used for shock experiment has a thickness of 1 mm and allows an easy applying and debonding of the confinement. Multiple other thicknesses are available (from 50 μm to 3 mm). Consequently a range of tapes have been bought to be tested and assess the effect of the thickness of a flexible polymer confinement on the laser shock process. The wider range of thicknesses covered compared to the epoxies can also give information on the potential effects induced by this characteristic compared with the experiments from 3.4.1. The characteristics and mechanical properties of the different tapes chosen are detailed in table 3.2.

Table 3.2: Technical sheet of the characteristics of the different acrylate tape polymer from Coroplast chosen to be used as confinement for the study of the effect of the thickness on the pressure produced (*: 1.0 kg, 625 mm^2).

Thickness	**50 μm**	**500 μm**	**1 mm**	**2 mm**	**3 mm**
Elongation at break	n.a	750 %	750 %	750 %	750 %
Tensile strength	n.a	10 N/25 mm	14 N/25 mm	25 N/25 mm	25 N/25 mm
Adhesion to steel	25 N/25 mm	50 N/25 mm	62 N/25 mm	75 N/25 mm	75 N/25 mm
Shear strength	10'000 min*	> 10'000 min*	> 10'000 min*	> 10'000 min*	> 10'000 min*
Temperature range	-40 to +120° C	-40 to +120° C	-40 to +120° C	-40 to +120° C	-40 to +120° C

The laser energy transmission measurement on the different acrylate tapes showed the same conclusion as with the epoxy ones; the optical transmission of these tapes is around 90% whatever the thickness of the tape measured, meaning the thickness has no effect on their transmission, the optical

losses happen at the interfaces by reflection.

3.4.2.1 Pressure and backface velocity measurements

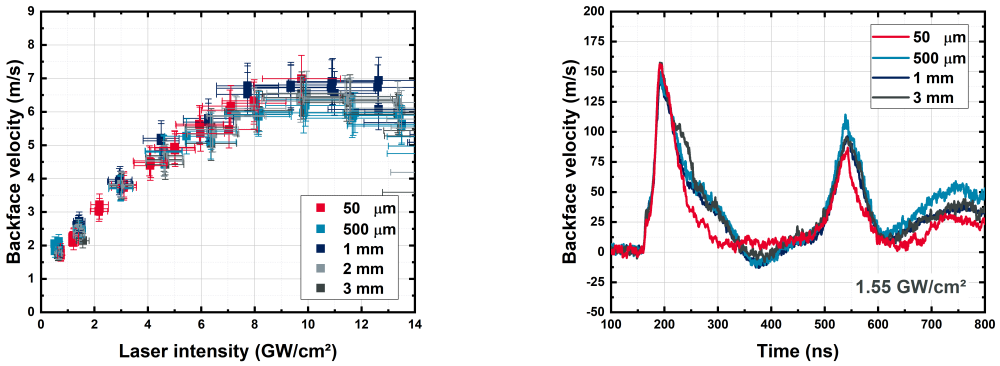

(a) (b)

Figure 3.11: Thickness influence of the acrylate tape confinement on (a) the pressure produced by laser shock with a 3 mm laser spot and a 7 ns pulse on 1 mm pure (99.0%) aluminium target and (b) the backface velocity profiles produced by VISAR with a 3.74 mm laser spot and a 7 ns pulse duration on the same targets shocked at 1.55 GW/cm^2.

Figure 3.11a shows the maximum pressure produced depending on the laser shot intensity for five different thicknesses of acrylate tape confinement ranging from 50 μm to 3 mm. The laser intensity ranged from 0.52 GW/cm^2 to more than 15 GW/cm^2 , the intensities displayed were stopped at 14 GW/cm^2 since the breakdown is situated at 7 GW/cm^2 for all the tapes tested. All the confinements studied demonstrated the same capability to produce pressure whatever the laser intensity chosen. This means that the maximum backface velocity reached is the same for all the tapes. However further study on the backface velocity profiles presented in figure 3.11b highlighted an effect of the thickness: in this case on the 50 μm one. The three others thicknesses demonstrate overlapping backface velocity profiles while the 50 μm one shows a slightly different profile. The the full width at half maximum (FWHM) is shorter, which is correlated to a shorter release compared to the other profile. This can induce multiple effects in the target treated under these conditions such as:

- Less thermal effects due to the shortening of the FWHM which induces a shorter time of application of the thermal loading, leading to a shorter thickness of the surface being thermally affected.

- A shallower depth of the residual stresses induced in the treated material. Due to the shortening of the FWHM, the pressure is applied for a shorter duration. The attenuation of the pressure in the thickness of the laser shocked piece leads to the reduced residual stresses compared to a classical treatment with a water confinement or a thicker acrylate tape confinement.

3.4.2.2 Full width half maximum shortening

To assess the shortening of the FWHM when thin confinements are used, multiple shots have been realised at different laser intensities with different thicknesses of acrylate tape confinement. The laser wavelength was 532 nm with a laser spot of 3.74 mm and a pulse duration of 7 ns. The targets were pure aluminium with a thickness of 1 mm.

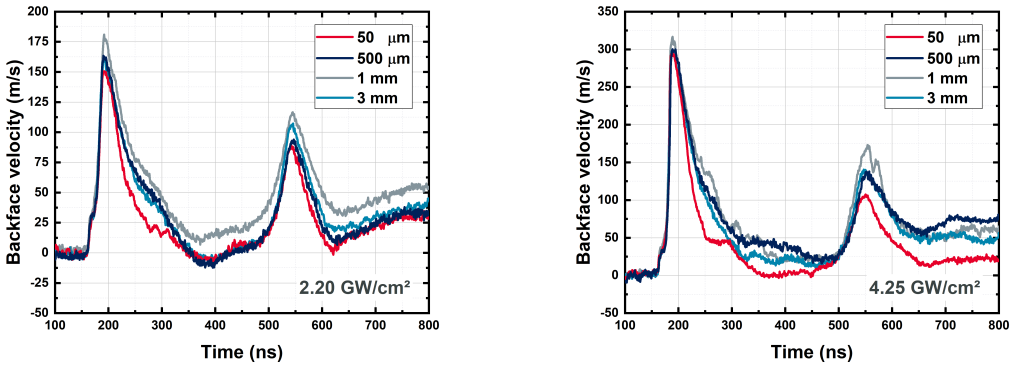

(a) (b)

Figure 3.12: Comparison of the backface velocity profiles at different thicknesses of acrylate tape confinement for different laser intensities (laser spot = 3.74 mm, pulse duration = 7 ns, target: (99.0%) aluminium 1 mm: (a) 2.20 GW/cm^2 and (b) 4.25 GW/cm^2

Figure 3.12 shows the backface velocity profiles obtained with four different acrylate tape confinement thicknesses at two different laser intensities. On both energies displayed, a shorter release for the 50 μm profile compared to the other three thicknesses is observed. On figure 3.12b, the velocity is quickly decreasing after the peak until reaching a small plateau at 250 ns followed by another fall which is associated with edge effects. In this case, the velocity is not going into negatives values due to the large laser spot chosen (3.74 mm) which reduce the edge effects in this configuration with a 1 mm target. The values of the full width half maximum for each profile presented is given in table 3.3.

The FWHM of the 50 μm confinement is always shorter than the one observed for the other

Table 3.3: Full width half maximum of the first peak of the profiles presented in figure 3.12.

Laser intensity	**Thickness**			
	50 μm	**500 μm**	**1 mm**	**3 mm**
1.55 GW/cm^2	43.2 ns	57.6 ns	51.2 ns	55.2 ns
2.20 GW/cm^2	43.6 ns	51.6 ns	55.2 ns	53.6 ns
4.25 GW/cm^2	36.4 ns	48.4 ns	53.2 ns	49.2 ns

tapes. Another point raised by table 3.3 is the apparent shortening of the FWHM at higher laser intensities, whatever the thickness of polymer tape used as a confinement. Figure 3.13 offers a better representation of this effect.

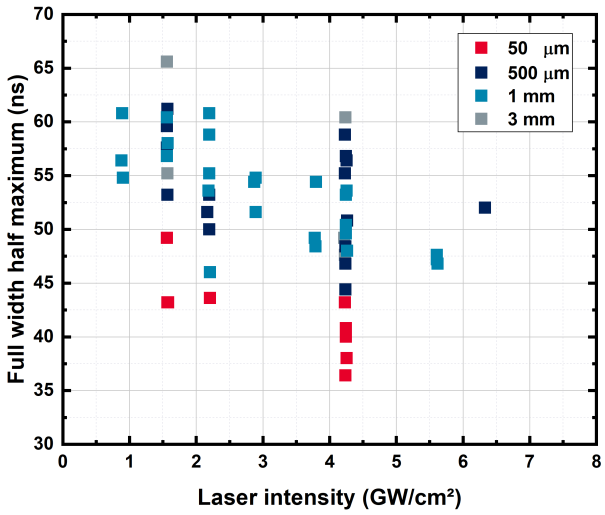

Figure 3.13: Full width half maximum depending on the laser intensity for different thicknesses of acrylate tape confinement with a laser spot of 3.74 mm, pulse duration = 7 ns on 1 mm aluminium targets.

The 50 μm tape exhibits shorter FWHMs compared to the other ones and the trend observed also confirms that the FWHM decreases with an increase of the laser intensity. An hypothesis would be that with higher laser energies, the tape will be tearing at an earlier time during the shot. If the tearing happens long after the peak pressure of the pulse, the effect will not be noticeable. On the contrary, if the hole happens during the release, the slow pressure decrease will be cut thus reducing the FWHM. This interpretation also suggests that with a confinement even thinner the tearing could

happen before the maximum pressure of the pulse is reached, causing a lower pressure to be produced by the shot besides it being shorter. It means that the pulse length could be tuned depending on the confinement tape thickness chosen to produce more or less thermal effect on the surface to be treated in the case of shots without thermal coating. Knowing that this process depends on the pressure produced, the thickness of the confinement medium and its mechanical properties, it is difficult to give a threshold and define parameters to control the tearing phenomenon to optimize the laser shock peening process

3.4.2.3 Plasma thickness versus confinement thickness

Due to the thinness of the 50 μm acrylate tape confinement, it has lower mechanical properties and breaks sooner than the other tape studied, causing the cutting of the release. If the tape breaks during the shock, the plasma starts to expand in the air, causing the interaction to pass from a confined regime to a direct one (see 1.2.1 and 1.2.2) causing a decreasing of the length of the interaction, due to the expanding of the plasma in the air, thus not being as efficiently heated while also not being confined at the interface between the target and confinement medium. The size determination of the plasma helps to put into perspective its size compared to the confinement thickness thanks to the equation developed by Fabbro et al. [201]:

$$L(\mu m) = 2.10^5 \, \frac{P(GPa)\,\tau(ns)}{Z(g.cm^{-2}.s^{-1})} \tag{3.5}$$

With:

L: the size of the interface, corresponding to the plasma thickness.

P: the pressure developped by the laser shock, obtained through equation 3.1.

τ: the pulse duration of the shot.

Z: the reduced impedance of the system target/confinement.

The method of calculation used to assess the impedance of the acrylate tape confinement makes the assumption that the mechanical properties of the acrylate tape is similar to that of an epoxy from the literature since their backface velocity profile obtained with VISAR measurements are the same. The density used for the calculations have been measured with a density scale at the laboratory ($\rho = 0.935$).

- This method allows the calculation of the impedance of the acrylate tape confinement based on the assumption described above. The parameters are calculated through the equation **??** ($P = \rho D u = Z u$ and $D = C_0 + S u$) under static condition with $u = 0$, leading to $D = C_0$. The shockwave speed D is calculated from shock experiment on different epoxies from the literature [197, 202, 203]. Figure 3.14 gives the Hugoniot curves and their fit allowing the obtention of their Hugoniot constant that can be used for the implementation of the Mie-Grüneisen equation of state (see 2.3.3.3), the value at $u = 0$ is given is figure 3.14a.

- A second possible method would be to make shock experiment directly on the acrylate confinement to obtain its impedance evolution depending on the laser intensity used. This would involve putting a coating on the two sides of the acrylate tape confinement, first for the laser not to go through the material and the opposite side, for the VISAR probe laser to be able to be reflected on the backface of the confinement. By extracting the pressure from the shots, the impedance can be calculated using $P = Z u$. The thickness of the plasma can then be extracted using equation 3.5. These experiments will be described in chapter IV.

The comparison between the two method would also be a good way to evaluate the difference between the assumption made for the calculation compared with the real behaviour of the acrylate tape confinement under laser shock conditions.

3.4.2.3.1 Impedance calculation from literature

Figure 3.14 gives the Hugoniot curves and their fit (which gives the S parameter) for shock experiments from [197, 202, 203]:

The different S extracted give a global approximated value of the parameter for epoxies under shock (≈ 1.6) than can be used for future simulation of the behaviour of the confinement under shock with the Mie-Grüneisen equation of state. The sound speed however is difficult to extract from these data except for figure 3.14a which gives shockwave velocity data starting from $u = 0$, thus giving a value of $C_0 = 2263$ m/s. The first part of the plot is a lot steeper than the rest of the plot, preventing the use of the Hugoniot constant S. For this reason the first part of the plot (from $u = 0$ to $u = 1500 m/s$) is fitted to obtain the shockwave velocity depending on the particle velocity in the range of interest for the laser shock experiment ($D = -0.47u^2 + 2.38u + 2.34$). This value of C_0 obtained is consistent with

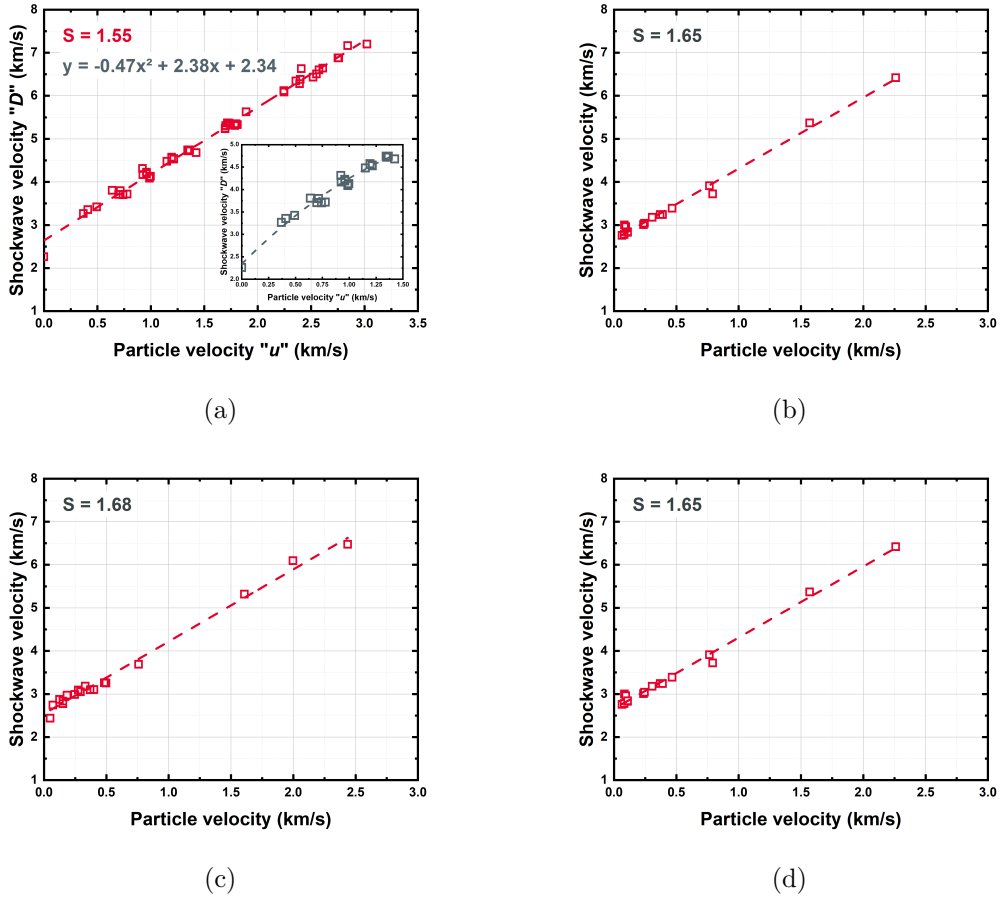

Figure 3.14: Shockwave velocity depending on the material velocity of different epoxies respectively from [197, 202, 203] and their linear fitting giving the S parameter from equation 3.3.

other value for epoxies found in the literature; 2000 and 2600 m/s, respectively from [204] and [205]. Since the backface velocity profiles using epoxy and acrylate confinement are the same, it is assumed that their mechanical properties and state are equivalent during shock. This obviously leads to some degree of approximation since the rubbery state and the transition to a state similar to the epoxy confinement is not taken into account in the calculation. The acrylate tape impedance calculated at $u = 0$ with a sound speed of 2263 m/s and a density of 0.935 is $Z = 2.12 * 10^5$ g.cm^{-2}.s^{-1}. The results of the calculation of the backface velocity, impedance and plasma size depending on the pressure are given in figure 3.15.

From figure 3.15c, the size of the plasma produced by the laser shock can be compared to the thickness of the confinement. The variation of the plasma thickness ranges from 0 to 13.8 μm. Even

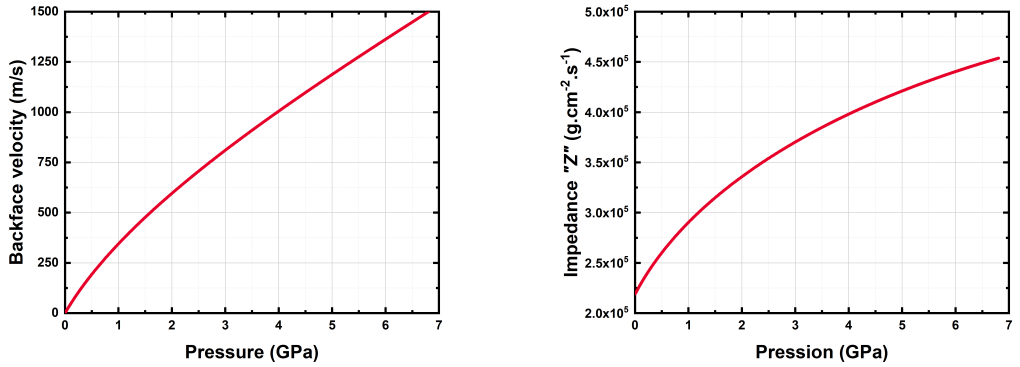

(a) (b)

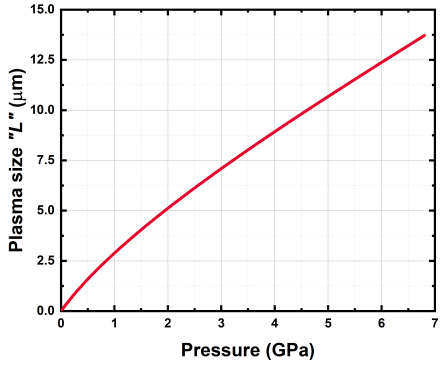

(c)

Figure 3.15: (a) material velocity depending on the pressure applied, (b) impedance of the confinement depending on the pressure applied and (c) plasma size depending on the pressure applied.

at low laser intensities (around 1 GW/cm^2) the plasma attains 2.7 μm which, in the case of the 50μm confinement represents $\approx$ 5% of its total thickness. The plasma size attains 10% of the total thickness of the confinement at 4.5 GW/cm^2 an energy close to the one used for industrial treatments. The important size of the plasma compared to the confinement thickness can explain its propensity to easily tear, even under low laser intensity shots.

3.4.2.3.2 Impedance calculation from experiments

Another way to approach the problem would consist in using the pressure, laser intensity and material velocity known from VISAR measurements performed directly on the acrylate tape. By coupling the results obtained with the equations 3.2 and 3.3 the impedance of the acrylate tape

depending on the pressure could be extracted.

3.4.2.4 Tape damaging under laser irradiation

A cause of optical transmission loss is the damaging of the confinements shot by laser. During laser shock process, multiple parameters can induce damaging of the confinement. In the classic case (i.e. with water) the problem is not encountered as the water flow is constantly renewed. However, in the case of a solid polymer confinement, replacing the confining medium is more difficult, time consuming and costly. For these reasons, knowing the state of the polymer after shots is important.

3.4.2.4.1 Transmission after shot

To assess the damaging of the confinements studied, the transmission of the acrylate tape was measured after a single shot for different laser intensities. The results given in figure 3.16 and 3.17.

The first figure shows the transmission of the acrylate tape confinement after one laser shot for different laser intensities and for the different thicknesses of confinement available. One can see that the two thinnest confining layers exhibit a decrease of their transmission after one shot sooner than the 2 mm and 3 mm confinements (the decrease for 500 μm and 1 mm confinements starts respectively at 2 and 2.5 GW/cm^2). The 2 and 3 mm ones show a decrease of their transmission at around 3 GW/cm^2 but the slope is a lot less steep, thus when the 3 mm confinement is shot with a laser intensity of 4 GW/cm^2 it still has a transmission of 70 to 80 % while the 500 μm one shows a transmission of 18 %.

Figure 3.17 shows the same phenomenon with the silicone confinement. The backface velocity was extracted by VISAR measurement for multiple laser shots on the same area of a 200 μm 99.0 % aluminium target. The velocity stays high for 2 shots (323 and 345 m/s) before decreasing rapidly to attain 103 m/s after five shots. A slower decrease is then observed until nearing 0 at 18 shots, showing a transmission close to 0 as well.

3.4.2.4.2 Tape imaging

Imaging of the acrylate polymer tape have been performed after mono-shot at different laser intensities to assess and better understand the damaging of the tape. Figure 3.18 shows the results of this experiment.

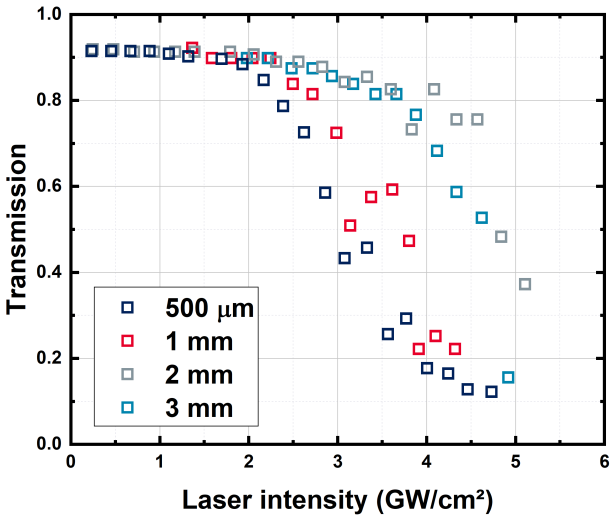

Figure 3.16: Transmission depending on the laser intensity taken after a single laser shot for different thicknesses of acrylate tape confinement. Wavelength = 532 nm, pulse duration = 9 ns.

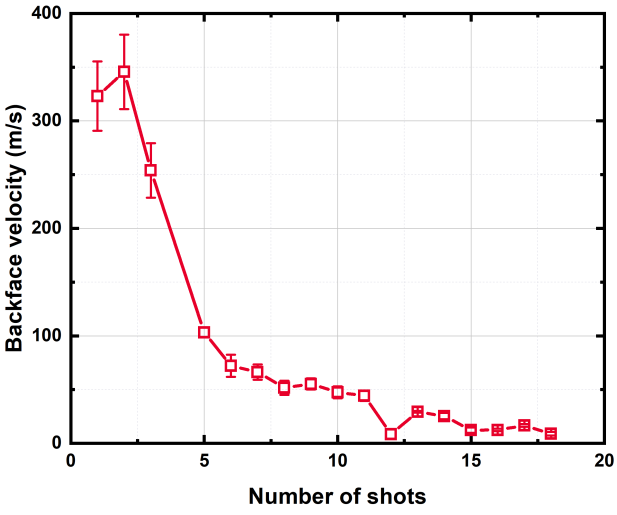

Figure 3.17: Velocity obtained by VISAR measurements for multiple shots on the same sample with the same silicone confinement. Laser intensity is 2.3 GW/cm², wavelength = 532 nm, pulse duration = 9 ns.

For every tape, a debonded area, larger than the laser spot used was observed after shock, preventing the direct application of a second laser pulse which would not be in a confined configuration

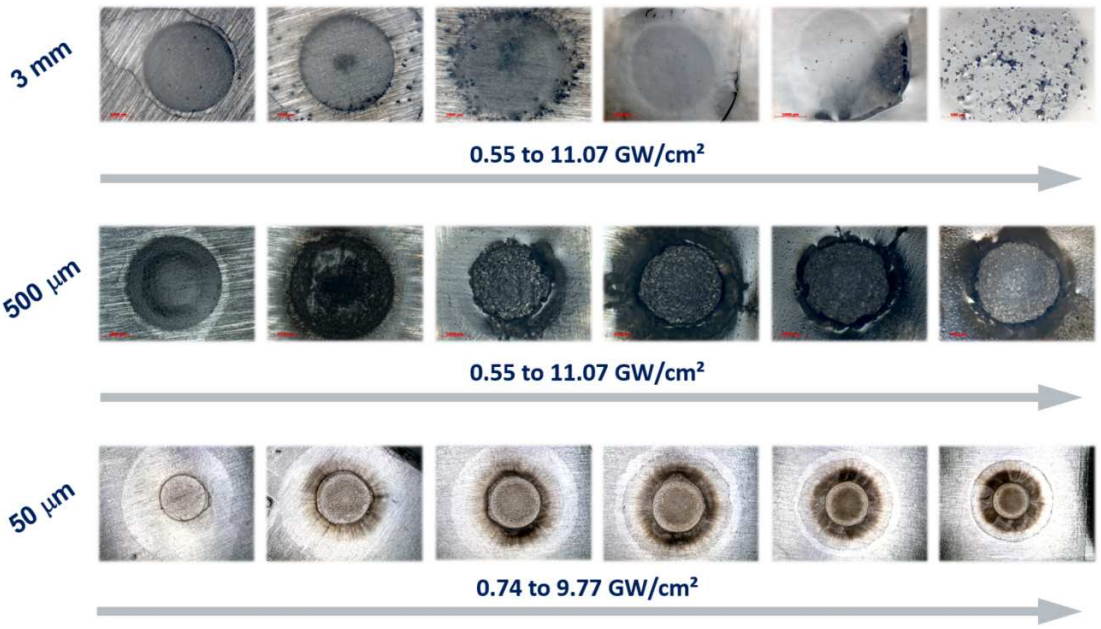

Figure 3.18: Influence of the thickness of the acrylate tape polymer and of the laser intensity on the confinement damaging after mono-shots with three different thicknesses of acrylate tape confinement on 1 mm aluminium targets.

and consequently produce a low pressure applied for a shorter duration. At low intensity all the tapes present signs of damage initiation mainly localized at the surface and subsurface of the confining medium while the backface of the acrylate tape, in contact with the aluminium target is also damaged and polluted but mainly by the effect of the plasma expansion. The plasma is composed of the matter present at the interface shocked, so to say, aluminium and the chosen confinement, meaning that aluminium ions and particles are projected on the confinement during shock, making it lose some of its transparency, again hindering the reusability of a polymer confinement after one shot. The plasma produced during shock also contain particles ripped off from the confinement. Due to its temperature, the plasma also induce potential thermal damaging to the confinement. Depending on the thickness of the acrylate tape confinement used, different effects are observed at different laser intensities:

- With a 3 mm tape, only low damaging is observed at low intensities in the form of black spots caused by impurities absorbing laser energy and initiating localized pyrolysis. At high intensities a surface opacification is observed as well as some tearing of the tape. Going at even higher laser intensities produces craters on the surface of the confinement as well as stronger opacification

due to the production of a breakdown plasma absorbing the incident energy from the laser pulse at the surface of the polymer tape.

- With a 500 μm tape, at low intensities only slight damaging and debonding are observed while going a slighlty higher energies will cause complete tearing of the tape on an area a little bit bigger than the laser spot size. Due to the tearing opacification is not observed , instead of having thermal effects localized at the surface of the confinement, they are localized at the surface of target, thus inducing thermal effect on the aluminium surface.

- With the 50 μm tape, even at low laser energies, the confinement tape is directly completely removed. Going higher in laser intensity causes a brown ring to appear around the laser spot size, caused by the plasma depositing aluminium particle around the impact point of the laser. This phenomenon could be used as a way to remove the confinement if the configuration chosen allow for a change of tape at each shot.

3.4.2.4.3 Infra-red characterization

Another way to assess the damaging of the acrylate tape confinement after laser shots consists in performing infra-red measurements on a sample of the tape before and after laser shot at different intensities or a different number of shots. In the case of damaging, the chemical changes induced by the bond breaking are visible on the IR spectra. Figure 3.19 shows the effect of shots at different laser intensities on the IR spectra of the acrylate tape. With this method only the surface of the acrylate tape confinement can be probed, the damaging occurring in the thickness of the material, although observable, cannot be studied.

The infra-red spectra presented show two areas of interest. First, between 3600 and 3000 cm^{-1}, a broad peak can be seen appearing with the spectrum in figure 3.19b with the increase of the laser energy used for the shot. The same phenomenon is observed for in the 1700 to 1500 cm^{-1} range in figure 3.19c. This is likely caused by the breaking of O-X chains, thus causing the creation of hydrogen bond between the H available in the surrounding environment and the oxygen. The creation of such bonds reduces the adhesive properties of the tape since the oxygen cannot link with the surface of which the confinement is layed on. The same effects are observed in figure 3.19d. In this case multiple laser shots were realised at a low laser intensity (2 GW/cm^2). The repetition of the shot induces the

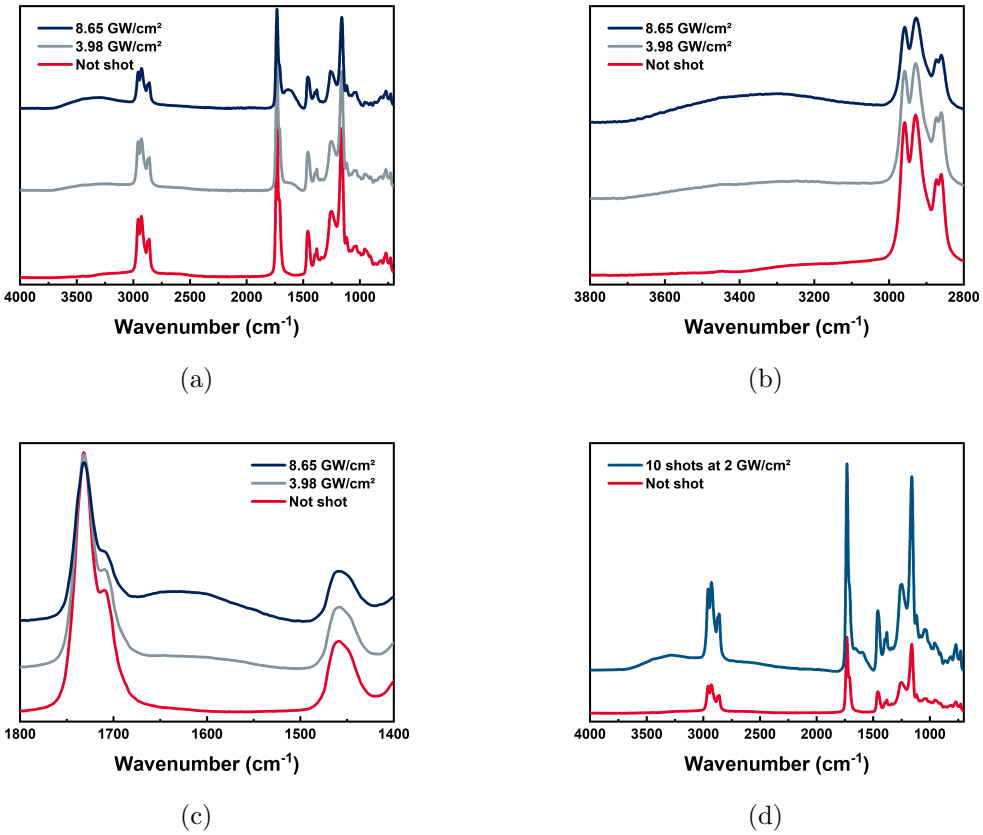

Figure 3.19: Infra-red spectra of the acrylate tape confinement before and after laser shot with a 3 mm laser spot, 7 ns pulse duration, 532 nm. (a) at two different laser intensities (3.98 and 8.65 GW/cm^2, (b) focus on the 3800 to 2800 cm^{-1} area, (c) focus on the 1800 to 1400 cm^{-1} area and (d) effect of 10 laser pulses at 2 GW/cm^2 on the acrylate tape confinement.

creation of defects that then act as absorbing points for the incident laser energy and speeds up further the damaging process.

3.4.2.5 Conclusion on the confinement thickness effects

The shot repetition during the laser shock peening treatment will be mainly limited by the decrease of the transmission of the confinement. It appears necessary to find a way to either replace the confinement after a set number of shots or to enhancement the resistance of the confinement to the laser interaction. It is also important to note that although the thickness of the polymer confinement chosen does not have any noticeable effect on the maximum pressure produced by a laser shot, other parameters are affected when the confinement reaches really low values (in this case 50 μm):

- The full width half maximum (FWHM) is shortened, causing the pressure to be applied for a shorter duration and finally resulting in residual stresses induced by the laser shock peening treatment to be shallower.

- The reduction of the FWHM affects the release of the pressure profile, causing the thermal effects to be applied for a shorter duration. In the case of a LSP treatment without thermal coating under this type of configuration, the thermal effects on the surface of the treated target should be mitigated allowing for better mechanical properties.

3.5 Adhesion

The time before the confining medium is debonded from the surface of the shocked target has been shown to have a significant role in the final pressure produced by a laser shock. For this reason, the adhesive properties of the confinement can have an influence on the process capability. The adhesive properties of different polymers were modified to be able to evaluate the effect of this parameter on the laser shock peening process. Two methods were used, for the first polymer, a silicone (Sylgard184, Dow Corning) was chosen, it is synthesized by mixing a base with a cross-liking agent with a 1:10 ratio. Changing the ratio modifies the curing of the polymer and as a result, changes its mechanical and adhesive properties as described in figure 3.20.

The second confining polymer chosen was the acrylate tape confinement already presented. To modify its adhesive properties a corona treatment was applied on it. The corona treatment consists in creating a corona discharge by applying a high electrical current to an apparatus tip to ionize air. The tip is placed close to the surface of the polymer to treat causing a change of surface energy. In practice, applying the plasma induce the rupture of chains at the surface of the polymer which, in turn creates dangling chains that participate to better adhesives properties. To assess the effectiveness of the process contact angle measurement were performed. After treatment if a lower contact angle should be observed that can be correlated to higher adhesive properties due to the increase of the surface energy. Figure 3.21 gives a representation of the corona treatment technique and of the contact angle one.

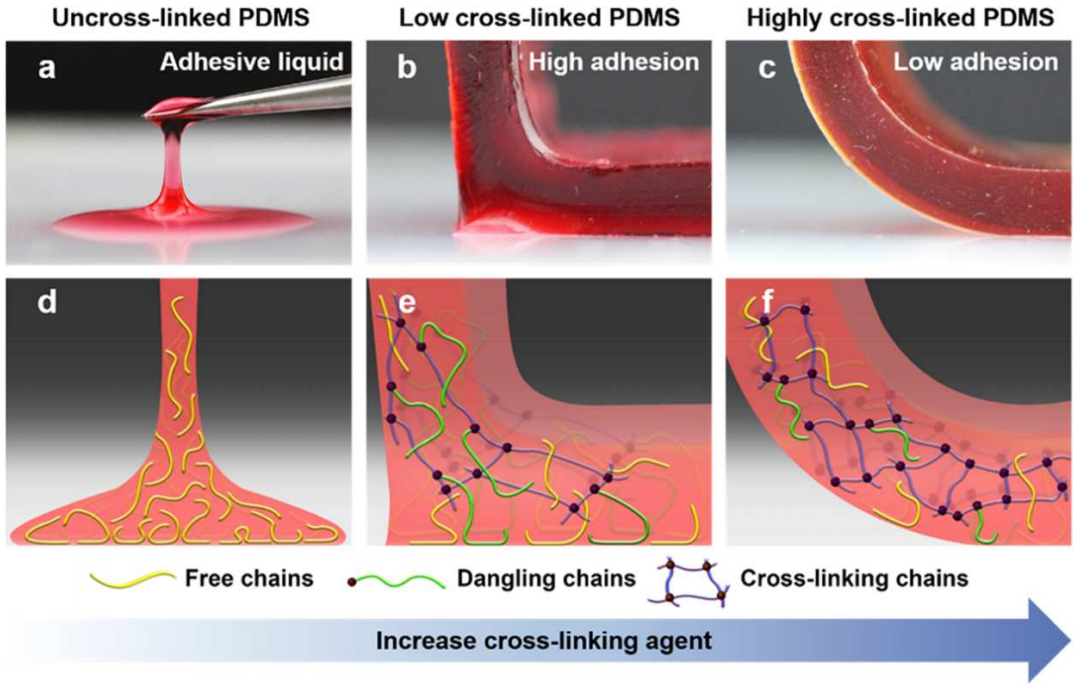

Figure 3.20: Design of patches of polydimethylsiloxanes (PDMS) by modification of the polymer chain mobility through its cross-linking. (a, d) uncross-linked PDMS adhesive that can easily spread on the surface because of the high mobility of the free chains. (b, e) low cross-linked PDMS with free and dangling chains that give the polymer a high adherence to the surface. (c, f) highly cross-linked PDMS that can easily be peeled off of the surface due to its reduced number of free and dangling chains (taken from [206]).

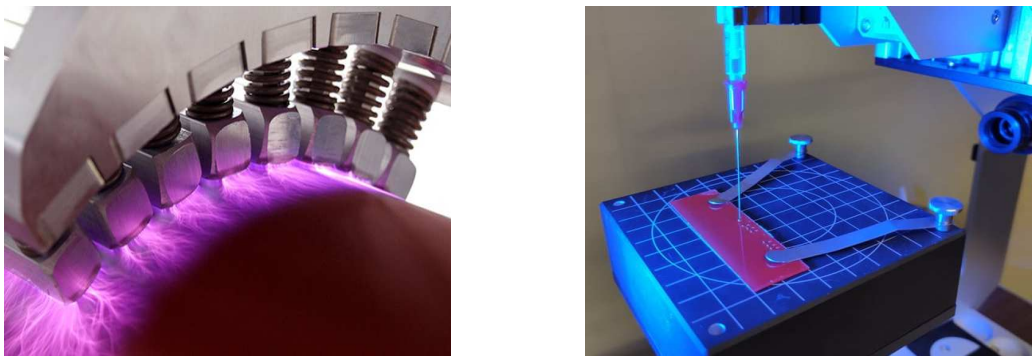

(a) (b)

Figure 3.21: (a) Corona treatment apparatus and (b) contact angle machine used during the experiments.

3.5.1 Silicone confinement

The silicone confinement was cured using two different ratio. The first one was synthesized using the classic recommended ratio of 1:10 hardener to base to produce a slightly tacky transparent adhesive

while the second ratio chosen was 6:100, giving a softer material with better adhesive properties. In both cases the base and hardener were thoroughly mixed before leaving it cross-liking for at least 24 hours at in air at ambient temperature. The mixture was covered to prevent any dust from coming into contact with it and small holes were placed on the lid to allow the gas produced by the reaction to escape from the container. The two polymers were then used as confinement during laser shock and the pressure produced was obtained from VISAR measurments. The laser spot size chosen was 3 mm on aluminium target with a 1 mm thickness. The silicone thickness was comprised between 300 to 600 μm depending on the sample. This thickness does not induce changes in the pressure produced as shown in the previous section. The laser intensities used ranged from 0.23 GW/cm^2 to 7.27 GW/cm^2, producing pressures up to 4.69 GW/cm^2. The results obtained are given in figure 3.22. Silicones with much higher quantity of cross-linking agent were not used because of their really low adhesive properties as well as their tendency to crack. On they contrary using lower quantity than 6% of curing agent would lead to a material too liquid to be used.

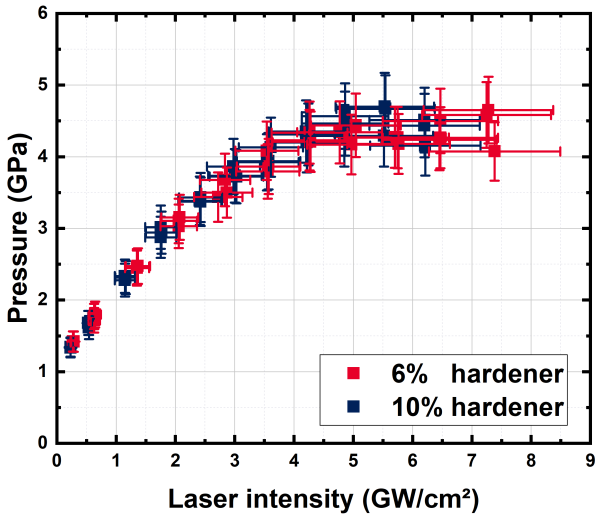

Figure 3.22: Pressure depending on the laser intensity on alumnium 1 mm thick with silicone confinements (Sylgard184) with different cross-linkings. The laser spot size used is 3 mm.

The pressure rising depending on the laser intensity does not change with variation of the adhesive properties through variation of the cross-linking of the silicone. Either the variation is too small for an effect to take place or it has no effect on the pressure production during shock. A slight difference that can be noted is the debonding on the confinement from the surface of the aluminium target. In

the case of a low cross-liking (the 6% curing agent for instance) the stronger adhesive properties can lead to more tearing of the confinement during the shock although this type of effect is also linked to the reduced mechanical properties caused by the lower cross-linking.

3.5.2 Acrylate tape confinement

The acrylate tape confinement was modified through corona treatment, the technique is commonly used to change the surface energy of materials. Since it breaking bond at the surface of the tape, the technique can be considered destructive but the thin surface affected does not lead to noticeable changes in the mechanical properties of the treated acrylate tape. The dangling chains created by the process are mainly O-H chains breaking, over time these chemical functions are recovered by reaction with the surrounding hydrogen in the air. Because of that the laser shock experiments were realised directly after application of the corona treatment and three days after. The results were then compared to the one obtained without any treatment. The assessment of the effect of the treatment was done with contact angle measurement at the PIMM laboratory with the help of Lauriane Truffault and Alain Guinault.

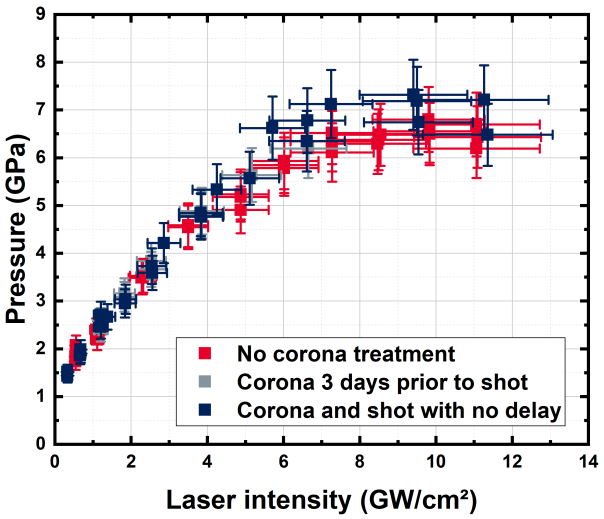

Figure 3.23: Pressure depending on the laser intensity for shots on 1mm aluminium targets with an acrylate tape confinement treated or not with the corona technique.

Figure 3.23 shows the effect of the corona treatment on the pressure produced by laser shock

depending on the laser intensity used for the shot. The trend followed is the same as with no treatment. A small difference is observed starting 6 GW/cm^2 between the samples shot after corona treatment with no delay and the others. Since the breakdown plasma formation starts at around 7 GW/cm^2 this small drift from the trend is not significant. The same breakdown phenomenon is observed with the formation of a pressure plateau after 6 GW/cm^2. The breaking of bonds at the surface of the acrylate tape confinement can explain the triggering of the breakdown phenomenon at a lower power density (6 GW/cm^2 versus 7 GW/cm^2 usually). The broken bonds act as defects that absorb more energy that undamaged matter and produce triggering points for further growing damages that favour a breakdown initiation. The same effect is not found with the shots realised 3 days after the corona treatment of the acrylate tape. This shows the recovery of the broken bond and by extension transparency by reaction chemical reaction of the dangling chains with the surrounding environment by the acrylate polymer.

3.6 Chemical composition

The chemical composition of the material used as a confinement for the laser shock peening process should have an influence on the process. The pressure produced is the same as shown previously with the pressure measurement with the different confinements. With the same measurements small differences were found in the breakdown thresholds of the different confinements and more particularly between the carbon-based and Si-based polymer chains. These differences are mainly due to the difference of optical transmission between the different material. A less transparent confining medium will absorb more incident laser energy, thus being damaged sooner and creating more starting points for further damaging. Because of that the breakdown will occur at lower laser energies compared to a material with less optical losses. The second explanation to the difference in breakdown threshold lies in the different backbone chains of the polymers used for the confining medium. A silicone chain typically has a higher bond strength compared to a carbon-carbon one which results in a silicone polymer having a higher resistance to damaging in most industrial uses. In the case of laser shock the energy involved is so high that defining an effect and decorrelating it from the optical transmission effect appears difficult.

A last point of differentiation between the use of two different backbone polymer chains as a confinement is the full width half maximum of the backface velocity profile, corresponding to the pressure duration produced by the laser shock with a certain set of parameters. To evaluate this variable,

laser shots have been realised with 1 mm acrylate tape and 300 to 600 μm silicones (Sylgard184, Dow Corning) synthesized at the laboratory using the normal 1:10 ratio. The laser spot size chosen was 3.74 mm with a pulse duration of 7 ns. Only the A beam of the Héphaïstos laser was used for these experiments to avoid any misalignment between the two beams. The laser intensity of the shots was 4.2 GW/cm^2, an energy allowing the production of an already large pressure while making sure that the breakdown threshold is not yet reached. Figure 3.24 shows the backface velocity profiles obtained for the experiments described on 1 mm 99% aluminium targets.

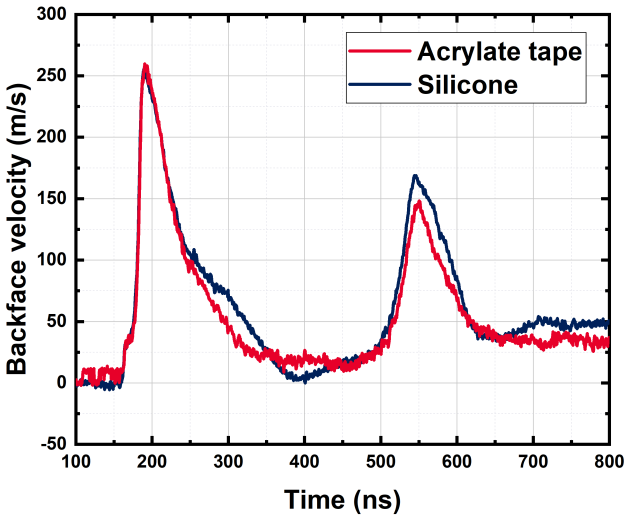

Figure 3.24: Comparison of the pressure depending on the laser intensity for the acrylate tape confinement and a silicone one. The two materials differ by their different backbone chain. The laser energy used was 4.2 GW/cm^2 with a laser spot size of 3.74 mm and a pulse duration of 7 ns. The shots were realised on 1 mm 99% aluminium targets.

The maximum velocity attained with the two confinements is the same as well as the full width half maximum with 48 ns for the acrylate tape and 52.4 for the silicone. A difference is observed during the release. The acrylate tape confinement shows a decrease of the backface velocity without any edge effects while the backface velocity profile of the silicone confinement show the beginning of the release followed by the edge effect at 300 ns, showing a minimum of 0 m/s at 400 ns. The second peaks do not present as much difference.

3.7 Residual stresses measurements

The last parts showed the calculation of the maximum pressure produced by laser shots while varying different properties of the polymer confinement. The results demonstrated the control over the pressure calculation with the different material used. Consequently the next step is to treat an area to realise residual stress measurement to assess the effect of a surface treatment using polymer confinements. The surface treatment, as opposed to the monopulse used up until now, induces 3D effects while a 2D axisymmetric representation was enough up until now. In the case of small laser spots (1 mm or less) coupled with high overlap between shots, the surface is homogenized and the residual stresses are uniformly distributed, hence allowing the use of an axisymmetric model to obtain a good representation of the residual stresses imparted by the laser shock treatment even if the ideal representation would still be involving a 3D model.

In the case of the use of bigger laser spots with lower overlap (20-70%) different areas of the treated surface do not see the same amount of laser shock. Because of that, the residual stress repartition can be affected and making a potential modelling of the process more complicated and the calculation more time-consuming due to the obligation to switch to a 3D modelling. Figure 3.25 gives an example of the described phenomenon in the case of a treatment using 50% overlap. Different areas see between 1 to 4 shots depending if they are on the edge of the treated region or in a specific location between lines of shots.

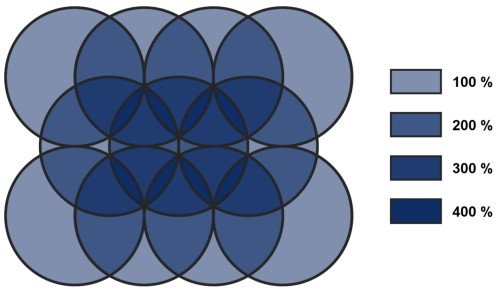

Figure 3.25: Number of laser shots seen by the matter in the case of a surface treatment using a 50% overlap.

3.7.1 Laser shock set-up

For the residual stress measurement, 7175-T7351 aluminium alloy coupons with a size of 60x60x30 mm were used. This alloys was supplied by Airbus and prepared the same way as the matter used directly on the aircraft in order to have transposable results to an industrial use. This aspect is of crucial importance due to the impossibility of performing residual stress measurements on plane piece after treatment. This means that the characterization of the process capability upstream need to be fully representative of the conditions that will be encountered in the final use to guaranty the efficiency of the treated material after laser peening without having to carry out characterization.

The set up used for the area treatment was had to be modified due to the specificities of the treatment with a flexible polymer as a confinement. Due to the damaging of the confinement in between shots coupled with the debonding when large spot are used, the area treatment had to be done by hand. For this reason, large spot of 4.7 mm were chosen with a laser intensity of 4 GW/cm^2 for each shot. An overlap of 50% was used and the area was covered three times to induce the residual stresses at an important depth. Moreover, to avoid the apparition of tensile residual stresses at the surface of the coupons treated, a thermal coating was used. For this purpose an aluminium adhesive was used, composed of 40 μm of adhesive an 50 μm of aluminium. The choice of aluminium as thermal coating, allows for an improvement of the pressure due to impedance mismatch in the case of treatment of steels or titanium alloys. In this case since the impedance of aluminium and the aluminium alloy coupon, the impedance is nearly the same and does not induce pressure changes.

Figure 3.26 shows different photos of the set up used for the treatment of the Al7175 blocks from the block placement to the block after residual stress analysis through incremental hole drilling technique. The displacement between each shot was realised with micrometric screws to obtain the desired overlap while covering an area at the center of the block of at least 20x20 mm. The acrylate tape confinement was replaced between each shot while the aluminium thermal coating was replaced after each line due to its width not covering the whole area of interest.

3.7.2 Surface state before and after treatment

The roughness of the surface was measured before and after the application of the first, second and third layer of lasers peening. The evolution of the roughness with the laser shock peening process

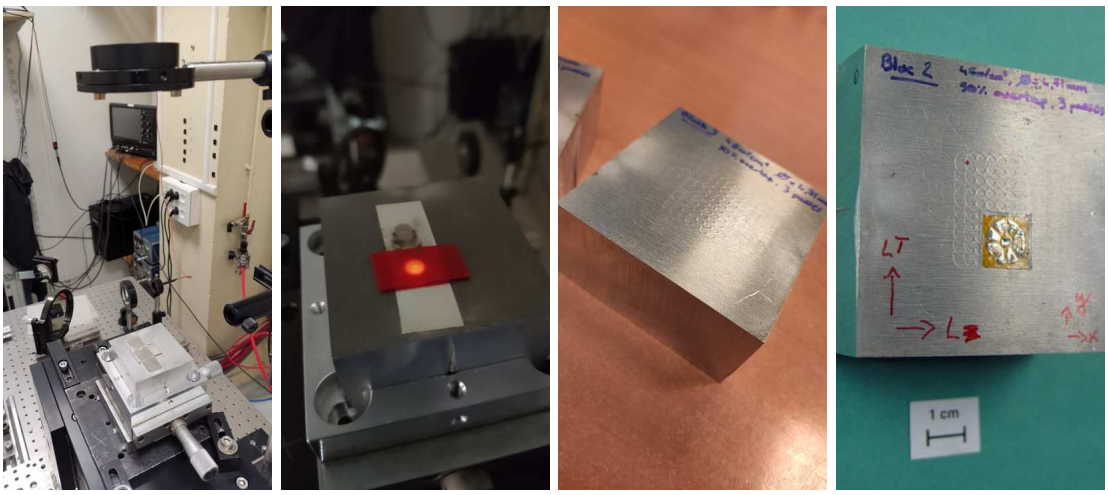

(a) (b) (c) (d)

Figure 3.26: Set up used for the residual stress treatment (a) Laser set up used for the treatment in the laboratory, (b) laser alignment with the aluminium thermal coating and the acrylate tape confinement with its liner, (c) coupon after treatment and (d) coupon after the residual stress measurement by incremental hole drilling technique.

is given in figure 3.27. The global roughness measured (Ra) before treatment on a 25x25 mm area is 1.90 μm. After one layer of laser treatment applied the roughness goes up to 2.10 μm and continues to get higher with the second and third layers applications (respectively 2.63 and 2.99 μm). Such an increase of the surface roughness is quite low but is still enough to need a resurfacing to reduce the final roughness of the treated piece to a desirable value. Due to the depth of the compressive residual stresses imparted in the material shocked, such a post-treatment is not problematic.

3.7.3 Residual stress measurement

Once the sample for residual stress measurement were ready, they were sent to Ulrike Heckenberger (Airbus Defence and Space, Brême) for analysis. The surface data were obtained using XRD measurement while the in-depth profile was obtained through incremental hole drilling technique up to 1 mm.

3.7.3.1 Surface measurement

For the evaluation of the surface residual stresses, X-ray diffraction was performed for the [311] plane with a Cr-tube using a 2 mm gauge and a 3 mm increment. The detail of the calculation is

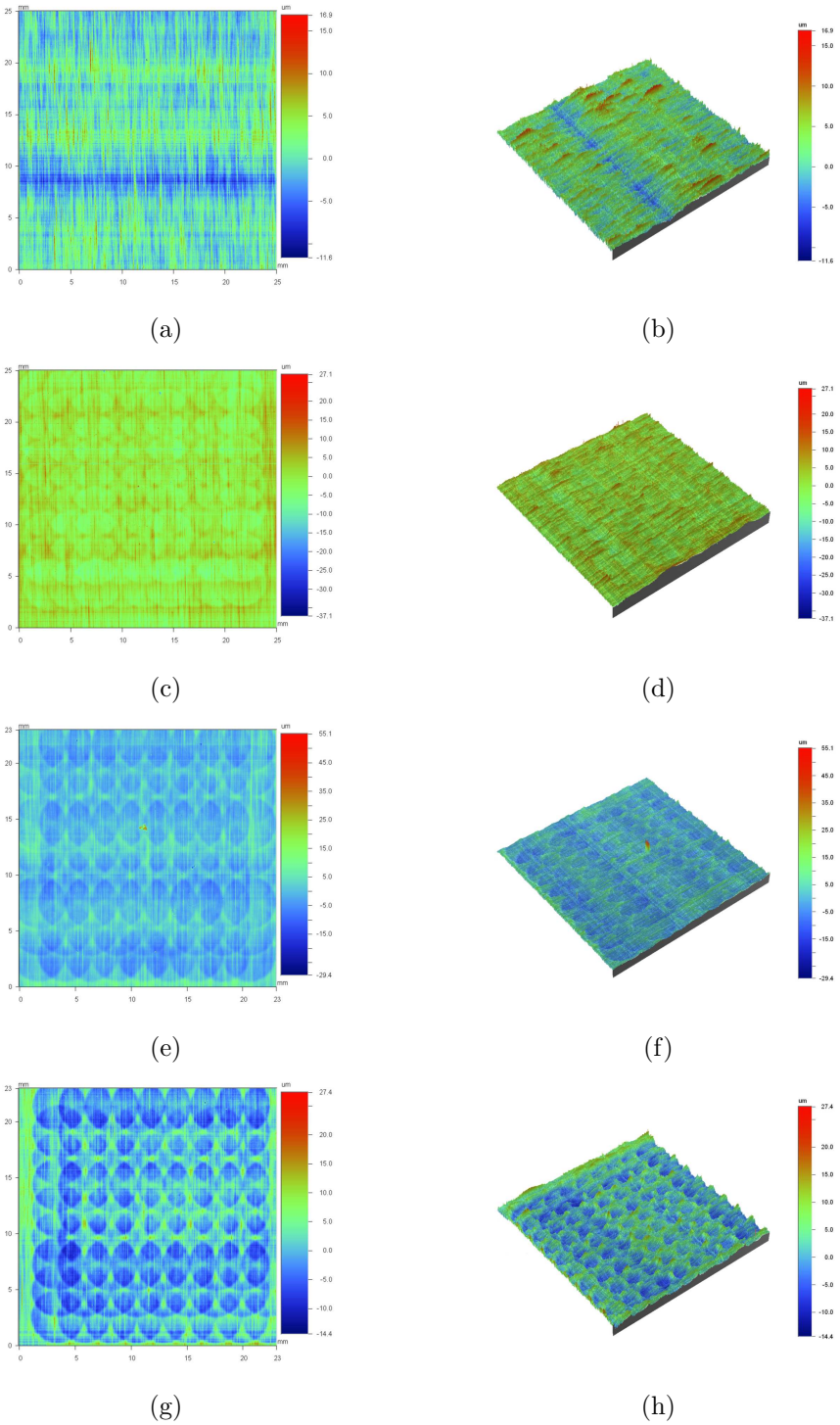

Figure 3.27: Surface roughness measurement with a DEKTAK apparatus on a 25x25 mm area for (a,b) non treated al7175 block, (c,d) after one layer of treatment, (e,f) after two layers of treatment, (g,h) after three layers of treatment.

given in chapter II (2.5).

3.7.3.2 Residual stresses calculation experiment

The experiment were realised by scanning the surface of the treated block at different positions along the edge of the treated area to make a line. The line was repeated lower and lower. The measurement was made in the two directions noted L and LT respectively the rolling direction of the sample and the orthogonal direction to it. Figure 3.28 give a representation of the points measured on the sample. The rolling direction can be observed on figure 3.28a with elongated light grey line from left to right. The measurement was also realised 10 mm above the peened area to have a non-treated reference and be able to attest that the laser shock peening treatment indeed induced compressive residual stresses in the matter.

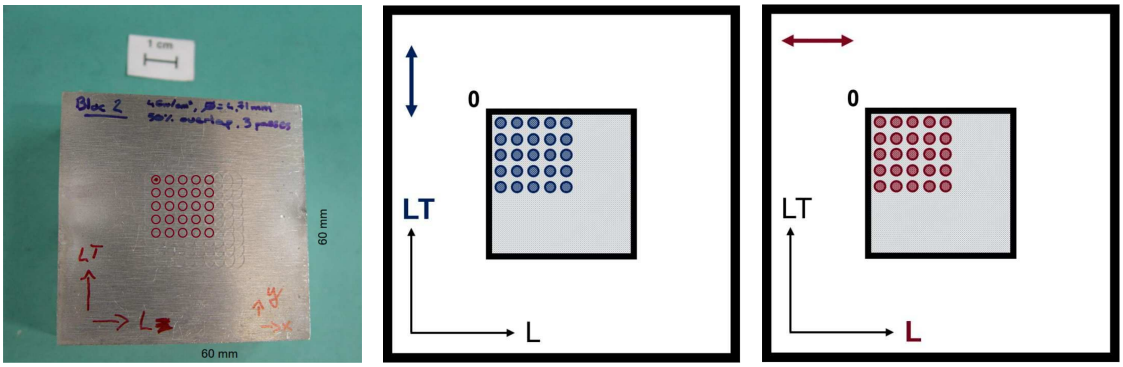

(a) (b) (c)

Figure 3.28: Surface XRD measurements realised on the al7175 coupon (a) coupon before the XRD measurement, (b) L direction, the rolling direction and (c) LT direction the orthogonal direction to the rolling one.

The results of the different measurement is given in figure 3.29 both in a treated and non-treated area . It is important to note that the XRD measurement gives access to the surface stresses averaged on the 50 to 100 first μm. In the case of these measurement it does not cause any problem since a thermal coating was used but in the case of a laser shock peening treatment without such a coating the tensile residual stresses at the extreme surface of the coupon will not be accurately represented. A solution to this problem would be to realise synchrotron measurements of the surface but this would also require a grain size sufficiently small as well as an isotropy of the grain orientation.

The measurements in the two directions give similar results. An average of -275 $\pm$ 15 MPa is found

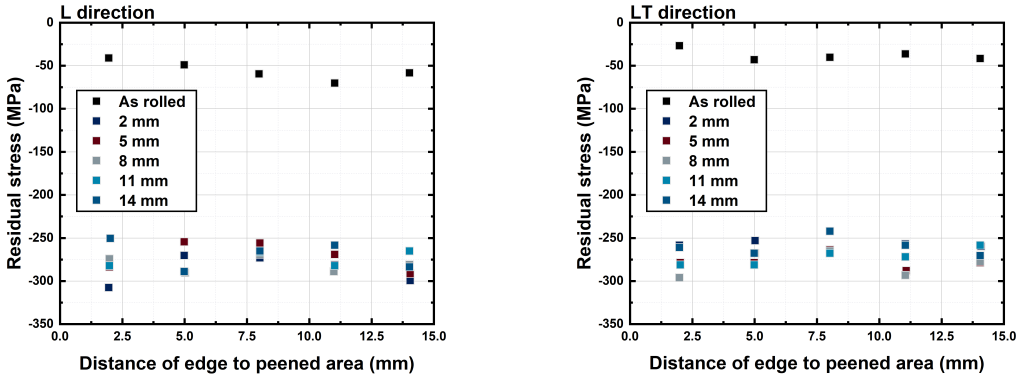

(a) (b)

Figure 3.29: Result of the XRD residual stress measurement at the surface of the treated block (a) along the L direction and (b) along the LT direction.

in the L direction while an average of -270 $\pm$ 15 MPa in the LT direction is obtained. The similar results indicate an homogeneous repartition of the residual stresses independently of the probed direction. The measurement in a non-treated area also resulted in negative values indicating compressive residual stresses although no compressive shock has been seen by the matter. This observation is explained by the rolling treatment that the alloy was subjected to during its pre-treatment. The surface values obtained are coherent with literature in close aluminium alloy such as al7075 treated by 3 water confined laser shots at 4 GW/cm^2 with a 25 ns Gaussian pulse duration at a 1064 nm wavelength and a 4.35 mm spot size and 67% overlapping by Peyre et al. [207].

3.7.3.3 In-depth measurement

For the in-depth measurement, incremental hole drilling was used. The technique consists in applying a strain rosette on the surface to be analysed before drilling in the middle of it to induce stress relaxation. The observation of the micro deformations of the piece surface is then used to calculate the residual stresses in the material. The full procedure is described more in detail in ASTM E837. For the experiment, the depth of drilling went up to 1 mm. Figure 3.26d show the rosette applied to the sample. The results obtained through the measurement are given in figure 3.30 and show high compressive residual stresses from the surface to the limit of 1 mm probed. The information was extracted, like with the XRD surface measurement in both the L and LT directions. Both of the directions exhibit similar values, confirming the isotropy of the stresses induced in the matter by the

laser treatment. The surface residual stresses are respectively for the L and LT directions -275 and -270 $\pm$ 15 MPa. The values slowly increases up to -191 and -166 MPa at 1 mm depending on the direction.

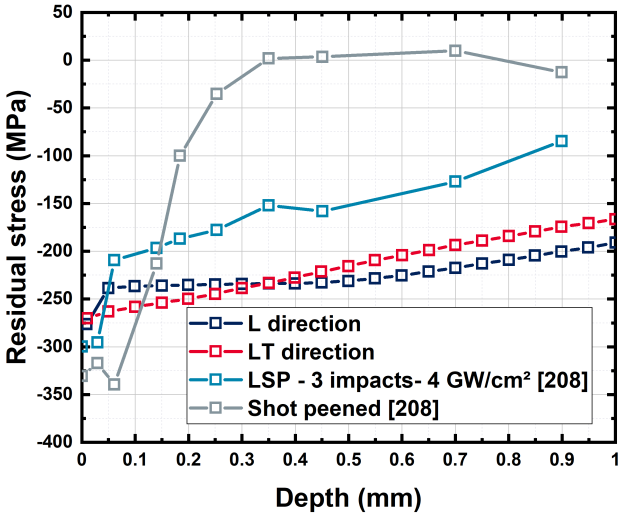

Figure 3.30: Residual stresses measured on a laser peened Al7175 coupon by incremental hole drilling method up to 1 mm and in-depth residual stress fields induced by LSP or shot-peening on 7075-T7351 by incremental hole-drilling method measurements (I = 3 GW/cm^2, pulse duration = 25 ns, Gaussian pulse, spot size =4.35 mm, water confined with al tape as thermal coating) (taken from [208]).

These results are similar to what was presented by Peyre et al. work from [207]). In the case of the treatment realised with the acrylate tape confinement the residual stresses induced are a little bit lower at the surface but stays higher in depth.

The similar results obtained with the laser treatment of two similar alloys with close laser parameters but with different confinement (i.e. water and acrylate tape) shows the capability of the flexible polymer confinement to be used as a replacement for the water confined configuration and allow the treatment of claustrated areas where laser shock peening could not be performed up until now. The problem to the complete implementation lies in the damaging of the tape through the process, both by thermal effect caused by the plasma creation and expansion but also by the mechanical loading inflicted to the polymer used as confinement during the shock propagation (see figure 3.31. Such as high pressure coupled with high strain rate, debond the confinement from the surface of the material treated. In the case of repeated laser shots the configuration is not in a confined mode anymore, mean-

ing that the pressures induced are greatly diminished as well as their length of application. Solutions are envisaged to mitigate these effects. For instance, the use of the final industrial configuration (spot size $\leqslant$ 1 mm, 1064 nm, 1 J) should produce less confinement damaging due to the smaller size of the plasmas created inducing lass polymer confinement debonding. Another way to avoid the damaging problem would be to automate the replacing of the confinement in between laser shots or between a defined number of shots.

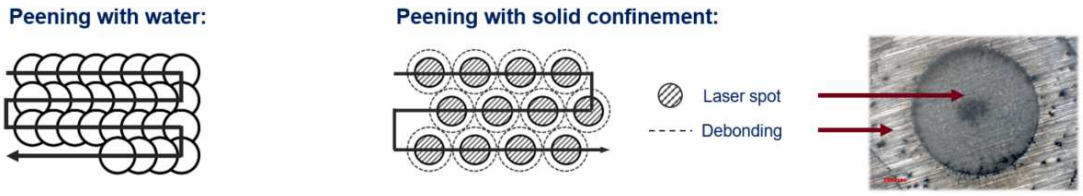

Figure 3.31: Peening pattern needed for treatment with water and solid confinement an description of the debonding phenomenon.

3.8 Conclusion

Different experiments were performed, first pressure measurement in order to determine the polymer able to deliver the highest pressure when used as a confinement. At the end of this step, the acrylate tape from Coroplast was chosen as it produces the same results as the water confined configuration in term of maximum pressure produced. Then, other experiments were performed to obtain information on the influence of various parameters such as:

- The optical transmission of the confinements studied at 532 and 1064 nm.
- The effect of the laser wavelength on the pressure produced by a laser shot.
- The influence of the polymer Young's modulus on the pressure produced.
- The confinement thickness influence.
- The effect of the adhesion properties of the polymer on the VISAR measurements.
- The influence of the backbone chain of the polymer used as a confinement.

After these characterizations, the acrylate tape confinement was used to produce a sample for residual stress measurement by XRD at the surface and hole drilling method in-depth. The results showed that the compressive residual stresses imparted in an Al 7175-T7351 block are equivalent to the residual stresses obtained for a similar, water confined treatment on a 7075 block with close mechanical properties. These results demonstrate the possibility to treat all types of alloys while using polymer confinement for the laser shock peening process.

The acrylate tape chosen gather all the properties needed in terms of interaction that were defined at the end of chapter I. The results obtained with the acrylate tape used as a confinement on aluminium targets are given in table 3.1.

Polymer confinement under shock

4 | Polymer confinement under shock

Content

4.1 Dynamic glass transition . . . 170
4.1.1 Material choice . . . 171
4.1.1.1 Polymer synthesis . . . 171
4.1.1.2 Transmission measurement . . . 172
4.1.1.3 Dielectric relaxation spectroscopy setup . . . 172
4.1.2 Dielectric relaxation spectroscopy results on acrylate tape . . . 172
4.1.3 Polycarbonate and polydimethylsiloxane study . . . 175
4.1.4 Comparison with laser experiment . . . 178
4.1.4.1 Rear free surface velocity profiles . . . 179
4.1.4.2 Simulation parameters . . . 180
4.1.4.2.1 Constitutive model . . . 182
4.1.4.2.2 Spatial and pressure profiles . . . 183
4.1.4.3 Simulation results - Strain rates extracted . . . 184
4.2 Acrylate tape mechanical characterization . . . 187
4.2.1 Shock experiment setup . . . 187
4.2.2 Spallation threshold . . . 187
4.2.3 Changes induced in the material . . . 193
4.2.3.1 Behaviour before damaging threshold . . . 193
4.2.3.2 Properties at higher pressures . . . 197
4.2.3.3 Mie-Grüneisen parameters extraction . . . 201
4.2.3.3.1 S parameter determination . . . 202
4.2.3.3.2 Grüneisen parameter determination . . . 204
4.2.3.3.3 Speed of the sound determination . . . 204
4.3 Conclusion on the acrylate behaviour under laser shock conditions . . . 205

Pour mieux comprendre les propriétés des matériaux de confinement utilisés lors des expériences de choc laser, une étude de leur comportement sous haute pression et vitesse de déformation est nécessaire. Les expériences réalisées dans les chapitres précédents étaient centrées sur des mesures VISAR sur des cibles d'aluminium et l'information était extraite de la face arrière de ladite cible. Dans cette configuration, le chargement de surface était obtenu au travers d'une méthode inverse de simulation numérique visant à reproduire les signaux VISAR en face arrière afin de remonter à la pression développée en face avant. Cette méthode permet l'obtention d'informations sur les propriétés de la cible aluminium ou de l'alliage traité par choc laser mais ne permet pas d'obtenir le comportement du matériau de confinement durant ces chocs laser. Or, les matériaux polymère flexibles présentent, sous chargement de haute pression et vitesse de déformation, une augmentation de leurs propriétés mécaniques avec un module d'Young pouvant passer de quelques MPa à quelques GPa. Cela à pour effet de modifier l'impédance réduite du système confinement/Cible et par extension la pression maximale finale produite par le choc laser. Afin d'être en mesure d'obtenir une meilleure compréhension des phénomènes mis en jeu dans les polymères exposés à des conditions mécaniques comme celles observées sous choc laser, différentes expériences ont été réalisées en se concentrant sur le confinement acrylique. Ces expériences donnent de nouvelles informations sur les propriétés mécaniques des polymères sous choc et permettent de se rapprocher d'une simulation numérique de leur comportement dans ces conditions. Un modèle FEM complet de ces polymères permettrait d'accéder à une meilleures compréhension des différents procédés mis en jeu mais aussi de gagner du temps pour la détermination et l'optimisation potentielle des paramètres laser dans un cadre industriel.

Transition vitreuse dynamique

Le phénomène de transition vitreuse correspond à la température à laquelle un matériau amorphe ou la phase amorphe d'un matériau subit une modification et transitionne d'un état vitreux à un état flexible ou inversement. En augmentant la température, les chaines d'un polymère gagnent en mobilité, faisant gagner par extension au matériau de la flexibilité. A l'inverse, en réduisant la température, la mobilité des chaines diminue progressivement jusqu'à un point ou elles déviennent "gelées" et le polymère atteint un état vitreux. La température de transition vitreuse est habituellement donnée pour conditions normales (régime statique et pression = 1 atm) mais sous chargement un décalage de cette température est observé [131]. De ce fait, le terme transition vitreuse dynamique est utilisé afin

de prendre en compte ces effets sous choc (voir 1.4.6.1 pour plus d'informations).

Durant les expériences de choc laser, la transition vitreuse dynamique intervient. Elle est causée par les fortes vitesses de déformation (de l'ordre de 10^6 s^{-1}) couplées à des pressions de l'ordre de quelques GPa. Habituellement, l'exprience utilisée pour déterminer le comportement des matériaux sous haute vitesse de déformation est le test des barres de Hopkinson ($\varepsilon < 10^5$ s^{-1}) [147, 148] mais ce dernier n'atteint pas les vitesses de déformation observées lors d'un choc laser. Une des seules méthodes permettant d'atteindre de telles vitesses de déformation est la spectroscopie diélectrique (DRS) qui peut atteindre les 10^7 s^{-1} en conditions normales et aller encore plus haut avec une configuration différente.

Pour évaluer les effets d'un choc laser sur un matériau de confinement, des expériences de DRS ont été réalisé (voir 1.4.4.1.2 et 2.4.2). L'objectif de ces expériences était d'obtenir des informations sur la mobilité des chaines des polymères sous haute vitesse de déformation avec une pression d'1 atm. De cette manière, il est possible de décorréler la contribution de la pression et de la vitesse de déformation sur la transition vitreuse dynamique. La même expérience a aussi été réalisée sous une pression isostatique de 600 MPa pour coupler les deux effets. Les résultats ont ensuite été comparés aux données obtenues lors des différentes expériences de choc laser.

Introduction

To better understand the properties of the confining material used during the laser shock experiments, a study of its behaviour under large pressure and strain rates is necessary. The experiments realised in the previous chapter were all focused on VISAR measurements on an aluminium target and the information was extracted from the backface of said target. In this type of configuration, the surface loading was obtained through inverse methods on with Abaqus modelling of the interaction. This method gave information about the consequences of the laser shock in the aluminium or alloys shot but did not give insight in the behaviour of the confinement material during these laser shocks. As said in previous chapters, under loading with a high strain rate, flexible polymers such as the acrylate tape or the silicone undergo a large change of mechanical properties with Young's modulus, going from MPa to GPa, thus changing the reduced impedance of the target/confinement system which influences the final pressure produced. To be able to achieve a deeper understanding of the interaction during shock as well as the reaction of the polymer confinement to said shock, experiments have been focused on the confining medium to obtain information about its mechanical properties changes during shock. A full set of parameters representing a polymer confinement during laser shock would also allow for its modelling. With an accurate simulation of the polymer confinement as well as the target, the full process could be modelled which would lead to a deeper understanding of the process while also saving time for the determination of the laser shock parameters for the process.

4.1 Dynamic glass transition

The glass transition phenomenon corresponds to the temperature at which the amorphous phase of a material undergoes a modification, transitioning from a glassy hard state to a soft flexible one or vice versa. By rising the temperature, the polymer chains gains mobility that grant flexibility to the material. On the contrary, by reducing the temperature, the mobility of the chains is gradually reduced up to a point where the chains are frozen and the material reaches a glassy hard state. The glass transition temperature is usually given under normal conditions (i.e static strain rate and a pressure of 1 atm) but under loading a shift of this value is observed [131]. For this reason the term dynamic glass transition is used to take into account those phenomena. More information on this topic can be found in 1.4.6.1.

During laser shock experiments, the dynamic glass transition phenomenon takes place. It is caused by the application of a high strain rate in the 10^6 s^{-1} order while a pressure in the GPa order is developed. The classic experiment chosen to obtain the behaviour of materials under high strain rate is the Hopkinson bar test ($< 10^5$ s^{-1}) [147, 148] but it does not reach the strain rates attained during laser shock making dielectric relaxation spectroscopy (DRS) one of the only alternative with its capability to go as high as 10^7 s^{-1} range or even higher with a different setup.

To assess the effect of a laser shock on a confining medium, Dielectric relaxation spectroscopy experiments were realised (see 1.4.4.1.2 and 2.4.2). The experiment objective was to obtain informations on the polymer chain mobility under high strain rate with an applied pressure close to 0 to decorrelate the two contributions on the dynamic glass transition. The same experiment was then realised under a 600 MPa hydrostatic pressure to have a representation of the two coupled effects. The results were then compared to the data obtained with the laser shock experiments.

4.1.1 Material choice

The choice of the polymers tested by DRS and laser shock was defined as follow: The acrylate tape confinement was selected as it is the reference confinement for end use with laser shock peening and the one that showed the most promising results. Two other polymers were selected, in this case on the basis of their glass transition temperature. To capture the effect of both the strain rate and pressure on the properties of a polymer, two extremes in term of glass transition temperature were chosen. A silicone, already studied in shock experiments (Sylgard184, Dow Corning) with T_g = 147 K (-126° C) and the second one a polycarbonate (Lexan 141, Sabic), already in the glassy state at ambient temperature with T_g = 415 K (142° C) (both the T_g were obtained through DRS measurement). The two materials were also chosen on the basis that they are amorphous to limit potential mechanical properties change induced by crystallization under stress or strain.

4.1.1.1 Polymer synthesis

The targets for laser shock were 99.0% aluminium with a thickness of 1 mm (AL000700, Goodfellows), the same as what was used for the other experiments.

The polycarbonate was bought in the form of pellets that were heated to make them easier to deform and that were then pressed on the 1 mm aluminium target at 250° C, 100 bar for 60 sec to

form an uniform film with a thickness of around 100 μm. The silicone (PDMS) chosen was Sylgard184 from Dow Corning. The standard 1:10 mix was used and the mixture was cured for 24h at ambient temperature to form films of around 700 μm thick.

4.1.1.2 Transmission measurement

The optical transmission of the polymers used was measured by using a calorimeter (QE50LP-H-MB-QED, Gentec) placed under the sample holder used for the experiments. The transmission was calculated using the lowest possible energy from the laser to produce the lowest laser intensity (0.2 GW/cm^2) as to avoid any potential damage to the polymer and then calculating the difference of energy with or without the polymer in the laser path. Polycarbonate showed a transmission of 87% while the silicone and the acrylate tape exhibited 90% transmission. The laser energy applied at the surface of the aluminium target was corrected according to this measurement for the laser intensity calculation.

4.1.1.3 Dielectric relaxation spectroscopy setup

The experiments were realised at the university of Rouen by Clément Fosse, the experiment under pressure was performed by Abdoulaye Soumaila Sounakoye under the supervision of Laurent Delbreilh. The DRS experiments were performed with an Alpha Analyser from Novocontrol Technologies GmbH in a frequency range going from 1.10^{-1} Hz to 2.10^6 Hz. The samples used were circular with a diameter of around 20 mm of the analyzed material and were placed between parallel gold electrodes. A Quatro Cryosystem (Novocontrol Technologies GmbH) was used to control the sample temperature with a stability of $\approx$ 0.5 K. For the silicone and polycarbonate, the temperature was increased from 123 K to 223 K using appropriate steps. For the acrylate the measurement was done from 173 K to 323 K with the same steps. For the silicone, measurement under an isostatic pressure of 600 MPa were realised with a specific setup.

4.1.2 Dielectric relaxation spectroscopy results on acrylate tape

The results of the DRS measurement on the acrylate tape confinement under atmospheric pressure are given in figure 4.1.

The 3D plot shows the imaginary part of the permittivity ϵ'' depending on the frequency and tem-

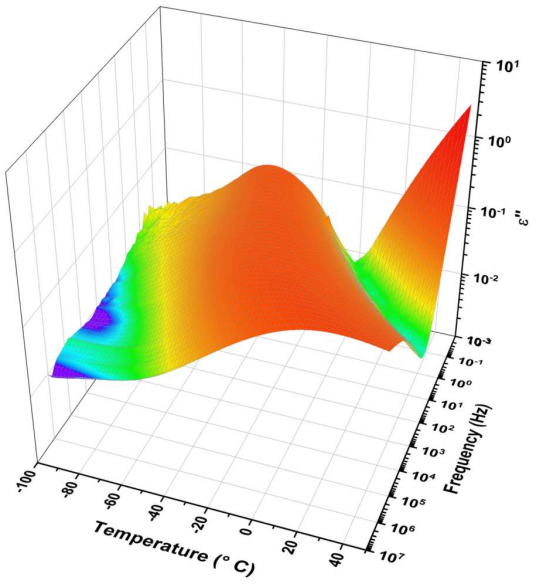

Figure 4.1: 3D plot of the dielectric relaxation spectroscopy results obtained with the acrylate tape confinement with a frequency varying from 0.1 to 2.10^6 s^{-1} over temperatures ranging from 173 to 323 K.

perature. The dynamic glass transition temperature is represented as the temperature and frequency at which a maximum of ϵ'' is observed. At high frequencies, one broad transition, covering from 223 to 323 K is observed while at low frequencies, two transitions are observed, respectively from 203 to 263 K and from 273 to more than 323 K. To better visualise the transition, the data are plotted on a 2D graph given in figure **??**. The figure represents the imaginary part of the permittivity depending on the frequency. For each experiment, a fixed temperature was chosen, the frequency was then varied while the permittivity was measured. The frequency can be compared to the strain rate thus giving information on the material behaviour up to 2.10^6 s^{-1}. Each line represents a measurement at a specific temperature ranging from 233 to 303 K. The maximum of each line shows the strain rate at which a transition occurs.

The different lines show the presence of two different transitions. Theses two transitions shows the probable presence of a copolymer in the material. Due to the presence of these two systems, the different glass transition temperatures present in the acrylate tape confinement allow for a large transition ranging on a wide temperature domain. This type of properties induces great adhesive properties and grant flexibility to the polymer.

The raw results are analysed with the Havriliak-Negami model to obtain the dielectric relaxation (see 2.4.2).

The relaxation map obtained represents $log_{10} f_{max}$ as a function of $1000/T$ and is given in figure 4.2. The points extracted with the Havriliak-Negami model represent the transition under fixed temperature and strain rate. Everything on the left of a point is rubbery while the right represents the glassy domain. An extrapolation of the results using the Vögel-Tammann-Fulcher (VTF) law is normally possible to extend the information on the material behaviour to a larger temperature and strain rate range. Due to the presence of two transitions on the acrylate confinement, the use of the VTF law is not possible for the acrylate tape confinement. The comparison between the results given by the two samples shows different behaviours. The dynamic glass transition temperature obtained at 10^2 Hz vary between 265.2 to 227.1 K. One of the explanation could be that the sample two was measured from 10^{-4} Hz while sample one started at 100 Hz. The ramp from 10 $^{-4}$ to 100 Hz could have induced a change in the material behaviour if the mobility of the chain is too small compared to the frequency used thus leading to a progressive rigidication of the polymer until its complete transition to a glassy state.

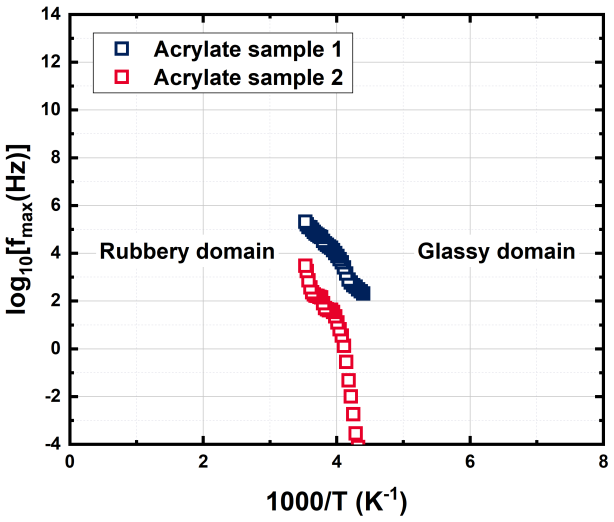

Figure 4.2: DRS measurements on two acrylate tape samples. The dots represent the results obtained using the Havriliak-Negami model [156].

4.1.3 Polycarbonate and polydimethylsiloxane study

In order to have access to an evaluation of the pressure and strain rate effect on a material that can be used as a confinement for the laser shock peening process, two other materials have been studied, polycarbonate (PC) and polydimethylsiloxane (PDMS). They are used as model material since they possess either a low glass transition temperature for the PDMS (147 K) or a high one for the PC (415 K). The PC is chosen because it is already in the glassy state even before being put in laser shock conditions. The PDMS, on the other hand, is used as a substitute to the acrylate tape confinement for its similar properties. It has a low glass transition temperature, is amorphous and is also a flexible adhesive. To complete the study a DRS experiment under isostatic pressure at 600 MPa was also realised to assess the effect of the pressure coupled with a high strain rate on the dynamic glass transition of such a material. The raw measurement on the PDMS are given in figure 4.3 and 4.5a, respectively for 3D and 2D plots. The 2D plots are given for both the measurements with no pressure and under an isostatic loading of 600 MPa. The raw results obtained with PC are not presented as they are not the main focus of this study since the material does not undergo a transition under laser shock conditions of pressure and strain rate.

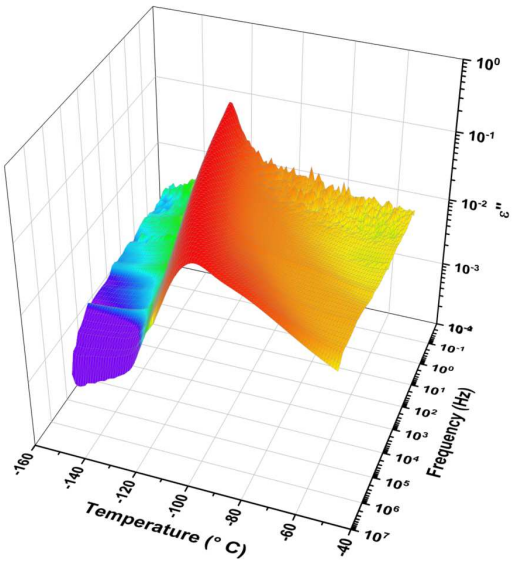

Figure 4.3: 3D plot of the dielectric relaxation spectroscopy results obtained with the polydimethylsiloxane (Sylgard184) confinement with a frequency varying from 0.1 to 2.10^6 s^{-1} over temperatures ranging from 173 to 323 K. Raw results obtained from the dielectric relaxation spectroscopy measurement of the polydimethylsiloxane (Sylgard184) confinement under atmospheric pressure.

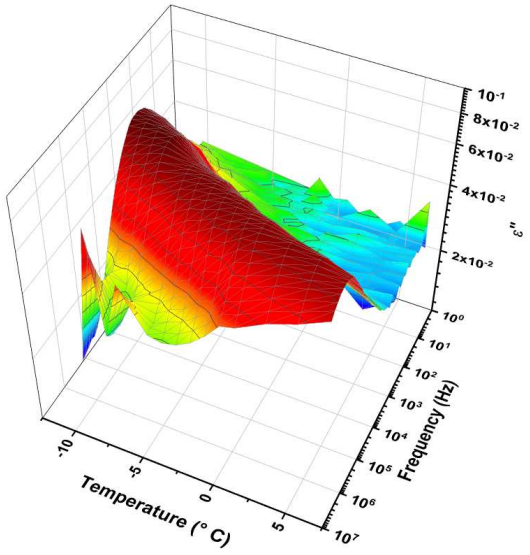

Figure 4.4: 3D plot of the dielectric relaxation spectroscopy results obtained with the polydimethylsiloxane (Sylard184) confinement with a frequency varying from 0.1 to 2.10^6 s^{-1} over temperature ranging from 262 to 279 K under a 600 MPa isostatic pressure.

With the polydimethylsiloxane, only one transition is observed and seems to be reasonably influenced by frequency applied which can be translated to the strain rate observed by the material during laser shock. To be able to have a better representation of the results the 2D plot is used with both the results without and under pressure.

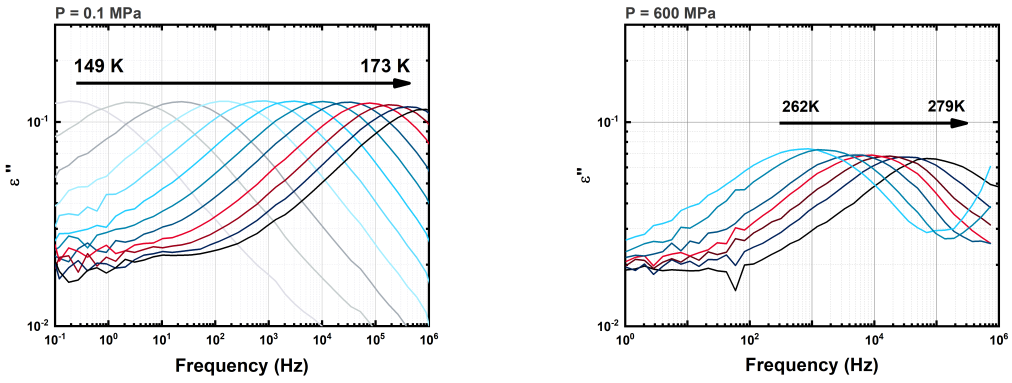

(a) (b)

Figure 4.5: Raw results obtained from the dielectric relaxation spectroscopy measurement of the polydimethylsiloxane (Sylgard184) confinement under (a) atmospheric pressure and (b) under an isostatic 600 MPa loading.

Each line represents a measurement at a specific temperature ranging from 149 K where the transition occurs at 10^{-1} s^{-1} to 173 K where it occurs at 8.9*10^5 s^{-1}.

The transition from a rubbery behaviour to a glassy one of each line is determined by the maximum, thus giving for a given temperature the strain rate necessary to induce a dynamic glass transition if any happens under the conditions of the experiment. In this case since only one transition is occurring, the determination of the dynamic glass temperature becomes easier. Under pressure, measurements were realised with temperature varying from 262 to 279 K. A shift of the dynamic glass transition is observed with a transition observed at 262 K for a strain rate of 5.10^2 s^{-1} while the measurement at 279 K showed a transition for a strain rate of 1.4*10^5 s^{-1}. An average shift of around 383 K is observed due to the loading applied during the experiment thus showing that the glass transition shift induced by pressure seems to have a significant impact compared to the effect of strain rate. To obtain a better representation of the data, the Havriliak-Negami model is used in the same way as with the acrylate tape measurements. From the information extracted with the model and since only one transition is observed, it is possible to extrapolate the behaviour of the Sylgard184 under a broader range of temperatures and strain rates by using the Vögel-Tammann-Fulcher (VTF) law:

$$\tau_{max} = \tau_0 \, exp\left(\frac{D\,T_0}{T - T_0}\right) \tag{4.1}$$

With:

τ_0: a pre-exponential factor

D: a dimensionless parameter related to the slope variation (steepness strength)

T_0 a reference temperature

The results presented in figure 4.6 give an accurate measurement of the silicone used during experiment with a glass transition temperature in static conditions ($\dot{\epsilon} = 10^{-2}$ s^{-1}) of 147 K, close to what is found in [209]. The fit obtained through the VTF law shows that under a pressure of 0.1 MPa the PDMS should always present a rubbery relaxation behaviour. In order for the PDMS to reach a glassy state, the strain rate would need to be as high as 10^{12} s^{-1}, a value largely higher than what can be reached by laser shock peening with the laser parameter used for the treatment and characterization. This means that by the effect of strain rate alone the silicone should stay in a rubbery

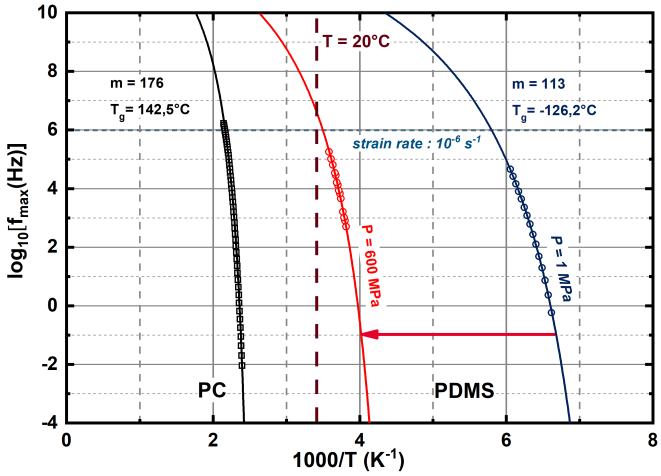

Figure 4.6: DRS measurements on PC and PDMS. The dots represent the measurement while the line represent the fit using the Havriliak-Negami model [156].

state even under laser shock conditions (10^6 s^{-1}). The glass transition temperature calculated for the silicone at 10^6 s^{-1} is 173 K meaning the shift induced by the strain rate is 299 K, a rather small effect compared to the assumed pressure effect. More precisely, it means that both stress and strain rate induce a consequent effect on the dynamic of the polymer chains that can be perceived, when looking at the macroscopic properties by a large dynamic glass transition shift which separates the rubbery and glassy behaviour of the materials studied. In the specific case of these experiments the pressure effect seems to be prevalent on the dynamic glass transition when compared to the strain rate effect. The polycarbonate on the other hand is not mechanically affected by the application of such strain since it is already in a glassy state at ambient temperature, its glass transition temperature variation depending on the strain rate applied is also smaller compared to what is observed with Sylgard184 as can be seen by comparing the steepness of the two fits.

4.1.4 Comparison with laser experiment

To compare the DRS results to a laser shock case scenario, shots were performed at different laser intensities with a camera setup coupled with the VISAR one. This allowed obtaining the backface velocity profiles of shots on 1 mm aluminium targets (99.0%) while also having images of the confinement deformation caused by the shock created. The backface velocity profiles were reproduced

via finite element modelling on Abaqus to extract the strain rate at the surface of the target while the camera imaging was used to complement this procedure and provide another rough estimation of the strain rate observed during shock. The strain rate extracted from the simulation and camera imaging gives the information at the surface of the aluminium target. The shock produced by the laser pulse induces two identical shockwaves, one going through the target and a second one going in the confinement. Since the two shockwaves are the same, the strain rate extracted at the surface of the shocked target is the same as the one seen by the face of the confining medium at the interface target/confinement. With this method, the strain rate along the thickness of the confinement cannot be known. This is important to note as in the case of a pressure and/or strain rate induced dynamic glass transition, the glassy state of the matter will only be known on the surface of the confinement, the thickness will not be able to be considered to have made a transition from the rubbery to the glassy state. The experimental setup used for the camera imaging coupled with VISAR measurement is presented in figure 4.7.

4.1.4.1 Rear free surface velocity profiles

The backface velocity profiles measured experimentally are given in figure 4.8 for four different confinements, respectively polycarbonate, acrylate tape, silicone and water. The shots were realised at 0.79 GW/cm^2 with a laser spot of 3.7 mm and a pulse duration of 7 ns. The targets chosen were 99.0%, 1 mm thick aluminium sheets.

The maximum velocity exhibited by the four confining media is the same, meaning that their mechanical properties under shock are at least of the same order of magnitude. Polycarbonate usually have a Young's modulus comprised between 2.0 to 2.4 GPa. The two other polymer confinements are rubbery with modulus in the MPa range. Their same pressure production when used as a confinement during laser irradiation, shows once again their shift to a Young's modulus in the GPa range due to a dynamic glass transition making the materials glassy. The water confined regime also produces the same pressure as the others, in accordance with studies showing the evolution of the mechanical impedance of water during laser shock (see figure 4.9).

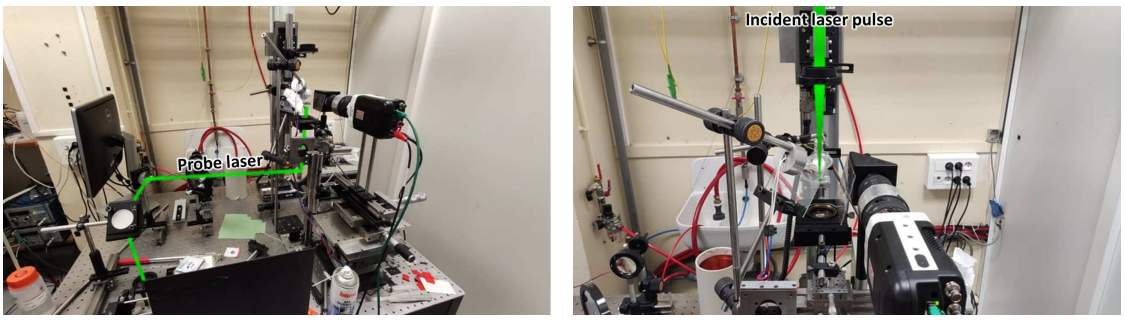

(a) (b)

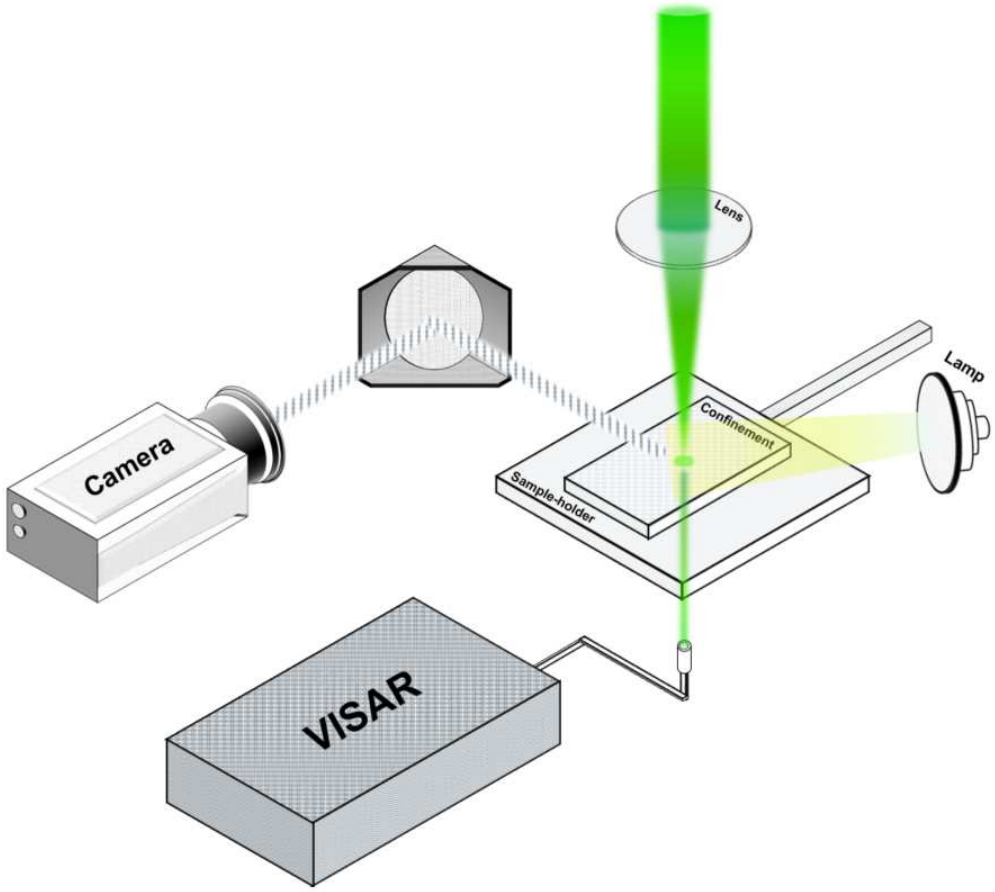

(c)

Figure 4.7: Setup used for the VISAR coupled with camera imaging for the strain rate measurements.

4.1.4.2 Simulation parameters

To obtain the strain rate of each laser shot, the backface velocity profiles are modelled on the FEM software Abaqus. The strain rate extracted is then correlated to either the pressure or laser intensity of the laser shot. A 2D axisymmetric model was used with an explicit solver to take into account all the

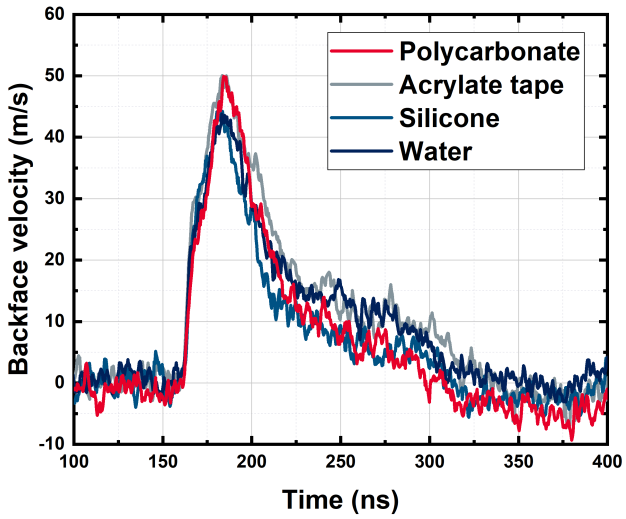

Figure 4.8: Backface velocity profiles for different confinements. Shots were realised with a laser spot of 3.7 mm, a pulse duration of 7 ns and a laser intensity of 0.79 GW/cm^2. 99.0%, 1 mm thick aluminium sheets were chosen for the targets.

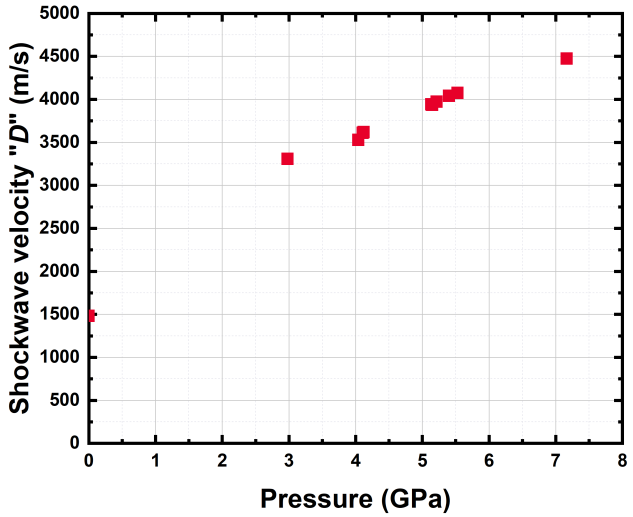

Figure 4.9: Experimental results describing the shockwave velocity evolution depending on the pressure in water (taken from [210]).

dynamic effects of the shock on the aluminium target. The modelled target was represented as a 1 mm thick pure aluminium plate with a width of 10 mm. The elements used were CAX4R (Continuum,

4-nodes bilinear axisymmetric, quadrilateral, reduced integration, hourglass control). The mesh was made finer in the shock area (1 μm x 1 μm) while it was made larger following a gradient the farthest it went from the center of the shock with a BIAS function in the X direction. The boundary condition were applied as follow: the bottom right corner, opposed to area where the shock was applied was fixed to represent the sample holder used during the experiment.

4.1.4.2.1 Constitutive model

The laser shock process induces high strain rates, reaching 10^6 s^{-1} and higher. For this type of solicitations the Johnson-Cook model is usually chosen [211]. It takes into account multiple parameters such as strain rate, strain hardening and thermal effects and is available in most FEM software [192].

Work by Amarchinta demonstrated the accuracy of the Jonhson-Cook model over elastic perfectly plastic or Zerilli-Armstrong models [212] for laser shock applications. For this simulation the Johnson-Cook model was coupled with the Mie-Grüneisen equation of state while also using the classical elasto-plastic material parameters. The parameters used are given in table 4.1.

Table 4.1: Simulation parameters used for the constitutive model

ν	ρ (kg/m^3)	**G** (MPa)	$\mathbf{C}_0$ (m/s)	**S**	Γ_0	σ_y (MPa)	**B**	**n**	**C**	ϵ_0 (s^{-1})
0.33	2700	25940	5380	1.338	2	80	200	0.3	0.035	0.01

Johnson-Cook

The model defines a Von Mises yield criterion as follow:

$$\sigma = (\sigma_y + B\epsilon_p^n)\left(1 + C\ ln\left(\frac{\dot{\epsilon}}{\dot{\epsilon_0}}\right)\right)\left(1 - \left(\frac{T - T_0}{T_{melt} - T_0}\right)^m\right) \tag{4.2}$$

The first part describes the strain hardening effect. The second part characterizes the strain rate effect and the last one is used to take into account the material temperature evolution during the plastic deformation. σ_y is the yield stress, B the strain hardening modulus, ϵ_p the equivalent plastic deformation, n the hardening coefficient, C the strain rate sensitivity, $\dot{\epsilon}$ the strain rate during the process, $\dot{\epsilon_0}$ the reference strain rate, T_0 the room temperature and T_{melt} the fusion temperature. G

is the shear modulus and ν is Poisson's ratio. Preliminary simulations showed that the thermal part has close to no effect on the results and is thus neglected.

Mie-Grüneisen equation of state

In order to accurately represent the hydrodynamic behaviour of the material, the Mie-Grüneisen equation of state is classically used. It allows the determination of the pressure in a material during shock. The equation stems from the Grüneisen model used to describe the effect of a crystal lattice volume variation on its vibrational properties. More information are given in 2.3.3.3.

4.1.4.2.2 Spatial and pressure profiles

The pressure profile used for the simulation was generated from the approach developed in Scius-Bertrand et al work [195] for a 532 nm wavelength. The pressure duration used is 7 ns with a Gaussian profile until the release. The laser spot spatial profile was directly measured from the experiment through camera imaging. The used spatial profile was then extracted from a filtering of the experimental profile through the Butterworth filter [193, 194]. Preliminary simulations showed that a small variation of intensity at the top of the experimental laser spot spatial profile did not have an influence on the backface velocity profile generated by the simulation. The spatial and pressure profiles used for the simulations are given in figure 4.10.

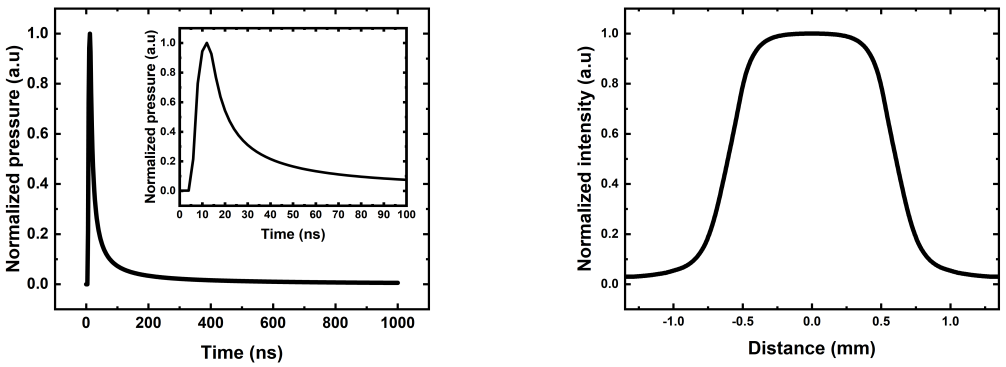

(a) (b)

Figure 4.10: (a) Normalized pressure profile obtained with the code from [195] for a 7 ns FWHM, 532 nm Gaussian pulse laser shot (b) Filtered laser spatial profile obtained with the Butterworth filter through a Python code and used for the simulation.

4.1.4.3 Simulation results - Strain rates extracted

The modelling of the backface velocity profile is given in figure 4.11a. Both the maximum velocity as well as the full width half maximum of the peak are well represented. The focus of the simulation was placed on the first peak of the velocity profile since the maximum and strain rate are only dependent on the first peak of the shockwave propagation. From the modelling of the backface velocity profile, the maximum plasma pressure of the shots is extracted as well as the maximum strain rate.

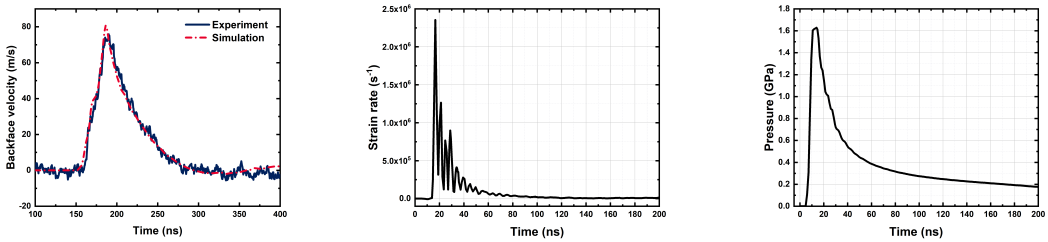

(a) (b) (c)

Figure 4.11: (a) Experimental and simulated profile for a laser shot with an intensity of 0.80 GW/cm^2 and a laser spot size of 3.7 mm diameter on a 1 mm 99.0% aluminium target. (b) Strain rate depending on the time extracted from the simulated backface velocity profile. (c) Pressure profile depending on the time extracted from the simulated backface velocity profile.

The pressure extracted from the modelling of the shot showed on figure 4.11a reaches 1.6 GPa and a strain rate of 2.4*10^6 s^{-1} at 0.79 GW/cm^2. The results confirm the strain rate values given in the literature in the 10^6 s^{-1} range [43]. The same procedure is applied to the velocity profiles for the different laser intensities used during the experiments shown in figure 4.12.

The strain rates extracted range from 1.91*10^6 s^{-1} at 0.79 GW/cm^2 to 4.01*10^6 s^{-1} at 4.37 GW/cm^2. By coupling these results with figure 4.6 shows that the silicone confinement, when exposed to a strain rate of 4.01*10^6 s^{-1} exhibit a glass transition temperature of 175 K. This means that the pressure produces a shift of glass transition temperature of at least 118 K for it to reach a glassy state during laser shock (thus reaching a glass transition temperature of 293 K, the ambient temperature). The strain rates effectively seen by PC, the acrylate tape or the silicone are considered close to these values. It is possible to evaluate a minimum strain rate seen by the silicone with camera imaging (figure 4.13). In the laser shock experiment, two identical shockwaves are created at the interface confinement/target. One goes in the target material while the second one goes in the confinement. This configuration means that the pressure applied is the same at the surfaces of both materials considered. The strain

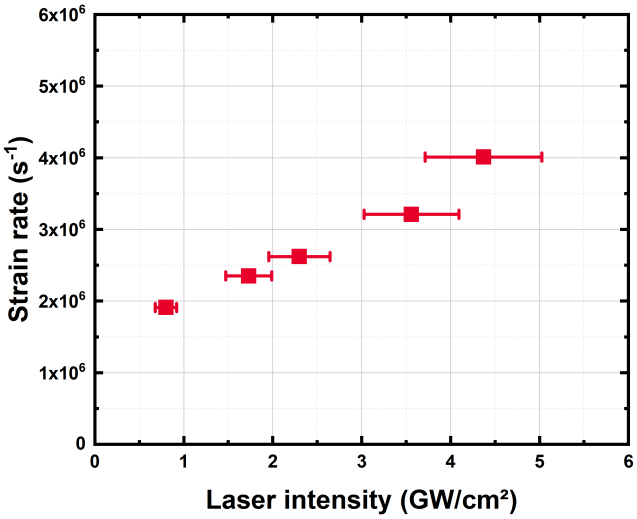

Figure 4.12: Strain rate depending on the laser intensity for a PDMS confinement, the values are extracted from Abaqus simulation at the surface of a pure aluminium target.

rate, on the other hand, is dependent on the mechanical properties of the material concerned. A simple calculation allows an assessment of the strain rate seen by the silicone confinement. From the camera imaging, one can observe that the deformation is superior to a half-circle. From the calculation of the perimeter, it is possible to estimate a minimum deformation induced by the laser shock. Figure 4.13a shows an image of the PDMS confinement 31 μs after the laser shock, long after the application of the maximum pressure and strain rate of the experiment since the laser pulse is 7 ns long. The initial length of the PDMS polymer tape L_0 is considered to be equal to the diameter of the laser shock while $L(t)$ is the length at a time t during shock. This length is equal to the perimeter of the half circle created by the shock expansion in the confinement. To simplify the case, a perfect half circle is considered for the calculation. The laser spot size is 3.74 mm so the perimeter of such an half-circle is roughly 5.81 mm. The time between the image taken in figure 4.13a and the laser shock is 31 μs. The strain rate obtained is $1.79.10^5$ s^{-1}. This means that long after the shock, the strain rate is still in the 10^5 s^{-1} range. It is safe to assume that at the time of the shock it would be a lot higher.

Moreover the Abaqus modelling shows that the maximum strain rate is attained after 16 ns for a 0.80 GW/cm^2 shot. From the same simulation, the strain rate is still in the 10^5 s^{-1} range.

It is also important to consider that the calculation with camera imaging is done based on the

face of the silicone opposed to the shockwave. The attenuation through the thickness reinforces the idea that at the interface target/confinement, the strain rate should be higher. From this result it is assumed that the strain rate seen by the PDMS at the interface of the laser shock is in the 10^6 s^{-1} range like the aluminium target from which the FEM strain rates have been extracted from.

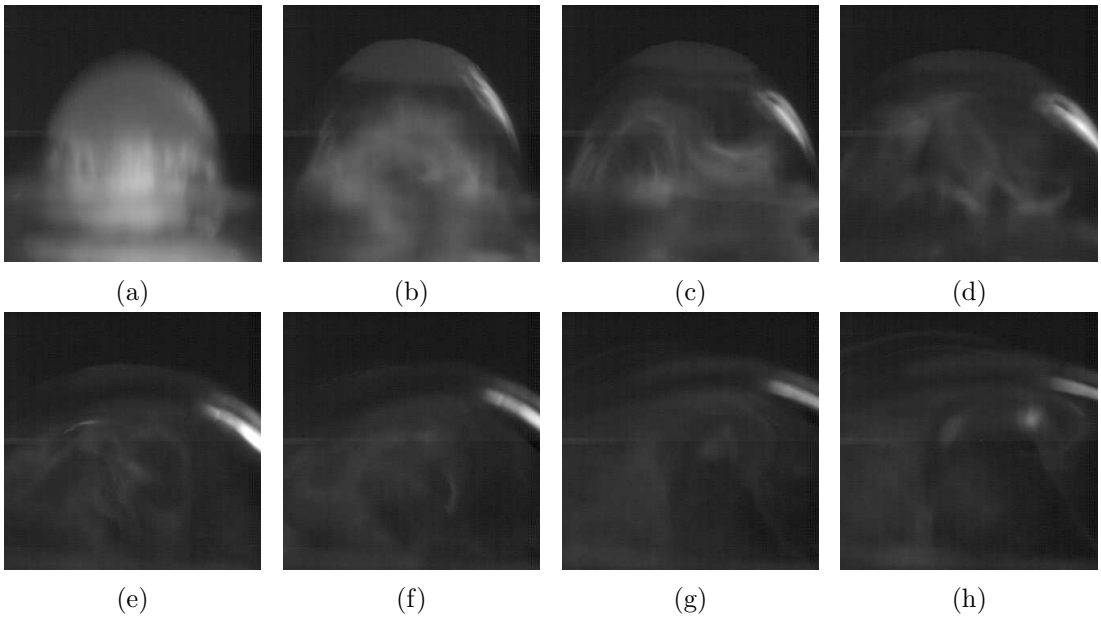

Figure 4.13: Images of the deformation of PDMS used as a confinement for laser shock, laser spot is 3.74 mm laser intensity is 4.23 GW/cm^2, pulse duration = 7 ns, maximum pressure at the interface aluminium/PDMS = 4.35 GPa. The image in the corner is the PDMS confinement 31 μs after the laser pulse with a high speed camera. The images after the first one are each increment from 37 μs

The values of pressure induced glass transition shift can be found in Aharoni's work [151]. In the case of PDMS, the average value found for amorphous polymer is 0.28 K/MPa. The pressure induced T_g shift calculated from the literature varies from 504 K for the lowest shot at 0.53 GW/cm^2 (1.8 GPa) to 1484 K at 5.5 GW/cm^2 (5.3 GPa). These values explain why every laser shot experiment always show a pressure produced that can be obtained only if the impedance of the confinement attain a value for which a Young's modulus in the GPa order is necessary. In order to stay in a rubbery state the pressure-induced shift should stay lower than 120 K, bringing the glass transition temperature around ambient temperature. The limit pressure to meet these criteria is 429 MPa.

To determine a more accurate value of the pressure induced shift in the silicone per MPa, a dielectric relaxation spectroscopy experiment is performed under isostatic pressure at 600 MPa as shown in figure 4.6 From the measurements realised by DRS under isostatic pressure at 600 MPa, the

coefficient can be corrected. The measurements at 0.1 and 600 MPa show a T_g shift of 100 K. The value of the shift can be adjusted 0.17 K/MPa at 1 s^{-1} and 0.18 K/MPa at 10^6 s^{-1} for the PDMS used for the experiments. These DRS results also show the prevalence of the pressure effect on the molecular chain mobility which induces the dynamic glass transition phenomenon compared to the strain rate.

4.2 Acrylate tape mechanical characterization

To obtain a better understanding of the effects induced by the laser shock process on the acrylate tape confinement chosen has the reference confining medium for the final industrial application. A specific experiment was designed to get data on the mechanical properties of the polymer tape under laser irradiation.

4.2.1 Shock experiment setup

To be able to assess the mechanical properties of the acrylate tape confinement under laser shock, a pure aluminium coating (99.9%) of the tape was realised by Dephys. A thickness of ≈ 10 μm was deposited on both face of the acrylate tape. VISAR measurements were then performed on the acrylate tape confinement with its coating. Figure 4.14 gives a representation of the laser setup. The confinement used for these laser shots were water droplets as the application of an acrylate tape confinement damages the aluminium coating.

Sollier et al. work shows the influence of the laser intensity used on the thickness ablated at the surface of the shocked target experimentally [34]. Figure 4.15 gives the thickness ablated at the surface of the shocked target depending on the laser intensity. The thickness ablated by the laser pulse between 0 to 6 GW/cm^2 varies from 0 to 4.6 μm. The thickness of the aluminium coating allows for the interaction to take place without inducing noticeable effects caused by the aluminium thickness in terms of shockwave attenuation while protecting the surface of the acrylate tape confinement.

4.2.2 Spallation threshold

First the value of the damage threshold was determined through the backface velocity profiles obtained. If the target is damaged on the impacted area, the shockwave will not be able to go back

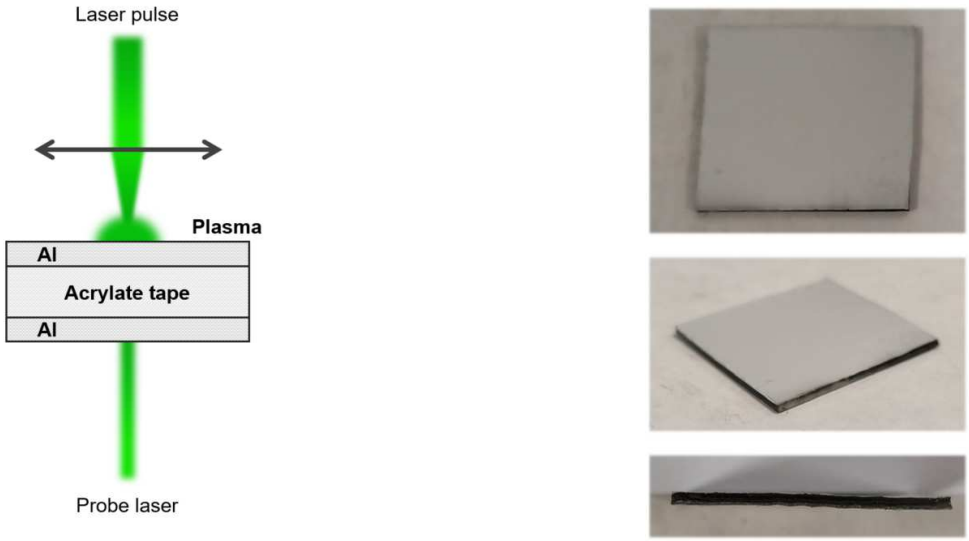

(a) (b)

Figure 4.14: (a) Set-up used for the VISAR measurement performed on the acrylate tape confinement with its aluminium coating. A water droplet was used as a confinement. (b) Images of the aluminium coated acrylate tape confinement.

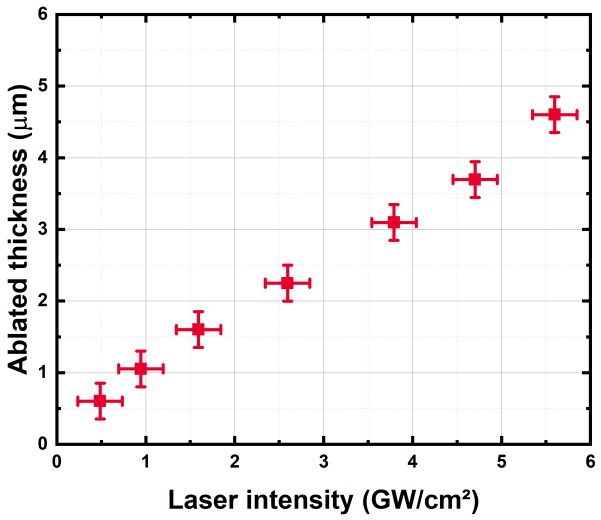

Figure 4.15: Ablated thickness depending on the laser intensity used. Targets are pure aluminium and the shots are performed with a 532 nm laser, 10 ns pulse, Gaussian pulse. (Results taken from [34]).

and forth in the material. Only the first peak will be present and the rest of the velocity profile will

show either a plateau or a slowly decreasing velocity. In some cases the material can be partially damaged and present peak witnesses of the shockwave being able to go back and forth in the material but while being strongly attenuated compared to a normal profile. Figure 4.16 shows the different backface velocity profiles obtained at different laser intensities for the shots on the acrylate tape coated in aluminium targets as well as the recap of the damaging threshold observed.

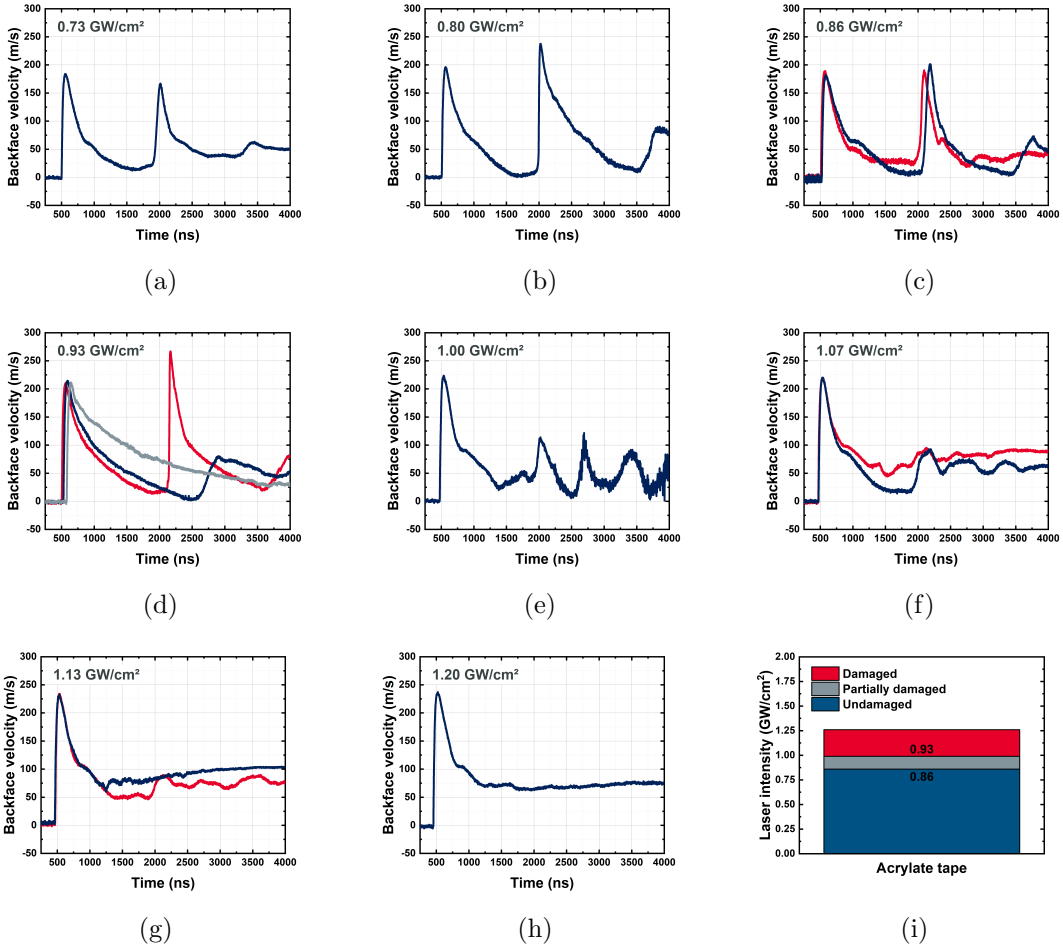

Figure 4.16: (a) to (h) Backface velocity profiles obtained through VISAR measurements on acrylate tape coated in 10μm 99.9% aluminium confined with water. The shots are realised at different laser intensities ranging from 0.73 to 1.20 GW/cm^2. (i) Damage threshold values found with the velocity profiles.

Figure 4.16 can be divided in three parts:

- Under 0.86 GW/cm^2: The shockwave goes back and forth the material without any problem, the shockwave velocity profile is similar to the ones observed in while shocking aluminium targets.

Another difference with a typical velocity profile obtained for a shot in an aluminium target, is the time of application of the pressure, seen with the difference in full width half maximum. In the case of aluminium the FWHM ranges between around 55 to 30 ns depending on the laser intensity chosen. In this experiment the acrylate tape confinement demonstrated a FWHM ranging from 240 to 407 ns depending on incident laser energy. This shows that the relaxation time of the polymer chains vastly changes depending on the pressure applied during the interaction. The profile at 0.80 GW/cm^2 presents a second peak at 2100 ns with a higher maximum velocity compared to the first peak. A possible explanation is that the pressure-induced dynamic glass transition does not take place as quickly as the speed at which the shockwave travels through the material. This leads to the first peak happening while the entirety of the shocked polymer is not yet fully glassy while the second peak which represents the second time the shockwave hits the back face of the polymer takes place at a time when a larger if not the whole material has undergone a dynamic glass transition to a glassy state, thus resulting in a higher mechanical impedance and consequently a higher material velocity. The third peak reaches a considerably lower maximum velocity due to the attenuation of the shockwave while it goes back and forth in the material.

- Between 0.86 and 0.93 GW/cm^2: The velocity profile shows signs of damaging or beginning of damaging. In figure 4.16c, the profile at 0.86 GW/cm^2 shows damaging during the release of the velocity profile as can be seen between 1000 and 1100 ns after the peak and again between 2340 and 2430 ns for the second peak. These two peaks are witnesses of damaging of the acrylate tape on its backface. The third peak follows a similar trend to the one observed for the lower laser intensities. The profiles at 0.93 GW/cm^2 shows different trend. The red line shows the same tendency as the profile at 0.80 GW/cm^2 in figure 4.16b with the second peak being higher than the first one. The blue line shows signs of material damaging with the second peak being a lot lower in velocity than the first one and also starting later at 2500 ns. On the 0.93 GW/cm^2 profile the grey line shows a fully damaged acrylate tape with no additional peaks after the first one. Only the release is present. The two other velocity profiles on this figure show either no damaging (red line) or partial damaging with the presence of a second attenuated peak (blue line).

- At intensities higher than 0.93 GW/cm^2: All the velocity profiles present damaging with either

residual peaks or not. The disappearing of the residual peaks is more pronounced as the incident energy applied is increased.

Overall, the maximum velocity of the different profiles obtained can be divided in two parts: the first one before the damaging threshold (up to 0.93 GW/cm^2) where the maximum velocity stays constant between 180 to 200 m/s. The second parts starts at 1 GW/cm^2 with the maximum of the first peak always around 220 m/s except for the profile at 1.20 GW/cm^2 where the backface velocity starts to increase again due to the pressure effects inducing an earlier raise of the Young's modulus during the shock. The images taken after the different laser shots on the front and back face are given in figure 4.17 for different laser intensities covering the cases before, during and after the damaging threshold.

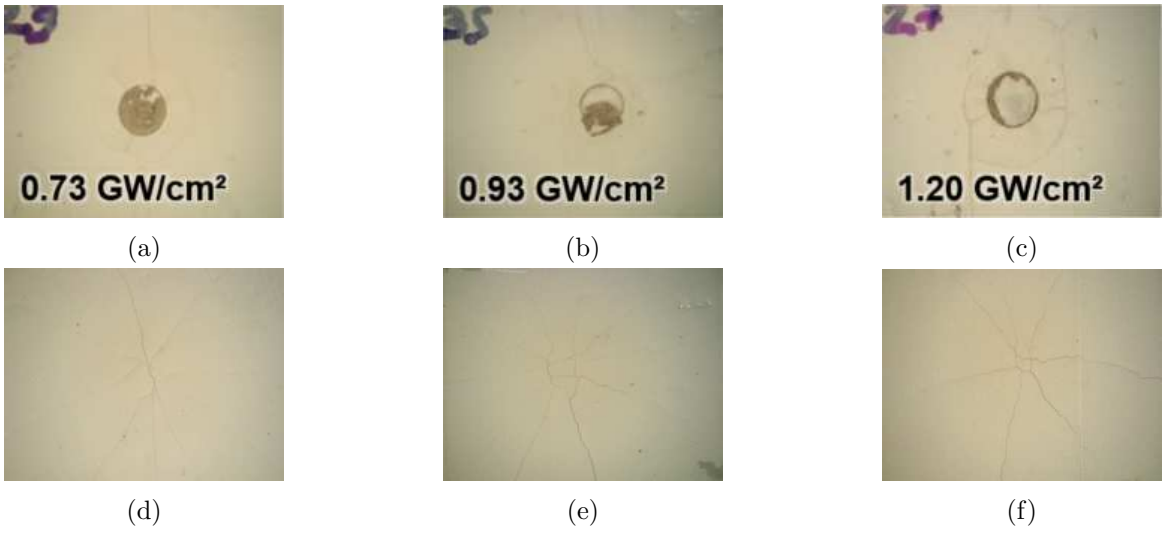

Figure 4.17: Images of the acrylate tape coated in alumnium after shots at different laser intensities. (a) front face and (d) back face before damaging threshold: 0.73 GW/cm^2, pulse duration 7 ns, spot size 3.68 mm. (b) front face and (e) back face at the damaging threshold: 0.93 GW/cm^2, same pulse duration and spot size. (c) front face and (f) back face, higher than the damaging threshold: 1.20 GW/cm^2, same pulse duration and spot size.

The different images show that before the damaging threshold (4.17a), the impact point of the laser pulse still shows a layer of aluminium coating that covers the acrylate tape beneath. This aluminium layer is scratched more and more while the damaging threshold is reached. At laser intensities higher than the damaging threshold the aluminium coating is fully removed. This means that the ablated depth is superior to 10 μm contrary to what had been found in Sollier's experiments [34]. The difference

in target material compared to Sollier's experiments is a possible explanation of those differing results. The back face of every targets presented show the same pattern of cracks induced by the pressure produced and transmitted to the back face. Reaching incident laser energies higher starts to induce a large deformation of the back face of the target.

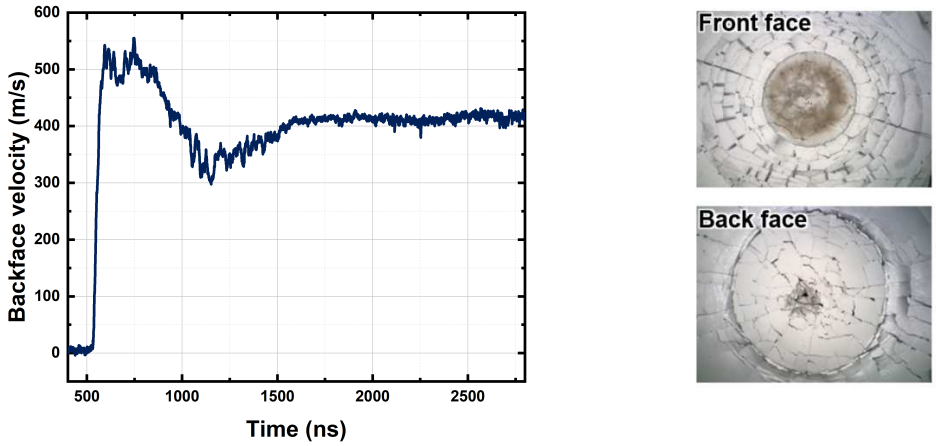

(a) (b)

Figure 4.18: (a) backface velocity profile of a laser shock at 2.85 GW/cm^2 with a laser spot of 5.54 mm and a pulse duration of 7 ns on a 1 mm acrylate tape coated on both sides with 10 μm pure (99.9%) aluminium. (b) Front and back face images of the target after shot.

Figure 4.18 gives an example of the front and back face observed on a target after a laser shock at 2.85 GW/cm^2 with a laser spot size of 5.54 mm and a pulse duration of 7 ns. At this type of laser intensity the front face of the target is totally stripped of its aluminium coating on the shocked side which leads to surface damaging of the acrylate tape. Darkening of the surface on the laser spot area shows the pyrolysis of defects in the polymer under laser irradiation. The back face shows the outline of the shockwave can be seen. The area covered by the shockwave on the backface appears to be larger than the laser spot size used. This observation is in agreement with the observations of the propagation of a shockwave in an aluminium or any metal alloys by finite element modelling (see figure 4.19). The dot observed in the middle of the backface corresponds to the VISAR probe laser going through the aluminium coating and starting to burn the polymer due to its high energy. Under the influence of the pressure on the back face, the aluminium coating is deteriorated, allowing the probe laser to starts damaging the acrylate tape underneath. The behaviour of the acrylate tape starting 1100 ns can be explained by the cracking of the backface of the target as well as the damaging of

the acrylate tape by the probe laser. Since the probe does not come into contact with the aluminium coating anymore, it cannot be reflected to the VISAR thus inducing the signal stagnation.

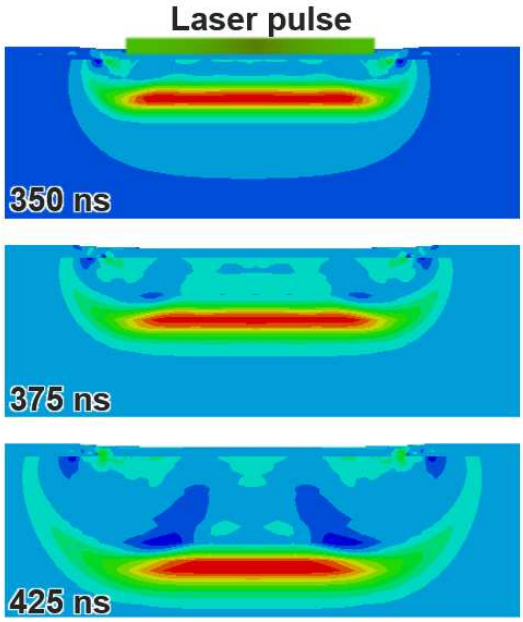

Figure 4.19: Finite element modelling from Abaqus software of al 7175, thickness 30 mm, showing the shockwave propagation through the material.

4.2.3 Changes induced in the material

4.2.3.1 Behaviour before damaging threshold

The observation of the different velocity profiles at different laser intensities showed no real difference on the shape of the signal observed. Instead the main difference observed was the change in the time at which the front shock reaches the backface of the target. With the use of a higher pressure the shock arrived earlier. Figure 4.21 shows the different backface velocity profiles obtained at different laser energies while using the acrylate tape coated in aluminium as target in a water confined regime under the damaging threshold.

The front shock reaching the backface sooner with higher pressure indicates that the mechanical properties of the acrylate tape evolve depending on the pressure applied on its surface. Following the equation 4.3 (for more information see B), the shockwave speed changes during the shock with the transition of the acrylate tape to a glassy state by the reduction of its molecular chain mobility under

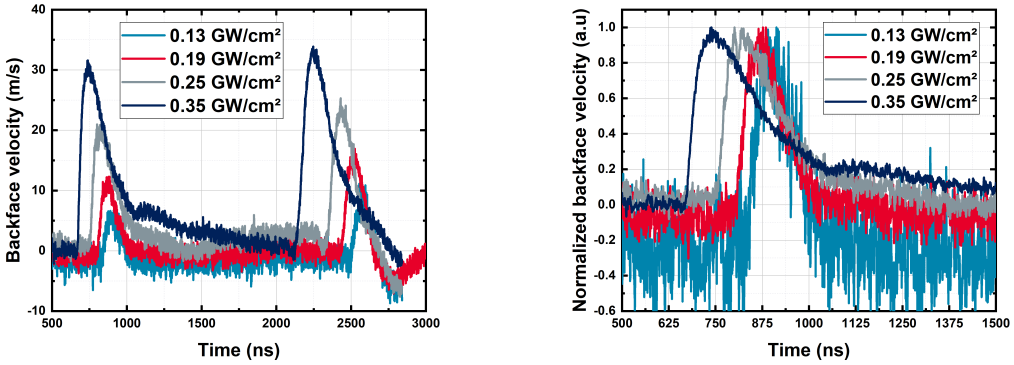

(a) (b)

Figure 4.20: (a) Backface velocity profiles obtained by VISAR measurement on 1 mm acrylate tape targets coated in 10 μm aluminium at different laser intensities. Pulse duration is 7 ns spot size for the shots ranging from 0.13 to 0.25 GW/cm^2 is 3.68 mm while the shot at 0.35 GW/cm^2 used a 5.54 mm spot size. (b) Normalized first peak of the different profiles presented.

stress and strain rate.

$$P = \rho\, D\, u \tag{4.3}$$

The increase of the shockwave velocity "D" can be seen on figure 4.20b with the time at which the first peaks appears. At the same time an increase of the full width half maximum is observed along the increase of the laser intensity.

The shockwave velocity can also be extracted from these experimental profiles by measuring the time between the first peak and the laser pulse. The result is then put in correlation with the target thickness (here 1 mm and 20 μm aluminium in total) to obtain the shockwave velocity. The same operation is used between the first and second peaks to obtain the average velocity of the shockwave during its travel once the shockwave already passed through the material one time inducing an at least partial glassy state. In this case, the thickness just has to be multiplied by two to take into account the wave going back and forth in the material to reach the backface once again.Table 4.2 gives a summary of the variation of the shockwave velocity, full width half maximum and material velocity on the first and second peaks depending on the laser intensity of the shock.

The shockwave velocity as well as the material velocity are increasing linearly with the laser intensity while the FWHM lose its linear behaviour at 0.35 GW/cm^2. The shockwave velocity in particular, is an indicator of the rigidification of the acrylate tape when used as a target under the

Table 4.2: Evolution of the shockwave speed "D", full width half maximum and material velocity "u" depending on the laser intensity used for a laser shock on a 1 mm acrylate tape target coated on both faces in 10 μm of pure (99.9%) aluminium.

Laser intensity	**D** $\mathbf{1^{st}}$ **peak**	**D** $\mathbf{2^{nd}}$ **peak**	**FWHM** $\mathbf{1^{st}}$ **peak**	**FWHM** $\mathbf{2^{nd}}$ **peak**	**u** $\mathbf{1^{st}}$ **peak**	**u** $\mathbf{2^{nd}}$ **peak**
GW/cm^2	m/s	m/s	ns	ns	m/s	m/s
0.13	1192	1206	73.2	64.8	6.7	11.4
0.19	1248	1230	111.6	121.2	12.3	16.9
0.25	1347	1263	159.2	150.8	21	25.3
0.35	1520	1363	175.6	203	31.6	33.7

influence of the pressure and strain rate since its encompasses the Young's modulus, speed of the sound and density of the material under shock. The difference on each parameter depending on the first or second peak is not as linear. The material velocity "u" always increases on the second peak while the shockwave velocity "D" only increases on the second peak for the shot at 0.13 GW/cm^2 and decreases for the three other ones. Finally the full width half maximum oscillates between a decrease and an increase at with each laser intensity increase. With the use of the equation $P = \rho\, D\, u$ (with u_s the rear free surface velocity, the maximum velocity of the first peak of the backface velocity profile obtained by VISAR and u the material velocity $u = u_s/2$) one can observe that the difference of pressure induced for the laser shock at 0.35 GW/cm^2 is mainly governed by the shockwave velocity variation since the material velocity practically does not change between the first and second peak. This leads to a lower pressure on the second peak at this laser intensity which in turn, induces a higher polymer chain mobility due to lesser rigidification. The lower fraction of the target transitioning to a glassy state causes the full width half maximum to increase. This observation indicates that in between the two peaks, the material is only partially glassy. This also means that by inducing a shockwave with a pressure high enough in the material, the entirety of its thickness can be transitioned to a glassy state. Reaching such a pressure would induce a "stable" set of mechanical properties parameters in the material as its state would not be evolving during the shockwave propagation.

The last mechanical parameter that can be studied through these velocity profiles is the strain rate evolution depending on the laser intensity used as well as between the first and second peaks. Figure 4.20b shows that the steepness of the first peak of the profile is independent of the laser intensity chosen, meaning that the strain rate is not affected by such a variation of incident laser energy. This can either mean that the strain rate is not affected by the laser energy in this material or that the

energy variation is too small to induce a noticeable effect in the material. The variation of the strain rate was also studied between the first and second peak of the same profile at different laser intensity. Figure 4.21 shows the two peaks superimposed at the four intensities already shown before. The steepness between the first and second peaks is decreasing on each plot.

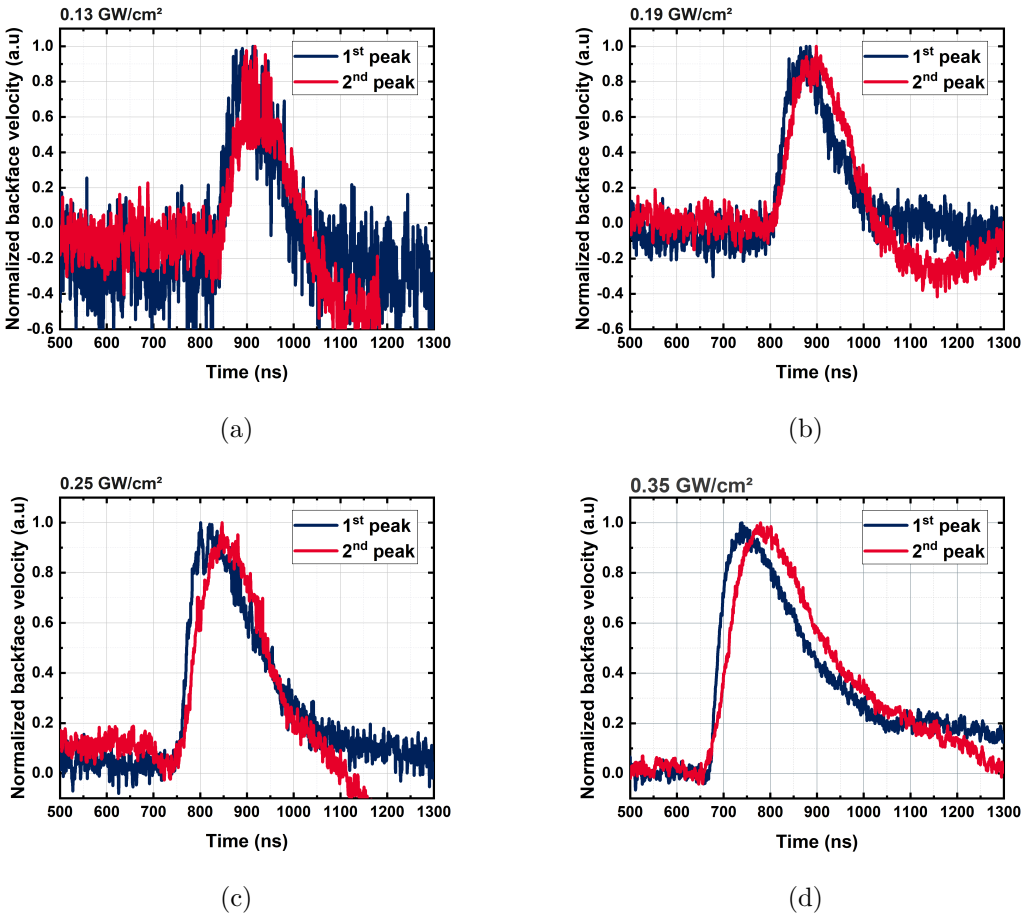

Figure 4.21: Superposition of the normalized first and second peaks of velocity profiles at different laser intensities. (a) 0.13 GW/cm^2, (b) 0.19 GW/cm^2, (c) 0.25 GW/cm^2 and (d) 0.35 GW/cm^2.

The steepness of the second peak decreases with higher laser intensities. The slope for 0.13, 0.19, 0.25 and 0.35 GW/cm^2 is respectively of 0.016, 0.015, 0.012 and 0.010). This steepness variation demonstrate a lowering of the strain rate while the laser intensity used gets higher contrary to what has been shown in figure 4.12. Under high pressure and strain rate a material like the acrylate tape with rubbery properties and subject to glassy transition seems to exhibit a different behaviour at low and high pressures (or laser intensity). Under a pressure of the order of hundreds of MPa the

material is only partially glassy and seems to exhibit rapidly evolving mechanical properties that are not necessarily the same as the one that can be observed with the use of laser intensities higher than the damaging threshold (≈ 0.86 GW/cm^2).

4.2.3.2 Properties at higher pressures

The characterization of the mechanical properties was extended to laser intensities higher than the damaging threshold (up to 10.13 GW/cm^2). Figure 4.24 shows the different backface velocity profiles obtained at different intensities ranging from 0.13 to 10.13 GW/cm^2 and the time needed for the shockwave to hit the backface of the target.

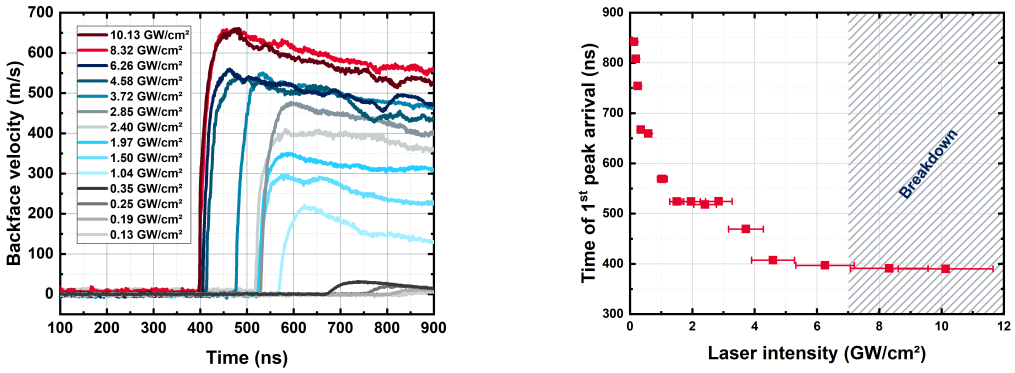

(a) (b)

Figure 4.22: (a) Backface velocity profiles extracted from VISAR experiments at laser intensities ranging from 0.13 to 10.13 GW/cm^2 on a 1 mm acrylate tape target coated on both sides by 10μm pure, 99.9% aluminium and shot with a 7 ns laser pulse, 532 nm wavelength. (b) Time needed for the shockwave to hit the backface of the target after the laser pulse depending on the laser intensity of the laser shot.

The shots previously shown in figure 4.20a are also added for comparison. The behaviour at higher laser intensities demonstrates different mechanical behaviour. The steepness of the profile becomes a lot more pronounced starting 1.04 GW/cm^2 and getting more and more steep until 8.32 GW/cm^2 where is stops evolving, mainly due to the breakdown threshold being reached thus preventing the pressure produced from going higher. The time needed for the shockwave to reach the backface of the target goes from 842 ns to 390 ns thus expressing the large evolution of the mechanical properties of the acrylate tape target under high stress/strain rate conditions. No study of the mechanical parameters between the first and second peaks of the profiles could be done here due to the damaging of the

confinement at intensities higher than the breakdown threshold, preventing the apparition of a second peak. The variation of the different parameters ("D", "u" but also the pressure "P" and the density "ρ" were calculated from these experiments.

The pressure calculation could not be done using the model provided in [195] since it has been validated between 1 to 10 GW/cm^2. Under 1 GW/cm^2 the interaction starts to change since the reflectivity becomes governed by metallic reflection rather than by a reflection on the plasma (see figure 1.5) thus the values given by most models at low intensities have higher uncertainties than the results at laser intensities above 1 GW/cm^2. Work from Bardy [210] shows experimental points obtained at low laser intensity in a confined regime with a 7 ns top-hat pulse at 532 nm. In this work, the pressures are extracted from the shots through the CEA internal code ESTHER which appears to be a better alternative compared to Abaqus for pressure prediction from laser experiments while also giving access to the plasma temperature and others variables through its calculations. The results given should still be taken carefully as they present an uncertainty higher than 15%, especially considering the measurements realised were done with a top-hat pulse instead of the Gaussian one used with the Héphaïstos laser. The pressure measurements under 1 GW/cm^2 are given in figure 4.23.

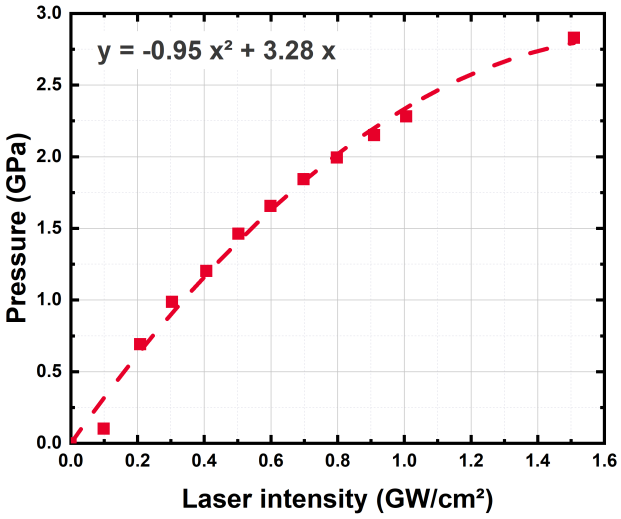

Figure 4.23: Maximum pressure depending on the laser intensity through the use of the ESTHER code, confined regime, 7 ns top-hat pulse, 532 nm (results taken from [210]).

The shockwave velocity as well as the material velocity are calculated using the same method

described above. Finally, the density is calculated using the Rankine-Hugoniot equation:

$$\rho_0 D = \rho(D - u) \tag{4.4}$$

With $\rho_0 = 0.935$, the value was calculated with a density scale on the acrylate tape polymer. Figure 4.24 shows the results of the calculation of these different parameters depending on the intensity of the laser shot chosen.

The variation of the different parameters studied depending on the intensity of the laser shot can be described as follow:

- The pressure plot in figure 4.24a describes the classic trend for laser shots with this type of set parameters. The pressure increases along with the laser intensity up to 7 GW/cm^2 when the breakdown threshold is reached, corresponding to a pressure of 8 GPa. After that point, the pressure reaches a plateau and the results extracted become more dispersed. This is caused by the breakdown plasma which absorbs incident laser energy. Due to the process not being really repeatable from one shot to another, the resulting pressures obtained are unstable.

- The material velocity "u", equal to the rear free surface velocity divided by two (the velocity obtained on the velocity profile generated by the VISAR experiment)follows a linear increasing with the pressure.

- The shockwave velocity "D" quickly rises with an increasing pressure up to 2 GPa. From 3.8 to 6 GPa a plateau is observed with a shockwave velocity staying at around 2125 m/s. This phenomenon can also be observed on figure 4.24 with multiple backface velocity profiles showing the beginning of their first peak at 520 ns despite the laser intensity between shot increasing. After 6 GPa, the shockwave velocity starts to increase again up to the breakdown threshold. Because the pressure stops rising, D stops going higher as well.

- Finally the density ρ variation matches the variation of the shockwave velocity. Considering equation 4.4, it is consistent with the calculation that is more influenced by the value of D than by the one of u. The same plateau is observed but starts around 4.8 GPa and stops at 5.8 GPa. Passed this value the density goes a little bit higher, reaching 1.097 at 6.6 GPa. A second plateau

caused by the breakdown phenomenon which prevents the density from going higher passed this laser intensity.

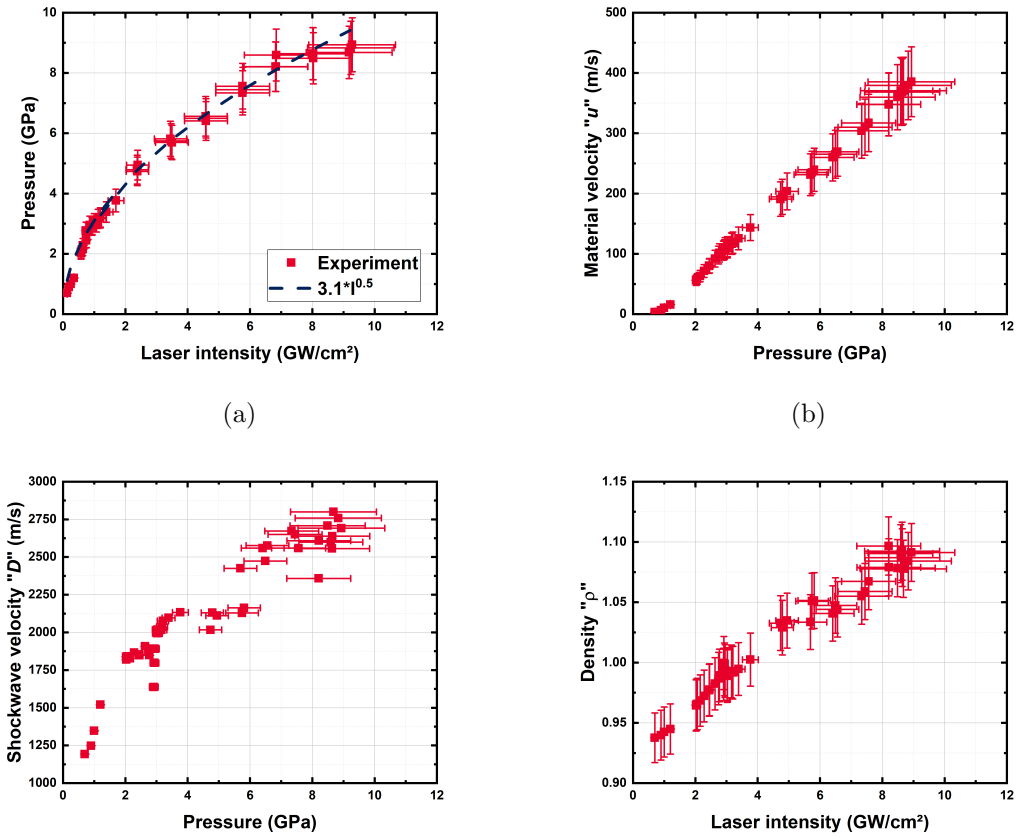

Figure 4.24: mechanical parameters extracted from the profiles obtained by VISAR measurements on shot with a 7 ns laser pulse, 532 nm on 1 mm acrylate tape targets coated on both sides by 10μm pure, 99.9% aluminium (a) Pressure depending on the laser intensity, (b) material velocity depending on the pressure produced, (c) shockwave velocity depending on the pressure produced and (d) density of the target depending on the pressure produced.

From these results the impedance Z of the acrylate tape confinement depending on the pressure applied is obtained using $Z = \rho D$. The result is given in figure 4.25 and compared with results obtained with water that have been extracted from measurement of the shockwave velocity depending on the pressure realised by Bardy et al. [210].

The results obtained show a lower impedance developed by the acrylate tape confinement under laser shock conditions compared to the water confined regime. Even though their impedance

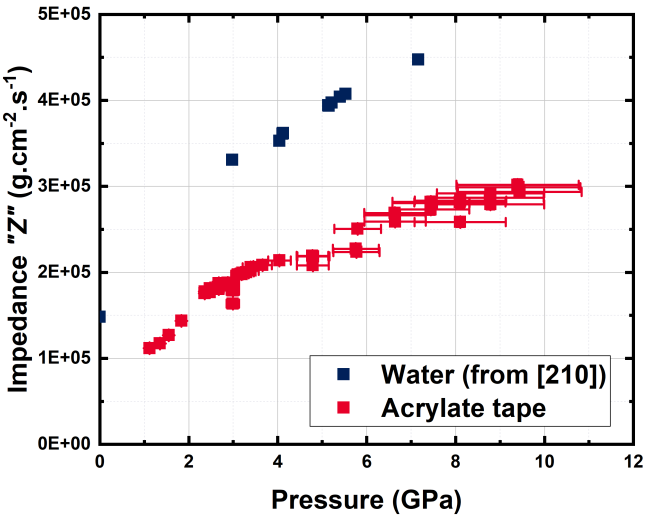

Figure 4.25: Impedance depending on the pressure applied for the acrylate tape confinement and water confinement from Bardy et al. work [210].

at P $\approx$ 0 GPa are close (Z_{water} = 1.48.10^5 g.cm^{-2}.s^{-1} for water at I = 0 GW/cm^2 and $Z_{acrylate}$ = 1.17.10^5 g.cm^{-2}.s^{-1} at 1.1 GPa for the acrylate tape confinement), the water impedance reaches higher impedances while under higher laser intensities and hence higher pressures. The maximum values reached are for water and acrylate tape, respectively 4.47.10^5 g.cm^{-2}.s^{-1} and 3.02.10^5 g.cm^{-2}.s^{-1}.

4.2.3.3 Mie-Grüneisen parameters extraction

The Mie-Grüneisen equation of state is linked to the pressure and volume in a solid at a set temperature. It can be written as:

$$\Gamma = V\left(\frac{dP}{de}\right)_V \tag{4.5}$$

With:

Γ: the Grüneisen parameter which represents the thermal pressure from a set of vibrating atoms.

V: the volume.

P: the pressure.

e: the energy.

If the Grüneisen parameter is considered to be independent from the pressure and energy then the

model can be integrated, giving:

$$P - P_0 = \frac{\Gamma}{V}(e - e_0) \tag{4.6}$$

The calculation of Γ is usually done with the Dugdale-MacDonald model [213] following:

$$\Gamma = -\frac{1}{3} - \frac{v}{2}\frac{d^2(p_c v^{2/3})/dv^2}{d(p_c v^{2/3})/dv} \tag{4.7}$$

Where p_c is the cold pressure. At the initial state, an approximation of Γ is given by the following equation described in [214] and obtained from work by Slater [215]:

$$\Gamma_0 = 2S - 1 \tag{4.8}$$

From the Hugoniot equations (conservation of mass, energy and momentum) a linear relation describing the behaviour of material under relatively low stress (< 10 GPa) allows the linking of the shock velocity D with the particle velocity u:

$$D = C_0 + Su \tag{4.9}$$

More information on the Mie-Grüneisen equation of state can be found in 2.3.3.3. For this type of equation to be implemented in a finite element modelling software like Abaqus some parameters are needed:

C_0: the speed of the sound in the material shocked.

S: the Hugoniot constant specific to the material.

4.2.3.3.1 S parameter determination

The first parameter that needs to be determined in the Mie-Grüneisen equation of state is the Hugoniot constant S that appears in the other parameters calculation. This parameter can be extracted from an Hugoniot plot of the concerned material using $S = dD/du$. The Hugoniot plot for the acrylate tape polymer is given in figure 4.26:

Usually one S parameter is extracted from the Hugoniot plot of a material. In this case, two main lines are observed, hence describing two S parameters, respectively 4.24 ± 0.67 and 6.02 ± 2.25. Some small divergences are observed at low backface velocities (corresponding to laser intensities lower than 1 GW/cm^2). A plateau separates the two different slopes for u ranging between 150 to 250 m/s, corresponding to the plateau observed for intensities I between 1.50 to 2.85 GW/cm^2. The

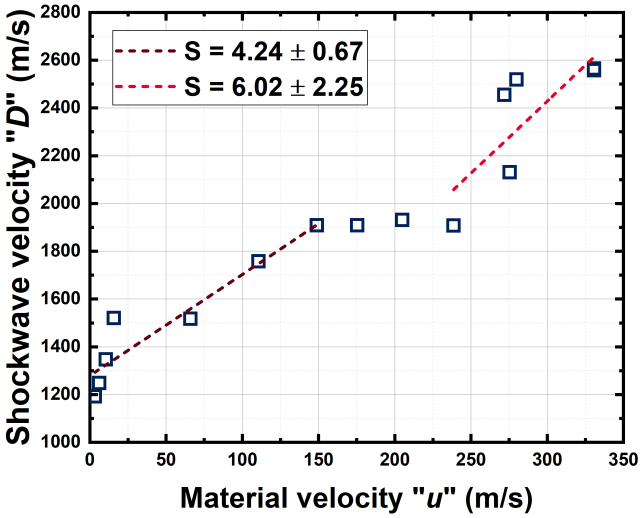

Figure 4.26: Hugoniot plot for the acrylate tape polymer corresponding to the shockwave velocity depending on the material velocity.

different ramps observed show different material behaviour depending on the pressure applied. Each of these behaviour is the witness of a phase transition of the material. In the case of the acrylate tape confinement, the pressures induced by laser shock should induce a transition to a glassy relaxation behaviour even at low pressures. The transition to a glassy behaviour in the Sylgard184 polymer under a 10^6 s^{-1} strain rate necessitate a pressure of at least 670 MPa. Considering that the static glass transition temperature of Sylgard184 under atmospheric pressure is 147 K while the acrylate tape exhibit a transition between 228 K, the pressure needed to induce a glassy behaviour in this material should be a lot lower than in the Sylgard184 if the value of the shift depending on the pressure is considered close (0.18 K/MPa). There are two possibilities to explain the plateau observed for material velocities between 150 to 250 m/s (equivalent to a pressure range $\approx$ from 3 to 6 GPa).

- The two glass transitions observed in the material are happening in this pressure range at ambient temperature (see **??**) but the material velocities in the acrylate tape polymer should have already induced a transition to a glassy behaviour.
- The plateau could also be an indicator of a beta transition (end-groups of the chain loosing mobility as opposed to the glass transition which concerns the backbone chain), either spread over a large temperature range like the glass transition of the material or could just be spread

by the diffusion of the transition through the thickness of the acrylate tape with the shock propagation. Complementary experiments with acrylate tapes of different thicknesses or with other polymer with a similar structure could give an answer to that question.

4.2.3.3.2 Grüneisen parameter determination

From the calculation of S, the Grüneisen parameter is also obtained using equation 4.8 giving respectively $\Gamma = 7.48 \pm 1.34$ and $\Gamma = 11.04 \pm 4.50$ for the two S values. This calculation is normally used for metals and gives a very good agreement with the values obtained using the thermodynamic parameters of the concerned material on which it was tested.

4.2.3.3.3 Speed of the sound determination

The results obtained from the precedent calculations allows to access to the sound of the speed in the material through the equation 4.9. The result of the calculation for the acrylate tape confinement depending on the laser intensity used is given in figure 4.27. The results are dispersed around 1250 m/s an oscillate between 910 to 1450 m/s. This dispersion of the results is partly caused by the S value calculated which give a linear fit between the shockwave velocity and backface velocity while the behaviour of the acrylate tape appears to fluctuate with the increasing material velocity. This can be caused by the reduced range of velocities attained with the experiments compared to the classical experiments that are usually done with material velocities reaching multiple km/s.

The Mie-Grüneisen equation of state allows a good representation of the shock but does not take into account the relaxation time of the polymer chains during the release.

The data obtained from the dielectric relaxation spectroscopy experiments could provide the necessary informations to produce an accurate modelling of the acrylate tape confinement. Such a model would allow a better understanding of the evolution of the mechanical properties of such a polymer under high pressure and strain rate. Moreover, a complete simulation of the polymer confinement behaviour would provide information about the effect induced in the material in all of its thickness rather than just on its surface.

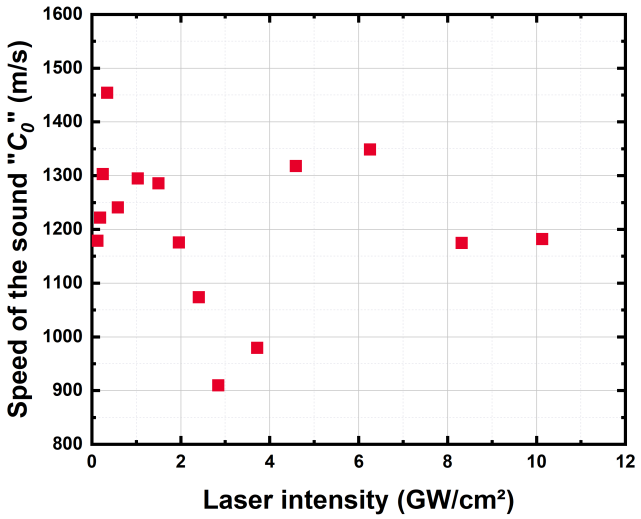

Figure 4.27: Speed of the sound in the acrylate tape confinement depending on the intensity of the laser shot.

4.3 Conclusion on the acrylate behaviour under laser shock conditions

Dielectric relaxation spectroscopy measurements were coupled with VISAR measurements on aluminium target confined with polydimethylsiloxane and polycarbonate. The first material was chosen for its low T_g (147 K) and properties close to the acrylate tape while the second material has a high T_g (415 K) and is solid even before shock. The coupling of the two experiments gave information on the effects induced in low T_g, flexible polymers when put under laser shock loading (high strain rate and pressure). The experiments showed the prevalence of the pressure on the transition to a glassy state of this type of flexible polymers. To complete the study the acrylate tape chosen for the LSP treatments was also studied with DRS but did not yield consistent results allowing an accurate interpretation.

To obtain further information on the behaviour of the acrylate tape confinement, VISAR measurements were performed on acrylate tape coated in ≈ 10 μm of aluminium on both sides and confined with water not to damage the aluminium coat. The results allowed to obtain parameters of the Mie-Grüneisen equation of state for this material. during these experiments a phase transition of the material under shock was also observed. It could correspond to the progressive plasticizing of the thickness of the acrylate tape confinement or be linked to the two T_g observed during the DRS measurements. Future experiments using the same setup but with different thicknesses of acrylate

tape could give information on this interrogation.

Conclusion

Conclusion

The purpose of this PhD was to replace the water confined regime used for the laser shock peening process in the industry by a polymer confined regime through the use of adhesive flexible transparent polymers. The study was part of a bigger project; the FORGE ANR, that aimed to cover all the aspects involved in the implementation of the laser shock peening process with polymer confinement, from the mastering of the confinement to the development of a laser and optic fiber adapted to the end use aimed.

The work was divided in different objectives. The first one was to be able to find a polymer to be used as a confinement that would be able to produce good pressures when used for laser shock. The second one was to have a better understanding of the laser-matter interaction in this specific configuration and at the different interfaces (air/confinement and confinement/target). The last objective was to understand the mechanisms involved in the polymer confinement degradation during laser shock both thermal and mechanical.

The first chapter presented a bibliography of the laser shock peening process with a description of all the important parameters as well as their effects on the interaction. A second bibliographic part presented the polymers properties under high temperature and pressure to give an overview of the expected effects of the lasers shock peening process on these types of materials.

The second chapter presented the different methods and diagnostic used for the material characterisation. First the laser characterization and all the metrology associated to the mastering of the energy of each shot. A very important parts linked to the next one which is the model used for the modelling of the back face velocity profiles obtained through VISAR experiment and allowed to extract the pressure produced by a laser shot directly from the experiment instead of having to use existing model that induce more uncertainties. Another focus of this chapter was to present the

different techniques used either for the polymer synthesis in some cases or for their characterization, in a static environment or under laser shock which involves high strain rate and pressure.

Chapter three was divided in three main axes. First defining a suitable polymer confinement for the end use intended. This involves the pressure measurement of multiple types of polymer, epoxies, silicones and acrylate based ones. Once the main polymer for the end use was defined, two more were chosen for the possibility to synthesize them at the laboratory. This allowed studies where the parameters influencing the properties of said polymers was possible. This leads to the second axis of the chapter in which different properties of the polymer confinements were tested such as the thickness, Young's modulus, adhesion properties and chemical composition of the polymers and their effects on the maximum pressure produced while also studying the water confined regime to have a reference point of comparison. Finally the last axis of this chapter consisted in defining the compressive residual stresses induced by a surface treatment using the chosen acrylate tape confinement to assess if the results obtained were suitable with what is expected to obtain good fatigue property behaviour after treatment.

The last chapter was focused on the study of mechanical behaviour of flexible polymers under laser shock conditions. These types of materials are typically studied under relatively low pressure and strain rate compared to what can be observed during a laser shock. For this reason laser experiments were coupled with dielectric relaxation spectroscopy (DRS) in order to obtain a better understanding of the polymer chains relaxation under high strain rate and pressure and explain the pressures produced by such polymers through the impedance mismatch theory. These experiments also allowed to obtain parameters of the Mie-Grüneisen equation of state that, coupled with chain relaxation informations obtained with the DRS experiment could allow an accurate modelling of the acrylate tape confinement.

Perspectives

This work showed that using flexible polymer confinements instead of the classically chosen water confined regime could yield equivalent maximum pressures and by extension equivalent compressive residual stresses and fatigue behaviour properties. Nevertheless, in order to completely master the laser shock peening process with polymer confinement, a certain number of experiments are still necessary.

- To better understand the phenomena at work during the laser-matter interaction with the polymer confinement a complete modelling of the confinement should be realised by coupling a Mie-Grüneisen model with a viscoelastic model or an extended Maxwell model to take into account the transition to a glassy state under shock and the long release induced by the chain relaxation. This type of modelling would allow to obtain information in the whole thickness of the material instead of just the surface data. To support this modelling, experiments on acrylate tape confinement covered in an aluminium coating but with different thicknesses than what was already done could give information on the material behaviour under laser shock. For example the transitions observed in the acrylate tape Hugoniot plot could be explained. New dielectric relaxation spectroscopy measurements could be realised since the results obtained from the experiments of this manuscript do not give reproducible results. To complete the experiment, new camera view of the acrylate confinement could be realised under laser shock with a better camera to obtain more accurate information of the deformation field of the material during the shock.

- In the same way, a 3D modelling of the residual stresses induced in the material could give a better representation of the compressive residual stresses induced by the laser shock peening treatment in large spot configuration (> 1 mm). In the case of small spot (< 1 mm) configuration, the high overlap an overall number of shots should induce a homogenisation of the residual stresses but a 3D modelling should still be realised to compared with an axisymmetric model to assess

the need for such a simulation.

- In order to further the use laser shock peening with polymer confinement in an industrial setting the problematic of the shot repetition must be solved. Although the process is working, it is, has of now, impossible to treat a typical work-piece surface ($\approx$ 30x30 mm) in a realistic time frame. To overcome this problem, two approach are envisioned. The first one consists in using even smaller laser spots and lower energies (100's of mJ) to induce smaller plasma that what was previously expected. That way the debonding could be avoided a well a thermal damaging of the confinement as well as its opacification due to the ablation of the surface aluminium particles ionised by the plasma. The second solution would be to automate the process to replace the polymer confinement at regular intervals, either between each shots or after a pattern that allow to use the maximum surface of the applied polymer tape before changing it.

Conclusion FR

L'objet de ce travail de doctorat était de remplacer l'eau de confinement utilisée pour le procédé de laser shock peening en industrie par un régime utilisant un confinement polymère par le biais de l'usage de polymères flexibles, transparents et adhésifs. L'étude prenait part dans le cadre d'un projet plus conséquent; l'ANR FORGE qui avait pour but de couvrir tous les aspects intervenant dans l'implémentation du procédé de laser shock peening utilisant un confinement polymère, de la maîtrise du-dit confinement jusqu'au développement d'un laser et d'une fibre optique adaptés à l'utilisation finale du procédé envisagé.

L'étude a été divisé en trois axes différents. Dans un premier temps l'objectif était de définir un polymère pouvant être utilisé pour l'application, c'est-à-dire qui serait capable de produire des pressions suffisantes quand utilisé comme confinement. Le deuxième objectif était d'obtenir une meilleure compréhension de l'intéraction laser-matière dans cette configuration confinée polymère aux différentes interface (air/polymère et polymère/cible aluminium). Le dernier objectif était de comprendre plus en profondeur les mécanismes mis en oeuvre lors de la dégradation du polymère de confinement, qu'elle soit thermique ou mécanique.

Le premier chapitre décrit une étude bibliographique du procédé de laser shock peening ainsi qu'une description des différents paramètres d'importance et de leur influence sur le procédé et l'intéraction laser-matière. Un deuxième volet bibliographique concerne les propriétés des polymères sous choc et haute température et donne une vue d'ensemble des effets potentiellements induits par le procédé de laser shock peening sur de tels matériaux.

Le deuxième chapitre présente les différentes méthodes et diagnostics utilisés pour la mesure des caractéristiques matériau. Tout d'abord la métrologie du laser a été effectuée pour s'assurer de l'énergie délivrée par chaque tir du laser. Cette partie du travail est intimement liée à la suivante qui consiste à

simuler les profils de vélocité en face arrière obtenus par mesures VISAR. La simulation de ces profils permet l'extraction de la pression maximale développée par un tir laser sans passer par l'utilisation de modèles déjà existants qui peuvent induire des incertitudes. Un autre point important de ce chapitre concerne la présentation de différentes techniques utilisées pour la synthèse des polymères ainsi que leur caractérisation dans un environnement statique et sous un chargement laser qui induit de fortes pressions et vitesses de déformation.

Le chapitre trois est divisé en trois axes principaux. Premièrement, la définition d'un polymère de confinement adapté à l'utilisation industrielle finale. Cette étape à fait l'objet d'études sur différentes familles de polymère; epoxy, silicones, acrylate. Une fois que le polymère d'intérêt était défini, deux de plus ont été choisis pour la possibilité de les synthétiser directement au laboratoire. Cela a permis de faire varier certaines de leurs propriétés de manière indépendante par rapport aux autres. Cette spécificité amène au second axe du chapitre dans lequel les différentes propriétés des polymères ont été testées une à une telles que l'épaisseur, le module d'Young, la composition chimique ou encore les propriétés adhésives ainsi que leurs effets sur les pressions maximales délivrées par le procédé de laser shock peening. Toutes les mesures ont été réalisées en parallèle avec un confinement par eau afin d'obtenir un point de référence. Le dernier axe du chapitre se concentre sur la mesure de contraintes résiduelles induites par le traitement en utilisant le confinement acrylate dans le but d'évaluer la viabilité des contraintes dans le matériau après LSP et si les valeurs atteintes permettent d'assurer un comportement en fatigue adéquat.

Le dernier chapitre étudie le comportement mécanique des polymères flexibles utilisés comme confinement lors de leur mise sous choc par laser. Ces matériaux sont typiquement étudiés sous des pressions et vitesses de déformation relativement basses comparées aux valeurs atteintes lors d'un traitement par choc laser. De ce fait les expériences laser ont été comparées avec des expériences de DRS (dielectric relaxation spectroscopy) dans le but d'obtenir une compréhension plus fine des phénomènes de relaxation de chaînes sous hautes pressions et vitesses de déformation et par extension expliquer les pressions développées par les polymères de confinement lors de leurs utilisation par le biais de la théorie de la rupture d'impédance. Ces expériences auront aussi permis d'obtenir les paramètres de l'équation d'état de Mie-Grüneisen qui, couplés avec les informations de relaxation de chaînes obtenues par DRS pourraient permettre une simulation fidèle du confinement acrylate.

Perspectives

Ce travail de thèse a permis de démontrer que l'utilisation de polymères en tant que confinement pour l'application de laser shock peening à l'instar de confinement par eau habituel permettait d'obtenir des pressions maximales équivalentes et par extension des contraintes résiduelles de compression et un comportement en fatigue similaires. Néanmoins, dans le but de complètement maîtriser l'utilisation du confinement polymère un certain nombre d'expériences doivent encore être réalisées:

- Pour mieux comprendre les phénomènes mis en jeu pendant l'intéraction laser-matière avec un confinement polymère, une modélisation complète du matériau doit être réalisée en couplant un modèle de Mie-Grüneisen avec un modèle viscoélastique ou un modèle de Maxwell étendu afin de prendre en compte la transition vitreuse sous choc des polymères utilisés ainsi que la relaxation lente de leurs chaînes qui provoque une détente lente. Ce type de modélisation permettrait d'obtenir des informations sur la totalité de l'épaisseur du confinement polymère alors que les expériences réalisées jusqu'alors ne donnent accès qu'au comportement de surface au niveau de l'interface confinement/cible. Pour accompagner cette modélisation, des expériences sur le confinement acrylate couvert d'une fine couche d'aluminium devraient être mises en oeuvre avec différentes épaisseurs de confinement. Cette expérience permettrait de mieux comprendre les effets de transitions observés dans la courbe d'Hugoniot du matériau sous choc. De nouvelles mesures DRS avec le confinement acrylate doivent aussi être faites afin d'obtenir un résultat plus stable que ceux disponibles pour l'instant. Pour compléter ces expériences, de l'imagerie par caméra rapide pourrait être faite sous choc pour obtenir de plus amples information sur le champs de déformation du polymère pendant l'intéraction laser-matière.

- De la même manière, une modélisation 3D des contraintes résiduelles induites dans la cible après traitement pourrait donner une meilleure représentation de la répartition des contraintes

comparé au modèle 2D axisymmétrique utlisé pour le moment. Ces expériences apparaissent nécéssaires dans le cas de l'utilisation de grandes tâches laser (> 1 mm) avec de faibles taux de recouvrement tir à tir. Dans le cas de traitements utilisants une petite tâche laser (< 1 mm) et induisant des contraintes de façon plus homogène, ce type de simulation permettrait de définir si un modèle 3D est nécessaire comparé à un modèle 2D axisymétrique.

- Afin de pouvoir aller plus loin dans l'utilisation du laser shock peening avec un confinement polymère dans un cadre industriel, la problématique de la répétition des tirs laser est cruciale et doit être résolue. Bien que les capacités du procédé soient démontrées, il est pour l'instant impossible de le transposer au traitement de pièces de surface représentatives des besoins industriels ($\approx$ 30x30 mm) en un temps réaliste. Pour contrecarrer ce problème, deux approches sont envisagées. La première consiste à utiliser une tâche d'encore plus faible diamètre et d'énergie également plus basse (100 aines de mJ) dans le but de produire des plasmas de taille plus petite. De cette manière le phénomène de décollement du confinement devrait pouvoir être réduit voir complètement évité. Un autre avantage de cette méthode est la réduction de l'endommagement par effet thermique et par extension de l'opacification tir à tir du confinement. La seconde solution serait d'automatiser le procédé en remplaçant le polymère de confinement à intervalle régulier, soit entre chaque tir, soit après un pattern permettant de maximiser la surface de confinement utilisée avant de la changer.

Appendixes

A | Ballard's model

Ballard's model gives information on the mechanical characteristics of a material after laser peening. The main results are as follow:
Plastification threshold for an uniaxial deformation:

$$P_H = \left(1 + \frac{\lambda}{2\mu}\right)\sigma_{Y_0} = \left(\frac{1-\nu}{1-2\nu}\right)\sigma_{Y_0} \tag{A.1}$$

With this calculation: $P_H = 1.7$ to $1.8\ \sigma_{Y_0}$ Depth plasticized for a triangular impulsion:

$$L_p = \frac{C_e C_p \tau_p}{C_e - C_p}\left(\frac{P - P_H}{2P_H}\right) \tag{A.2}$$

The depth affected linearly depends on the pressure pulse duration τ_P Plastic deformation rate:

$$\varepsilon^p = -\frac{2P_H}{3\lambda + 2\mu}\left(\frac{P}{P_H} - 1\right) \tag{A.3}$$

The plastic deformation rate calculated is correct once the material is plasticized, numerically it works between P_H and $2P_H$ and linearly depends on P Optimal treatment pressure:

$$P = 2 \quad \text{to} \quad 2.5P_H \tag{A.4}$$

The optimal treatment pressure is close to the saturation pressure of ε^p Superficial residual stress for a circular impact with a radius r_0:

$$\sigma_{surface} = -\sigma_{Y_0}\left(1 - \frac{4\sqrt{2}}{\pi}(1+\nu)\frac{L_P}{r_0\sqrt{2}}\right) \tag{A.5}$$

The superficial residual stress is dependent on some parameters, thus $\sigma_{surface}$ vary as follow:

- It increases with ε^p and r_0
- It decreases with L_P

B | Impedance mismatch and shockwave theory

A shock is a pressure wave propagating though a material modifying it during a short time and on a brief length (about a few atomic planes). A shockwave can be determined by three main parameters:

- Pressure P
- Internal energy E
- Density ρ

The shock propagation induce a change of these characteristic variables.

B.1 State equations

During the shockwave propagation the material goes from an initial state (P_0, E_0, ρ_0) to a final state (P, E, ρ). At first approximation, a material under shock can be described as a liquid. The modifications brought by the shockwave can be predicted by three conservation hydrodynamic equations. In order to do so, two new parameters need to be introduced:

- D, the speed of the shockwave propagation
- u, the material speed induced in the material

For a material at $u_0 = 0$, Rankine-Hugoniot equations are used [216, 217]:

$$\rho_0 D = \rho(D-u) \quad \text{(mass)} \tag{1}$$

$$E - E_0 = \frac{1}{2}(P+P_0)(\frac{1}{\rho_0} - \frac{1}{\rho}) \quad \text{(energy)} \tag{2}$$

$$P - P_0 = \rho_0 D u \quad \text{(quantity of movement)} \tag{3}$$

The three equations are completed by a state equation $f(P, E, \rho) = 0$ specific to each material in order to close the system. To study shockwaves with low pressures ($P < 10\ GPa$), such as the ones observed during the laser shock peening process in confined environnement, the hydrodynamic approach just described is not sufficient. The interaction must be described with an hydrodynamic part linked to high deformation speeds ($d\varepsilon/dt \simeq 10^6 s^{-1}$) in which the material behave like a liquid, but also an elastic part where it is considered as a solid. In this case the pressure (P) is not the relevant characteristic value. The one that must be considered is the longitudinal stress (σ_x) in the material. Following these formalisms, the shockwave propagates through the solid under two regimes, bounded by the Hugoniot elastic limit of the material by:

$$P_H = 1 + \frac{\lambda}{2\mu}\sigma_{Y_0} \tag{B.4}$$

Where:

- λ and μ are the Lamé coefficients
- σ_{Y_0} is the static elastic limit of the material

B.1.1 $P_x < P_H$ Elastic regime

For pressures lower than P_H, the shockwave propagates as an elastic wave with a speed C_e given by:

$$C_e = \sqrt{\frac{\lambda + 2\mu}{\rho}} \tag{B.5}$$

And the induced pressure is written:

$$Px = \rho_0 C_e u \tag{B.6}$$

B.1.2 $P_x > P_H$ Plastic regime

For pressures higher than P_H, shockwave propagates as a combination of elastic and plastic waves, the latter is defined by a lower speed C_p:

$$C_p = \sqrt{\frac{\lambda + \frac{2}{3}\mu}{\rho}} \tag{B.7}$$

The induced pressure becomes:

$$P_x = \rho_0 C_p u + \frac{2}{3}\sigma_{Y_0} \tag{B.8}$$

where $(2\sigma_{Y_0})/3$ is the elastic contribution

The celerity of elastic waves is superior to the one of the plastic waves (C_e>C_p)

B.2 Shockwave propagation

B.2.1 Front shock stiffening

In the case of a compressive shock, the pressure variation ΔP induced by a shock is linked to the material speed u following eq.B.6. If the pressure variation is positive, ΔP is also positive, thus Δu is the same sign as the wave celerity. The medium is accelerated following the shockwave propagation path and the compression ramp is stiffened, up to the formation of a front moving at a given speed, as described in figure B.2

$$p_1 > p_0 \quad \text{so} \quad c(p_1) > c(p_0)$$

$$\Delta p = p_1 - p_0 = \rho_0(c(p_0))(u_1 - u_0) > 0 \quad \text{so} \quad u_1 > u_0$$

The two successive compressive shockwave are catching up one to the other as shown in fig. B.1

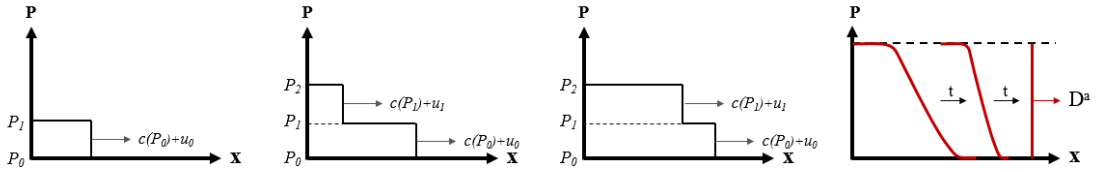

Figure B.1: Stiffening of a compressive shockwave

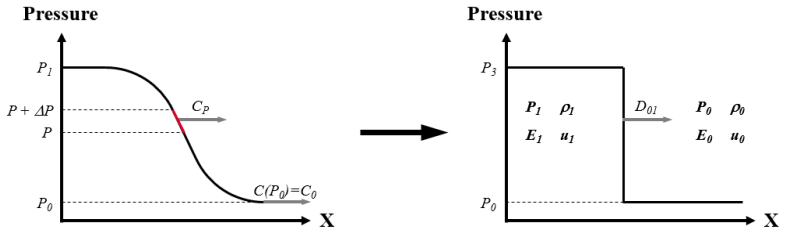

Figure B.2: Stiffening of a compressive shockwave from [218]

B.2.2 Release spreading

Apart from the hydrodynamic attenuation, the shockwave is also attenuated by an elasto-plastic component during its propagation in the material. Since $C_e > C_p$, the elastic component of the release wave is faster than the shock front, thus catching it up and clipping it.

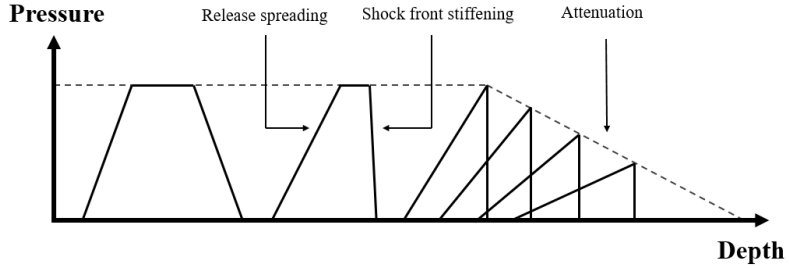

Figure B.3: Pressure profile evolution during its propagation in the target

In this case:

$$p_1 < p_0 \quad \text{so} \quad c(p_1) < c(p_0)$$

$$\Delta p = p_1 - p_0 = \rho_0(c(p_0))(u_1 - u_0) < 0 \quad \text{so} \quad u_1 < u_0$$

Two successive releases are getting further apart from one another.

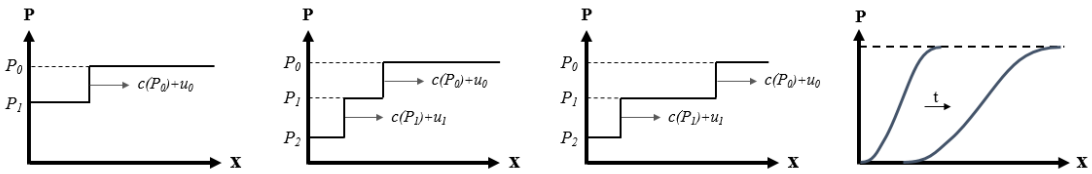

Figure B.4: Broadening of a release wave

The two phenomena are observed in the pressure profile of a laser shock. At the beginning a compressive shock induces a sharp rise in pressure up to the maximum and then the release tail is slowly going back to the initial state. fig. B.5

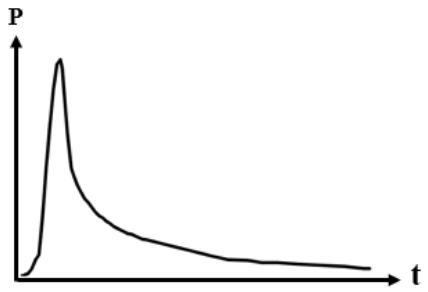

Figure B.5: Pressure profile of a laser shot

B.3 Hugoniot curve

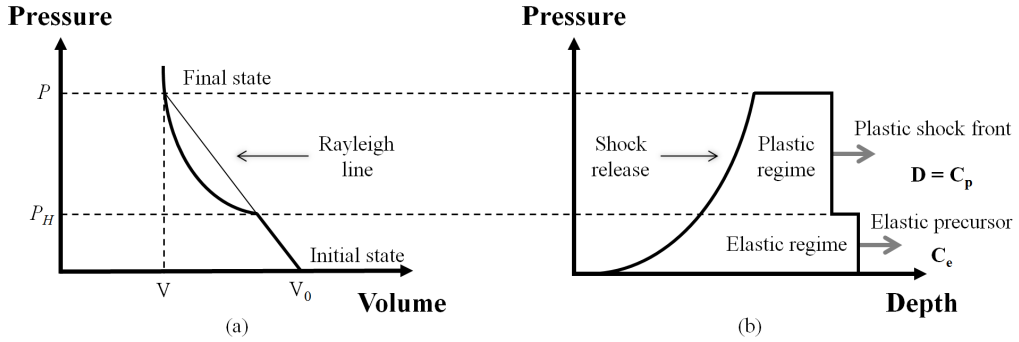

Figure B.6: (a) Hugoniot curve and (b) its equivalent representation as pressure = f(depth) diagram from [34]

Figure B.6 shows the Hugoniot curve. It is a representation of the possible states (P, V) of a material from an initial state at $P = P_{amb}$. The curve can be divided in three parts:

1. An elastic part which moves the precursor P_H up, the speed is not affected by the shock pressure.

2. A plastic wave front between the elastic-plastic limit and the point defining the solid under shock, characterized by the crossing of the Rayleigh line (the prolongation of the elastic part) and the Hugoniot curve.

3. An hydrodynamic part, above the Rayleigh line, the relaxation front, in which the elasto-plastic behavior of the material can be neglected.

B.4 Shock polar

The shock polar of a material is similar to its Hugoniot curve as it gives the Pressure attained by a medium depending on the material speed u. More specifically it is a representation $P_x(u)$ which allows the characterization og a shock in a material from the initial state. The shock polar of a material is given by eq. B.9.

$$P_x = \rho_0(C_0 + Su)u + \frac{2}{3}\sigma_{Y_0} \tag{B.9}$$

The part

$$\frac{2}{3}\sigma_{Y_0}$$

is used because of the elasto-plastic component of the material which shifts the shock polar in the plastic part as seen in figure B.7.

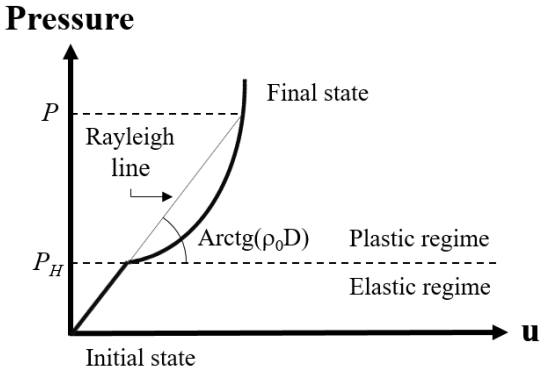

Figure B.7: Shock polar representation from [33]

Much like the Hugoniot curve, the shock polar is composed of three parts if the elasto-plastic behavior of the material is taken into account:

1. When $P < P_H$ The shock speed is not affected by the pressure as shown in eq.B.6. The material exhibit a linear behavior.

2. When $P > P_H$ the shock speed D is given by the slope of the Rayleigh line, linking the intersection elasto-plastic point and the final state point. The slope is defined by $Z = \rho_0 D$, Z being the shock impedance of the material. The evolution of the system is described by eq.B.9.

3. Over these points, the final state is reached. It is characterized by the crossing of the Rayleigh line and the shock polar. The elasto-plastic behavior can be neglected and the pressure is obtained with the hydrodynamic equations.

Movement quantity conservation:

$$p_1 = \rho_0 D_{01} u_1 \tag{B.10}$$

Closing equation:

$$D_{01} = C_0 + S u_1 \tag{B.11}$$

With:

- D is the shock speed
- C_0 is the velocity of the sound in the material
- S is the Hugoniot constant specific to the material
- u is the material speed

B.4.1 Shock polar properties

The parable arc represent all the accessible states of the material when exposed to a shock from the initial state. It does not represent a thermodynamical route. The shock polar is specific to each material (ρ_0, c_0, S) and allows the determination of the material state after shock. The Rayleigh line slope determine the shock impedance $Z = \rho_0 D_{01}$

B.4.1.1 Isentropic approximation

The increase of the entropy in the shock front can be large but its influence on (P-u) plane is negligible when the pressures are moderates. $(H_0) \sim (S_1)$

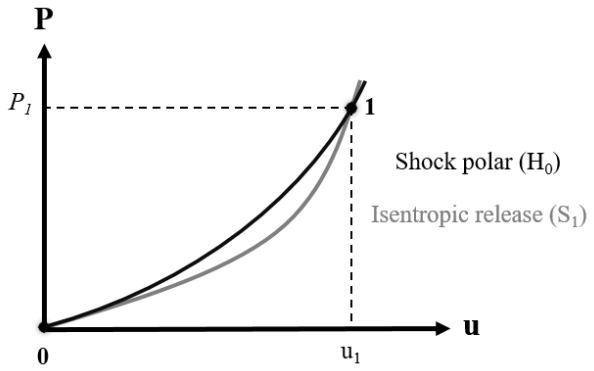

Figure B.8: Isentropic approximation in the (P-u) plane

B.4.1.2 Unique polar approximation

In the case of two successive shocks, the calculation of the energy cannot be obtained by the addition of the energy of the two shocks:

$$e_1 - e_0 = \frac{1}{2}(p_1 + p_0)(\frac{1}{\rho_0} - \frac{1}{\rho_1})$$

$$e_2 - e_1 = \frac{1}{2}(p_2 + p_1)(\frac{1}{\rho_1} - \frac{1}{\rho_2})$$

Is not equal to:

$$e_2 - e_0 = \frac{1}{2}(p_2 + p_0)(\frac{1}{\rho_0} - \frac{1}{\rho_2})$$

But by the unique shock polar approximation it can be considered that the two polars in the (P-u) plane are equivalent ($H_0 \sim H_1$)

B.4.1.3 Unique adiabatic approximation

With the two first approximations, the accessible states (u_1, P_1) for a shock from an initial state are situated on:

- On the (H_0) curve if the wave is incident (positive)
- On the curve (H_0^-), symmetrical of (H_0) in relation to u_1 if the wave is reflected.

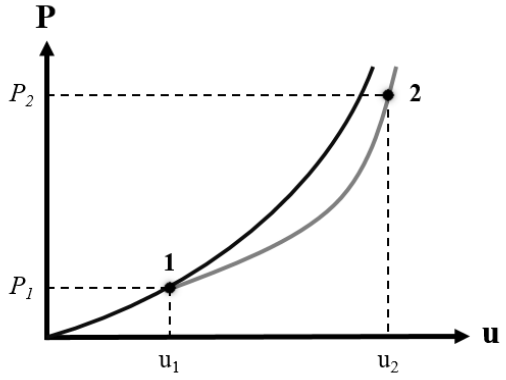

Figure B.9: Unique polar approximation in the (P-u) plane

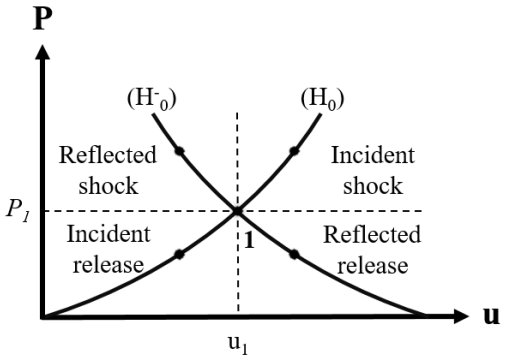

Figure B.10: Unique adiabatic approximation in the (P-u) plane

B.5 Shock transfer between two media A and B

When an incident shock (P_i) propagating in a medium A, goes throught an interface with a medium B, a shockwave is transmitted (P_t) to the second environment B while a shockwave or a release wave (P_r) is reflected in A depending on the shock polar of the two mediums. On both sides of the interface, the new stable state (P_t, u_t) is determined by mass and material speed conservation.

B.5.1 General case: A and B are solids

The nature of the reflected wave is dependant on the impedance ratio between the two materials (ie the position of the two shock polars to one another):

- if Z_A<Z_B (H_A under H_B), the reflected wave is a shock ($P_2 > P_1$)

- if $Z_A > Z_B$ (H_B under H_A), the reflected wave is a release ($P_2 < P_1$)

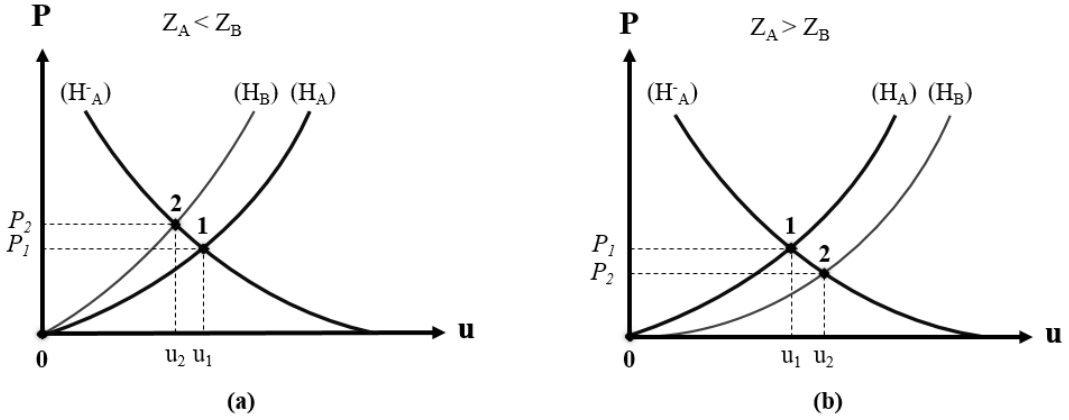

Figure B.11: Shockwave transmission between two medium A and B. (a) Amplified transmitted shock. (b) Dampened transmitted shock.

B.5.2 B is a gas or void

If A is a solid and B is void or a gas, the shock amplitude P_2 transmitted to B is negligible and considered to be 0 since the shock polar of B is far bellow that of A and can be approximated as the x-axis where $P = 0$. The shock is entirely reflected inside of A in order to return the interface to a stress-free state. The material speed u_1 at the interface is the crossing of the point placed at the intersection of the shock polar and the release polar (which is the shock polar symmetrical passing on (P_1, u_1)) and the u axis on which $P = 0$ (figure B.12).

The speed obtained is the free surface speed (u_s) written:

$$u_s = 2u_i \tag{B.12}$$

The above equation is important since u_s can be obtained expererimentally (through VISAR measurements for exemple), allowing, thanks to equation B.12, to retrieve the material speed of the target u. Then, by using the equations B.10 and B.11, it is possible to access the pressure induced in the target, through the material shock polar which links P to u.

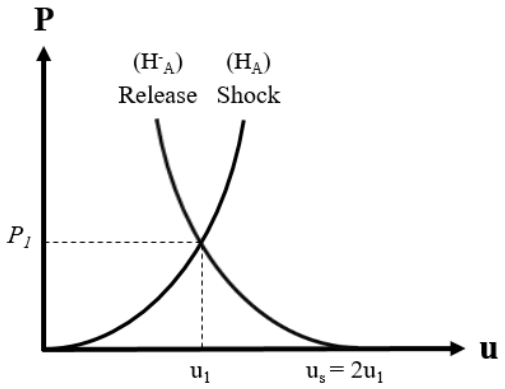

Figure B.12: Free surface speed in the case of a shock propagation through an interface between a medium A and a gas or void B

B.5.3 Example of a shockwave propagating between two media

When a shock propagates from a medium A to an interface with a second medium B, the hydrodynamic equilibrium imposes a mechanic continuity at the interface. It implies that a shockwave is transmitted in the medium B while another one is reflected in medium A. It is the impedance mismatch phenomenon. When studying the propagation of a shockwave, 3 main questions should be asked:

- In which material is the shockwave propagating?
  Used to chose the reference shock polar
- In which direction is the shockwave propagating?
  Will a direct polar or a reflected one be used?
- In which state (P, u) is the shockwave propagating?
  From (P_0, u_0) to (P_1, u_1) for example.

The following example uses this method: The example describes a shock propagated through two materials A and B (fig. B.13).

First information needed is in which material is the shockwave propagating? The choice between the two polars (fig. B.14 (a)) H_A and H_B depends on the material studied. In this case the polar H_B is above H_A since $Z_A < Z_B$.

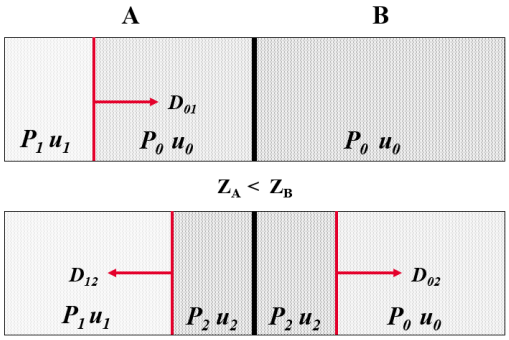

Figure B.13: Shockwave propagating through an interface between two materials A and B.

The shockwave is transmitted in B while a reflected wave goes through A. B will be studied first (fig. B.14 (b).

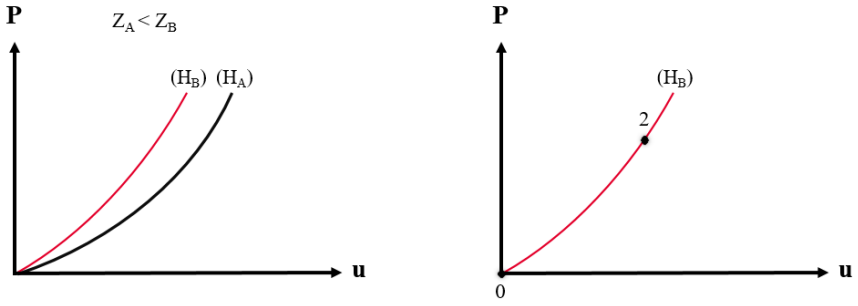

Figure B.14: Shock polars of materials A and B

Once the polar is chosen, the direction of propagation of the shockwave must be determined. The shock is transmitted to the material B, a direct polar is used, as shown on fig. B.14 (b). To finish the state (P, u) of the propagating shockwave is determined. (P_0, u_0) is the initial state and is placed at the origin of the polar. The new state (P_2, u_2) is situated somewhere on the shock polar.

The next step is to determine the new state of the medium A. After hitting the interface, a part of the shockwave is reflected in A. The reflected polar H_A^- of H_A is used. It is the symmetry of H_A from the pressure axis. B.15 (a). The new state of the material (P_1, u_1) is then determined (fig. B.15 (b) and the polar translated horizontally to cross that point (P_1, u_1) (fig. B.15 (c).

The final state of the material B can now be obtained and corresponds to the intersection point of H_A^- and H_B fig. B.15 (d).

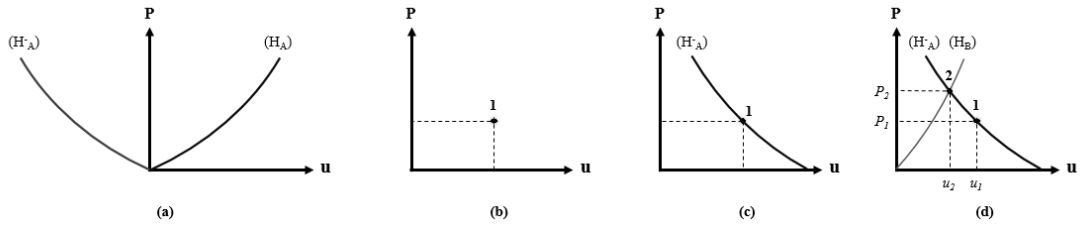

Figure B.15: (P,u) state determination in of the materials A and B

In this case the difference in impedance between the two media induces an increase of the pressure at the interface.

C | Fatigue testing principle

The principle of fatigue testing is to determinate the fatigue strength of a material, so to say its ability to resist cyclic loading for the longest possible duration and number of cycle at a given temperature. Multiple types of loading can be applied for testing such as: torsion, tensile loading or a combination of them. A load cycle is characterized by its load ratio noted R and stress amplitude σ_a given by the following:

$$R = \frac{\sigma_{min}}{\sigma_{max}} \tag{C.1}$$

with σ_{min} the minimum load applied and σ_{max} the maximum load. The stress amplitude is defined as follow:

$$\sigma_a = (\sigma_{max} - \sigma_{min})/2 \tag{C.2}$$

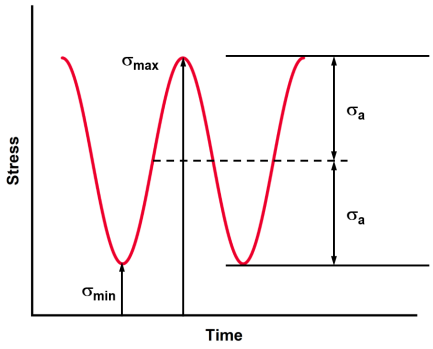

Figure C.1: Cyclic loading for fatigue test and its parameters.

For a fatigue strength test the values measured are the stress depending on the number of cycle of applying said stress. The plot obtained with these information is called a S-N curve. The term

fatigue strength represents the number of load cycles at a defined stress level where the material tested has a 50% probability of failing due to fatigue damage. The fatigue limit, on the contrary represents the limit stress level at which no fatigue damaging is expected for the material independently of the number of cycle realised. An example of a classical S-N curve is given in Figure C.2 for aluminium.

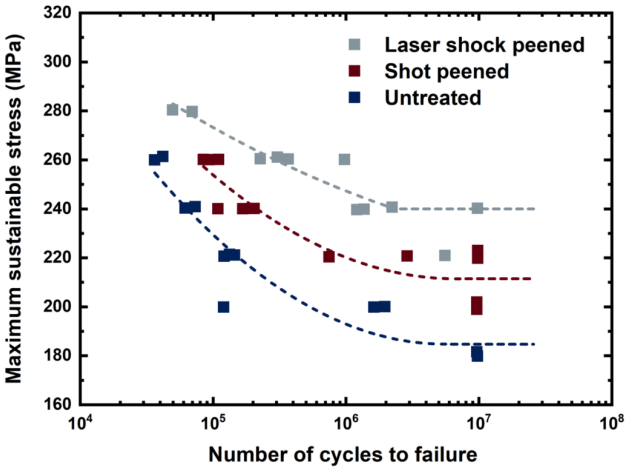

Figure C.2: S-N curves of aluminium 7075. Tests done at 40-50 Hz with a 100 kN material testing machine on specimen having a K_t = 1.6-1.7. (Taken from [219])

C.1 Fatigue testing methods

Multiple methods are available to test metallic airframe structures such as Stress-life (S-N), Strain-life (ϵ-N) or Damage Tolerance to obtain multiple information about the structure studied but each of these methods need a specific type of coupon for the measurements. Usually a classic traction testing machine is used, the geometry and size of the sample can slightly change depending on the machine and the method of testing chosen.

Another option is the 3 and 4 points bending tests. On the first one, the sample is placed on two supporting pins and subjected to a loading in the middle of the material with a third support pin placed on the opposite side of the sample to the two other ones. For the second one, instead of a third supporting pin in the middle of the sample, two others are placed at an equal distance from the center of the sample. These two loading are lowered on the tested material with a determined cyclic loading up to the fatigue failure of the material. The two techniques have some differences that need

to be taken into account when choosing the testing option for a material. The maximum bend stress seen by the sample during the loading is concentrated on a small surface with the three point bending while with four points bending it is spread out on a section of the material. This means that 3 points bending might show early failure of the tested material if the area put under loading has a default. It also means that this type of testing is not adapted for non homogeneous materials such as composites.

For materials used in the aerospace an example of 4 points bending fatigue test sample is given in figure C.3. Correa et al. showed that the edge of the tested material play a role in the final fatigue results obtained due to edge effects [72]. To compensate for this phenomenon the edges of the four points bending sample are titled with a low angle. This geometry concentrate the loading on a smaller area of the fatigue sample not affected by the edge effects.

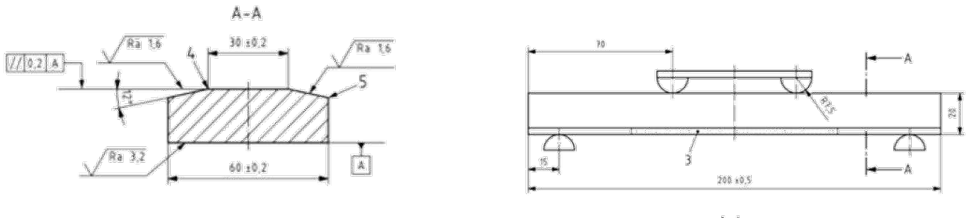

(a) (b)

Figure C.3: Sample geometry used for fatigue life measurement on aerospace pieces treated by laser shock peening.(a) front view (b) side view.

Unfortunately these types of testing are sometimes not fully representative of the final assembled structure. Some operations such as surface treatments and finishes necessary for production aircrafts are not taken into account. An accurate surface representation is all the more important given that fatigue cracks are mainly influenced by the surface quality. In order to take into account all type of possible failure initiation the full scale fatigue testing is the best option as the test includes the effects of component geometry and production. An example of Full Scale Fatigue Test is given in Figure C.4 for an Airbus A380 MegaLiner Barrel.

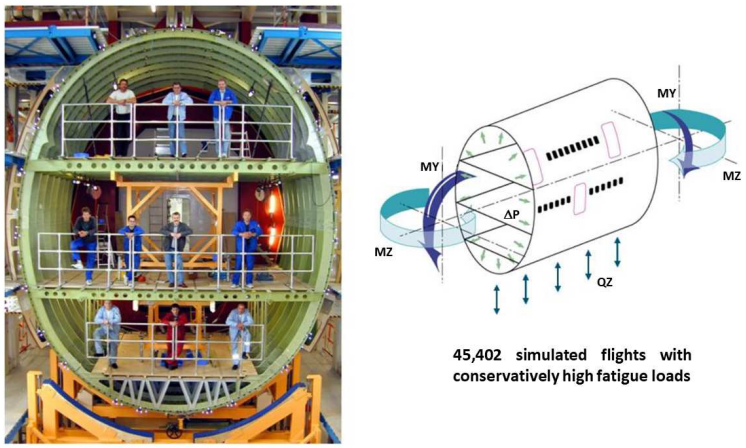

Figure C.4: Airbus A380 MegaLiner Barrel (MLB) full scale fatigue test specimen with the number of simulated flight and loading conditions. (Taken from [220]).

D | Paris' law

To model fatigue crack growth, Paris-Erdogan equation is used. The concept was introduced in 1961 with hypothesis that the rate of crack growth may be dependent on the stress intensity factor[221]. In 1963, Paris and Erdogan, confirmed the theory and introduced the equation [222]. It describes the rate of growth of a fatigue crack depending on the range of stress intensity following:

$$\frac{da}{dN} = C(\Delta K)^m \tag{D.1}$$

With a the crack length, da/dN the fatigue crack growth for a loading cycle N. C and m are experimentally defined coefficients specific to the material. These two parameters are influenced by environment, frequency, temperature or stress ratio [223, 224]. ΔK is the stress intensity range

$$\Delta K = K_{max} - K_{min} \tag{D.2}$$

With K_{max} and K_{min} are the maximum and minimum intensity values during the load cycles applied. Figure D.1 shows that the Paris equation works only in the mid range of crack propagation. If the stress intensity range is too low or too high (i.e approaching the material's fracture toughness K_Ic) the equation will not apply. Paris et al. paper demonstrates experimentally the similitude principle. Equal fatigue crack growth rate is observed for equal applied stress intensity ranges, independent of load, crack size, component or specimen geometry [225]. The principle extended in 1989 by Wei and Gangloff to describe corrosion fatigue crack propagation in aggressive gas and environments [226]. These two principles are used to predict materials fatigue behaviour, either in terms of applied stress range ($\Delta\sigma$) depending on the total life (N_f) or crack length (a) versus number of cycles (N). Crack propagation can be divided in 3 regions represented in Figure D.1 during stress corrosion cracking.

- I: The crack is dominated by chemical attack of strained bonds in the crack.
- II: The propagation is controlled by diffusion of chemical into the crack.

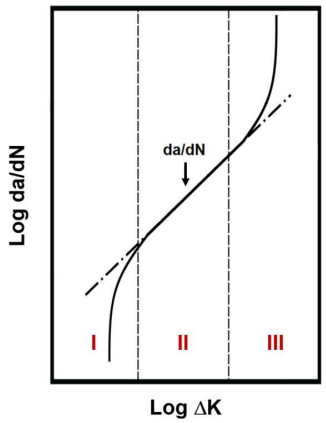

Figure D.1: Plot of the crack growth rate depending on the stress intensity range, the Paris's equation fit the part II of the plot.

- III: The stress intensity reach its critical value and propagates independent if its environment.

E | Mullins and Payne effects

E.1 Mullins effect

The Mullins effect represent the stress softening of filled elastomers at low and high strains. Fillers are generally used in elastomers in order to enhance their mechanical properties by creating aggregates with polymer chains in between them, thus reducing the mobility of the chains surrounding the filler surface causing a modulus increase. During a cyclic loading the stress required on reloading is less than that on the initial loading for stretches up to the maximum reached before during the last loading [132]. The Mullins effect is explained by the rupture of bonds between filler aggregates during the loading cycle, if the broken bond is the shortest linking two filler parts then the new possible stretching will be higher [133] as shown in figure E.1. Different models are able to describe this kind of effects [134, 135].

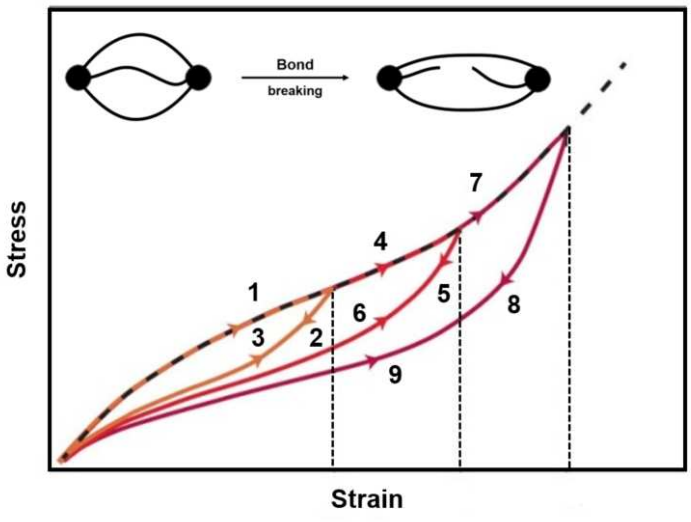

Figure E.1: Principle of stress softening through Mullins effect and physical explanation of the Mullins effect.

Other phenomena can participate in the stress softening via Mullins effect along bond breaking such as molecule slipping, filler rupture, disentanglement or double-layer model. These are described in more details in [136].

E.2 Payne effect

The Payne effect is specific to the stress strain behaviour of elastomers and rubbers under cyclic loading with small strain amplitude. The effect is manifested by an influence on the viscoelastic storage modulus depending on the applied strain [137, 138]. The effect is induced by filler content and consequently disappear for unfilled elastomers. Due to the random repartition of polymer chains between filler aggregates, the stress-strain relationship in filled elastomers are highly non-linear even for small strains however some models are still able to represent the effects at work [130, 139].

Bibliography

[1] GA Askaryan and EM Morozov. Pressure in the evaporation of a substance in ray-radiation. *Journal of Experimental and Theoretical Physics*, 43(6):2319–2320, 1962.

[2] G. A. Askar'yan and E. M. Moroz. Pressure on Evaporation of Matter in a Radiation Beam. *Soviet Journal of Experimental and Theoretical Physics*, 16:1638, 1963.

[3] NC Anderholm. Laser-generated stress waves. *Applied Physics Letters*, 16(3):113–115, 1970.

[4] B. P. Fairand, B. A. Wilcox, W. J. Gallagher, and D. N. Williams. Laser shock-induced microstructural and mechanical property changes in 7075 aluminum. *Journal of Applied Physics*, 43(9):3893–3895, 1972.

[5] J. Fournier. *Génération d'ondes de choc par laser pulsé de forte énergie. Application mécaniques et métallurgiques.* PhD thesis, Ecole polytechnique, 1989.

[6] R Fabbro, J Fournier, P Ballard, D Devaux, and J Virmont. Physical study of laser-produced plasma in confined geometry. *Journal of applied physics*, 68(2):775–784, 1990.

[7] D. Devaux. *Caractérisation des plasmas formés par impulsion en géométrie confinée. Application au choc laser.* PhD thesis, Université de Paris XI, 1993.

[8] D Devaux, R Fabbro, L Tollier, and E Bartnicki. Generation of shock waves by laser-induced plasma in confined geometry. *Journal of Applied Physics*, 74(4):2268–2273, 1993.

[9] P Peyre and R Fabbro. Electromagnetic gauge study of laser-induced shock waves in aluminium alloys. *Journal de Physique III*, 5(12):1953–1964, 1995.

[10] P. Ballard. *Contraintes résiduelles induites par impact rapide. Application au choc laser.* PhD thesis, Ecole polytechnique, 1991.

[11] P Ballard, J Fournier, R Fabbro, and J Frelat. Residual stresses induced by laser-shocks. *Le Journal de Physique IV*, 1(C3):C3–487, 1991.

[12] P Ballard, J Fournier, R Fabbro, J Frelat, and L Castex. Study of the plastification of metallic targets shocked by a laser pulse of high energy. *Le Journal de Physique Colloques*, 49(C3):C3–401, 1988.

[13] C. Dubouchet. *Traitements thermomécaniques de surfaces métalliques à l'aide de lasers CO2 et de laser impulsionnel.* PhD thesis, Université de Paris XI, 1993.

[14] P. Peyre. *Traitement mécanique superficiel d'alliages d'Aluminium par onde de choc laser. Caractérisation des effets induits et application à l'amélioration de la tenue en fatigue.* PhD thesis, Université de Technologie de Compiègne, 1993.

[15] M.Boustie. *Etude de l'endommagement dynamique sous l'action d'une onde de choc induite par une impulsion laser de forte puissance dans une cible solide.* PhD thesis, Université de Poitiers, 1991.

[16] L. Tollier. *Caractérisation de chocs laser à éclairements modérés par interférométrie VISAR. Application à l'étude de l'endommagement par écaillage de matériaux métalliques.* PhD thesis, Université de Poitiers.

[17] P. Darquey. *Ondes de choc et acelération de geuille mince par impulsion laser en interaction confinéd. Test d'application à la compaction dyamique de poudres métalliques.* PhD thesis, Université de Poitiers, 1989.

[18] M Boustie, S Couturier, JP Romain, D Zagouri, and H Simonnet. Shock pressure and free surface velocity measurements in confined interaction—response of new vf 2/vf 3 piezoelectric gauges. *Laser and particle beams*, 14(2):171–179, 1996.

[19] T De Resseguier, S Couturier, M Boustie, J David, G Nierat, and F Bauer. Characterization of laser-driven shocks of high intensity using piezoelectric polymers. *Journal of applied physics*, 80(7):3656–3661, 1996.

[20] SR Mannava. Us patents us5591009a. *US5584662A, US5584586*, 1995.

[21] Yuji Sano, Naruhiko Mukai, Koki Okazaki, and Minoru Obata. Residual stress improvement in metal surface by underwater laser irradiation. *Nuclear Instruments and Methods in Physics Research Section B: Beam Interactions with Materials and Atoms*, 121(1-4):432–436, 1997.

[22] P. Virmoux. *Caractérisation en élastoplasticité et fatigue de ontact de l'acier Z100CD17 durci superficiellement par choc laser.* PhD thesis, Ecole nationale supérieure d'arts et metiers, 1996.

[23] Xavier Scherpereel, Patrice Peyre, Remy Fabbro, Glenn Lederer, and N Celati. Modifications of mechanical and electrochemical properties of stainless steel surfaces by laser shock processing. In *Lasers in Material Processing*, volume 3097, pages 546–557. International Society for Optics and Photonics, 1997.

[24] J. R. Desforges. *Propagation en fatigue des fissures courtes dans alliages d'aluminium.* PhD thesis, Université de Poitiers.

[25] Yongkang Zhang, Shuyi Zhang, Chengye Yu, Yaxin Tang, Hong Zhang, Hongxing Wu, Dahao Guo, Shengbo Wang, Xiaoping Xia, Mingsong Chen, et al. Laser shock-processing for fatigue and fracture resistance. *Science in China Series E: Technological Sciences*, 40(2):170–177, 1997.

[26] Allan H Clauer. Laser shock peening, the path to production. *Metals*, 9(6):626, 2019.

[27] Ahmed Maamoun, Mohamed Elbestawi, and Stephen Veldhuis. Influence of shot peening on alsi10mg parts fabricated by additive manufacturing. *Journal of Manufacturing and Materials Processing*, 2(3):40, 2018.

[28] Lloyd Hackel, Jon R Rankin, Alexander Rubenchik, Wayne E King, and Manyalibo Matthews. Laser peening: A tool for additive manufacturing post-processing. *Additive Manufacturing*, 24:67–75, 2018.

[29] Xin Hong, Shengbo Wang, Dahao Guo, Hongxing Wu, Jie Wang, Yusheng Dai, Xiaoping Xia, and Yanning Xie. Confining medium and absorptive overlay: Their effects on a laser-induced shock wave. *Optics and Lasers in Engineering*, 29(6):447 – 455, 1998.

[30] N Mukai, N Aoki, M Obata, A Ito, Y Sano, and C Konagai. Laser processing for underwater maintenance in nuclear plants. 1995.

[31] R Fabbro, B Faral, J Virmont, F Cottet, JP Romain, and H Pépin. Experimental study of ablation pressures and target velocities obtained in 0.26 μm wavelength laser experiments in planar geometry. *The Physics of fluids*, 28(11):3414–3423, 1985.

[32] F Cottet and JP Romain. Formation and decay of laser-generated shock waves. *Physical Review A*, 25(1):576, 1982.

[33] Laurent Berthe. *Processus de claquage de milieux transparents sous irradiation laser. Application au choc laser en regime de confinement par eau.* PhD thesis, Université Paris XI Orsay, 1998. Thèse de doctorat dirigée par Fabbro, Rémy Physique Paris 11 1998.

[34] Arnaud Sollier. *Etude des plasmas générés par interaction laser-matière en régime confiné : application au traitement des matériaux par choc laser.* PhD thesis, Université de Versailles St-Quentin, 2002. Thèse de doctorat dirigée par Fabbro, Rémy Physique Versailles-St Quentin en Yvelines 2002.

[35] L Berthe, R Fabbro, P Peyre, and E Bartnicki. Experimental study of the transmission of breakdown plasma generated during laser shock processing. *The European Physical Journal-Applied Physics*, 3(2):215–218, 1998.

[36] L. Berthe, R. Fabbro, P. Peyre, L. Tollier, and E. Bartnicki. Shock waves from a water-confined laser-generated plasma. *Journal of Applied Physics*, 82(6):2826–2832, 1997.

[37] A Sollier, L Berthe, and R Fabbro. Numerical modeling of the transmission of breakdown plasma generated in water during laser shock processing. *The European Physical Journal-Applied Physics*, 16(2):131–139, 2001.

[38] A Vaidyanathan, T Walker, and A Guenther. The relative roles of avalanche multiplication and multiphoton absorption in laser-induced damage of dielectrics. *IEEE journal of Quantum Electronics*, 16(1):89–93, 1980.

[39] Laurent Berthe. *Processus de claquage de milieux transparents sous irradiation laser. Application au choc laser en regime de confinement par eau.* PhD thesis, Université Paris XI Orsay, 1998. Thèse de doctorat dirigée par Fabbro, Rémy Physique Paris 11 1998.

[40] P Peyre, L Berthe, R Fabbro, and A Sollier. Experimental determination by pvdf and emv techniques of shock amplitudes induced by 0.6-3 ns laser pulses in a confined regime with water. *Journal of physics D: Applied physics*, 33(5):498, 2000.

[41] PE Schoen and AJ Campillo. Characteristics of compressional shocks resulting from picosecond heating of confined foils. *Applied physics letters*, 45(10):1049–1051, 1984.

[42] R v Mises. Mechanik der festen körper im plastisch-deformablen zustand. *Nachrichten von der Gesellschaft der Wissenschaften zu Göttingen, Mathematisch-Physikalische Klasse*, 1913:582–592, 1913.

[43] P Peyre, R Fabbro, P Merrien, and HP Lieurade. Laser shock processing of aluminium alloys. application to high cycle fatigue behaviour. *Materials Science and Engineering: A*, 210(1-2):102–113, 1996.

[44] G Banaś, HE Elsayed-Ali, FV Lawrence Jr, and JM Rigsbee. Laser shock-induced mechanical and microstructural modification of welded maraging steel. *Journal of Applied Physics*, 67(5):2380–2384, 1990.

[45] Tiantian He, Yi Xiong, Zhiqiang Guo, Lingfeng Zhang, Fengzhang Ren, and Alex A Volinsky. Microstructure and hardness of laser shocked ultra-fine-grained aluminum. *Journal of Materials Science and Technology*, 27(9):793–796, 2011.

[46] C Rubio-González, G Gomez-Rosas, JL Ocaña, C Molpeceres, A Banderas, J Porro, and M Morales. Effect of an absorbent overlay on the residual stress field induced by laser shock processing on aluminum samples. *Applied Surface Science*, 252(18):6201–6205, 2006.

[47] Uroš Trdan, José Luis Ocaña, and Janez Grum. Surface modification of aluminium alloys with laser shock processing. *Strojniški vestnik-Journal of Mechanical Engineering*, 57(5):385–393, 2011.

[48] Janez Grum, Uros Trdan, and Michael R Hill. Laser shock processing of enaw 6082 aluminium alloy surface. In *Materials science forum*, volume 589, pages 379–384. Trans Tech Publ, 2008.

[49] Arpith Siddaiah, Bo Mao, Yiliang Liao, and Pradeep L Menezes. Surface characterization and tribological performance of laser shock peened steel surfaces. *Surface and Coatings Technology*, 351:188–197, 2018.

[50] Luca Petan, José Luis Ocaña, and Janez Grum. Influence of laser shock peening pulse density and spot size on the surface integrity of x2nicomo18-9-5 maraging steel. *Surface and Coatings Technology*, 307:262–270, 2016.

[51] Xiaojun Shen, Pratik Shukla, Subhasisa Nath, and Jonathan Lawrence. Improvement in mechanical properties of titanium alloy (ti-6al-7nb) subject to multiple laser shock peening. *Surface and Coatings Technology*, 327:101–109, 2017.

[52] P Peyre, L Berthe, X Scherpereel, and R Fabbro. Laser-shock processing of aluminium-coated 55c1 steel in water-confinement regime, characterization and application to high-cycle fatigue behaviour. *Journal of Materials Science*, 33(6):1421–1429, 1998.

[53] Amrinder S. Gill, Abhishek Telang, and Vijay K. Vasudevan. Characteristics of surface layers formed on inconel 718 by laser shock peening with and without a protective coating. *Journal of Materials Processing Technology*, 225:463–472, 2015.

[54] P. Peyre and R. Fabbro. Laser shock processing: a review of the physics and applications. *Optical and Quantum Electronics*, 27(12):1213–1229, Dec 1995.

[55] Xiang Ling, Weiwei Peng, and Gang Ma. Influence of laser peening parameters on residual stress field of 304 stainless steel. *Journal of pressure vessel technology*, 130(2), 2008.

[56] XC Zhang, YK Zhang, JZ Lu, FZ Xuan, ZD Wang, and ST Tu. Improvement of fatigue life of ti–6al–4v alloy by laser shock peening. *Materials Science and Engineering: A*, 527(15):3411–3415, 2010.

[57] Qiao Hongchao. Experimental investigation of laser peening on ti17 titanium alloy for rotor blade applications. *Applied surface science*, 351:524–530, 2015.

[58] Allan Clauer and John Koucky. Laser shock processing increases the fatigue life of metal parts. *Materials and Processing Report*, 6(6):3–5, 1991.

[59] Y Sano. Underwater maintenance and repair technologies for reactor components by laser material processing. In *Proc. 7th Int. Welding Symposium (7WS)*, volume 439, 2001.

[60] Yuji Sano, Minoru Obata, Tatsuya Kubo, Naruhiko Mukai, Masaki Yoda, Kiyotaka Masaki, and Yasuo Ochi. Retardation of crack initiation and growth in austenitic stainless steels by laser peening without protective coating. *Materials Science and Engineering: A*, 417(1-2):334–340, 2006.

[61] Y Sano, K Masaki, T Gushi, and T Sano. Improvement in fatigue performance of friction stir welded a6061-t6 aluminum alloy by laser peening without coating. *Materials and Design (1980-2015)*, 36:809–814, 2012.

[62] Yuji Sano. Quarter century development of laser peening without coating. *Metals*, 10(1):152, 2020.

[63] Alexandre Rondepierre, Selen Ünaldi, Yann Rouchausse, Laurent Videau, Rémy Fabbro, Olivier Casagrande, Christophe Simon-Boisson, Hervé Besaucéle, Olivier Castelnau, and Laurent Berthe. Beam size dependency of a laser-induced plasma in confined regime: Shortening of the plasma release. influence on pressure and thermal loading. *Optics & Laser Technology*, 135:106689, 2021.

[64] Yuji Sano, Motohiko Kimura, Naruhiko Mukai, Masaki Yoda, Minoru Obata, and Tatsuki Ogisu. Process and application of shock compression by nanosecond pulses of frequency-doubled nd: Yag laser. In *High-Power Lasers in Manufacturing*, volume 3888, pages 294–306. International Society for Optics and Photonics, 2000.

[65] Allan H Clauer, Barry P Fairand, and Ben A Wilcox. Pulsed laser induced deformation in an fe-3 wt pct si alloy. *Metallurgical Transactions A*, 8(1):119–125, 1977.

[66] L Berthe, R Fabbro, P Peyre, and E Bartnicki. Wavelength dependent of laser shock-wave generation in the water-confinement regime. *Journal of Applied Physics*, 85(11):7552–7555, 1999.

[67] Mikhail N Polyanskiy. Refractive index database. 2014.

[68] William D. CowieJames E. GutknechtHerbert HalilaSeetharamaiah MannavaAlbert E. McdanielJames E. Rhoda. Laser shock peened gas turbine engine fan blade edges, 1996. European Patent 0 794 264 B1.

[69] Yongxiang Hu, Han Cheng, Jianhua Yu, and Zhenqiang Yao. An experimental study on crack closure induced by laser peening in pre-cracked aluminum alloy 2024-t351 and fatigue life extension. *International Journal of Fatigue*, 130:105232, 2020.

[70] S. Huang, J.Z. Zhou, J. Sheng, K.Y. Luo, J.Z. Lu, Z.C. Xu, X.K. Meng, L. Dai, L.D. Zuo, H.Y. Ruan, and H.S. Chen. Effects of laser peening with different coverage areas on fatigue crack growth properties of 6061-t6 aluminum alloy. *International Journal of Fatigue*, 47:292–299, 2013.

[71] C. Correa, L. Ruiz de Lara, M. Díaz, A. Gil-Santos, J.A. Porro, and J.L. Ocaña. Effect of advancing direction on fatigue life of 316l stainless steel specimens treated by double-sided laser shock peening. *International Journal of Fatigue*, 79:1–9, 2015.

[72] C. Correa, L. Ruiz de Lara, M. Díaz, J.A. Porro, A. García-Beltrán, and J.L. Ocaña. Influence of pulse sequence and edge material effect on fatigue life of al2024-t351 specimens treated by laser shock processing. *International Journal of Fatigue*, 70:196–204, 2015.

[73] Samuel Adu-Gyamfi, XD Ren, Enoch Asuako Larson, Yunpeng Ren, and Zhaopong Tong. The effects of laser shock peening scanning patterns on residual stress distribution and fatigue life of aa2024 aluminium alloy. *Optics & Laser Technology*, 108:177–185, 2018.

[74] Samuel Adu-Gyamfi, X.D. Ren, Enoch Asuako Larson, Yunpeng Ren, and Zhaopong Tong. The effects of laser shock peening scanning patterns on residual stress distribution and fatigue life of aa2024 aluminium alloy. *Optics and Laser Technology*, 108:177–185, 2018.

[75] Timur Canel, Muzaffer Zeren, and Tamer Sınmazçelik. Laser parameters optimization of surface treating of al 6082-t6 with taguchi method. *Optics and Laser Technology*, 120:105714, 2019.

[76] VS Raja and Tetsuo Shoji. *Stress corrosion cracking: theory and practice*. Elsevier, 2011.

[77] Bing Han, Yanbin Chen, Wang Tao, Hao Li, and Liqun Li. Microstructural evolution and interfacial crack corrosion behavior of double-sided laser beam welded 2060/2099 al-li alloys t-joints. *Materials and Design*, 135:353–365, 2017.

[78] A Turnbull, K Mingard, JD Lord, B Roebuck, DR Tice, KJ Mottershead, ND Fairweather, and AK Bradbury. Sensitivity of stress corrosion cracking of stainless steel to surface machining and grinding procedure. *Corrosion science*, 53(10):3398–3415, 2011.

[79] SC Wu, Y Luo, Z Shen, LC Zhou, WH Zhang, and GZ Kang. Collaborative crack initiation mechanism of 25crmo4 alloy steels subjected to foreign object damages. *Engineering Fracture Mechanics*, 225:106844, 2020.

[80] JI Dikcosn, L Shiquiong, J-P Bailon, and D Tromans. The fractography of transgranular scc in fcc metals: mechanistic implications. In *Parkins Symposium on Fundamental Aspects of Stress Corrosion Cracking*, pages 303–322, 1991.

[81] Yuji Sano, Yoshihiro Sakino, Naruhiko Mukai, Minoru Obata, Itaru Chida, Takuya Uehara, Masaki Yoda, and You Chul Kim. Laser peening without coating to mitigate stress corrosion cracking and fatigue failure of welded components. In *Materials Science Forum*, volume 580, pages 519–522. Trans Tech Publ, 2008.

[82] P Peyre, X Scherpereel, L Berthe, C Carboni, R Fabbro, G Béranger, and C Lemaitre. Surface modifications induced in 316l steel by laser peening and shot-peening. influence on pitting corrosion resistance. *Materials Science and Engineering: A*, 280(2):294 – 302, 2000.

[83] Uroš Trdan and Janez Grum. Evaluation of corrosion resistance of aa6082-t651 aluminium alloy after laser shock peening by means of cyclic polarisation and els methods. *Corrosion Science*, 59:324–333, 2012.

[84] J Sheng, S Huang, JZ Zhou, JZ Lu, SQ Xu, and HF Zhang. Effect of laser peening with different energies on fatigue fracture evolution of 6061-t6 aluminum alloy. *Optics and Laser Technology*, 77:169–176, 2016.

[85] Hyunjung Lee, Youngjoo Kim, Yooin Jeong, and Sangshik Kim. Effects of testing variables on stress corrosion cracking susceptibility of al 2024-t351. *Corrosion science*, 55:10–19, 2012.

[86] Yuji Sano, Koichi Akita, Kiyotaka Masaki, Yasuo Ochi, Igor Altenberger, and Berthold Scholtes. Laser peening without coating as a surface enhancement technology. *Pulse*, 100(40):250mJ, 2006.

[87] Benjamin Floyd Brown. *Stress-corrosion cracking in high strength steels and in titanium and aluminum alloys*. Naval Research Laboratory, 1972.

[88] R Sundar, P Ganesh, B Sunil Kumar, RK Gupta, DC Nagpure, R Kaul, K Ranganathan, KS Bindra, V Kain, SM Oak, et al. Mitigation of stress corrosion cracking susceptibility of machined 304l stainless steel through laser peening. *Journal of Materials Engineering and Performance*, 25(9):3710–3724, 2016.

[89] JZ Lu, KY Luo, DK Yang, XN Cheng, JL Hu, FZ Dai, H Qi, L Zhang, JS Zhong, QW Wang, et al. Effects of laser peening on stress corrosion cracking (scc) of ansi 304 austenitic stainless steel. *Corrosion Science*, 60:145–152, 2012.

[90] PR Chalker, SJ Bull, and DS Rickerby. A review of the methods for the evaluation of coating-substrate adhesion. *Materials Science and Engineering: A*, 140:583–592, 1991.

[91] M Arrigoni, Sophie Barradas, M Braccini, M Dupeux, Michel Jeandin, M Boustie, C Bolis, and L Berthe. A comparative study of three adhesion tests (en 582, similar to astm c633, lasat (laser adhesion test), and bulge and blister test) performed on plasma sprayed copper deposited on aluminium 2017 substrates. *Journal of adhesion science and technology*, 20(5):471–487, 2006.

[92] JL Vossen. Measurements of film-substrate bond strength by laser spallation. 1978.

[93] John S Foley and Philip A Barone. Automated laser paint stripping. *Metal finishing*, 90:48–50, 1992.

[94] Selen Ünaldi, Kosmas Papadopoulos, Alexandre Rondepierre, Yann Rouchausse, Alexandra Karanika, Florent Deliane, Konstantinos Tserpes, Giannis Floros, Emmanuel Richaud, and Laurent Berthe. Towards selective laser paint stripping using shock waves produced by laser-plasma interaction for aeronautical applications on aa 2024 based substrates. *Optics and Laser Technology*, 141:107095, 2021.

[95] Arthur Kantrowitz. Propulsion to orbit by ground-based laser. *Astronaut. Aeronaut.*, 10:74, 1972.

[96] C William Larson. Perspective on one decade of laser propulsion research at air force research laboratory. In *AIP Conference Proceedings*, volume 997, pages 84–96. American Institute of Physics, 2008.

[97] Massoud Malaki and Hongtao Ding. A review of ultrasonic peening treatment. *Materials and Design*, 87:1072–1086, 2015.

[98] Hitoshi Soyama. Cavitation peening: A review. *Metals*, 10(2):270, 2020.

[99] Jörn Bonse, JM Wrobel, Jörg Krüger, and Wolfgang Kautek. Ultrashort-pulse laser ablation of indium phosphide in air. *Applied Physics A*, 72(1):89–94, 2001.

[100] Yong Jee, Michael F Becker, and Rodger M Walser. Laser-induced damage on single-crystal metal surfaces. *JOSA B*, 5(3):648–659, 1988.

[101] David Gómez and Igor Goenaga. On the incubation effect on two thermoplastics when irradiated with ultrashort laser pulses: Broadening effects when machining microchannels. *Applied Surface Science*, 253(4):2230–2236, 2006.

[102] AV Butenin and B Ya Kogan. Damage mechanism in transparent polymer materials on multiple exposure to pulsed laser-radiation, 1976.

[103] Mikhail B Agranat, NP Novikov, VP Perminov, and Yampol'skiĭ. Some aspects of the initial stage of the development of laser damage in polymethylmethacrylate.

[104] Stefan Nolte, Cl Momma, H Jacobs, A Tünnermann, Boris N Chichkov, Bernd Wellegehausen, and Herbert Welling. Ablation of metals by ultrashort laser pulses. *JOSA B*, 14(10):2716–2722, 1997.

[105] JK Chen, DY Tzou, and JE Beraun. Numerical investigation of ultrashort laser damage in semiconductors. *International Journal of Heat and Mass Transfer*, 48(3-4):501–509, 2005.

[106] BC Stuart, MD Feit, S Herman, AM Rubenchik, BW Shore, and MD Perry. Nanosecond-to-femtosecond laser-induced breakdown in dielectrics. *Physical review B*, 53(4):1749, 1996.

[107] CWo Carr, HB Radousky, and SG Demos. Wavelength dependence of laser-induced damage: determining the damage initiation mechanisms. *Physical Review Letters*, 91(12):127402, 2003.

[108] Boris N Chichkov, C Momma, Stefan Nolte, F Von Alvensleben, and A Tünnermann. Femtosecond, picosecond and nanosecond laser ablation of solids. *Applied physics A*, 63(2):109–115, 1996.

[109] Detlev Ristau. *Laser-induced damage in optical materials*. CRC Press, 2014.

[110] RW Hopper and Donald R Uhlmann. Mechanism of inclusion damage in laser glass. *Journal of Applied Physics*, 41(10):4023–4037, 1970.

[111] Aleksandr A Manenkov, GA Matyushin, and Nechitaĭ. Nature of the cumulative effect in laser damage to optical materials.

[112] SN Zhurkov and VE Korsukov. Atomic mechanism of fracture of solid polymers. *Journal of Polymer Science: Polymer Physics Edition*, 12(2):385–398, 1974.

[113] Leonid Borisovich Glebov, Oleg M Efimov, and Petrovskiĭ. Influence of the mode composition of laser radiation on the optical breakdown of silicate glasses.

[114] Dimitrios Kitriotis and Larry D Merkle. Multiple pulse laser-induced damage phenomena in silicates. *Applied optics*, 28(5):949–958, 1989.

[115] George B Kaufman. Inorganic chemistry: principles of structure and reactivity, (huheey, james e.; keiter, ellen a.; keiter, richard l.), 1993.

[116] Istvan Benedek. *Pressure-sensitive design, theoretical aspects*. CRC Press, 2006.

[117] Donatas Satas. *Handbook of pressure sensitive adhesive technology*. 1989.

[118] C Creton and P Fabre. Adhesion science and engineering, da dillard and av pocius ed., 1, 2002.

[119] Xavier Callies, Olivier Herscher, Cécile Fonteneau, Alexis Robert, Sandrine Pensec, Laurent Bouteiller, Guylaine Ducouret, and Costantino Creton. Combined effect of chain extension and supramolecular interactions on rheological and adhesive properties of acrylic pressure-sensitive adhesives. *ACS applied materials and interfaces*, 8(48):33307–33315, 2016.

[120] Zbigniew Czech. Synthesis and cross-linking of acrylic psa systems. *Journal of adhesion science and technology*, 21(7):625–635, 2007.

[121] Kelly Brown, Jacob C Hooker, and Costantino Creton. Micromechanisms of tack of soft adhesives based on styrenic block copolymers. *Macromolecular Materials and Engineering*, 287(3):163–179, 2002.

[122] GK Schalau, Alexis Bobenrieth, Robert O Huber, Linda S Nartker, and Xavier Thomas. Silicone adhesives in medical applications. *Applied Adhesive Bonding in Science and Technology*, pages 93–117, 2018.

[123] Adrian Krzysztof Antosik, Karolina Mozelewska, Robert Pełech, Zbigniew Czech, and Nataniel Adrian Antosik. Conductive electric tapes based on silicone pressure-sensitive adhesives. *Silicon*, 13:867–875, 2021.

[124] Samuel Ansorge, Frank Schmuck, and Konstantin O Papailiou. Impact of different fillers and filler treatments on the erosion suppression mechanism of silicone rubber for use as outdoor insulation material. *IEEE Transactions on Dielectrics and Electrical Insulation*, 22(2):979–988, 2015.

[125] Adhesion Zosel. Adhesion and tack of polymers: Influence of mechanical properties and surface tensions. *Colloid and Polymer Science*, 263(7):541–553, 1985.

[126] A Zosel. Adhesive failure and deformation behaviour of polymers. *The journal of adhesion*, 30(1-4):135–149, 1989.

[127] Costantino Creton. Pressure-sensitive adhesives: an introductory course. *MRS bulletin*, 28(6):434–439, 2003.

[128] A Zosel. Effect of cross-linking on tack and peel strength of polymers. *The Journal of Adhesion*, 34(1-4):201–209, 1991.

[129] Frederick Harwood Norton. *The creep of steel at high temperatures*. Number 35. McGraw-Hill Book Company, Incorporated, 1929.

[130] Davide Colombo, Hélène Montes, François Lequeux, and Sabine Cantournet. Thermo-mechanical modeling of a filled elastomer based on the physics of mobility reduction. *Mechanics of Materials*, 143:103319, 2020.

[131] Dirk Willem Van Krevelen and Klaas Te Nijenhuis. *Properties of polymers: their correlation with chemical structure; their numerical estimation and prediction from additive group contributions*. Elsevier, 2009.

[132] Leonard Mullins. Effect of stretching on the properties of rubber. *Rubber chemistry and technology*, 21(2):281–300, 1948.

[133] Shamsul Zakaria, Liyun Yu, Guggi Kofod, and Anne Ladegaard Skov. The influence of static prestretching on the mechanical ageing of filled silicone rubbers for dielectric elastomer applications. *Materials Today Communications*, 4:204–213, 2015.

[134] Roozbeh Dargazany and Mikhail Itskov. Constitutive modeling of the mullins effect and cyclic stress softening in filled elastomers. *Physical Review E*, 88(1):012602, 2013.

[135] Guilherme Machado, Grégory Chagnon, and Denis Favier. Analysis of the isotropic models of the mullins effect based on filled silicone rubber experimental results. *Mechanics of Materials*, 42(9):841–851, 2010.

[136] Julie Diani, Bruno Fayolle, and Pierre Gilormini. A review on the mullins effect. *European Polymer Journal*, 45(3):601–612, 2009.

[137] Arthur R Payne. The dynamic properties of carbon black-loaded natural rubber vulcanizates. part i. *Journal of applied polymer science*, 6(19):57–63, 1962.

[138] Arthur R Payne. The dynamic properties of carbon black loaded natural rubber vulcanizates. part ii. *Journal of Applied Polymer Science*, 6(21):368–372, 1962.

[139] A Lion and C Kardelky. The payne effect in finite viscoelasticity: constitutive modelling based on fractional derivatives and intrinsic time scales. *International Journal of Plasticity*, 20(7):1313–1345, 2004.

[140] Ravi S Gorur, George G Karady, Anurag Jagota, Minesh Shah, and Ann M Yates. Aging in silicone rubber used for outdoor insulation. *IEEE Transactions on Power Delivery*, 7(2):525–538, 1992.

[141] R. N. Peacock. Practical selection of elastomer materials for vacuum seals. *Journal of Vacuum Science and Technology*, 17(1):330–336, 1980.

[142] J David Carlson and Mark R Jolly. Mr fluid, foam and elastomer devices. *mechatronics*, 10(4-5):555–569, 2000.

[143] Barkan Kavlicoglu, Bryce Wallis, Huseyin Sahin, and Yanming Liu. Magnetorheological elastomer mount for shock and vibration isolation. In *Active and passive smart structures and integrated systems 2011*, volume 7977, page 79770Y. International Society for Optics and Photonics, 2011.

[144] RB Bogoslovov, CM Roland, and RM Gamache. Impact-induced glass transition in elastomeric coatings. *Applied physics letters*, 90(22):221910, 2007.

[145] CM Roland, S Hensel-Bielowka, M Paluch, and R Casalini. Supercooled dynamics of glass-forming liquids and polymers under hydrostatic pressure. *Reports on Progress in Physics*, 68(6):1405, 2005.

[146] Jordan Jennifer L. Siviour, Clive R. High strain rate mechanics of polymers: A review. *Journal of Dynamic Behavior of Materials*, 2:15–32, 2016.

[147] Bertram Hopkinson. X. a method of measuring the pressure produced in the detonation of high, explosives or by the impact of bullets. *Philosophical Transactions of the Royal Society of London. Series A, Containing Papers of a Mathematical or Physical Character*, 213(497-508):437–456, 1914.

[148] RM Davies. A critical study of the hopkinson pressure bar. *Philosophical Transactions of the Royal Society of London. Series A, Mathematical and Physical Sciences*, 240(821):375–457, 1948.

[149] Paul Zoller. A study of the pressure-volume-temperature relationships of four related amorphous polymers: polycarbonate, polyarylate, phenoxy, and polysulfone. *Journal of Polymer Science: Polymer Physics Edition*, 20(8):1453–1464, 1982.

[150] Paul Zoller, Thomas A Kehl, Howard W Starkweather Jr, and Glover A Jones. The equation of state and heat of fusion of poly (ether ether ketone). *Journal of Polymer Science Part B: Polymer Physics*, 27(5):993–1007, 1989.

[151] Shaul M Aharoni. Increased glass transition temperature in motionally constrained semicrystalline polymers. *Polymers for Advanced Technologies*, 9(3):169–201, 1998.

[152] Nijenhuis te K Krevelen Van DW. Properties of polymers, 2009.

[153] JA Soto Puente, B Rijal, Laurent Delbreilh, K Fatyeyeva, Allisson Saiter, and E Dargent. Segmental mobility and glass transition of poly (ethylene-vinyl acetate) copolymers: Is there a continuum in the dynamic glass transitions from pvac to pe? *Polymer*, 76:213–219, 2015.

[154] John D Ferry. *Viscoelastic properties of polymers*. John Wiley and Sons, 1980.

[155] Alen Oseli, Alexandra Aulova, Marina Gergesova, and Igor Emri. Time-temperature superposition in linear and non-linear domain. *Materials Today: Proceedings*, 3(4):1118–1123, 2016.

[156] S Havriliak and S Negami. A complex plane analysis of α-dispersions in some polymer systems. In *Journal of Polymer Science Part C: Polymer Symposia*, volume 14, pages 99–117. Wiley Online Library, 1966.

[157] S Havriliak and S Negami. A complex plane representation of dielectric and mechanical relaxation processes in some polymers. *Polymer*, 8:161–210, 1967.

[158] Gilles Marckmann and Erwan Verron. Comparison of hyperelastic models for rubber-like materials. *Rubber chemistry and technology*, 79(5):835–858, 2006.

[159] Melvin Mooney. A theory of large elastic deformation. *Journal of applied physics*, 11(9):582–592, 1940.

[160] LRG Treloar. The elasticity of a network of long-chain molecules. i. *Transactions of the Faraday Society*, 39:36–41, 1943.

[161] LRG Treloar. The elasticity of a network of long-chain molecules—ii. *Transactions of the Faraday Society*, 39:241–246, 1943.

[162] Hubert M James and Eugene Guth. Theory of the elastic properties of rubber. *The Journal of Chemical Physics*, 11(10):455–481, 1943.

[163] Akira Isihara, Natsuki Hashitsume, and Masao Tatibana. Statistical theory of rubber-like elasticity. iv.(two-dimensional stretching). *The Journal of Chemical Physics*, 19(12):1508–1512, 1951.

[164] VL Biderman. Calculations of rubber parts. *Rascheti na prochnost*, 40, 1958.

[165] Alan N Gent and AG Thomas. Forms for the stored (strain) energy function for vulcanized rubber. *Journal of Polymer Science*, 28(118):625–628, 1958.

[166] LJ Hart-Smith. Elasticity parameters for finite deformations of rubber-like materials. *Zeitschrift für angewandte Mathematik und Physik ZAMP*, 17(5):608–626, 1966.

[167] KC Valanis and Robert F Landel. The strain-energy function of a hyperelastic material in terms of the extension ratios. *Journal of Applied Physics*, 38(7):2997–3002, 1967.

[168] Raymond William Ogden. Large deformation isotropic elasticity–on the correlation of theory and experiment for incompressible rubberlike solids. *Proceedings of the Royal Society of London. A. Mathematical and Physical Sciences*, 326(1567):565–584, 1972.

[169] AG James, A Green, and GM Simpson. Strain energy functions of rubber. i. characterization of gum vulcanizates. *Journal of Applied Polymer Science*, 19(7):2033–2058, 1975.

[170] RC Ball, M Doi, SF Edwards, and M Warner. Elasticity of entangled networks. *Polymer*, 22(8):1010–1018, 1981.

[171] Burak Erman and Paul J Flory. Relationships between stress, strain, and molecular constitution of polymer networks. comparison of theory with experiments. *Macromolecules*, 15(3):806–811, 1982.

[172] Paul J Flory and Burak Erman. Theory of elasticity of polymer networks. 3. *Macromolecules*, 15(3):800–806, 1982.

[173] H-G Kilian, HF Enderle, and K Unseld. The use of the van der waals model to elucidate universal aspects of structure-property relationships in simply extended dry and swollen rubbers. *Colloid and Polymer Science*, 264(10):866–876, 1986.

[174] Ellen M Arruda and Mary C Boyce. A three-dimensional constitutive model for the large stretch behavior of rubber elastic materials. *Journal of the Mechanics and Physics of Solids*, 41(2):389–412, 1993.

[175] Alan N Gent. A new constitutive relation for rubber. *Rubber chemistry and technology*, 69(1):59–61, 1996.

[176] Oon H Yeoh and PD Fleming. A new attempt to reconcile the statistical and phenomenological theories of rubber elasticity. *Journal of Polymer Science Part B: Polymer Physics*, 35(12):1919–1931, 1997.

[177] G Heinrich and M Kaliske. Theoretical and numerical formulation of a molecular based constitutive tube-model of rubber elasticity. *Computational and Theoretical Polymer Science*, 7(3-4):227–241, 1997.

[178] M Kaliske and G Heinrich. An extended tube-model for rubber elasticity: statistical-mechanical theory and finite element implementation. *Rubber Chemistry and Technology*, 72(4):602–632, 1999.

[179] MHBM Shariff. Strain energy function for filled and unfilled rubberlike material. *Rubber chemistry and technology*, 73(1):1–18, 2000.

[180] C Miehe, Serdar Göktepe, and F Lulei. A micro-macro approach to rubber-like materials—part i: the non-affine micro-sphere model of rubber elasticity. *Journal of the Mechanics and Physics of Solids*, 52(11):2617–2660, 2004.

[181] H Khajehsaeid, J Arghavani, and R Naghdabadi. A hyperelastic constitutive model for rubber-like materials. *European Journal of Mechanics-A/Solids*, 38:144–151, 2013.

[182] İsmail Doğan Külcü. A hyperelastic constitutive model for rubber-like materials. *Archive of Applied Mechanics*, 90(3):615–622, 2020.

[183] Morrel H Cohen and David Turnbull. Metastability of amorphous structures. *Nature*, 203(4948):964–964, 1964.

[184] FE Karasz, HE Bair, and JM O'reilly. Thermal properties of atactic and isotactic polystyrene. *The Journal of Physical Chemistry*, 69(8):2657–2667, 1965.

[185] Mary C Boyce, David M Parks, and Ali S Argon. Large inelastic deformation of glassy polymers. part i: rate dependent constitutive model. *Mechanics of materials*, 7(1):15–33, 1988.

[186] Johannes Schindelin, Ignacio Arganda-Carreras, Erwin Frise, Verena Kaynig, Mark Longair, Tobias Pietzsch, Stephan Preibisch, Curtis Rueden, Stephan Saalfeld, Benjamin Schmid, et al. Fiji: an open-source platform for biological-image analysis. *Nature methods*, 9(7):676–682, 2012.

[187] L. M. Barker and K. W. Schuler. Correction to the velocity-per-fringe relationship for the visar interferometer. *Journal of Applied Physics*, 45(8):3692–3693, 1974.

[188] LM Barker and RE Hollenbach. Laser interferometer for measuring high velocities of any reflecting surface. *Journal of Applied Physics*, 43(11):4669–4675, 1972.

[189] G. Hansen Z. *Instrumentenk*, 61:411, 1941.

[190] L. Tollier, R. Fabbro, and E. Bartnicki. Study of the laser-driven spallation process by the velocity interferometer system for any reflector interferometry technique. i. laser-shock characterization. *Journal of Applied Physics*, 83(3):1224–1230, 1998.

[191] L Tollier and R Fabbro. Study of the laser-driven spallation process by the visar interferometry technique. ii. experiment and simulation of the spallation process. *Journal of applied physics*, 83(3):1231–1237, 1998.

[192] Michael Smith. *ABAQUS/Standard User's Manual, Version 6.9*. Simulia, 2009.

[193] Stephen Butterworth. Experimental wireless and the wireless engineer. *Wireless Eng*, 7:536, 1930.

[194] Guido Van Rossum and Fred L Drake Jr. *Python reference manual*. Centrum voor Wiskunde en Informatica Amsterdam, 1995.

[195] Marine Scius-Bertrand, Laurent Videau, Alexandre Rondepierre, Emilien Lescoute, Yann Rouchausse, Jan Kaufman, Danijela Rostohar, Jan Brajer, and Laurent Berthe. Laser induced plasma characterization in direct and water confined regimes: new advances in experimental studies and numerical modelling. *Journal of Physics D: Applied Physics*, 54(5):055204, February 2021.

[196] Corentin Le Bras, Alexandre Rondepierre, Raoudha Seddik, Marine Scius-Bertrand, Yann Rouchausse, Laurent Videau, Bruno Fayolle, Matthieu Gervais, Leo Morin, Stéphane Valadon, et al. Laser shock peening: toward the use of pliable solid polymers for confinement. *Metals*, 9(7):793, 2019.

[197] Stanley P Marsh. *LASL shock Hugoniot data*, volume 5. Univ of California Press, 1980.

[198] D. Loison. Propagation des ondes dans un milieu condensé. 2016.

[199] Roland Böhmer, KL Ngai, C Austen Angell, and DJ Plazek. Nonexponential relaxations in strong and fragile glass formers. *The Journal of chemical physics*, 99(5):4201–4209, 1993.

[200] Esteve Ernault. *Thermo-oxydation de resines epoxy/amine*. PhD thesis, 2016. These de doctorat dirigee par Fayolle, Bruno et Richaud, Emmanuel Mecanique-materiaux Paris, ENSAM 2016.

[201] R. Fabbro, J. Fournier, P. Ballard, D. Devaux, and J. Virmont. Physical study of laser-produced plasma in confined geometry. *Journal of Applied Physics*, 68(2):775–784, 1990.

[202] M Van Thiel, J Shaner, and E Salinas. Compendium of shock wave data. volume 3. section c. organic compounds excluding hydrocarbons. section d. mixtures. section e. mixtures and solutions without chemical characterization. compendium index. Technical report, LAWRENCE LIVERMORE NATIONAL LAB CA, 1977.

[203] DE Munson and RP May. Dynamically determined high-pressure compressibilities of three epoxy resin systems. *Journal of Applied Physics*, 43(3):962–971, 1972.

[204] Romain Ecault. *Etude expérimentale et numérique du comportement dynamique de composites aéronautiques sous choc laser. Optimisation du test d'adhérence par ondes de choc sur les assemblages composites collés*. PhD thesis, 2013. Thèse de doctorat dirigée par Boustie, Michel-Touchard, Fabienne et Berthe, Laurent Mécanique des solides, des matériaux, des structures et des surfaces Chasseneuil-du-Poitou, Ecole nationale supérieure de mécanique et d'aérotechnique 2013.

[205] Elise Gay. *Comportement de composites sous choc induit par laser : développement de l'essai d'adhérence par choc des assemblages de composites collés*. PhD thesis, 2011. Thèse de doctorat dirigée par Berthe, LaurentBoustie, Michel et Arrigoni, Michel Matériaux et mécanique Paris, ENSAM 2011.

[206] Zhen Gu, Xizi Wan, Zheng Lou, Feilong Zhang, Lianxin Shi, Siheng Li, Bing Dai, Guozhen Shen, and Shutao Wang. Skin adhesives with controlled adhesion by polymer chain mobility. *ACS applied materials & interfaces*, 11(1):1496–1502, 2018.

[207] P Peyre, R Fabbro, L Berthe, and C Dubouchet. Laser shock processing of materials, physical processes involved and examples of applications. *Journal of Laser applications*, 8(3):135–141, 1996.

[208] P Peyre, P Merrien, RP Lieurade, and R Fabbro. Laser induced shock waves as surface treatment for 7075–t7351 aluminium alloy. *Surface Engineering*, 11(1):47–52, 1995.

[209] Stephen J Harley, Elizabeth A Glascoe, and Robert S Maxwell. Thermodynamic study on dynamic water vapor sorption in sylgard-184. *The Journal of Physical Chemistry B*, 116(48):14183–14190, 2012.

[210] Simon BARDY. *Contrôle et optimisation du test d'adhérence par choc laser sur assemblages collés*. Theses, Ecole nationale supérieure d'arts et métiers - ENSAM, December 2017.

[211] Gordon R Johnson. A constitutive model and data for materials subjected to large strains, high strain rates, and high temperatures. *Proc. 7th Inf. Sympo. Ballistics*, pages 541–547, 1983.

[212] HK Amarchinta, RV Grandhi, K Langer, and DS Stargel. Material model validation for laser shock peening process simulation. *Modelling and simulation in materials science and engineering*, 17(1):015010, 2008.

[213] JS Dugdale and DKC MacDonald. The thermal expansion of solids. *Physical Review*, 89(4):832, 1953.

[214] MH Rice, R Go McQueen, and JM Walsh. Compression of solids by strong shock waves. In *Solid state physics*, volume 6, pages 1–63. Elsevier, 1958.

[215] John Clarke Slater. *Introduction to chemical physics*. Read Books Ltd, 2011.

[216] William John Macquorn Rankine. Xv. on the thermodynamic theory of waves of finite longitudinal disturbance. *Philosophical Transactions of the Royal Society of London*, 1870.

[217] Henri Hugoniot. Memoir on the propagation of movements in bodies, especially perfect gases (first part). *J. de l'Ecole Polytechnique*, 57:3–97, 1887.

[218] Damien Courapied. *Etude de l'interaction laser matière en régime de confinement par eau avec deux impulsions laser. Application au test d'adhérence par choc laser.* PhD thesis, 2016. Thèse de doctorat dirigée par Berthe, Laurent et Peyre, Patrice Mécanique-matériaux Paris, ENSAM 2016.

[219] P. Peyre, R. Fabbro, P. Merrien, and H.P. Lieurade. Laser shock processing of aluminium alloys. application to high cycle fatigue behaviour. *Materials Science and Engineering: A*, 210(1):102 – 113, 1996.

[220] RJH Wanhill. Fatigue requirements for aircraft structures. In *Aerospace materials and material technologies*, pages 331–352. Springer, 2017.

[221] Paul C Paris. A rational analytic theory of fatigue. *The trend in engineering*, 13:9, 1961.

[222] Paul Paris and Fazil Erdogan. A critical analysis of crack propagation laws. 1963.

[223] K Sadananda, A.K Vasudevan, and R.L Holtz. Extension of the unified approach to fatigue crack growth to environmental interactions. *International Journal of Fatigue*, 23:277–286, 2001.

[224] Tianwen Zhao, Jixi Zhang, and Yanyao Jiang. A study of fatigue crack growth of 7075-t651 aluminum alloy. *International Journal of Fatigue*, 30(7):1169–1180, 2008.

[225] Paul C Paris, Mario P Gomez, and William E Anderson. The trend in engineering. *University of Washington*, 13(1), 1961.

[226] Robert Peh-ying Wei. *Fracture Mechanics: Perspectives and Directions (twentieth Symposium)*, volume 1020. Astm International, 1989.

Corentin LE BRAS

Etude de matériaux polymères comme confineurs solides dans l'application choc laser LSP

Résumé : Le procédé de laser shock peening (LSP) est couramment utilisé dans l'industrie aéronautique afin de renforcer le comportement en fatigue des pièces critiques. Il consiste à focaliser une impulsion laser à la surface d'une pièce métallique. Au contact, un plasma se crée et se détend dans l'air tout en induisant la création d'une onde de choc dans la cible. Afin de produire des pressions suffisantes au traitement d'alliages utilisés dans l'aéronautique, une couche d'eau est placée sur la surface de la pièce à traiter. Dans cette configuration, la détente du plasma produit une pression de l'ordre du GPa. En conséquence, des contraintes résiduelles de compression sont induites dans le matériau qui induisent elles-mêmes un meilleur comportement en fatigue. Cependant, le régime confiné par eau ne permet pas le traitement de certaines pièces d'avion dans lesquelles de l'eau ne peut pas être amenée. Dans ce manuscrit de thèse, l'utilisation d'un polymère transparent et flexible comme confinement pour le LSP démontre de bons résultats permettant de démontrer l'efficacité des polymères pour des applications de grenaillage laser dans lesquelles l'eau ne peut être utilisée. Le manuscrit présente le choix d'un polymère de confinement suivi de son évaluation ainsi que de ses propriétés mécaniques sous régime de choc laser.

Mots clés : Grenaillage laser, Adhésif, Transition vitreuse dynamique, Contraintes résiduelles

Abstract : The laser shock peening (LSP) process is commonly used in the aerospace industry to reinforce the fatigue life behaviour of aircraft parts. It consists in focusing a laser pulse at the surface of a metallic target. Upon contact, a plasma is created and starts to expand in the air and induces the creation of a shockwave in the material. In order to reach sufficient pressures to treat the alloys of interest, a water layer is usually placed on top of the surface of the metallic target. In this configuration, plasma release produces a pressure in the GPa range that plasticises the matter. As a result, compressive residual stresses are induced in the material and are themselves the cause of the final increased fatigue life behaviour. However, this configuration does not allow for the treatment of some specific parts of aircrafts that cannot support water in their environment. In this work, the use of flexible, transparent polymers as confinement for LSP is studied and demonstrates good results allowing to consider polymer for laser peening applications where water cannot be used. The results present the choice of a polymer to be used as a confinement for the LSP process, followed by its characterization as well as its properties under laser shock loading.

Keywords : Laser shock peening, Adhesive, Dynamic glass transition, Residual stresses